Coal pellets as an alternative fuel for a semi-continuous coal stove

CW Meyer

orcid.org/ 0000-0001- 5795- 3863

Dissertation accepted in fulfilment of the requirements for the degree *Master of Engineering in Chemical Engineering* at the North-West University

Supervisor:	Prof HWJP Neomagus
Co-supervisor:	Prof JR Bunt
Co-supervisor:	Dr FH Conradie

Graduation: June 2025

DECLARATION

I, Coenraad Wilhelmus Meyer, hereby declare that the dissertation entitled: “Coal pellets as an alternative fuel for a semi-continuous coal stove”, submitted in fulfilment of the requirements for the degree of Master of Engineering in Chemical Engineering, is my own work except where acknowledged in the text where the appropriate references have been provided. Language and grammar editing was conducted with the help of AI technology. This dissertation has not been submitted to any other tertiary institution in whole or in part. I understand that the copies handed in for examination are the property of the Noth-West University. Opinions, findings and conclusions or recommendations expressed in any publication generated by the NRF supported research are that of the author(s) alone, and the NRF accepts no liability whatsoever in this regard.

Signed at Sasolburg on the 26th of November 2024.

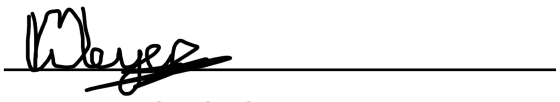

CW Meyer (Author)

ACKNOWLEDGEMENTS

I give praise to our Heavenly Father for the opportunities, talents, and perseverance He has granted me. Without His guidance, I would not be where I am today.

I wish to acknowledge the following for their contributions toward the completion of my thesis:

- To my parents, Mom and Dad, thank you for your unwavering support, motivation, and pep talks. Your love and care have carried me through the tough times when giving up seemed like the only option.
- To my close family, Nico du Plooy, Ronelle du Plooy, and Ria Vermaak, thank you for doing more than I could ever ask for. Your contributions to my growth and development are immeasurable.
- To my primary supervisor, Prof. Hein Neomagus, thank you for never giving up on me. Your knowledge, experience, and honesty have been invaluable throughout this process.
- To my secondary supervisors, Prof. John Bunt and Dr. Frikkie Conradie, I could not ask for better mentors, role models, and teachers. I will always cherish the moments we shared and the lessons I learned from you.
- To the Climatology Research Group, Mr. Richhein du Preez and Prof. Stuart Picketh, thank you for your assistance with assembling the equipment and your patience when things did not go as planned.
- To the fourth-year students, Mr. Rikus Horn, Mr. Jan Witbooi, and Mr. Tjasse Biewenga, your contributions to my work have not gone unnoticed. Thank you for staying by my side during the long nights and cold winter mornings in the coal lab.
- To the lab staff, Ms. Rene Bekker, Mr. Clement Mgano, Mr. Adrian Brock, Mr. Jan Kroeze, and Mr. Elias Mofokeng, your assistance with the technical aspects of my work is greatly appreciated.
- To my friends and confidants, Mr. Marcus Keulder and Mr. Marco de Sousa, you have been there for me through all the ups and downs, both academically and personally. May our friendships stand the test of time.
- To the National Research Foundation (NRF) [Coal Research Chair Grant No. 86880] who financially supported this work.
- To my fiancé, Cara Prinsloo, thank you for always standing by my side. I know my academic endeavours have taken much of our time together, but I trust the rewards will make up for it.

Thank you for never allowing me to feel hopeless and discouraged and for being strong when I could not.

ABSTRACT

Around four million South African households depend on coal for fuel. Despite gaining electricity access, many continue using coal due to its affordability and cultural significance. Low-income households often rely on damaged or homemade stoves, leading to inefficient combustion and higher indoor emissions. In 2016, household pollutants contributed to roughly 3.8 million deaths globally. Approximately 11% of South Africa's run-of-mine coal consists of fines, often discarded due to costly disposal processes. While coal agglomeration (e.g., pellets) can add value to these fines by addressing storage and transport issues, studies have revealed that they are seldom adopted in low-income South African communities.

This study aims to determine the thermal performance and emissions quality of coal pellets, in order to evaluate the suitability thereof as an alternative to current domestic fuel sources. To achieve this aim, lump coal and coal pellets with different characteristics were combusted in a semi-continuous coal stove developed by *New Dawn Engineering* in collaboration with the North-West University. Six fuel batches were tested: lump coal (C), binderless pellets (P-B), and four variations of PVA binder pellets, both with and without waterproofing (P-2.5, P-5, P-2.5-W, and P-5-W).

Key findings indicate that combustion behaviour differed significantly between lump coal and coal pellets. The lump coal run exhibited the highest power output of 8.0 kW, and an overall thermal efficiency of 71.2%. In comparison, the binderless pellets displayed the lowest power rating of 4.2 kW, whereas the P-2.5 pellet run displayed the highest overall thermal efficiency of 77.5%. In terms of emissions, the semi-continuous coal stove achieved lower emission levels than a typical domestic coal stove burning both lump coal and low smoke fuel. The lump coal exhibited the lowest carbon monoxide CO emission factor of 0.67 ± 0.04 g/MJ, while most pellet runs, particularly P-2.5, produced CO emission levels more than double that of lump coal. The high CO emission factors of the coal pellets were attributed to the combustion in oxygen deficient conditions, which was observed during all the pellet fuel experiments. The SO_X emission factors remained relatively comparable between the different fuel batches with no significant correlation to operating parameters. Variations in NO_x emissions was mainly attributed to combustion in a reductive environment, with lump coal producing the highest NO_x emission factor of 120 ± 6 mg/MJ. Particulate matter emissions showed no significant correlation with fuel type or characteristics. The P-5 run produced the lowest PM levels with an emission factor of 15 ± 1 mg/MJ. Overall, the lump coal and P-5 stove-fuel combinations exhibited superior performance relative to the other combinations evaluated across both low- and high-power settings. The P-5

pellets is therefore identified as a suitable alternative fuel for the semi-continuous coal stove. The fuel PSD of -19 mm +13.2 mm is also recommended for domestic use.

Keywords: Coal; Combustion; Coal pellets; Coal stove.

TABLE OF CONTENTS

LIST OF TABLES

LIST OF FIGURES

CHAPTER 1 – INTRODUCTION

1.1 BACKGROUND AND RATIONALE

1.1.1 Domestic dependence on solid fuels

South Africa's energy resources are dominated by coal and processed coal products [1], [2], [3]. The Department of Energy (DoE) indicated that the combustion of coal and coal-derived fuels satisfies approximately 70% of South Africa's industrial and domestic energy demands [1], [2], [4]. Coal-fired powerplants are the main source of electricity in South Africa, producing approximately 85% - 90% of Eskom's (Electricity Supply Commission) total electricity output [5], [6]. Although coal in South Africa is mainly used in power stations and petrochemical processes, less than 4% of the total annual coal produced is purchased by local merchants and sold for domestic use [1], [3]. Currently, it is estimated that approximately 30% of the global population relies on the household combustion of solid fuel [7]. Most of these households use combustion equipment that emits pollutants continuously that are potentially harmful to both human health and the current climate [8], [9]. It was reported that the global dependence of households on cookstoves and domestic solid fuels decreased from 62% to 41% between 1980 and 2010 [9]. However, because of the increase in global population, the number of individuals that depend on household solid fuel energy generation remains approximately constant at 2.8 billion [9]. Most of these households are situated in Africa and Southeast Asia (regions where more than 60% of households utilise solid fuels) [9]. Approximately 4 million South African households still rely on coal as a fuel source, especially during the winter seasons [10]. The DoE reports that households mainly rely on coal combustion for domestic activities since it is a relatively cheap fuel source, especially for informal settlements that are situated near coal mines [2]. For these households, the combustion of coal has two primary purposes, which are heating the living environment, and providing heat for cooking [3]. In addition, domestic fuel combustion can also be used for lighting, and various other applications such as personal hygiene [11], [12]. Households that receive access to electricity rarely move away from coal combustion since electrical appliances are seen as unaffordable and untraditional [3]. A study conducted in Africa also reported the possibility that households which are situated more than 5 km away from "cleaner" fuel sources (like liquid petroleum gas (LPG) or low smoke-fuel) are less likely to adopt these fuels [13]. Further research indicated that households in low-income settlements follow the "energy ladder" hypothesis, which states that residents will adopt cleaner forms of energy as their income increases [14], [15]. Therefore, with a current (and increasing) South African unemployment rate of 32.9% [16], millions of residents will continue to rely on coal and biomass combustion for energy demands in the near future.

1.1.2 Effect of household emissions

Several fuel sources are utilised in low-income settlements during daily household activities. The two main solid fuels burnt in these settlements have been identified as wood and coal [17]. Additional energy resources include electricity, paraffin, LPG, and any available biomass other than wood (*e.g.,* animal dung) [17]. Coal, wood, and other biomass resources are relatively inexpensive and easily accessible but potentially produce harmful indoor emissions when used [11], [17]. A correlation can be identified between a country's stage of development and the source of emissions in these regions [18]. The pollution levels in developed countries are primarily produced by traffic and industrial operations, while the combustion of solid cooking fuel is one of the main pollutant contributors in developing countries [18]. The combustion of these solid fuels produces harmful emissions such as carbon monoxide (incomplete combustion), sulphur dioxide, nitrogen dioxide, particulate matter, volatile organic compounds and polycyclic aromatic hydrocarbons [11], [15]. The *Clean Cooking Catalog* [19] and *The World Bank* [20] provide information on more than 800 unique combustion appliances and cookstoves. The data pertains to appliances used in combination with solid or liquid fuels for everyday cooking and heating purposes. These stoves or appliances range from the traditional wood-fuelled three-stone fire (TSF) to clean-burning liquefied petroleum gas (LPG) improved cookstoves [19], [20]. Even the most advanced stoves still produce harmful emissions when used in living environments. These emissions are commonly referred to in literature as household air pollution (HAP). When exposure to harmful indoor pollutants is considered, there are two types of exposure that the stove user can experience: indirect (distal) and direct (proximal) exposure [21]. The combustion of fuel, living room volume, pollutant ventilation, and stove application are all direct factors that determine the proximal exposure to HAP whereas income, education level, cooking habits and other socio-economic factors indirectly influence the degree of exposure to members of stove-using households [22]. In 2016, WHO reported that prolonged exposure to HAP contributed to approximately 3.8 million deaths worldwide [23]. Several studies on the health effects of HAP were conducted in the past 10 years and concluded that these indoor emissions contribute to an average global mortality of between 3 - 4 million deaths annually, which mainly occurs in middle- and low-income countries [8], [22], [23], [24]. Particulate matter produced by household combustion can often contain acids, heavy metals such as lead (Pb), manganese (Mn) and organic substances that are harmful to human life upon chronic exposure [18]. Indoor pollutants generated from hydrocarbon combustion often contribute to the development of respiratory diseases and cardiovascular ailments [15]. Various studies indicated that members of households exposed to HAP when compared to households that utilise a cleaner form of energy, have increased risks of all-cause mortality in addition to the reported respiratory diseases and cardiovascular ailments, [25].

In 2010, the World Health Organization International Agency for Research on Cancer (IARC) concluded that household pollutants from coal or coal-related fuels are a Group 1 carcinogen [8]. Studies also indicate that indoor pollutants are associated with childhood chronic lung diseases and pneumonia [26], [27].

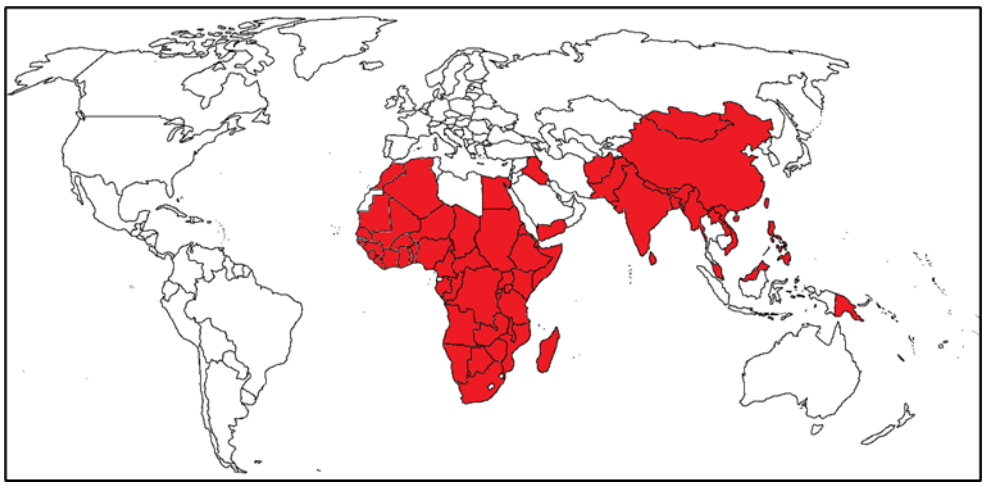

Figure 1-1: Countries with more than 300 indoor air pollution deaths per million population (adapted from [26]).

Most of the solid fuel combustion-related diseases and health impacts are mainly recorded in developing countries, such as most Sub-Saharan African countries as well as Southeast Asian countries as indicated in Figure 1-1 [26], [28]. A definitive correlation between poverty, household pollution and respiratory diseases can also be identified [26]. Poverty is thus a key factor that leads to the dependence on coal combustion which could ultimately result in a higher mortality rate due to the inevitability of continued exposure to the aforementioned pollutants [26].

1.1.3 Coal fines accumulation

Coal fines or coal mine tailings are historically seen as a waste by-product of the coal mining and post-mining processes [29], [30]. Tailings are generally classified as fine (-0.5 mm) or ultra-fine (-0.1 mm). Coal fines produced by mining processes are suspended in a slurry and have to be dewatered and thermally dried before it can be used [31]. This is known as the beneficiation of coal fines and is typically economically unfeasible due to the high cost of dewatering and the low market value of coal [30], [31]. Furthermore, due to the high disposal cost, fines are normally left in slurry ponds or abandoned stockpiles [29]. Some dewatered coal fines are also sold to local power plants as feedstock [30]. The total amount of coal fines in the top ten coal producing countries is estimated to exceed 30 billion tons and are mostly discarded and unused [29]. The South African coal mining industry is estimated to produce more than 250 million tonnes of coal

per year, of which 4% (10 million tonnes) are found to be ultra-fine coal [31]. These coal fines have an average size fraction of 150 μm and a calorific value (CV) of approximately 23 MJ/kg [31]. Discarded coal fines present several risks and hazards that include acid mine drainage, dust release and spontaneous combustion [31]. The marketing of waste coal fines faces significant difficulties such as storage, handling, transport, *etc.* especially when the fines are wet or contain aeratable dust particles from dry fines [32]. Waste coal fines that do not cake easily, can be utilised as combustion fuel in its unrefined state but require specialised grates [33]. Even when special construction is used in combustion appliances, the fines are difficult to handle and result in fuel waste much greater than when lump coal is used [33]. Therefore, the value of coal fines as fuel is significantly lower than lump coal from the same batch.

1.1.4 Coal agglomeration

Coal agglomerates can be defined as the product of combining coal fines into coherent particles with a substance called the binder. Binders are usually chemical mixtures but can also be derived from direct liquefaction of biomass material [32]. The coal agglomeration process can be used to address the handling disadvantages of coal fines, as previously mentioned, and ensure the value addition of coal fines. Due to the formation of coherent particles, coal agglomeration can also be utilised to prepare fuel for combustion appliances that are typically designed for lump coal [33]. These agglomerates (coal briquettes or coal pellets) can have a market value equal to, or more than the original lump coal of which the fines were separated (depending on the quality thereof) [33]. Since coal is a non-renewable source of energy, it is of significant importance to reduce coal fines waste and find cost effective methods of utilising current discarded coal fines. A study was conducted by Muzenda, [30] to investigate the potential uses of South African coal fines. The reported methods of low-cost coal fines utilisations are summarised in Figure 1-2.

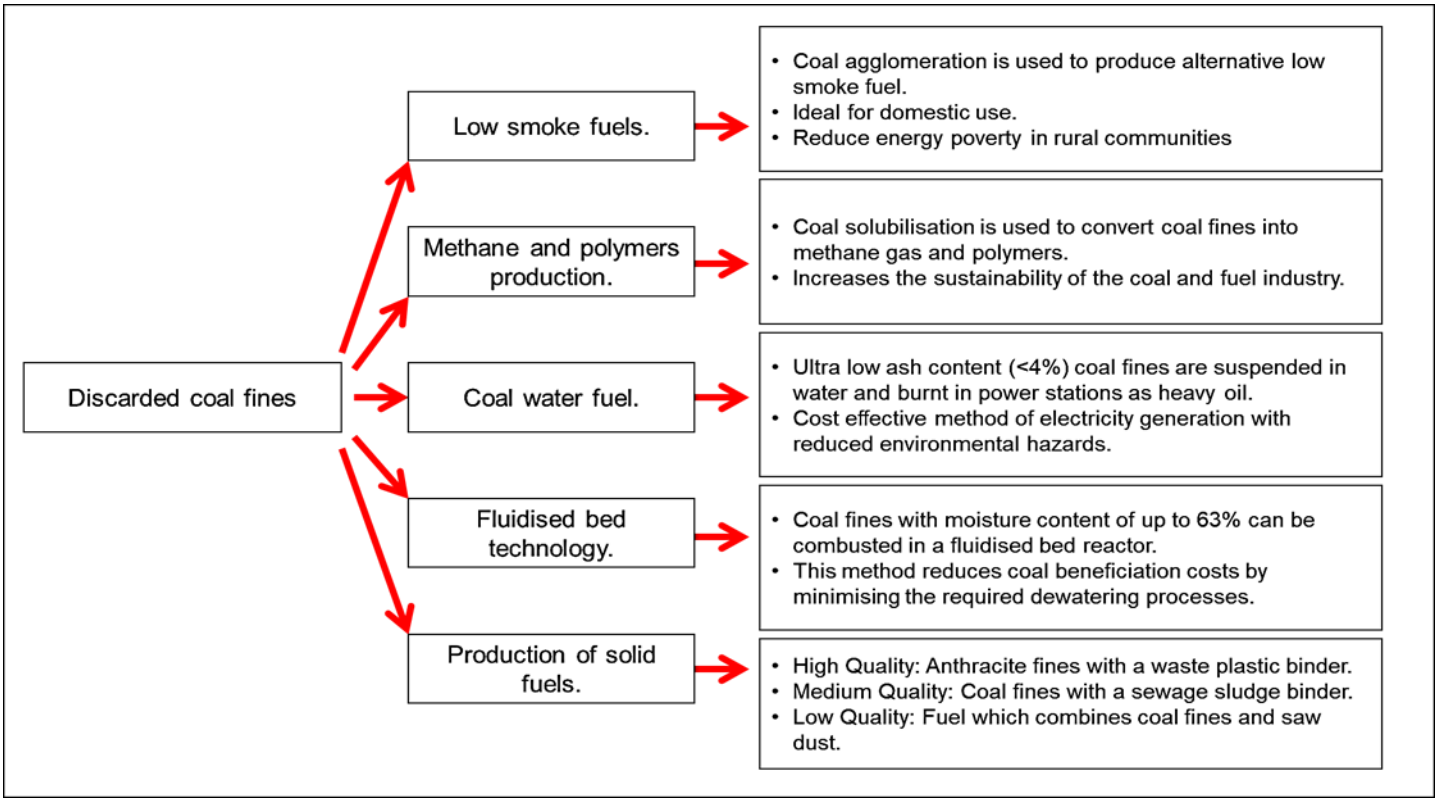

Figure 1-2: Potential uses of South African coal fines (adapted from [30]).

The utilisation of coal fines to produce low smoke fuels (LSFs) is an already existing method of energy generation in South Africa, while most of the other presented methods of coal fines utilisation are still in the theoretical/planning stages of implementation [30]. Producing LSFs requires coal fines agglomeration which can be done by several methods, such as pelletising, briquetting, or extrusion [30], [34]. Coal agglomeration can be defined as the process of particle enlargement, whereby material fines are upgraded into larger coherent pellets or granules [35]. Furthermore, in literature, several advantages, disadvantages and requirements have been given for the coal (LSF) agglomeration process and are summarised in **Table 1-1**.

It is clear from literature that the main advantages of coal agglomeration include the value addition of coal fines, the ease of handling, the prevention of environmental hazards, and the economic benefits thereof. The only clear disadvantages of coal agglomeration are the technical and economic resources that are required for the agglomeration process [36]. The coal fines are carefully prepared for the agglomeration process, which can be time and labour consuming, and relatively expensive [36].

Table 1-1: Summary of the coal fines to LSF agglomeration process [30], [35].

Advantages	Disadvantages	Requirements
• Can provide rural communities with an affordable alternative improved energy source. • Coal agglomeration can prevent environmental hazards such as spontaneous combustion of coal fines. • Coal agglomeration improves the handling and storage of coal fines and reduces losses due to aeratable coal fines.	• Ultra-fine coal particles can cause several process blockages and can easily clog up process equipment which was designed for coarser coal fines.	• Homogeneous particle size range. • Coal agglomerates must be water resistant for outdoor usage. • High agglomerate strength to prevent disintegration during handling and transport. • Agglomerates should have similar characteristics to lump coal (such as calorific value, ash yield, etc.)

Several studies suggested that cookstoves which utilise packed bed combustion with homogeneous fuel particles (both in geometry and composition; for example, pellets) have improved emissions performance compared to ordinary cookstoves [8]. Even though coal agglomerates can be used as an alternative fuel for combustion appliances, various studies conducted in South African low-income settlements indicate that these are rarely utilised [3]. The semi-continuous coal stove that was developed at the North-West University in a collaborative effort with *New Dawn Engineering* [37], is currently part of a project to reduce the local HAP of the Highveld rural settlements such as in the Witbank and Sasolburg regions. Similar studies were conducted by Sumbane et al. [38] and Kuhn et al. [39], where the fuel size, emissions levels and thermal efficiency were tested in an attempt to reduce local HAP. The application of alternative fuels like coal fine agglomerates was however not tested in any of these studies.

1.2 PROBLEM STATEMENT, AIM AND OBJECTIVES

Millions of households in South Africa still depend on coal combustion to satisfy their basic needs. However, prolonged exposure to coal combustion emissions induces respiratory illnesses and other health ailments. Mining and post-mining processes result in an accumulation of coal fines that are unused and ultimately discarded. Agglomeration results in the value addition of coal fines, but the utilisation of coal pellets in domestic combustion appliances is not documented in literature.

Therefore, this study aims to determine the thermal and emissions performance of the semi-continuous coal stove with coal pellets as fuel, in order to evaluate the suitability of coal pellets as an alternative to current domestic fuel sources.

To attain the aim of this study, the following objectives are outlined:

- Procure and characterise coal pellets.
- Measure the thermal and emissions operating parameters during the operation of a semi-continuous stove.
- Determine emission factors and thermal efficiencies.
- Compare the performance parameters of coal pellets and conventional domestic solid fuels.
- Identify possible stove design improvements to accommodate the combustion of coal pellets.

1.3 SCOPE OF STUDY

1.3.1 General approach and limitations

This study focuses on coal pellets as an alternative fuel for a semi-continuous coal stove. As such, the scope of this study is limited to combusting coal pellets in a novel coal stove. Lump coal is included in this study as a basis of comparison. These stove-fuel combinations specifically focus on pellets formed from the tumble-growth agglomeration process. The agglomerate binder used in this study is selected from preliminary testing of several binders that were made available by the fuel vendor. The semi-continuous coal stove is fabricated from a combination of cast iron, mild steel, refractory brick, and fitted with a chimney. No modifications to the design of this coal stove were incorporated during this study to ensure scientific consistency, however design improvement recommendations are included for future research.

The stove-fuel experiments included in the scope of this study is varied based on i) fuel characteristics, ii) stove power setting, and iii) fuel size range and packing. During fuel selection, different pellet binders were tested, including a starch binder. However, for bulk experimentation and fuel characterisation, one binder was chosen (PVA) at three varying quantities (0 wt.%, 2.5 wt.% or 5 wt.%). Furthermore, only one waterproofing agent was used in this study as recommended by the fuel vendor. During the stove power setting experiments (high- and low-power) the inlet airflow opening was either fully closed or opened to control the internal natural draft of the stove. Based on packing properties (bed density, voidage, etc.), the experiments included three varying size ranges of selected mixtures (-19 mm +13.2 mm, -19 mm +9.5 mm, and -13.2 mm +6.7 mm).

The lump coal and coal pellets are compared based on combustion, thermal, and emissions parameters as set out in the aim of this study. Emission sampling and thermal measurements is based on the setup proposed by Sumbane et al. [38], Kuhn et al. [39] and Altanzul [40]. Some modifications (such as water traps) were made to improve the setup and allow for accurate sampling, while maintaining the health and reliability of the analyser equipment. This equipment setup and use thereof was conducted in a controlled laboratory environment.

The stove operation, measurement of emissions and thermal parameters were conducted per standard operating procedure (SOP) as set up by the coal stove designer. However, some SOP recommendations were made to allow improved ignition and combustion of coal agglomerates. The emissions measurements were limited to the capability of the gas analyser and includes CO, CO_2, SO_2 NO_X, and O_2. No other species in the flue gas (such as H_2S, COS, or CH_4) were tested for in this study. Similarly, due to equipment limitations total PM (and not size-specified fractions)

is reported in this study. Finally, emission factors shown in this study are only reported on an energy basis instead of on a mass basis.

1.3.2 Dissertation outline

This dissertation will contain six chapters that are outlined as follows:

- The study is introduced in Chapter 1 where a contemporary problem is identified and a solution for the problem is suggested in the form of this study. The problem statement, aim, and objectives are stated, and a brief overview of the dissertation is given.
- In Chapter 2, literature relevant to the aim of this study is presented, and comparable literature research data is provided. In the literature survey, an overview of both coal fines accumulation in South Africa and pollutant formation in domestic combustion appliances is given. However, the main theme of this chapter is to discuss recent studies conducted in the field of improvements in the operation of cookstoves globally.
- The fuel characterisation is given in Chapter 3. All relevant chemical and physical/mechanical characteristic parameters of the lump coal and coal pellets are presented and discussed. The experimental methods used for the fuel characterisation are also listed.
- Chapter 4 details the experimental methodology, including the materials and methods, equipment setup, and the operating procedures. Furthermore, in this chapter data processing methodology for both thermal and emission parameters are given and discussed.
- In Chapter 5, the results of the experimental work and data calculations are provided. An overview of general observations and trends are provided, whereafter the comparisons between performance parameters of stove-fuel combinations are made. A comprehensive discussion comparing high-power runs with different fuel characteristics is given, while the remaining sub-sections offer brief summaries regarding the comparison of low- and high-power runs, as well as the impact of fuel PSD on thermal and emission performance parameters.
- Finally, the experimental work and discussions are summarised in Chapter 6. A conclusion and recommendations regarding the suitability of coal pellets as alternative fuel for a semi-continuous coal stove are given to address the problem statement, aim and objectives stated in Chapter 1.

CHAPTER 2 – LITERATURE SURVEY

In this section, the literature survey is centred on two key aspects. Firstly, it provides an overview of the origin and classification of coal fines and discusses their utilization. This establishes a comprehensive background of research and published literature concerning the challenges associated with coal fines and the suggested solutions. The second part of this chapter delves deeply into domestic stoves and the relevant literature regarding their operation and the implementation of improved cookstoves. The chapter is then concluded, highlighting the pertinent parameters related to improved cookstove performance.

2.1 COAL FINES OVERVIEW

2.1.1 Origin and formation of coal fines

Coal is utilised as the primary fuel source in global energy generation, with its combustion process being the predominant method for energy production [41]. Bituminous coal is South Africa's primary fuel source for both domestic and commercial energy production and will continue to dominate this sector for the foreseeable future [42]. Although several coalfields in the Gauteng, Free State, and Mpumalanga provinces have been explored and exploited, it was estimated in 2014 that more than 70% of South Africa's remaining coal resources were situated in the Limpopo region, which remained unexplored until recently [42] These four coalfields in combination with the remaining coal reserves across the country, could persist for more than 100 years at current coal consumption rates [30], [42]. South Africa first entered commercial coal production in 1857 and is currently among the top 10 global coal-producing countries, with a production rate of approximately 250 million tonnes per annum [30], [42]. During the production process, run of mine (ROM) coal is processed to extract and liberate the higher value coal from low value mineral rock, ash forming minerals, and other undesirable matter like pyrite (sulphur containing mineral) [42], [43]. Beneficiation processes can be in the form of chemical cleaning or, more commonly, mechanical/physical cleaning. In the latter, coal ore is separated from contaminants using mechanical machinery such as crushers and industrial screens [43], [44], [45]. During this process, ROM coal is crushed into a smaller size range and screened using industrial sieves with common aperture sizes ranging between 3 and 1 mm in diameter [43], [44]. Up to 60% of the bottom size coal can fall below a particle size of 35 μm, however it has been reported that South African coal tailings have an average particle size of 150 μm in diameter [30], [43]. Where liberation characteristics allow, the coal fines are beneficiated in several processing units which separate low ash yield (low density) coal from other higher density impurities and high ash forming mineral matter (high density) coal/shale depending on market quality requirements, i.e., calorific

value, ash, and sulphur content, etc. [43], [44]. The low ash yield coal fines (average calorific value of 23 MJ/kg on a dry basis) are usually dried and mixed in with the coarse lump coal or sold to local power plants or metal refining processes as energy generation feedstock [30], [45]. Finally, the retained low grade coal tailings are directed to waste plants where it is used as land fill material or abandoned in stockpiles. This is due to the high supply and low market demand, particle size (<500µm), high sulphur content, high ash yield, and handling difficulties thereof [30], [34], [43].

2.1.2 Classification and characterisation of South African coal fines

In 2001, it was estimated that more than 1 billion tonnes of waste coal and coal fines were available in South Africa [46]. At current reported discard rates, the availability of abandoned coarse coal, unsold duff coal, and coal tailings are estimated to exceed 2.4 billion tonnes (estimations for the year 2020) [47]. It is also reported that the majority of the discarded coal resides in the Witbank-Highveld coal region and could theoretically be extracted for reuse as feedstock for energy production [48]. In 2014, it was reported that there were 29 active discard coal tailing dumps (approximately 310 million tonnes), and 17 active discard slurry ponds (50 million tonnes) [30]. The characteristics of discarded coal material can vary depending on the reason for its abandonment. Coal mine tailings typically have high ash and sulphur content, whereas coal material abandoned due to excess production and low market demand usually has lower ash and sulphur content and a higher calorific value compared to the aforementioned coal tailings. The minimum and maximum reported characteristic values for discarded coal material mentioned in literature can be seen in Table 2-1 [49], [50].

Table 2-1: Summary of South African coal fines' composition reported in literature (air dried basis).

Characteristic	Minimum reported	Maximum reported
Sulphur Content *(%)*	0.8	8
Volatile Matter *(%)*	8	30
Ash Yield *(%)*	10	70
Calorific Value *(MJ/kg)*	2	26

Eskom (Electricity Supply Commission), the South African electricity utility, indicated that at current and projected discarding rates, if the waste coal material is used as energy generation

feedstock, it could sustain all current power stations for up to 15 years of continuous operation [50]. It is also reported that the 2.4 billion tonnes of available waste coal material in South Africa could produce up to 4.6 TWh of electricity, which is three times the estimated Sub-Saharan electricity demand in 2040 [47].

2.2 AGGLOMERATION PROCESSES

The agglomeration of coal fines can typically be divided into two distinct sections: Pressure agglomeration (such as briquetting and extrusion), and non-pressure agglomeration (such as pelletisation) [35]. Pressure agglomeration utilises mechanical compressions to press the fine material into a certain cohesive shape. This process commonly uses the moisture of the material to act as a binding agent [35], or can make use of a common binding agent. Non-pressure agglomeration utilises a tumbling process to agglomerate material into a spherical pellet, and typically requires a binding agent to assist in the fines' coalescence process [35]. Before the pelletisation process (also referred to as the tumble-growth agglomeration process) can occur, several techniques can be applied, which include micro pelletising and conditioning [35]. Micro pelletising refers to the process where small quantities of solid material are mixed with the binding agent to produce "seed pellets" (particles with a large enough diameter to induce external material accumulation during the tumble process) [35]. Conditioning refers to the process of adding binders to the raw material, which not only reduces airborne fines and dust but also prepares the material for the pelletisation process [35]. Once these pre-treatment techniques are performed, the material is directed to the main process unit in which the tumble-growth agglomeration process occurs.

Table 2-2: Process units commonly used in the pelletisation process (adapted from [35]).

Process unit	Uses	Capacity
Disc/drum pelletiser	• Agglomeration	100 ton/hr
Rotary drum pelletiser	• Agglomeration • Coating	3500 ton/hr
Pin mixer	• Micro Pelletising • Mixing • Conditioning • Agglomerating	70 ton/hr
Pugmill mixer	• Mixing • Conditioning • Agglomerating	250 ton/hr

In Table 2-2, a summary of the main process units in which the agglomeration process can take place is provided; some of these process units can also be used for the micro pelletising and conditioning procedures [35]. The most common process unit used for the non-pressure agglomeration process worldwide is the disc/drum pelletiser [35]. The disc or drum of this unit is typically operated at an angle of 45° - 50° to ensure a suitable pellet size during the tumble process [51]. Due to the minimal pressure that occurs inside the drum/disc, it is critical to ensure that sufficient binder and moisture (18% – 25%) is present to obtain durable pellets for downstream handling [51]. The material feedstock as well as the binder are constantly fed into the process unit, which ensures continuous operation [35]. There are several process variables which need to be considered to achieve the desired end product. These variables include binder feed rate, material feed rate, disc/drum speed, disc/drum angle, *etc.* [35]. All these process variables influence the exiting pellet size, strength, and production rate. Once the material exits the pelletiser, it is directed to a rotary dryer or fixed oven to "cure" the agglomerates and reduce excess moisture in the granules [35]. The oven is typically operated at a temperature of between 250 °C and 300 °C, with a pellet residence time of between 30- and 90-min dependant on the binding agent used [51]. An overview of the entire process is given in Figure 2-1 [35].

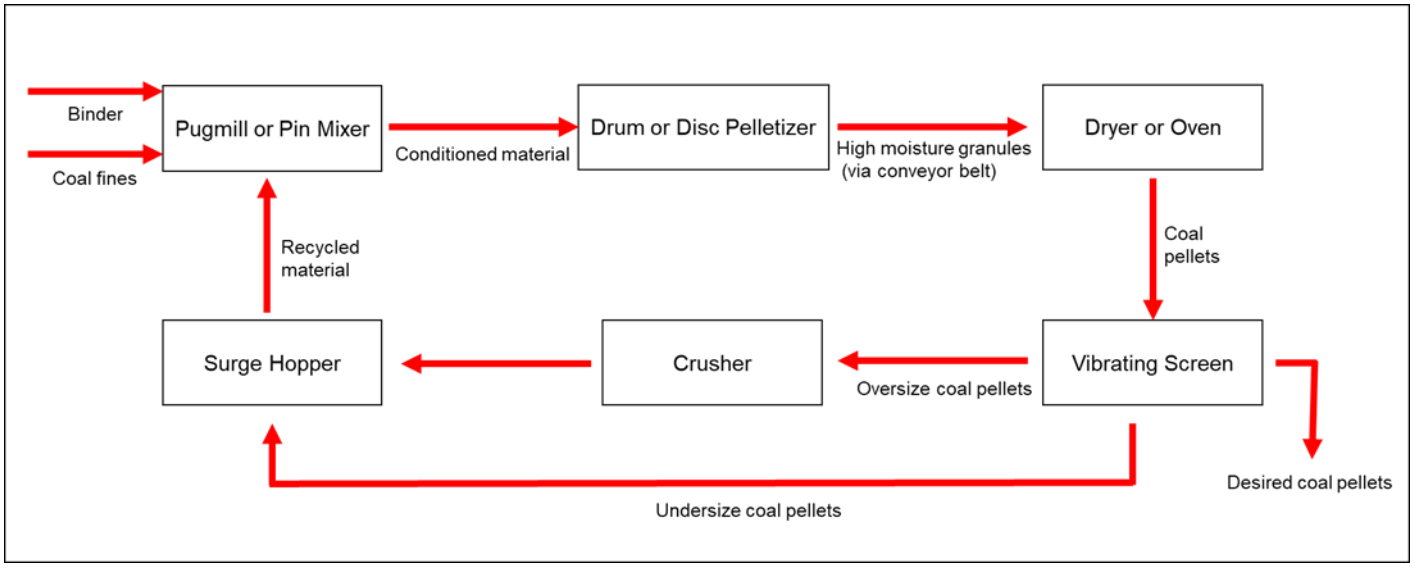

Figure 2-1: Process flow diagram of a typical pelletisation plant (adapted from [35]).

Although the pelletisation process can be utilised to produce low LSF from discarded coal tailings, the large-scale economic feasibility thereof is still questioned [52]. To test the technical feasibility of this process, preliminary tests have been conducted on the production of LSF from ultra-fines in South Africa [52]. These tests confirmed that pelletising coal fines is indeed technically feasible in the South African context [52].

2.2.1 Economic feasibility of agglomerates as domestic fuel source

In Chapter 1 the technical feasibility of South African coal fines as feedstock for coal agglomeration was briefly discussed, however it is clear form the literature that households will only approach a new fuel source if their financial capabilities permit it ("energy ladder hypothesis"). A study on the economic aspects of converting un-beneficiated coal tailings into marketable fuel, was conducted in the late 1990's in South Africa. The focus of the study was to demonstrate the influence of coal beneficiation methods on the economics in a coal tailings processing plant [51], [53]. One of the investigated methods was the thermal dewatering of coal fines, whereafter coal pelletisation was applied to reduce the surface moisture uptake after beneficiation. The first step in the feasibility analysis was to calculate the contribution to annual gross profit. This was done by evaluating the quality of the coal fines before and after the dewatering and pelletisation phases. It was reported that as the moisture content of the coal tailings decreases, the calorific value increases, and consequently the market value of the fines also increases. Accordingly, it was found that thermal dewatering of coal fines and their pelletisation are more financially promising at higher calorific values (26 MJ/kg) [51].

In the same study, the economics of three main agglomeration methods — pelletisation, briquetting, and extrusion — were investigated. Both capital costs and operating costs were compared. It was found that pelletisation required the largest initial capital investment, while briquetting incurred the highest ongoing operating costs. In contrast, binderless briquetting required the least capital and operating costs due to savings associated with binder and binder equipment expenses. The feasibility analysis in this study concluded with a Net Present Value (NPV) calculation to assess the viability of coal pelletisation and thermal beneficiation methods over a 10-year period. It was determined that pelletisation and thermal beneficiation of coal fines were marginally feasible at a calorific value of 25.5 MJ/kg and could become unfeasible at lower calorific values due to reduced market values. To maintain financial viability, it was recommended that the agglomerates should be sold at higher market rates, such as those in the global coal agglomerates export market. However, despite the technical feasibility of coal agglomerates as LSFs, their use as domestic fuel was deemed unfeasible at the time of the study. This was because the cost of coal agglomeration exceeded that of commercial D-grade lump coal. Therefore, despite its technical feasibility, coal agglomeration was unlikely to be adopted in South African households according to the findings [51], [53].

2.2.2 Coal pellet characteristics and combustion

A study was conducted by Altun et.al., [54] to determine the main parameters influencing the thermal performance and combustion efficiency of appliances when using coal agglomerates as fuel. The following parameters were found to be significant:

- The type of binder used for coal agglomeration.
- The amount of binder added to the pre-agglomeration coal mixture.
- The moisture content of the pre-agglomeration mixture.

A similar topic was discussed by Garcia-Maraver et. al. [55], who outlined the critical factors affecting the quality and performance of a biomass pellet. These factors are also applicable to coal pellets and the characterisation thereof. In this study, it was reported that the quality and combustion performance of pellets depends on two main factors: i) the chemical characteristics of the raw material, which outlines the composition of the agglomerates, and ii) the operating variables of the fuel pelletisation process, which determines the mechanical and physical properties of the fuel pellets [55]. In this study, the pellet characteristic outline, as presented in Table 2-3, was given and discussed; these factors are also the outline for pelletisation criteria as set out in the European documents for pelletisation standards [55].

Table 2-3: The characteristics that influence the performance of agglomerates (adapted from [55]).

Chemical Properties	Mechanical and Physical Properties
• Elemental composition. • Calorific value. • Moisture content. • Ash yield. • Volatile matter. • Material thermal behaviour.	• Pellet durability. • Pellet hardness. • Bulk density. • Particle density. • Pellet size range.

The binder, which is added to the agglomeration mixture, presents a significant influence on both the mechanical and chemical characteristics of the derived coal pellets, and consequently influences both the thermal performance and emission levels of any device that it is utilised in. In a study evaluating the combustion and emission characteristics of coal agglomerates using various binders, poly(vinyl alcohol) (PVA) was identified as a binder that positively influenced the combustion performance and emission levels of coal pellets in a fixed-bed lab-scale combustor [56]. The study also compared the results of pellet combustion with lump coal combustion. It was

observed that the PVA binder enhanced the ignitability of coal and increased the combustion rate, albeit at the expense of overall combustion efficiency in bituminous coal agglomerates [56]. Additionally, all tested binders were found to increase the ash yield and decrease the volatile matter content of bituminous coal agglomerates [56]. The addition of a PVA binder also reduced the fixed carbon content of the coal agglomerates, resulting in a decrease in their lower heating values (LHVs).

The utilisation of coal fines to produce low smoke fuel has already been studied in literature [30]. However, recent studies have introduced a novel approach to further reduce emissions by using coal pellets as fuel. One such study investigated the simultaneous removal of SO_X and NO_X from typical flue gas by utilising both calcium pellets and potassium-containing coal pellets. The potassium in the coal pellets reduces NO_X compounds to N_2, while calcium pellets absorb SO_2 during combustion [41]. The potassium-containing coal pellets are produced using a binder with high potassium content, and KOH is added to the coal slurry mixture, whereas the calcium pellets are made from a $Ca(OH)_2$ water slurry [41]. During combustion, calcium pellets are placed on top of the coal pellet bed. The study determined that the optimal temperature for combined SO_2 capture, and NO_X reduction is 450 °C [41]. Ultimately, both calcium pellets and potassium-containing coal pellets were found to significantly reduce NO_X and SO_X emissions in flue gas [41]. Other research also suggests that $Ca(OH)_2$ can be directly added into coal pellets to achieve similar emissions reduction effects. Despite the potential for reducing emissions in combustion devices, there is no combustion data of coal pellets in household appliances available in the literature.

2.3 PROPERTIES OF HOUSEHOLD COOKSTOVES

2.3.1 Literature attention of coal stoves

Since the health and environmental risks attributed to traditional cookstoves and domestic combustion have been realised, research on this topic has increased substantially. To validate if the field of improved coal stoves is still relevant in contemporary research, and where the absence in research is, an attempt was made to investigate the literature tendencies and focus points. To achieve this goal, the North-West University's *EBSOC^{TM} Discovery Service (EDS)* academic search platform was used to create a summary of literature in the field of household cookstoves. The EDS search platform was chosen due to the wide range of sub-platforms (like *Scopus, Science Direct, Web of Science*, etc.) that is utilised to produce a comprehensive list of search results. Only peer reviewed and acknowledged academic publications were included in this summary. An investigation was conducted on the type of cookstove (improved or traditional stove), stove operating parameter (thermal performance or emissions quantification) and stove fuel (biomass material, coal material, or coal briquettes). The publication summary over the period of the past 20 years can be seen in Figure 2-2.

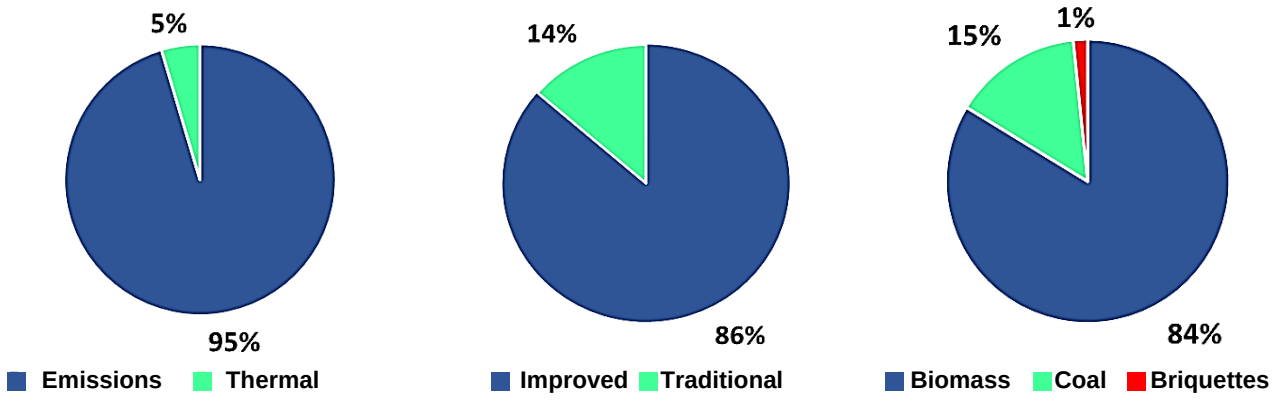

Figure 2-2: EDS search results on relevant subjects.

From Figure 2-2 it can be seen that the majority of publications focused on the emissions quantification of cookstoves rather than the thermal performance. This is mainly due to the health ailments induced by household cookstoves and associated HAP, as discussed in Section 1.1. It is possible that the thermal performance is regarded as an objective of lesser importance since the variability thereof has little impact on human health and living conditions. This would explain why only 5% of cookstove related publications focused on thermal related characteristics over the past 20 years. Furthermore, the subject of improved cookstoves is also favoured among

researchers since the field mainly associates with the reduction of cookstove emissions and directly addresses the HAP negative health impacts. Most of the research that was conducted on traditional stoves aimed to define and quantify the health impacts and corresponding pollutants that these stoves are associated with. Finally, in the context of household cookstoves, the most publicised fuel in literature, irrespective of combustion appliance, was found to be biomass (mainly wood, animal dung, charcoal, and various types of crop residue). This can be attributed to the primary use of biomass in cookstoves globally. Coal is only used in regions where an abundance of low-cost, low-grade coal is available, like parts of China, India, and South Africa. The majority of households in central Africa do not have access to low-cost coal, and therefore rely on the combustion of nearby collected biomass in traditional stoves. The use of coal briquettes as domestic fuel source was found to be one of the least published subjects in the cookstove field, and no publications was found on the utilisation of (tumble-growth) coal pellets in domestic cookstoves.

The yearly increase in literature publications can be seen in Figure 2-3. From the data, it is clear that the domestic cookstove research field is dominated by emissions specific, improved cookstove, and biomass fuel publications. All three of these research subjects received a significant increase in yearly publications after 2007, and a peak number of publications can be seen between 2017 and 2019. However, a current decrease in number of publications in all three subject areas are also observed, which might be due to the extensive research that already exist in this field over the past decade. It was also observed that recent publications focused more on the aftermath of improved cookstove and intervention programs, rather than the development of upgraded cookstoves and emissions reduction programs. Finally, some publications reporting the use of coal as cookstove fuel were published between 2007 – 2010 and 2014 – 2020. With regards to coal agglomerates, only briquettes were studied as a fuel for cookstoves (excluding coal-biomass hybrid agglomerates) and have only received some attention between 2007 – 2010 and 2016 – 2020. In conclusion, there is a clear and noticeable lack of publications reported in the field of coal agglomerates as fuel source for cookstoves, with specific attention to thermal performance and emissions quantification.

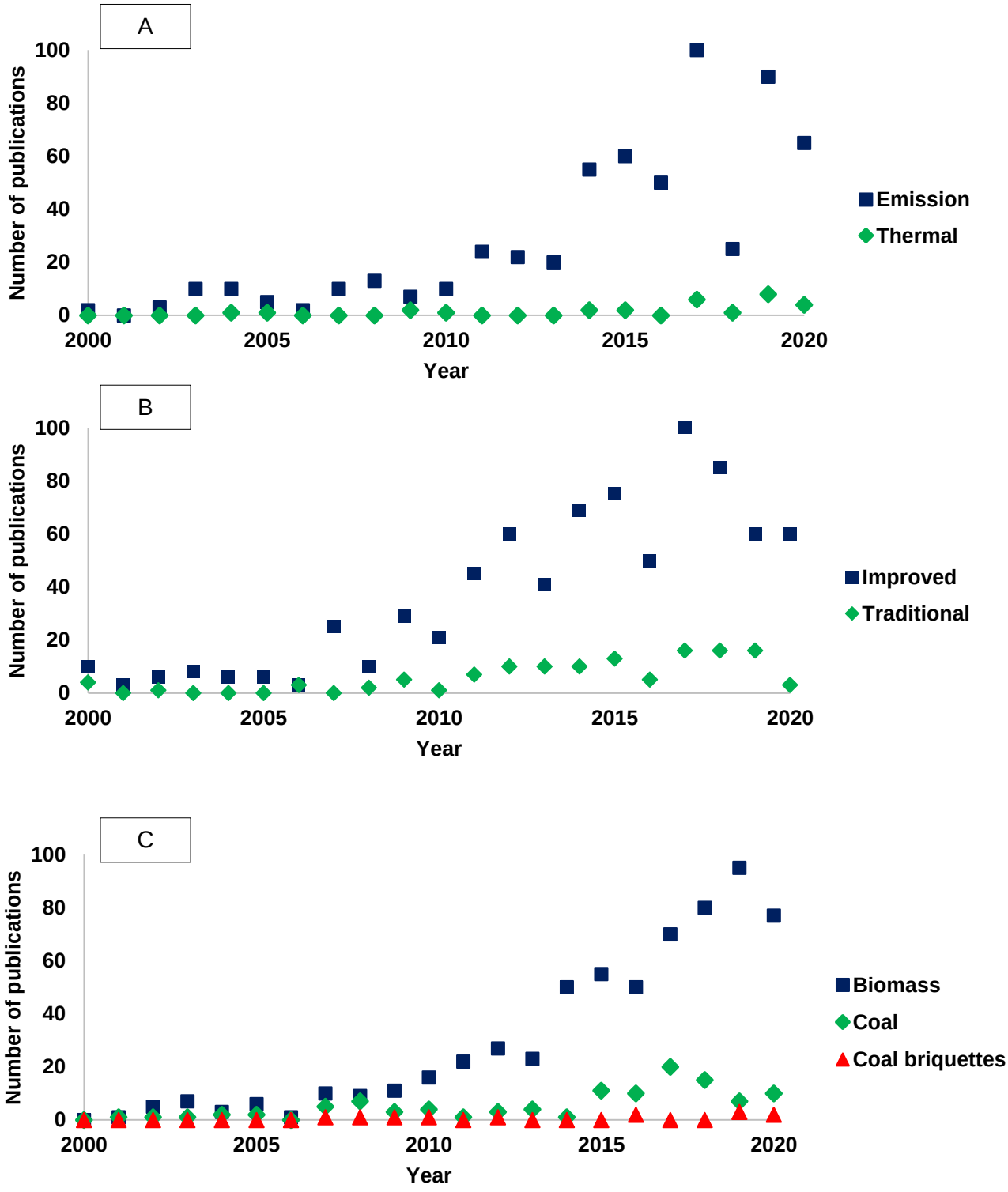

Figure 2-3: Yearly publication of cookstove research with regards to A) thermal or emissions quantification, B) tradition or improved cookstoves, and C) fuel type.

2.3.2 Advantages and disadvantages of improved coal stoves

The advantages of improved cookstoves are undeniable. A recent article summarised that a combination of improved cooking fuels and improved stoves resulted in significant improvements in air quality and human health across several countries, affecting almost 1 billion households [22]. Moreover, another study conducted in Africa reported the effect that improved cookstoves had on the food security, energy security, and socio-economic factors of rural households [13]. The primary motivation of households to adopt the improved cookstove was for food security [13]. As the food security increased, other factors such as the socio-economic conditions improved as well [13]. These cookstoves exhibited the largest effect on food security and reduced the poverty of households [13]. Thereafter improved education, environmental sustainability, reduced climate change, and the adoption of cleaner energy sources were also linked with the improved cookstove intervention program [13]. In conclusion, the increase in food security and quality of living, which is induced by improved cookstoves, can improve the households' overall wellbeing and thereby increasing their socio-economic conditions, energy security, and reducing the environmental emissions [13].

Although improved cookstoves are widely practised as a solution to HAP, the use thereof is still controversial since coal and biomass combustion are still a major source of air pollution [57]. Furthermore, it is observed that some improved cookstoves can produce a high statistical variability with regards to HAP estimates [58]. Studies conducted on the implementation of improved coal and cookstoves reported that the emission levels obtained on laboratory scale were much lower than that during field tests [59]. It is also reported that even though improved cookstoves drastically reduced indoor air pollution levels, these reduced levels are still above the WHO recommended guidelines [11], [22]. A recent study in Ethiopia reported that the implementation of improved biomass stoves reduced the indoor particulate matter by 46%, however a follow-up study on the same improved stove and HAP reduction program reported that the long-term chances of acute lower respiratory infection among children and stove users were not significantly lowered by the improved stove program [60]. Moreover, a similar study reported that the implementation of an improved cookstove had no significant effect on the personal exposure to particulate matter among stove users and children [61]. Therefore, it is clear that even though improved cookstoves can reduce indoor emissions, it is possible that the health effects thereof may remain unchanged. Additionally, a key factor to the ineffectiveness of emission reduction research and programs such as improved coal and biomass stoves, was the inability for scaling-up [62].

A common problem that is also faced when implementing an improved stove intervention program, is the households' willingness to adopt these technologies. There are several factors

that need to be overcome before a household will adopt the cleaner stove. These factors can be described by the “KHAIWAL” model (Knowledge, Housing characteristics, Awareness, Interventions, Willingness to pay, Adoption, Lower emissions) [22]. A major disadvantage to the implementation of clean cookstoves is the willingness for households to change the way that they generate energy daily. A study was carried out on 1000 households in Nigeria which received improved cookstoves as part of an intervention program [13]. It was reported that 90% of these households were willing to continue the use of improved cookstoves and adopt the clean energy generation methods only after the program was completed, compared to 10% of the households that were willing to adopt it at the start of the project [13]. Furthermore, in the study it was also reported that 85% of the households will adopt the improved cookstoves primarily for food security, while the other 15% showed interest in improving their energy security for cooking, reduction of environmental pollutants, and ensuring environmental sustainability [13]. This clearly illustrates households’ state of mind towards emissions reduction and improved cook stoves.

2.3.3 Classification of cookstoves and solid fuels

In South Africa and neighbouring countries, the most common household solid fuels are identified as coal, wood, charcoal, and briquettes [63]. In contrast to South- and East Asian countries, dung and crop waste are seldomly utilised as solid fuel source [63]. Therefore, the household combustion and emission factors reviewed in this, and subsequent sections of the thesis, will only focus of the solid fuels utilised in the Southern African region. The most common and traditional type of cooking method that rural households still rely on, is the three stone fires [64]. This method of energy production is mainly combined with biomass (like wood and crop rests); however, coal and charcoal are also used [63]. The main two disadvantages of three stone fires are: 1) The user is in direct contact with the emissions generated by combustion, due to the lack of ventilation and a chimney, and 2) the three stone fire uses up to 90% more fuel, which results in the ineffective use of time and money that can be applied to other areas like education, health and food security, especially in low-income settlements [64].

Cookstoves can generally be described by two important characteristics: i) The nature of the airflow/draft within the stove, and ii) the proximity of the ignition zone to the fuel. These characteristics are usually used to describe a combustion appliance.

Improved cookstoves can be generally classified into six main types, i) Rocket/side-fed cookstove, ii) Gasifier cookstove, iii) Charcoal cookstoves, iv) Forced-draft/fan cookstove, v) Batch operated cookstoves, and vi) Continuously fed cookstoves [65].

- Rocket or side-fed cookstove

The fuel of a Rocket improved cookstove (typically uses biomass like wood and other plant material) is continuously fed through the side of the stove, and rests on top of a grate where the combustion occurs. The ash and inert matter fall through the grate towards the bottom of the stove, while the air is supplied to the combustion zone through the same inlets as where the fuel is fed. The Rocket type stove can be operated on a natural or forced draft principal dependant on the requirements. Typical examples of this type of stove includes the *Envirofit G-3300* and the *Grameen Greenway Smart stove* [65].

- Gasifier cookstove

These cookstoves operate on the gasification principal where a specific two-phase system is utilised. In the first section (gas generation), the gasification of carbonaceous fuel occurs by means of pyrolysis, and combustible volatiles and vapours are directed towards the combustion zone. In the second zone (gas burner), the pyrolysis vapour is ignited and combusted to produce energy [65]. Combustion efficiencies and emission levels differ between each improved stove,

however it is evident that gasification based cookstoves exhibit improved combustion performance and lower emission levels when compared to other stove types [66]. Typical examples of these stoves include the *Mimi Moto, Awamu Troika,* and the *Philips ACE 1* [65].

- Charcoal cookstoves

The charcoal stoves utilise charred biomass (charcoal) as fuel and is typically batch operated. The fuel is mainly carbonised/pyrolysed to remove most of the volatile matter and increase the energy per mass unit of the fuel (increased calorific value). Some examples of the charcoal cookstove include the *Burn Jikokoa, Kenyan Ceramic Jiko,* and the *Envirofit CH-2200* [65].

- Forced draft/fan cookstove

Cookstoves are usually operated on a natural draft principal, however forced draft or fan cookstoves utilise an electric component (fan or blower) to increase the air inlet to the combustion zone, which enhances turbulence within the stove and consequently promotes cleaner combustion and reduced emissions [65]. However, it has been reported in literature that the forced draft cookstoves exhibit higher levels of harmful pollutants when compared to natural draft cookstoves [66]. The is due to the increased airflow through the forced draft stove, which decreases the combustion flame length and consequently reduces the residence time of the volatile organic compounds in the combustion zone. Therefore, an increase in emission levels is observed [66]. Examples of a forced draft cookstove include the *Philips Model No. HD4012 LS*, *BioLite HomeStove* and the *Quad TLUD*.

- Other cookstoves

In addition to the aforementioned types of stoves, batch- and continuous operated improved cookstoves are also among common classifications. Batch operated stoves require a single fuel loading phase prior to operation, which can last for the remainder of the cooking period depending on the amount of fuel loaded. Continuous cookstoves require a constant addition of fuel into the combustion zone to ensure prolonged operation. In addition, several other classifications of improved cookstoves exist, for example the liquid fuel stove, gas stove, electric stove, and solar stove [65], which are rarely used in poverty engulfed rural communities.

2.3.4 Formation of emissions in coal stoves

One key characteristic of South African coals and coal fines are the high levels of inherent inorganic mineral content, when compared to coals mined in the northern hemisphere [42], [67]. Furthermore, South African coal generally has lower inherent sulphur and halogen levels compared with northern hemisphere coal [67]. The presence of sulphur in South African coals have been identified as a primary source of sulphur dioxide, hydrogen sulphide, and sulphuric acid pollutants, which poses significant environmental and human health hazards [42]. The sulphur in coal is present in three main forms; sulphide and sulphate (also collectively referred to as inorganic sulphur), and organic sulphur [42]. Inorganic sulphur is typically present as pyrite, siderite and marcasite minerals which form in the coal deposits along fractures and cleats, while the organic sulphur forms because of sulphur capture in the organic matrix when peat is formed [42]. A recent study described the SO_2 emissions data obtained from the combustion of coal agglomerates. In this study, two distinctive peaks of SO_2 were observed during combustion. This was reported to be due to both organic and inorganic sulphur being present in the coal [68]. The organic sulphur is less stable than the inorganic sulphur, which results in an initial peak in SO_2 emission during the devolatilization of the coal agglomerates [56]. This was observed for temperatures lower than 300 °C [56]. Similar mechanisms for organic and inorganic nitrogen exists. During combustion, atmospheric air is typically used as O_2 source for the combustion reaction. Atmospheric nitrogen (N_2) is therefore also present during combustion and can be converted to NO at elevated temperatures (above 1300 °C) [41], which is commonly referred to as “thermal NO_x”. Further, organically bound nitrogen compounds in the fuel are typically oxidised to NO during combustion (at temperatures between 300 °C and 800 °C) [41], which is the most common source of NO emission in household combustion appliances. Similarly, the organically bound sulphur is oxidised to form SO_2 [41]. In an abundance of oxygen, NO can be converted to NO_2, while SO_2 can be converted to SO_3 [41]. Consequently, the collective term for all the nitrogen oxides is “NO_x”, and the collective term for all the sulphur oxides is “SO_x”.

2.3.5 Performance of stove-fuel combinations

Household emissions had been thoroughly researched in literature using numerous fuel sources. Various approaches to the reduction in these emissions have been attempted, which include optimisation of combustion appliances, switching to alternative fuels, and providing improved methods of ignition.

An investigation regarding the particulate matter and carbon emissions from coal and biomass combustion was conducted using typical Chinese household stoves [69]. The implementation of a carbon mass balance method was mainly utilised to obtain particulate matter and elemental carbon emission factors [69]. In the study, it was concluded that for coal combustion, that particulate matter emission factors were primarily affected by the coal volatile matter content, whereas the elemental carbon emission factors were significantly influenced by the coal ash yield, volatile matter, and the calorific value [69]. Similar research was done to determine the organic and black carbon emission factors of household combustion [70]. Bituminous and anthracitic coals and coal agglomerates having different compositions were combusted in three different household combustion appliances to evaluate the respective carbon emission factors [70]. It was observed that the coal maturity (organic content) was the most influential factor in combustion performance and overall stove thermal efficiency [70]. Furthermore, the average-volatile bituminous coal was found to be the largest black carbon and organic carbon emissions contributor [70]. Finally, it was also reported that the agglomerated coal had a substantial improved emissions performance when compared to the lump coal [70]. This improvement was attributed to the use of a binding agent. As the agglomerates combust, the binder increased the likelihood for combustion of volatile matter and acted as a catalyst in the cracking process of heavy tars to combustible gases. This accelerated the combustion zone propagation from the gas phase to the solid phase which resulted in lower emission factors [71].

A recent emissions measurement campaign was conducted by Islam et. al. ([72] as part of the multiyear cookstove intervention trial, which took place in two rural locations in India. In total, 253 uncontrolled cookstove tests was performed during a 3-month measurement period, to estimate the household emissions that were emitted during typical household activities [72]. A vast variety of cookstoves were tested, which included traditional solid fuel stoves as well as modern LPG cookstoves. In this study, it was found that the LPG cookstoves produced the least number of indoor pollutants, while the traditional cookstoves showed that the largest variability in emission factors [72]. It was also found that the measurement period, fuel properties, relative humidity, and cooking duration were the main factors that influenced the variability of cookstove emission factors [72]. The study was concluded by pointing out that “real life” emission factor data was

much higher than laboratory experiments due to non-ideal combustion performance, and the influence of other combustion sources [72].

Sumbane *et al.* [38] investigated the performance and emission reductions of a low smoke fuel combusted in a conventional household coal stove. The fuel size was also investigated in the study with specific consideration given to ignition time and combustion efficiency [38]. The performance of low smoke fuels was compared to lump coal with a CV of approximately 20 MJ/kg [38]. It was concluded that low smoke fuels showed reduction in particulate matter emissions with sacrifice to heat retention and combustion efficiency [38]. Furthermore, small fuel particles provided a higher combustion efficiency and showed reduction in emissions compared to larger particles, with ignition time being higher for larger particles [38]. Finally, it was stated that the economics of substituting coal with any other fuel source should be thoroughly considered before any program is implemented [38].In Table 2-4, a brief summary of emission factors found in literature, is given. The data presented is illustrative of various combustion appliances, which predominantly use lump coal as fuel.

Table 2-4: Summary of literature cited for lump coal emission factors.

Reporting basis	Fuel	Combustion appliance	Average emission factors	Reference
Mass	Bituminous coal	Typical Chinese household stove	EF_{PM} = 3.17 ± 4.67 g/kg EF_{EC} = 0.23 ± 0.36 g/kg	[69]
	Three bituminous coals (varying maturity)	Three different coal stoves	EF_{BC} = 3.05 g/kg EF_{OC} = 5.05 g/kg	[70]
	Nine bituminous coals (varying maturity)	Coal stove	EF_{PM} = 16.77 g/kg EF_{BC} = 3.32 g/kg EF_{OC} = 8.29 g/kg	[73]
	Bituminous coal	Dover King™ coal stove	EF_{PM} = 12.33 ± 3.44 g/kg	[38]
	Low Smoke Fuel	Dover King™ coal stove	EF_{PM} = 2.37 ± 0.32 g/kg	[38]
Energy	Bituminous coal	TJ4.0 improved coal stove	EF_{PM} = 0.11 ± 0.03 mg/MJ EF_{CO} = 0.7 ± 0.3 g/MJ	[40]
	Bituminous coal	Typical Chinese updraft coal stove	EF_{PM} = 4.2 ± 1.41 mg/MJ EF_{CO} = 11.9 ± 4.53 g/MJ	[40]

***Where EF_{PM} is the particulate matter emission factor, EF_{EC} is the elemental carbon emission factor, EF_{BC} is the black carbon emission factor, EF_{OC} is the organic carbon emission factor and EF_{CO} is the carbon monoxide emission factor.**

Coal briquetting is an alternative fuel source to lump coal since it can be integrated with sustainable biomass fuels. The use of coal agglomerates is also advantageous since it can be used in combination with improved combustion stoves to reduce air pollution and health impacts and is recommended by the Chinese government [74]. In Table 2-5, a summary of data regarding the emissions performance of coal agglomerates in various cookstoves are given. It is noticeable that no combustion performance data is available for tumble-growth coal pellets, as the focus in literature is mostly on coal briquettes and biomass pellets.

Table 2-5: Summary of literature cited coal agglomerate emission factors.

Reporting basis	Fuel	Combustion appliance	Emission factors	Reference
Mass	Honeycomb coal briquettes	Three different coal stoves	EF_{BC} = 0.051 g/kg EF_{OC} = 2.49 g/kg	[70]
Energy	Semi-coked coal briquettes	TJ4.0 improved coal stove	EF_{PM} = 0.03 ± 0.04 mg/MJ EF_{CO} = 0.8 ± 0.4 g/MJ	[40]
	Semi-coked coal briquettes	Typical Chinese updraft coal stove	EF_{PM} = 7.2 ± 1.80 mg/MJ EF_{CO} = 5.7 ± 1.00 g/MJ	[40]

Where EF_{PM} is the particulate matter emission factor, EF_{EC} is the elemental carbon emission factor, EF_{BC} is the black carbon emission factor, EF_{OC} is the organic carbon emission factor and EF_{CO} is the carbon monoxide emission factor.

The literature cited results displayed in Table 2-4 and Table 2-5 can be compared to determine how the performance of stove-fuel combinations can improve when households switch from lump coal to coal agglomerates. It can be seen from these tables that the emission factors for agglomerated fuel are significantly lower than for lump coal. The use of honeycomb coal briquettes reduced both organic and black carbon emissions, while the use of semi-coked coal briquettes resulted in reduced PM and CO emissions in some cases. However, from the results in Table 2-4 and Table 2-5 it can be seen that in the case of a typical Chinese updraft coal stove, the PM emission factors increased as the fuel was switched from lump coal to coal agglomerates. Furthermore, from the results reported for the TJ4.0 improved coal stove it can be seen that the change from lump coal to coal agglomerates had little influence on CO emissions. Both these observations highlight the importance of testing various stove-fuel combinations, to achieve optimal emissions reduction. The results presented in Table 2-4 and Table 2-5 will also be used as a literature baseline for experimental findings in this study.

2.3.6 Recent developments: Improved coal stoves

Several attempts to develop alternative coal combustion appliances for the South African rural communities were investigated in the past century. A bottom-lit downdraft (BLDD) clean burning coal stove was developed at the University of Johannesburg [75]. This stove is developed as a multi-purpose combustion appliance that provides increased thermal performance with lower overall emissions compared to current domestic appliances [75]. The stove was optimised using a combination of computational fluid dynamics and combustion experiments where coarse bituminous coal was burned. It is reported that the coal stove can produce approximately 4 kW of energy and can reach temperatures of 900 °C in the combustion zone [75]. From combustion experiments, an overall CO/CO_2 ratio of 5.3% was reported, compared to paraffin appliances (CO/CO_2 ratio of 2%), and an improved brazier stove (CO/CO_2 ratio of 30%) [75].

Like the coal stove developed at the University of Johannesburg, Altanzul ([40]) investigated the structural optimisation and emissions performance improvement of a household coal stove. The improved cross-draft coal stove (called TJ4.0) was experimentally used to combust both lump coal as well as coal agglomerates [40]. The design of the TJ4.0 improved coal stove is nearly identical to the semi-continuous coal stove used in this study. The thermal and emissions performance of the stove was studied and compared to the performance of typical Chinese up-draft coal stoves. The operation and measurement of the TJ4.0 coal stove performance is similar to the setup described by Sumbane ([21]). In addition to investigating the stove's performance using both coal and semi-coked coal briquettes, the size range of the fuel was also varied to determine the impact of the fuel size on combustion [40]. It was found that the combustion emissions formed, were significantly lower for the TJ4.0 coal stove when compared with typical Chinese coal stoves [40]. The TJ4.0 stove emitted on average 95% less particulate matter and carbon monoxide emissions than for domestic coal stoves, which was attributed to the natural draft direction in the stove [40]. The use of coal briquettes resulted in further particulate matter emission reductions (approximately 99.5% less than for domestic coal stoves) and resulted in a higher thermal efficiency than for lump coal [40]. The stove achieved a maximum thermal efficiency of 90.7% and a maximum fire power of 7.0 kW [40]. Finally, a minimum CO/CO_2 ratio for the TJ4.0 was determined as 1.90% ± 0.9% (lump coal) and a maximum of 2.89% ± 1.6% (semi-coked briquettes) in the fuel size range of -25 mm +16 mm [40].

CHAPTER 3 – FUEL PREPARATION AND CHARACTERISATION

Fuel characterisation is performed since the combined properties of a fuel directly influence its behaviour during production, transport, handling, and combustion. Understanding these properties enables a comprehensive evaluation of the fuel's combustion performance in the semi-continuous coal stove. In this chapter, various chemical and mechanical properties of the fuel are investigated and reported. The chapter begins with an overview of the fuel's origin and preparation (Section 3.1), including the naming convention for the respective fuel batches. Subsequently, the experimental details are discussed in Section 3.2, with a summary of the different characterisation experiments and the respective methods provided. The bulk of this chapter focuses on the characterisation results and discussion presented in Section 3.3, with reference to the fuel composition, particle properties, mechanical strength, and water resistance of the various batches. The chapter is concluded in Section 3.4 with a summary of the main findings.

3.1 MATERIAL ORIGIN AND PREPARATION

For this study, six fuel batches were prepared and procured from an external vendor, *CoalTech™.* These batches consisted of five coal pellet batches with different properties, and one lump coal batch as a baseline. The test work leading to the selection of these batches is given in ANNEXURE A. The identification of the six fuel batches and the differentiating properties are indicated in Table 3-1.

Table 3-1: Fuel identification and description.

Batch	Batch Key	Description
1	**C**	Standard lump coal, D grade.
2	**P-B**	Pellets, binderless, no waterproofing.
3	**P-5-W**	Pellets, 5% PVA binder, with waterproofing.
4	**P-5**	Pellets, 5% PVA binder, no waterproofing.
5	**P-2.5-W**	Pellets, 2.5% PVA binder, with waterproofing.
6	**P-2.5**	Pellets, 2.5% PVA binder, no waterproofing.

The pellet batches were obtained from *CoalTech™* and manufactured according to the tumble-growth agglomeration process as given and discussed in Section 2.2. In Figure 3-1 the production of these pellet batches in their respective process units is illustrated. The PVA binder in Table 3-1 was selected as the main binding agent after preliminary testing (ANNEXURE A). The binderless

pellets were produced by adding excess amounts of water to the drum pelletiser, which acted as a substitute for a binding agent in the agglomeration process. It is for this reason that these pellets are also referred to as water binder pellets. For experimental reliability purposes, all the above indicated pellet batches were made from one coal fines stock, whereas the lump coal was sourced from a local mine (representative of household used coal). It was ensured that the production process was identical for all fuel batches, excluding binder quantity and the addition of waterproofing. The ideal size range criteria for the pellets used in the semi-continuous coal stove is indicated as -19 mm +6.7 mm based on the dimensions of the stove internals. The lower limit of this size range is based on the grate aperture size whereas the upper limit is based on the cookstove combustion chamber width to fuel diameter ratio. All the coal pellet batches were manufactured according to this size criteria. The agglomeration process that was used for these pellets differ slightly from the general production method since sun-baking was the final step in the agglomeration process instead of oven baking as per norm. This method increases financial feasibility by reducing the production cost.

Figure 3-1: Production process of coal pellets, including drum pelletiser (left), conveyor system (middle), and rotary dryer (right) (provided by *CoalTech™).*

Throughout this study, the six batch keys as given in Table 3-1 will be used when referring to the different individual fuel sets or experimental runs. The fuel batches are distinguished by five

independent variables to investigate which properties would result in ideal implementation and combustion performance. These variables are:

- Fuel type (pellets vs lump coal)
- Waterproofing (with or without)
- Binder type (PVA or water)
- Binder quantity (2.5 wt.% or 5.0 wt.%)
- Fuel PSD (-19 mm +13.2 mm; -19 mm +9.5 mm; -13.2 mm +6.7 mm)

For the characterization experiments described in this section, the only material required in addition to the fuel was standard cooking oil, which was obtained from *Builders Express*. During the particle density characterization where water submersion was used, the pellets (specifically P-B and P-2.5) disintegrated. To avoid this, standard cooking oil was used as a substitute. The cooking oil prevented fluid from entering the pellet pores during submersion, thereby maintaining the integrity of the pellets and preventing them from crumbling and disintegrating.

3.2 CHARACTERISATION PROCEDURES

The main performance influencing characteristics of agglomerates is clearly stated in literature as composition, particle properties (size, density, mechanical strength, etc.), and water resistance [55]. A summary of the characterisation experiments and the respective methods are given in Table 3-2. International standards were prioritised, where possible, whereas literature methods were used for less common characterisation methods. All the composition analyses were done by and external vendor, *Bureau Veritas Testing and Inspections South Africa.*

Table 3-2: Characterisation experiments and methods.

Characteristic	Experiment	Method
Composition	Sample Preparation	• ISO 13909-4: 2001
	Moisture	• ISO11722: 1999
	Ash Yield	• ISO 1171: 2010
	Volatile Matter	• ISO 562: 2010
	Total Sulphur	• ISO 19579: 2006
	Ultimate Analyses	• ISO 12902 - CHN Instrumental method
	Ash Fusion Temperature	• ISO 540:2008
Particle Properties	Particle Size Distribution (PSD)	• Based on ISO 728:2021 with adapted method as proposed by Sumbane [21].
	Material Density	• Based on method proposed by Dan-Asabe et al. [76].
	Circularity	• Based on ISO 9276-6 with specific method proposed by Meyer [77].
	Friability	• Based on method proposed by Temmerman et al. [78].
Mechanical Strength	Drop Shatter	• ASTM-D440-86-1994
	Shatter Index	• ISO 616:2021
	Compressive Strength	• Based on JP JIS Z 8841-1993 with adapted method as proposed by England [51].
Water resistance	Water Resistance	• Based on method proposed by Leokaoke et al. [79] and Mangena et al. [80]
	Water submersion	• Based on method proposed by Leokaoke et al. [79] and Mangena et al. [80]
	Water Retention	• Based on method proposed by Botha [81] and Modiri [82].
	Wet Strength	• Based on JP JIS Z 8841-1993 with adapted method as proposed by England [51] and Leokaoke et al. [79].

The characterisation methods displayed in Table 3-2 were selected not only for performance evaluation but also to assess the feasibility of large-scale implementation. Fuel used in rural environments must withstand handling, transport, and long-term environmental exposure. The following characteristics are intended for this assessment:

- Drop Shatter Characterization: Indicates the brittleness of the fuel during production, transport, storage, and loading.

- Compressive Strength Characterization: Assesses feasibility concerning handling, such as fuel stacking during transport and storage.

- Friability: Represents the integrity of the fuel. Higher friability decreases implementation feasibility due to increased material losses.

- Water Resistance: Evaluates the performance of coal pellets in wet conditions, crucial for real-life applications in rural areas where environmental moisture (e.g., rain) is prevalent.

3.3 RESULTS AND DISCUSSION

3.3.1 Composition

To investigate the composition of the different fuel batches, several analyses were conducted. The results of the various analyses are displayed in Table 3-3. According to the general coal classification (whereby South African coals are classified from A – D grade based on its composition and calorific value [83], [84]) it can be seen that all six fuel batched falls within the classification of D grade coal. This was intentionally chosen to be representative of the fuel that is currently being used in rural areas in South Africa [1], [3]. From the proximate analyses results in Table 3-3, it can be seen that the moisture content of the coal pellets batches is roughly 50% higher when compared to that of the lump coal. This is mainly due to the agglomeration process, where water is added to the tumble-growth process. When the pellets are oven dried during the agglomeration process, the moisture content is significant lower when compared to the sun-dried pellets. This explains the relatively high moisture content of the pellets seen in Table 3-3.

Table 3-3: Composition analyses results.

		Fuel identification					
	Analyses component *(air-dried basis)*	**C**	**P-5**	**P-5-W**	**P-2.5**	**P-2.5-W**	**P-B**
Combustion composition	% Inherent moisture	4.0	6.0	5.9	6.0	5.5	5.8
	% Volatile matter	24.5	22.9	22.7	22.1	22.1	21.5
	% Ash yield	21.4	25.7	25.8	27.1	26.7	26.0
	% Fixed carbon (by difference)	50.1	45.4	45.6	44.8	45.7	46.7
Elemental composition	% Total carbon	60.6	53.1	53.6	52.4	53.0	53.6
	% Hydrogen	3.5	2.8	2.9	2.8	2.8	2.8
	% Nitrogen	1.4	1.3	1.4	1.3	1.4	1.4
	% Sulphur	0.5	0.7	0.7	0.8	0.8	0.8
	% Oxygen (by difference)	8.7	10.4	9.7	9.7	9.8	9.7
	Gross calorific value *(MJ/kg)*	23.6	20.3	20.4	19.8	20.2	20.5

The moisture content of the water binder pellets is also similar to the PVA binder pellets even though increased amounts of moisture is used during the agglomeration process to account for the lack of a binder. The volatile matter, ash yield and fixed carbon for the pellet batches are similar, indicating that the addition of a binding agent did not influence the composition of the fuel significantly. The volatile matter and the fixed carbon content of the lump coal was found to be higher than the coal pellets while the ash yield was lower. The lower ash yield and increased fixed carbon content of the lump coal is also reflected in the calorific value. Consequently, the gross heating value was the highest for the lump coal while relatively constant between the different pellet batches. The similar calorific value between the pellet batches also indicates that the addition of a PVA binder, the quantity thereof, or the addition of a waterproofing agent did not significantly influence the pellet energy content or overall chemical characteristics. Similarly, the elemental composition as obtained from the ultimate analyses also indicated that the chemical characteristics of the fuel remained similar for all the pellets batches.

The ash fusion temperature characterisation was also requested and done by an external vendor since clinkering was observed during initial test work. The results are displayed in Table 3-4.

Table 3-4: Ash fusion test results.

		Fuel identification					
	Analyses Component	**C**	**P-5**	**P-5-W**	**P-2.5**	**P-2.5-W**	**P-B**
AFT (Reducing)	Initial deformation temperature (°C)	>1550	1340	1332	1326	1326	1340
	Softening temperature (°C)	>1550	1352	1343	1334	1328	1354
	Hemispherical temperature (°C)	>1550	1360	1360	1348	1338	1368
	Fluid temperature (°C)	>1550	1420	1406	1384	1376	1398
AFT (Oxidising)	Initial deformation temperature (°C)	>1550	1336	1340	1321	1324	1341
	Softening temperature (°C)	>1550	1346	1346	1328	1332	1352
	Hemispherical temperature (°C)	>1550	1355	1364	1332	1345	1365
	Fluid temperature (°C)	>1550	1410	1419	1374	1378	1409

In Table 3-4 the temperatures for a reducing and oxidising environment can be seen. In both the oxidising and reducing environments, the ash fusion temperatures for the coal pellets was found to be approximately 1350 °C while the lump coal is above measurement range greater than 1550 °C. Similar ash fusion temperatures were reported in literature for South African Highveld coal and coal fines [85]. The relatively lower ash fusion temperature of the coal pellets might be due to increased pyrite content of in the coal fines, which is also reflected in the total sulphur content results displayed in Table 3-3. Finally, it can also be seen that the addition of PVA binder, the quantity therefor or the addition of a waterproofing agent did not significantly influence the ash fusion temperature of the coal pellets. Therefore, it can be assumed that no fluxing compound is present in the PVA binder or the waterproofing agent.

3.3.2 Particle properties

The results shown in Figure 3-2 illustrate the cumulative passing particle size distribution of the coal pellets as received from the manufacturer. These PSD graphs were created by screening the coal pellets into size ranges from 26.5 mm to 4.75 mm.

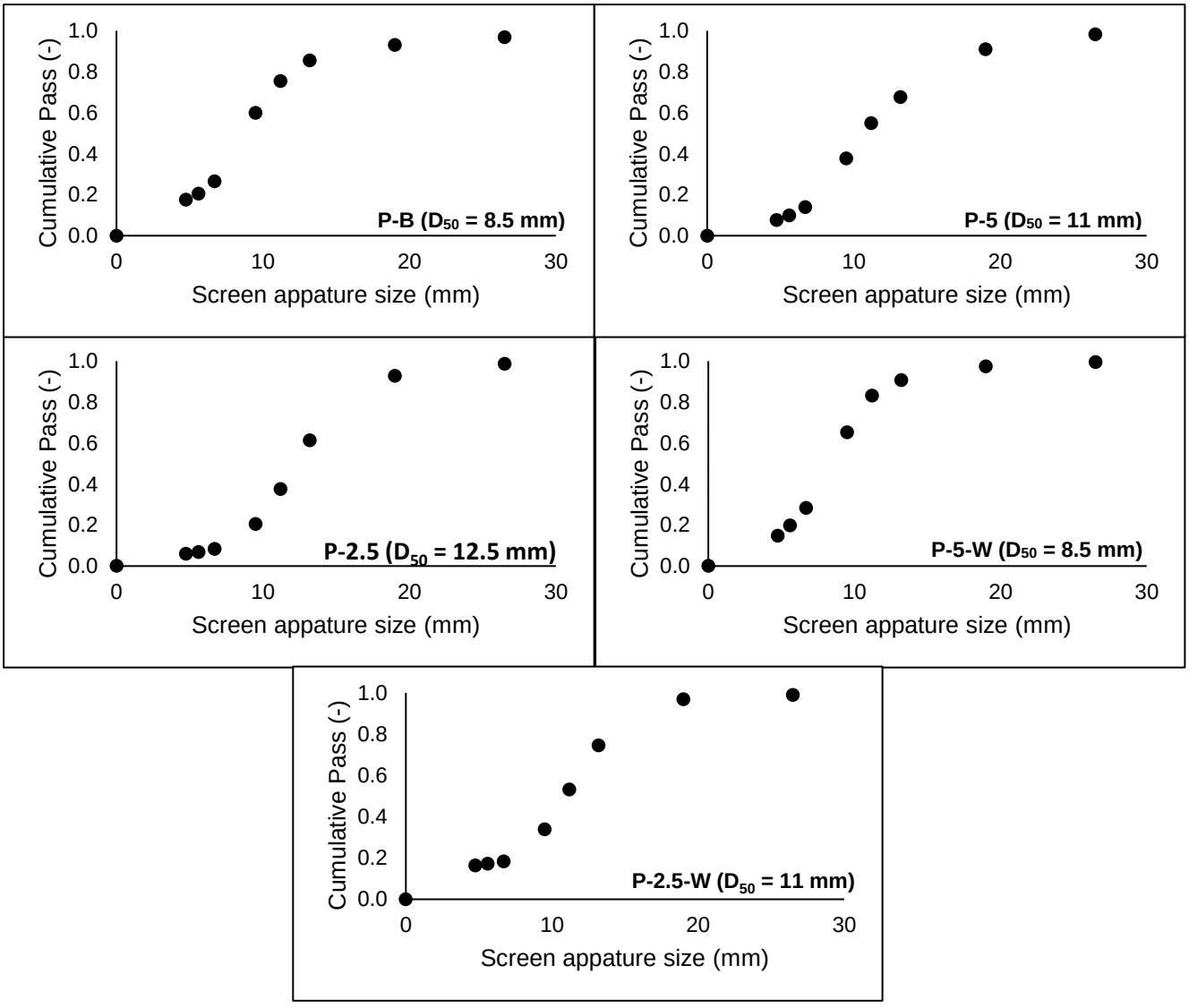

Figure 3-2: Particle size distribution of coal pellet batches.

The D_{50} of each batch, ranging between 8.5 mm and 12.5 mm, is shown in Figure 3-2. This correlates with the ideal size range criteria of the fuel as stated in Section 3.1. When considering the ideal size range (-19 mm +6.7 mm), the P-2.5 pellets in Figure 3-2 exhibited an ideal PSD. The P-B as well as the P-5-W pellet batches had the smallest D_{50} values of below 9 mm. While screening the binderless pellets, it was observed that a significant quantity of fines was present

in the transport containers which suggests that these pellets had a high friability and led to significant material loss. Conversely, the low D_{50} of the P-5-W pellets was not due to fines and was rectified with screening techniques.

Table 3-5: Comparison of pellet properties (-19mm +13.2mm).

		C	**P-B**	**P-5-W**	**P-5**	**P-2.5-W**	**P-2.5**
Material density	*(g/ml)*	1.6 ± 0.3	1.5 ± 0.2	1.5 ± 0.1	1.4 ± 0.1	1.4 ± 0.1	1.4 ± 0.2
Circularity	*(-)*	0.75 ± 0.03	0.85 ± 0.01	0.87 ± 0.01	0.87 ± 0.01	0.88 ± 0.01	0.88 ± 0.01

The properties of the fuel are given in Table 3-5. The following conclusions could be made regarding the material density:

- No significant difference was noted in the material density between the fuel batches and the addition of pellet binder or waterproofing did not influence the density of the pellets.
- The greater variance in the lump coal density could likely be attributed to the different inherent organic and inorganic materials within the particles.
- The pellet density's lower variance could be traced back to the use of homogeneous coal fines in its manufacture.

Considering the fuel circularity, the lump coal exhibited a lower circularity when compared to the coal pellets. A lower circularity generally indicates an increased packing density when considering a single size range [77]. The similar circularity between the coal pellet batches suggest that a similar bulk packing can be expected within the geometry of a cookstove. The relatively high circularity and sphericity of the pellets was due to the tumble growth agglomeration process that was used to produce it.

3.3.3 Mechanical strength properties

To determine if the coal agglomerates will be able to meet the necessary standard, the strength characterisation was performed through a drop shatter test and compressive strength test. The results are displayed in Table 3-6 and Table 3-7 respectively.

Table 3-6: Strength properties measured by a drop shatter test.

Drop Shatter						
	C	**P-B**	**P-5-W**	**P-5**	**P-2.5-W**	**P-2.5**
Drops before breakage	4 ± 2	0 ± 1	15 ± 3	11 ± 2	1 ± 1	2 ± 1
Shatter Index						
	C	**P-B**	**P-5-W**	**P-5**	**P-2.5-W**	**P-2.5**
+ 6.7 mm	0.95	0.52	0.93	0.92	0.88	0.85
- 6.7 mm + 4.75 mm	0.02	0.09	0.01	0.01	0.03	0.04
- 4.75 mm + 2.8 mm	0.01	0.10	0.02	0.02	0.02	0.03
- 2.8 mm + 2 mm	0.01	0.08	0.01	0.02	0.02	0.02
- 2 mm + 1.18 mm	0.01	0.09	0.01	0.02	0.02	0.02
- 1.18 mm	0.01	0.12	0.02	0.02	0.03	0.04

The average drop before breakage as well as the shatter index is given in Table 3-6. The results are displayed for a total of 10 tests, where the fuel particles were dropped continuously until the breakpoint was reached, as per method in Table 3-2. In this study, the breakpoint is defined as the drop at which disintegration or failure occurs, in accordance with ASTM-D440-86-1994 and ISO 616:2021 standards. This breakpoint is characterised by the separation (shattering) of one or more pieces from the original particle. The shatter index subsequently determines the size distribution of the material after the breakpoint, represented as the percentage of the material retained on a sieve with a specified aperture size. It can be seen that the binderless pellets failed on average upon the first drop and shattered in a wide range of sizes. Furthermore, it can be seen that the 2.5% PVA binder pellets failed within the first four drops. The 5% PVA pellets failed only after more than ten drops. The shatter index of the 5% PVA pellets indicated that more than 90% of the pellet remained coherent after shattering, which compares to the shatter results of lump coal. In contrast to the high number of drops for the 5% PVA binder pellets, the lump coal only remained coherent for approximately four drops before shattering. This might be attributed to the irregular shape of lump coal. Since lump coal has an average circularity of 0.75, it is likely that

the elongated areas of the lump coal resulted in early shattering, while the majority of the particle remains intact. This is supported by the shatter index that revealed approximately 95% of the lump coal particles remained intact upon shattering, and small fragments (±1%) were found in each of the smaller shatter size ranges. Supporting information regarding this observation and the relative low number of drops could not be retrieved from literature. Finally, from Table 3-6 it can also be seen that no significant correlation can be made between the addition of waterproofing agent, and the structural integrity of the coal pellets. The compressive strength test results of the different fuel particles can be seen in Table 3-7.

Table 3-7: Dry particle compressive strength characterisation.

Compressive strength *(MPa)*					
C	**P-B**	**P-2.5**	**P-5**	**P-2.5-W**	**P-5-W**
22.3 ± 5.7	2.7 ± 0.2	11 ± 0.6	21.6 ± 0.7	8.6 ± 0.5	19.7 ± 2

In Table 3-7, it is found that the lump coal particles and 5% PVA particles have similar compressive strength characteristics. This is followed by the 2.5% PVA pellets that required significantly less pressure to fragment the particles. The binderless pellets required the least pressure for structural failure, which can be attributed to the absence of a binding agent. Again, it can be seen that the addition of a waterproofing agent did not influence the integrity and compressive strength of the pellets, as no significant correlation can be made between the pellets with and without a waterproofing agent. Finally, all the pellet batches exceeded the minimum compressive strength required for coal agglomerates (0.35 – 0.38 MPa) as stated in literature [86]. Therefore, from a mechanical strength and integrity point of view, all the pellet batches are fit for large scale implementation. In Table 3-8 a summary of the particle friability results is shown for each fuel batch. The material fraction lost indicated in this table corresponds to material smaller than 6.7 mm, which aligns with the stove grate aperture size.

Table 3-8: Particle friability results.

		C	**P-B**	**P-5-W**	**P-5**	**P-2.5-W**	**P-2.5**
Friability	*(% lost)*	0.2 ± 0.1	20 ± 8	0.2 ± 0.1	0.2 ± 0.08	1.0 ± 0.2	0.8 ± 0.3

The binderless pellets showed the highest material loss during the test, primarily due to the lack of a binding agent. This finding corresponds to the lower D_{50} as discussed previously. Furthermore, the increased quantity of the PVA binder added to the pellets improved the integrity of the fuel which resulted in lower material loss for the 5 wt.% PVA pellets when compared to the 2.5 wt.% PVA pellets. The higher material loss that would be expected from using pellets instead of lump coal can be minimised by adding a sufficient amount of PVA binder. This is shown in Table 3-8 that the friability of the 5 wt.% PVA pellets was the closest to the lump coal. Any increase in PVA binder beyond 5 wt.% to minimise handling losses might not be feasible since the effect of particle integrity gain would be minimal. Finally, it was also found that the addition of a waterproofing agent did not significantly influence the friability of the fuel.

3.3.4 Water resistance

In the Table 3-9, the results of a water submersion test are displayed. These results show the effectiveness of the coal pellets' binder and waterproofing agent in wet conditions.

Table 3-9: Water resistance test results.

	Time after water submersion						
Fuel ***(- 19mm + 13.2mm)***	0 *(sec)*	5 *(sec)*	10 *(sec)*	15 *(sec)*	20 *(sec)*	30 *(sec)*	60 *(sec)*
P-B	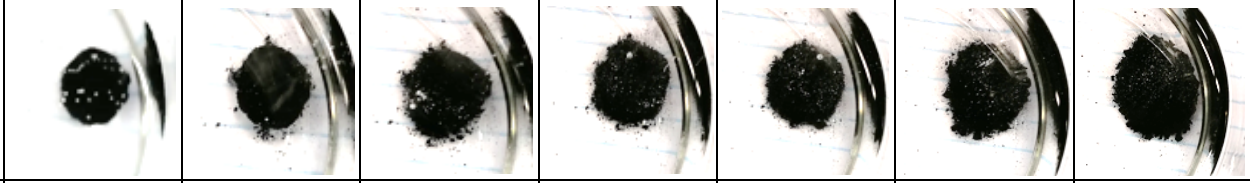						
P-2.5	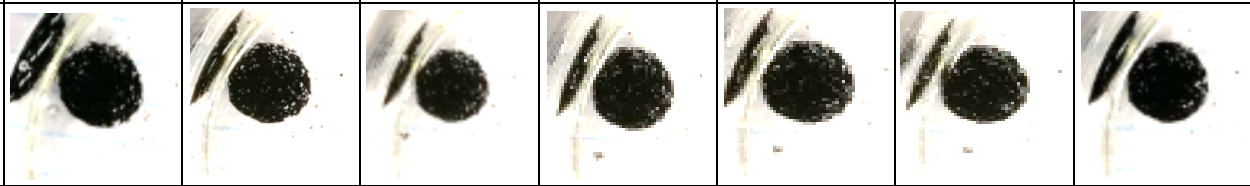						
P-5	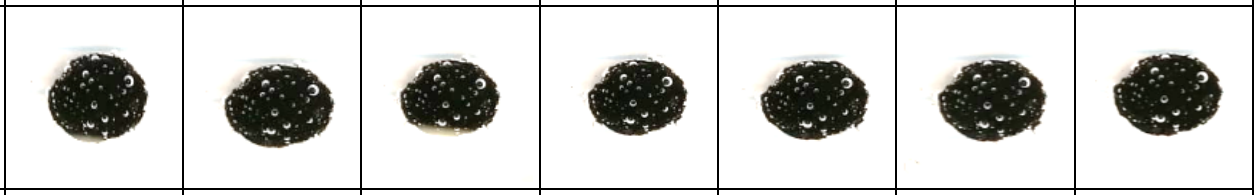						
P-2.5-W	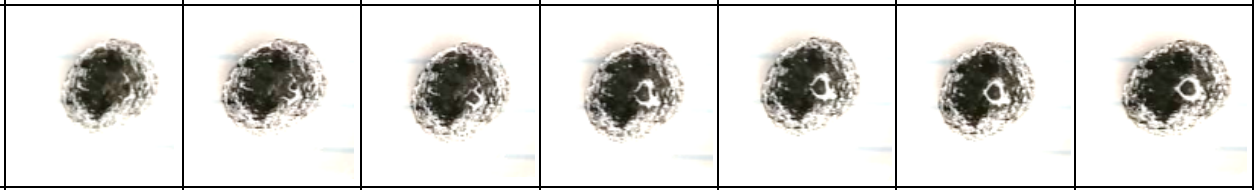						
P-5-W							

Observations were made and recorded after submerging the pellets in water for a total of 24 hours. The pellet conditions for the time intervals of 0 sec – 60 sec are given in Table 3-9 while the crumble and disintegration points are given in Table 3-10. Crumbling of the binderless pellets could be observed after 5 seconds, and complete disintegration after 60 seconds. All the other pellet batches remained coherent for the remainder of the 60 seconds after submersion. From the images in the table, the influence of binder quantity as well as the waterproofing agent is

clearly visible. The effect of the waterproofing layer can be seen for pellet batches P-2.5-W & P-5-W as it creates a sealing layer on the outer surface of the coal pellet preventing water from entering the porous structure of the agglomerate. For the P-5 pellets, small bubbles on the outer surface of the pellet can be seen which might be attributed to the hydrophilic nature of the binder. It is well documented in literature that PVA binder has film-forming properties that makes it suitable for water resistance applications [81], [87]. The molecular structure of the binder prevents water permeation into the pores and inherently waterproofs the agglomerate. This means that even if the outer water proofing layer is damaged or pellet fracture occurs, disintegration would not take place when the fragments come in contact with water. However, this is not the case with the P-2.5 and P-B pellets. As can be seen in Table 3-9, the air pockets did not form on the outer surface of the pellets indicating water permeation. This led to the results in Table 3-10 where the crumble and disintegration instances are displayed.

Table 3-10: Water submersion observation summary.

	C	**P-B**	**P-2.5**	**P-5**	**P-2.5-W**	**P-5-W**
Crumble point	> 24 hr	5 sec	3.5 min	> 24 hr	> 24 hr	> 24 hr
Disintegration point	> 24 hr	60 sec	9 min	> 24 hr	> 24 hr	> 24 hr

The P-2.5 pellets crumbled after just 3 min of submersion and completely disintegrated after approximately 9 minutes of submersion. This is mainly due to the lack of PVA binder as it remained coherent longer than the binderless pellets but still disintegrated since not enough PVA binder was present to fully waterproof the fuel. Finally, all three other pellet batches, as well as the lump coal remained coherent for the remainder of the submersion experiment.

Table 3-11: Water retention and wet strength test results summary.

		C	**P-5**	**P-2.5-W**	**P-5-W**
Water retention	*(-)*	0.02 ± 0.01	0.07 ± 0.01	0.09 ± 0.01	0.04 ± 0.01
Wet strength	*(MPa)*	>20.0	4.0 ± 0.3	1.9 ± 0.2	4.1 ± 0.5

In Table 3-11 the water retention and wet strength quantification results are shown. The water retention, as a fraction of the particle mass, represents the quantity of water that permeated into the particle pores and remained entrained after an air-drying period of 1 hour. The P-B & P-2.5 pellet batches were not included in the test since these pellets did not remain intact after water submersion. The lump coal retained the least amount of water after submersion, followed by the P-5-W pellet batch. Therefore, the addition of a waterproofing agent and the quantity of PVA binder directly influences the amount of water retained by the fuel particles. It should also be noted that the pellets with only 5 wt.% PVA binder exhibited an improved retention performance when compared to the P-2.5-W pellet particles. Therefore, it can be argued that the addition of 2.5 wt.% binder provides a better waterproofing characteristic than the addition of a waterproofing agent. Similar observations can be made for the wet strength test results. The compressive strength of lump coal remained relatively unchanged compared with the dry compressive strength as presented in Table 3-7. The wet compressive strength of the P-5 & P-5-W particles was similar while the P-2.5-W particles required the least amount of pressure before structural failure was observed. This is in direct correlation with the water retention test results. It can also be seen that the P-5, P-2.5-W, and P-5-W still maintained a structural strength above the minimum strength required for coal agglomerates (0.35 – 0.38 MPa) as given in literature [86]. For practical purposes, another batch of P-5 pellets was sun dried instead of air dried after water submersion. This was done to test how the compressive strength would change based on drying conditions. It was found that a pressure of 6.9 ± 0.4 MPa is needed to compromise the structural integrity of these P-5 pellets.

3.4 CONCLUSION

Several mechanical and chemical properties were investigated and characterised in this chapter. It was confirmed that, based on the fuel composition, all six fuel batches fall within the classification of D-grade coal, representative of the fuel currently used in rural households. Furthermore, the results from the proximate analyses indicated that the addition of a PVA binder, the quantity thereof, or the addition of a waterproofing agent did not significantly influence the fuel composition or chemical characteristics. Similarly, the elemental composition remained constant across all pellet batches. It was found that the ash fusion temperatures for the coal pellets were significantly lower than those determined for lump coal.

Regarding the fuel particle properties, there was no significant difference in material density between the coal pellets. An identical bulk packing can be expected within the geometry of the stove, as a similar circularity was obtained for all coal pellet batches. The mechanical strength of the coal pellets increased proportionally with the amount of binder incorporated into the fuel. The binderless pellets exhibited the weakest mechanical strength and integrity, in contrast to the 5 wt.% PVA pellets, which showed similar mechanical properties to lump coal. In these result sets, the waterproofing agent also showed no influence on the mechanical characteristics. The friability results indicated that the binderless pellets showed the highest material loss during the test, primarily due to the lack of a binding agent. Furthermore, the integrity of the fuel increased with an increase in the binding agent. The addition of the waterproofing agent did not influence the friability characteristic of the fuel.

It was also found that the waterproofed pellets and 5 wt.% PVA pellets remained intact after being submerged in water for 24 hours. Here, the amount of binder and the addition of a waterproofing agent were critical to the structural integrity of the fuel after prolonged exposure to moisture. It is also recommended that the fuel be sun-dried after prolonged exposure to moisture, as this significantly increased the strength of the fuel compared to air drying alone. This can be further explored during large-scale implementation when fuel wetting might be a risk. Finally, when considering the logistics of field implementation of the coal agglomerates, the P-5 pellets are recommended. This fuel displayed similar characteristics to lump coal and did not require a waterproofing agent to remain intact after water submersion. The feasibility of the other pellet fuels is dependent on the specific application and implementation objectives.

CHAPTER 4 – MATERIALS AND METHODS

This chapter outlines the materials and methods employed during the experimental phase, as well as the data processing techniques utilised. Section 4.1 begins with a detailed description of the experimental procedure and setup, including the materials used. It provides an in-depth explanation of the semi-continuous coal stove and its operating principles, the instrumentation setup for data collection, and the standard operating procedures (SOPs) followed. The experimental schedule is also outlined and discussed within this context. Next, Sections 4.2 and 4.3 provides detailed summaries of the data processing methodologies applied to quantify the emissions and thermal performance parameters, which form the primary focus of the results and discussion. The chapter concludes with an evaluation of experimental repeatability in Section 4.4, where the results of five experiments conducted under similar operating conditions are compared and subjected to statistical analysis.

4.1 EXPERIMENTAL PROCEDURE AND SETUP

The experimental procedure and setup discussed in this section is similar to what was proposed by Sumbane et al. [38], Kuhn et al. [39] and Altanzul [40]. Some improvements have been made to allow for coal pellet combustion and to increase equipment reliability.

4.1.1 Materials

A summary of the experimental material can be seen in Table 4-1. In this table, the item category (function) is given as well as its source and specifications.

Table 4-1: Consumable materials used during experimental phase.

Item category	Consumable material	Source	Specifications
Fuel	Coal Pellets	*CoalTech™*	See Section 3.1.
	Lump Coal	*CoalTech™*	See Section 3.1.
	Wood Kindling	Builders Express	Pine wood (10mm x 15mm x 50mm).
	Paraffin	Builders Express	Kerosene >98 vol.% and naphthalene <1 vol.%.
Calibration gas	CO	African Oxygen Limited (AFROX)	3901 ppm CO with balance N_2.
	CO_2	African Oxygen Limited (AFROX)	21.10 vol.% CO_2 with balance N_2.
	SO_2	African Oxygen Limited (AFROX)	494 ppm SO_2 with balance N_2.
	NO	African Oxygen Limited (AFROX)	69.8 ppm NO with balance N_2.
	Air	African Oxygen Limited (AFROX)	21.8 vol.% O2 with balance Ar, CO_2, N_2, and H_2O <10 ppm.
	N_2	African Oxygen Limited (AFROX)	N_2 99.999 vol.%.
Equipment consumables	PM Thimbles	Envirocon Instrumentation	Silica fibre thimble.
	Sorbent Tubes	Envirocon Instrumentation	Activated charcoal.
	Filters	Envirocon Instrumentation	Filter element for Horiba PG 350s.
	Pre-filters	Envirocon Instrumentation	Moisture and particulates removal.
	Filter Kits	Envirocon Instrumentation	Internal filter kit for DustTrak II unit.
Cleaning chemicals	Ethanol	Glassworld & Chemical Suppliers	99.9 vol.% purity.
	Acetone	Glassworld & Chemical Suppliers	99.9 vol.% purity.
	Toluene	Glassworld & Chemical Suppliers	99.9 vol.% purity.

4.1.2 The semi-continuous coal stove

As discussed in Section 3.1, for experimentation in this study, both lump coal and coal pellets were used as fuel source. The primary combustion appliance used in combination with the six fuel batches, is the semi-continuous coal stove. The improved stove and relevant internal and external components are displayed in Figure 4-1.

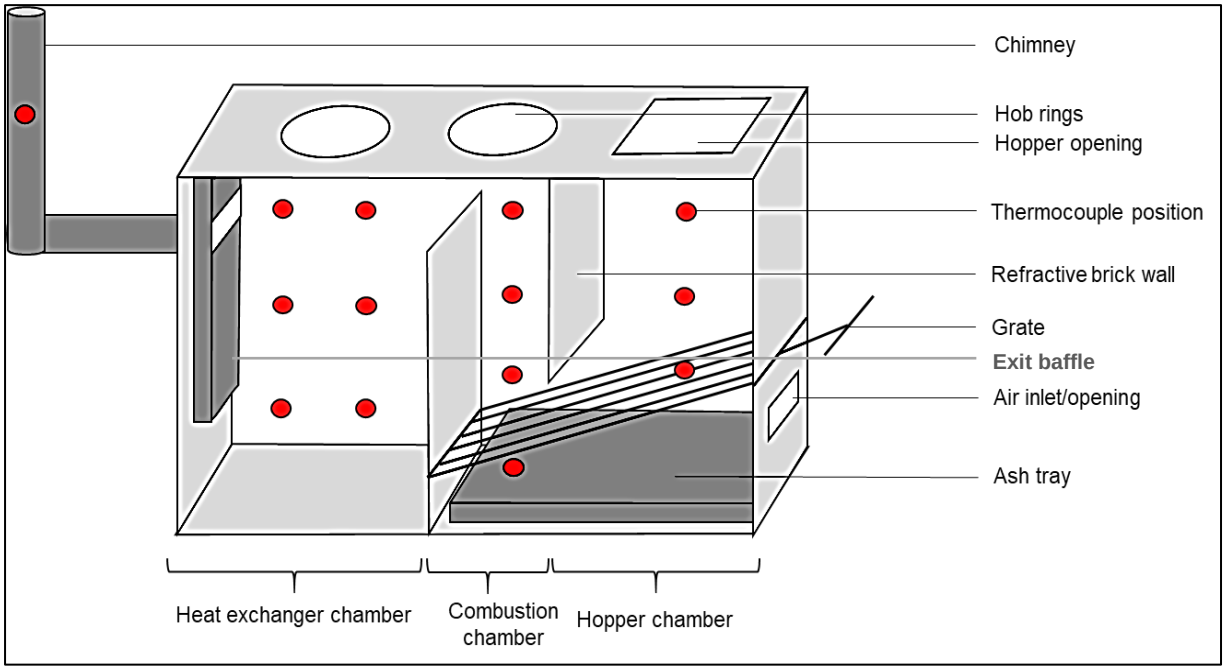

Figure 4-1: Cross section of the semi-continuous coal stove with relevant components.

The coal stove used in this study was developed by *New Dawn Engineering* [37] in collaboration with the North-West University. This stove contains a grate (fuel support), a chimney, heat resistance construction materials, a heat exchanger chamber, and operates on a cross-draft principal (right to left in the figure). The coal stove is designed with three distinct sections, the hopper chamber, the combustion chamber, and the heat exchanger chamber. These chambers are also shown in Figure 4-1 with the location of the respective thermocouples (red dots). The typical and ideal operation of the coal stove is explained by investigating the function of the three stove chambers. The hopper chamber ensures a semi-continuous operation by continuously feeding solid fuel to the combustion chamber. In the combustion chamber, the combustion zone forms on the grate where a portion of the solid fuel ignites, while the remaining fuel is gravity-fed into the hot burning zone. The solid combustion products and inert compounds fall through the grate onto the ash tray eliminating the influence thereof on the combustion zone. This allows for

a semi-continuous operation where the user can operate the stove for long periods with minimal stove operator intervention. The heat released from combustion is directed to the hob rings and upper plate of the coal stove which provides a heated surface for cooking purposes. The gaseous combustion products flow from the combustion chamber to the heat exchanger chamber where heat is exchanged with the metallic surfaces of the stove. Within the heat exchanger chamber, internal circulation occurs, which allows for 1) increased energy transfer from the hot fluid to the metallic surfaces of the stove, and 2) promotes ash and particulate matter settling by reducing the gas velocity in the chamber. Therefore, the use of a heat exchanger chamber not only improves the thermal efficiency of the stove but also aids in overall emissions reduction. In addition to the cooking surface, thermal convection and radiation across all the stove surfaces allows for living space heating. Finally, the emissions are ventilated through the chimney to the atmosphere and thus reducing direct inhalation by the stove user. The flow of gas in the coal stove is controlled by the natural air draft between the air inlet and the stove chimney. The air opening is used to control the fuel combustion rate by varying the opening size and consequently the oxygen supply to the combustion zone. The varying of the air inlet is mainly used to control the power rating of the coal stove based on application.

4.1.3 Operating principle

The semi-continuous coal stove was designed to operate similarly to a top-lit updraft gasification stove since the production of combustible gases and volatiles are separated from the combustion thereof [66]. However, these gasification stoves exhibit a gasification stage and a combustion stage, while the semi-continuous coal stove operates with four distinct stages. The four operating stages, and the location thereof are displayed in Figure 4-2. These stages are:

i) Pyrolysis

In this stage most of the moisture, organic and inorganic volatiles, and heavy gaseous hydrocarbons are separated from the fuel. This takes place inside the hopper chamber as the combustion zone propagates towards the front end of the stove. Oxygen is consumed in the combustion zone on the grate, therefore the local oxygen concentration in the hopper above the combustion zone decreases. Consequently, pyrolysis of fuel occurs in the hopper chamber in an oxygen lean environment. A portion of the heavy pyrolysis products and volatilised tars condense on the cold stove surfaces (e.g., the hopper lid) and on the remaining cold fuel at the top of the hopper chamber. Some of these condensed tars gets cracked during operation or are burnt off during the course of the run. The remaining uncondensed pyrolysis products are directed to the combustion chamber where gas phase combustion occurs.

ii) Cracking of hydrocarbons

Complex long-chain hydrocarbons are thermally cracked in an oxygen lean environment due to the extreme temperatures of the horizontal combustion zone that formed along the stove grate. These complex hydrocarbons are transformed into light carbonaceous gases that are combustible in the combustion chamber in the vapour phase.

iii) Char combustion

As the volatiles, inherent moisture, and tars are removed from the fuel, char forms. This char usually consists of carbon, minerals, and inert matter. The char combustion occurs on top of the grate and provides a large portion of the energy that is delivered to the stove surfaces. Some of the energy released from the char combustion is also used for pyrolysis and heating of air permeating through the bed.

iv) Gas combustion

The volatile matter (pyrolysis products), cracked tars, and light hydrocarbons are combusted in the vapour phase in the combustion chamber. This is typically observed by a flame present in the mid-top area of the combustion chamber. This greatly contributes to the high temperature and energy flux of the stove cooking zone (hob rings). This design principle also improves the combustion of carbonaceous particulate matter, minimising the emission thereof.

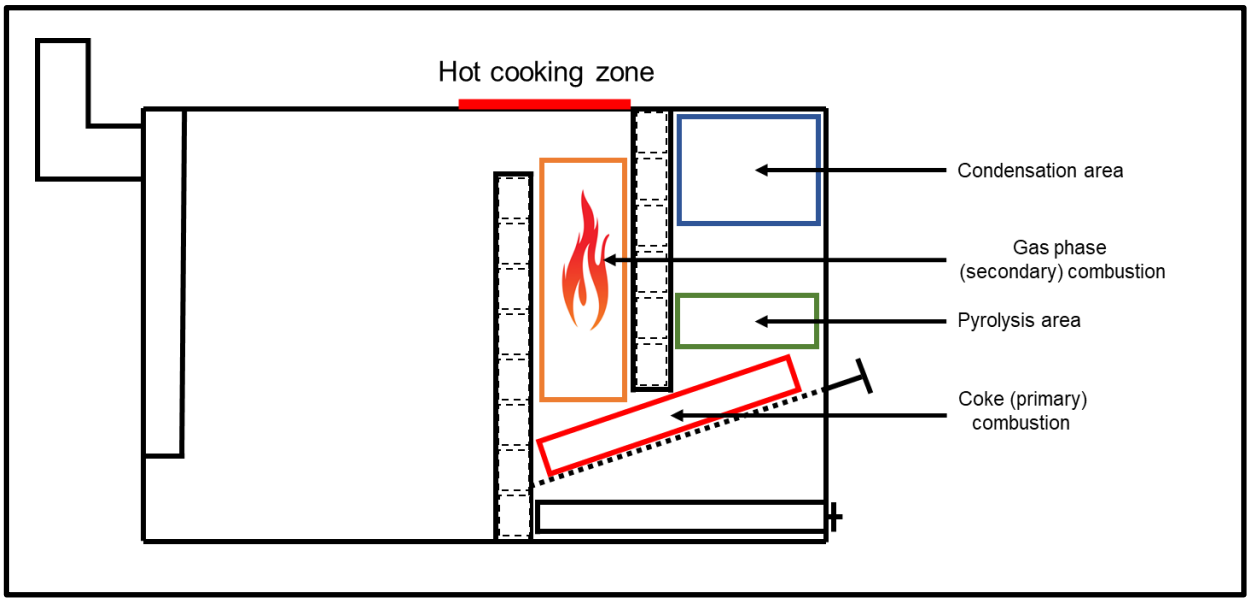

Figure 4-2: Operating principle of the semi-continuous coal stove.

Based on the operating principles, the combustion zone can be divided into two sections: the solid phase combustion region and gas phase combustion region. The solid phase combustion occurs on top of the grate and is where the primary oxygen consumption occurs. The remaining oxygen that did not take part of the solid phase combustion gets heated and flows through the bed towards the centre of the combustion chamber. Here, the gas phase combustion occurs, and oxygen is further consumed to form combustion products.

4.1.4 Equipment setup

The experimental setup used for this study is based on the setup used by Sumbane et al. ([38]), Kuhn et al. ([39]) and Altanzul ([40]).

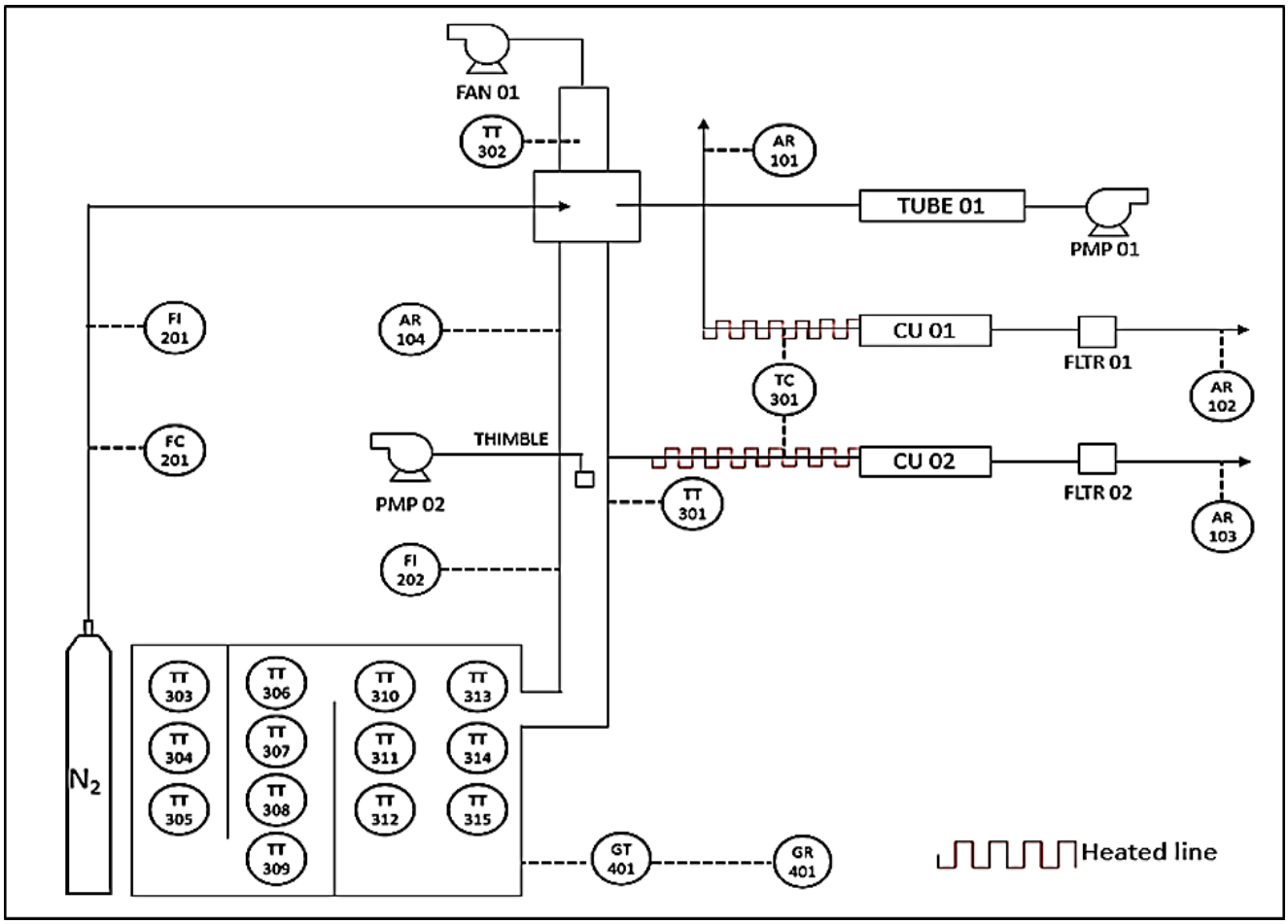

Figure 4-3: Piping and instrumentation diagram (P&ID) for the experimental setup.

The setup can be divided into two categories: thermal data collection equipment, and emissions data collection equipment. For thermal data, the following equipment was used: (i) K-Type thermocouples which indicate the internal stove temperature profiles (including chimney and roofline vent sections), (ii) a pyrometer and thermal camera to determine stove external surface temperature profiles and (iii) standard water boiling test instruments to obtain the stove thermal performance data. For the emissions data collection the following equipment was used: (i) Two Horiba PG350 gas analysers for the chimney emissions (SO_X, NO_X, CO_2, CO, and O_2), (ii) a DustTrak II gas analyser together with a particulate matter (PM) thimble to determine particulate matter emissions and (iii) activated carbon tubes for volatile organic matter emissions data. The Horiba PG 350 gas analysers mainly measure SO_2 with minimal error from the presence of SO_3,

therefore this study refers to any sulphur oxide emissions measured during the experimental phase as SO_x. In addition to thermal and emissions equipment, a load cell was used to record the weight of the stove during operation. Three water traps were also installed to eliminate condensate from forming in the sampling lines that could possibly interfere with the sampling conditioning or damage the equipment. A diagram of the equipment setup is shown in Figure 4-3 and the key components are indicated in Table 4-2. The equipment shown in the figure was frequently cleaned, and the gas analysers were calibrated before each experiment.

Table 4-2: Equipment list (key to Figure 4-3).

Component	Description
AR 101	DustTrak II
AR 102	Horiba PG 350 analyser (diluted)
AR 103	Horiba PG 350 analyser (undiluted)
AR 104	Hygrometer & data logger
FI 201	Nitrogen rotameter
FI 202	Differential flow meter
FC 201	Cylinder valve
TT 301-315	K-type thermocouples
TC 301	Heat controller
GT 401	Sartorius platform scale
TUBE 01	Activated carbon tube
GR 401	Combix 2 data recorder
CU 01	Conditioning unit
CU 02	Conditioning unit
FAN 01	Extractor fan
FLTR 01	Moisture and PM filter
FLTR 02	Moisture and PM filter
PMP 01	GilAir Plus Pump
PMP 02	Aquaria CF20 pump

4.1.5 Ignition procedure and operation

The first step in the ignition and stove standard operating procedure (SOP) is to prepare the necessary equipment. Before each experiment, all analysers are calibrated using the calibration gas shown in Table 4-1. In addition, all equipment filters are inspected, cleaned, and replaced if necessary. The cleaning chemicals shown in Table 4-1 is used for cleaning the previously mentioned filters, glass equipment, sampling equipment, and sampling lines. The fuel ignition within the semi-continuous coal stove is based on the top-lit up draft (TLUD) ignition method as discussed in various literature publications [88]. The ignition process is started by closing the stove openings such as the air inlet, ash tray, and hob rings, and opening the hopper chamber lid. This is done to promote the formation of a natural cross-draft through the hopper lid, down the hopper chamber and directly into the combustion chamber as fuel ignition commences. Next, a fraction of the fuel (1.5 kg) is deposited on top of the stove grate to form an evenly distributed layer of fuel thick enough to prevent major airflow through the grate during ignition.

After the fuel bed has been prepared, wood kindling (200 g) is placed on top of the bed, with the longest side parallel to the grate. This is done to ensure that air can flow through the kindling and underneath the stove bridge (refractory material separating the hopper- and combustion chamber). Small fuel pieces (50 g with a PSD of less than 6.7 mm) are placed on top of the wood in the combustion chamber which, once ignited, rapidly combusts with the wood, and produces some initial combustible vapours before the rest of the fuel is ignited. Finally, more wood kindling (100 g) is placed on top of the small fuel pieces in the combustion chamber and in the back of the hopper chamber, with the longest side perpendicular to the stove grate. The final addition of wood is to improve the propagation of flames form the combustion chamber to the back of the hopper chamber. The wood kindling is spread out on the fuel bed to ensure that the entire top section of coal/pellets are ignited before filling the hopper with the remaining fuel. It is critical that the entire horizontal fuel bed is ignited in order for devolatilization to occur. If this does not happen before the bulk of the fuel is loaded into the hopper, an ideal combustion zone will not form (cold ignition). Once the final wood chips have been placed, two paraffin-soaked woodchips are ignited in the combustion chamber and underneath the bridge. All the biomass used in the ignition process are *Pinus Radiata* (“Pine”) wood, which was found to be the easiest to ignite and produced the most reliable and repeatable ignition in the semi-continuous stove during preliminary testing. The combination of pine wood and paraffin acts as an ignition accelerant which ensures a quick and uniform formation of the combustion zone with minimal smouldering.

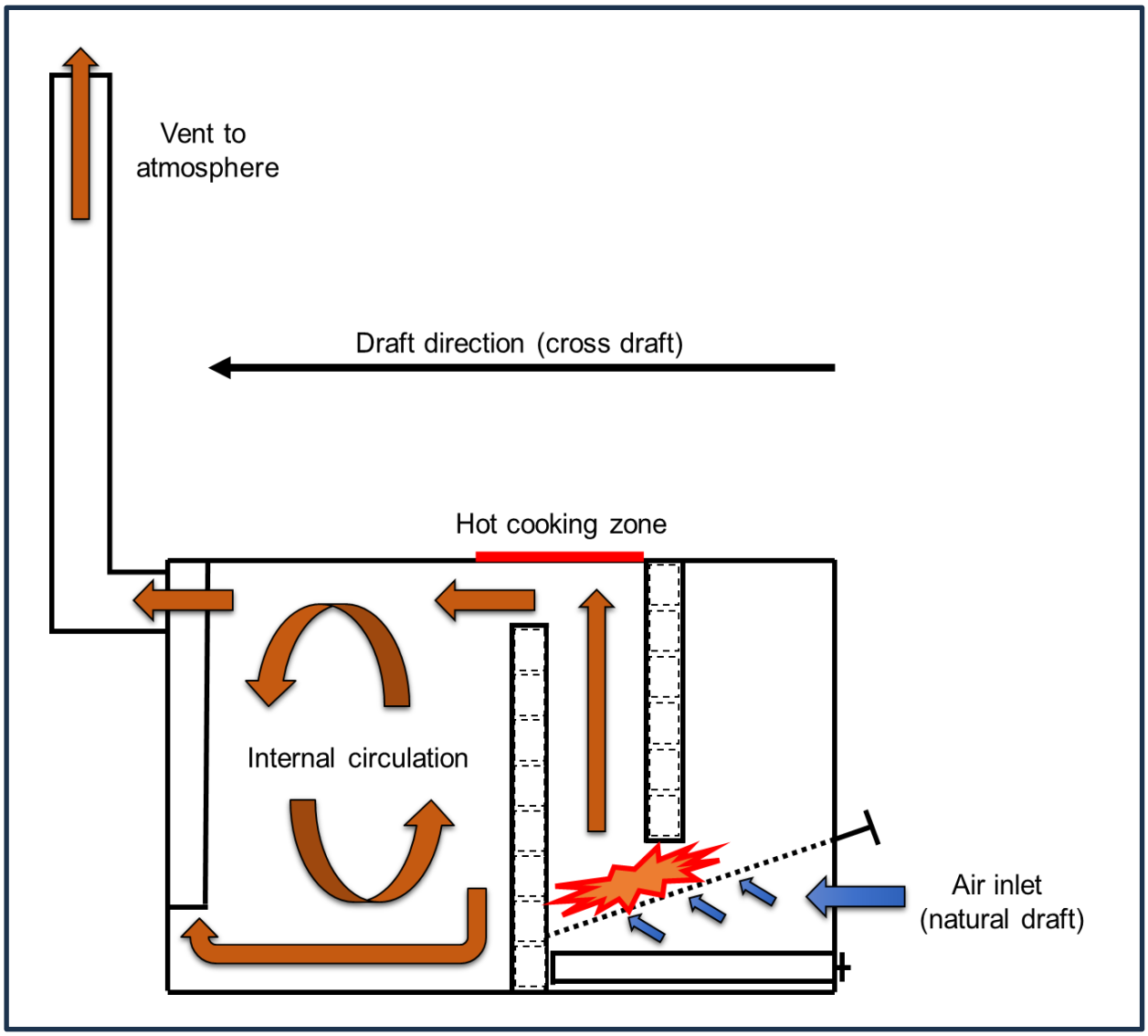

Figure 4-4: Semi-continuous coal stove internal fluid flow scheme.

The aforementioned procedure (top-lit ignition of coal material) has been found to be the most effective method of igniting a coal fuel with the least amount of emissions produced during the ignition phase [88]. Once the wood in the hopper chamber have developed into char material, a fraction of the remaining coal is added into the hopper chamber. The reason for not adding all the remaining fuel is to prevent a slow ignition process with elevated emission levels, which was found to occur if the hopper is instantly filled after ignition. Then, once a fully developed combustion zone is present in the combustion chamber and underneath the bridge, the hopper is filled with the remaining fuel and the air controller is set to the desired level. The hopper is filled with fuel to approximately 1 cm below the hopper lid. This is done to prevent downward force on the packed bed and to prevent combustion gases from escaping through a partially open hopper lid. The

adjusted air controller can be set to 5.5 cm (high-power), 2.5 cm (medium-power), and 0.5 - 0 cm (low-power). The motivation for the low-power setting is to let the stove operate on “ingress air” – air that flows into the stove via unintended openings like seams or small holes in the stove design. Even though the air controller is fully closed and therefore reduces the available combustion oxygen in the stove, the operating principal of the semi-continuous coal stove ensures minimal production of incomplete combustion gases (e.g., carbon monoxide).

After the ignition phase is complete, grate shakes are required as part of normal operation. Some criteria were set to reduce the variability of this procedure and standardise the grate shakes for all runs. It was decided that grate shakes would be performed when:

- Significant dead zones are observed in the combustion chamber.
- A 300 °C decrease in the combustion zone temperature is observed (from the peak of the previous grate shake).
- High oxygen levels were observed in the flue gas (approximately 10% – 13% by volume O_2).

During normal operation, all three criteria occurred simultaneously due to ash accumulation in the combustion zone, however during abnormal conditions (e.g., smouldering, channelling, severe clinkering, etc.) grate shakes were also performed when only one or two of the criteria points were met. As part of the preliminary test work, it was observed that frequent grate shakes can result in inconsistent performance parameters. The decision was made to continue experimentation with grate shakes to evaluate the typical operation of the stove as per design intent. This would provide the most representative performance data of household application, minimising the difference between lab and field results. Furthermore, grate shakes are an essential part of the stove's continuous operation, and therefore the criteria were included in an attempt to minimise its effect on performance results.

4.1.6 Experimental schedule

The experimental schedule was developed based on the several independent variables that were chosen for this study (fuel type, waterproofing, binder type, fuel PSD, and binder quantity, as was discussed in Section 3.1). The experimental matrix can be seen in Figure 4-5.

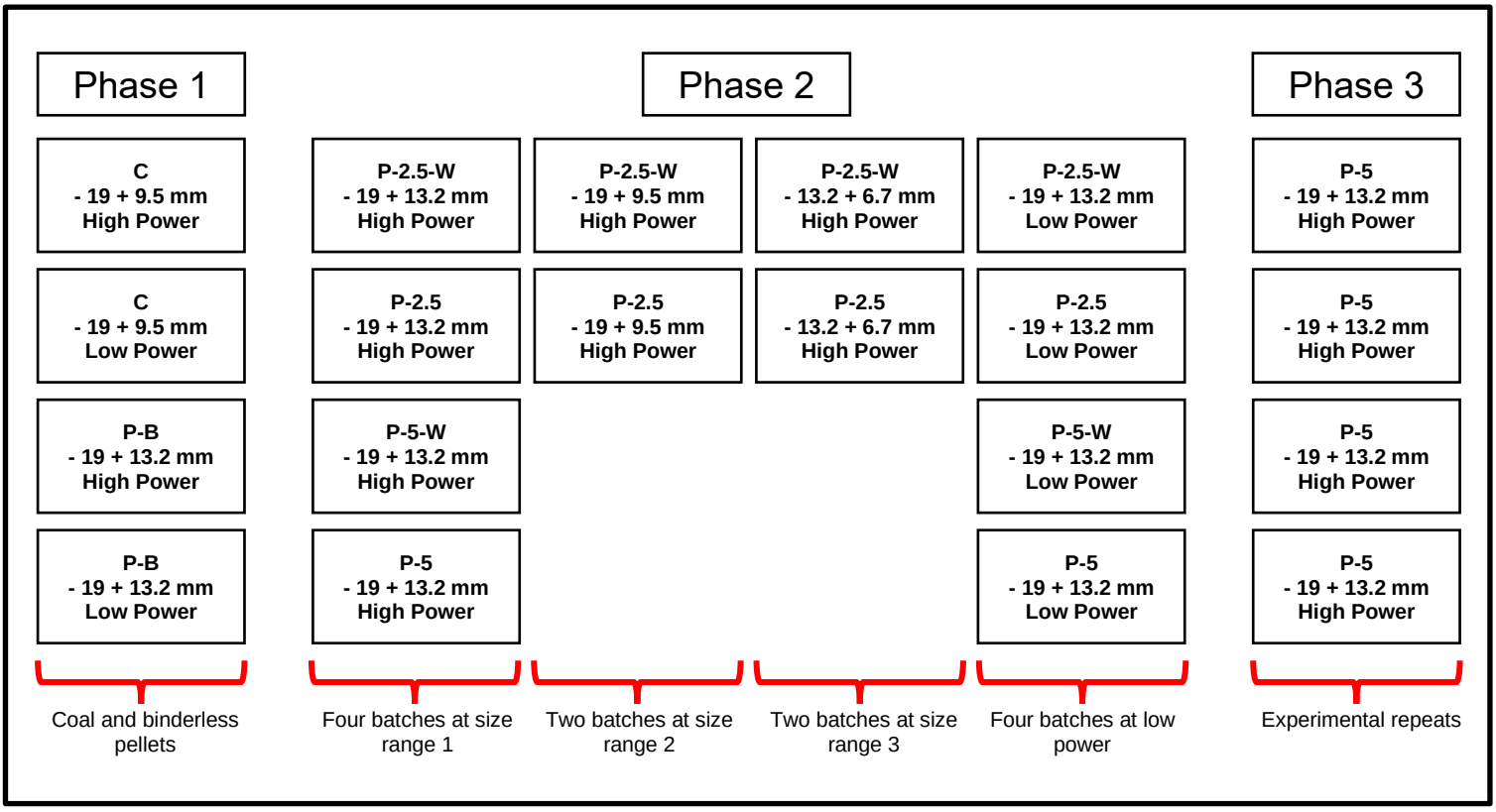

Figure 4-5: The experimental matrix with reference to the chosen independent variables.

The experimental schedule is divided into three phases of experiments. The first phase experimental runs were intended to compare the performance of lump coal against binderless pellets at both high- and low-power settings. For this purpose, the size range of the fuel was kept constant. The phase 2 experiments were intended to compare fuel PSDs, stove power setting, and the effect of the fuel characteristics. For this purpose, all the PVA binder pellet batches were utilised. Finally, the phase 3 experiments were repeats chosen to determine the repeatability and accuracy of results given in this study. A total of 20 experiments were conducted and completed. In total, four unscheduled repeat runs were necessary due to operational challenges, equipment failures, and external disturbances.

For the bulk of the experimentation, it was necessary to select three size ranges in order to correlate different packing parameters with the combustion performance. Taking the ideal size range criteria into consideration (-19 mm +6.7 mm as discussed in Section 3.3.2), the following size ranges were selected based on the packing parameters discussed in this ANNEXURE B:

- -19 mm +13.2 mm
- -19 mm +9.5 mm
- -13.2 mm +6.7 mm

Table 4-3: Summary of selected size rages' packing parameters.

	-19 mm +13.2 mm	**-19 mm +9.5 mm**	**-13.2 mm +6.7 mm**
Bed density *(kg/l)*	0.72	0.76	0.80
Bed voidage fraction *(-)*	0.52	0.49	0.48
Surface area to volume ratio *(mm^2/mm^3)*	0.37	0.48	0.62
Surface area per fuel mass *(m^2/kg)*	0.52	0.63	0.77

A summary of the three size ranges' packing characteristics is given in Table 4-3. A significant difference in the packing parameters between the three selected size ranges is present and is therefore used for combustion performance correlation.

4.2 EMISSIONS DATA PROCESSING

The determination of the flue gas emissions plays a critical role in the evaluation of the semi-continuous coal stove's performance. The emission quantification methodology, which was developed as part of this study's objectives, depicts combustion and stack emissions on a time basis, and includes the impact of disturbances such as grate shakes. The calculation results also illustrate fluctuations in mass loss rates and internal gas flow rates. The stack velocity is a key parameter in emissions quantification since the velocity translates to flue gas volumetric flow and further, by using the ideal gas law, relates to total mole flow through the stack. When the chimney mole flow is known, determining the emission factors is possible when the flue gas composition is also known. For this study, however, the use of velocity measurement equipment was not available. It was therefore decided to approximate the chimney mole flow from combustion and emissions data. The approximation starts by removing any outliers, or noise, from the mass loss data set. These outliers are created as part of normal operations (such as fuel loading) or when grate shakes are performed. This can be removed with a simple logic algorithm which is applied to each mass reading in a chronological order ($m_0 \rightarrow m_f$). The logic algorithm is presented in Equation 4-1. After any outlier data is removed, the combustion rate is calculated using Equation 4-2.

$$m = \boldsymbol{IF}\left(\boldsymbol{OR}\left(m_{j+1} > m_j;\ m_j - m_{j+1} > \dot{m}_{fuel}\right)\right)\boldsymbol{THEN}\ m_{j-1}\ \boldsymbol{ELSE}\ m_{j+1} \qquad 4\text{-}1$$

$$\dot{m}_{fuel} = \frac{dm}{dt} = \frac{m_j - m_{j+1}}{t_{j+1} - t_j} \qquad 4\text{-}2$$

Where:

m	is the corrected mass value *(kg).*
m_j	is the mass reading recorded for the instance "j" *(kg).*
m_{j+1}	is the mass reading recorded for the instance "$j+1$" *(kg).*
m_{j-1}	is the mass reading recorded for the instance "$j-1$" *(kg).*
t_j	is the time recorded for the instance "j" *(kg).*
t_{j+1}	is the time reading recorded for the instance "$j+1$" *(kg).*
$\dot{m}_{fuel}$	is the average mass loss rate for interval "$j \rightarrow j+1$" *(kg/s).*
$\frac{dm}{dt}$	is the change in fuel mass per time unit (combustion rate) *(kg/hr).*

Once the average mass loss rate for a certain interval is known, the theoretical mole flow of pollutants can be determined. The detailed coal composition obtained from proximate and ultimate analyses is used for this purpose. Using the flue gas composition data obtained from the Horiba gas analysers, the equation can be solved to determine the total flue gas flow rate. However, this method relies on the following assumptions:

i. The CO_2 pollutant species is used as the basis of this calculation since it has the largest flue gas concentration which minimises the effect of measurement error on the emission factor calculations.
ii. The organic matter reacts (combusts) homogeneously according to the ratios given by the ultimate analysis.
iii. A fixed α value of between 0.96 - 0.99 was assumed for each scenario. This is not a true description of reality as α varies with time during the experimental runs and can be described as a function of excess air.
iv. A fixed $y_{dry/wet}$ fraction of 0.94 - 0.96 was used to convert the flue gas from a dry basis to a wet basis. This value was determined based on the fuel moisture content, total hydrogen and oxygen in the fuel, and the relative humidity of the inlet air (y_{H_2O}). This is not a true description of reality as the water vapour fraction significantly varies with time. It was observed that the water vapour in the flue gas decreased as the run progressed.

Using the above assumptions, Equations 4-3 to 4-11 can be applied. This method is an alternative approximation of flue gas flow rate without the use of direct measurements such as chimney velocity. When both the CO and CO_2 concentrations in the flue gas are known, Equation 4-4 and the latter part of Equation 4-5 can be applied rather than Equation 4-3.

$$\dot{n}_{CO2} = \dot{m}_{fuel} \frac{x_C}{MW_C} \alpha \quad \text{4-3}$$

$$\dot{n}_C = \frac{\dot{m}_{fuel}\, x_C}{MW_C} \quad \text{4-4}$$

$$\dot{n}_{chim} = \frac{\dot{n}_{CO2}}{(y_{CO2})(y_{dry/wet})} = \frac{\dot{n}_C}{(y_{CO} + y_{CO_2})(y_{dry/wet})} \quad \text{4-5}$$

$$\dot{V} = \frac{\dot{n}_{chim} R\, T}{P} \quad \text{4-6}$$

$$\dot{m}_i = (y_i)(\dot{n}_{chim})(MW_i) \quad \text{4-7}$$

$$\dot{m}_{PM} = C_{PM}\, \dot{V} \quad \text{4-8}$$

$$m_{i,tot} = \int \dot{m}_i\, dt \quad \text{4-9}$$

$$CV_{corr} = \frac{CV}{1 - x_{ash}} \quad \text{4-10}$$

$$EF_i = \frac{m_{i,tot}}{(\Delta m_{fuel})(CV_{corr})} \quad \text{4-11}$$

Where:

$\dot{n}_{CO2}$	is the mole flow of CO_2 in the flue gas *(mol/hr).*
$\dot{m}_{fuel}$	is the average mass loss rate *(kg/s).*
x_C	is the carbon content of the fuel on a dry & ash free basis *(-).*
MW_C	is the molecular weight of carbon *(g/mol).*
α	Is the fraction of carbon that is oxidised to CO_2 *(-).*
$\dot{n}_C$	is the mole flow of carbon in the flue gas *(mol/hr).*
$\dot{n}_{chim}$	is the chimney flue gas mole flow rate (*mol/hr*).
y_{CO}	is the vapour fraction of CO in the chimney *(-).*
y_{CO2}	is the vapour fraction of CO_2 in the chimney *(-).*
$y_{dry/wet}$	is the correction factor for water vapour in the flue gas *(-).*
$\dot{V}$	is the volumetric chimney flow rate exiting the stove (*m^3/hr*).
P	is the system pressure (assumed atmospheric at chimney outlet) *(kPa).*
R	is the ideal gas constant *(J/K.mol).*
T	is the flue gas temperature *(K).*
$\dot{m}_i$	is the mass flow of pollutant species i in the flue gas *(g/hr).*
$\dot{m}_{PM}$	is the mass flow of total particulate matter in the flue gas *(g/hr).*
y_i	is the vapour fraction of pollutant species i in the flue gas *(-).*
C_{PM}	is the vapour concentration of particulate matter in the flue gas *(g/m^3).*
MW_i	is the molecular weight of pollutant species i *(g/mol).*
$m_{i,tot}$	is the total mass emitted of species i *(g).*

Δm_{fuel} is the difference between the initial and final mass of fuel *(kg).*

CV is the calorific value determined by lab analyses (air-dried) (*MJ/kg*).

CV_{corr} is the corrected calorific value for ash yield *(MJ/kg).*

x_{ash} is the ash yield of the fuel *(-).*

EF_i is the emission factor of pollutant species i *(g/MJ).*

The emission factor unit basis of "g/MJ" was chosen for this study. In addition to the main emissions data processing methodology shown above, further supporting calculations and information can be found in ANNEXURE E:

- Section E.1: Determining emission factors. The emission data processing methodology is applied to the P-5 run as an example calculation.

- Section E.2: Determining emissions mass balance. Using the approximation given in Equations 4-3 to 4-11, the mass balance of each component species (carbon, sulphur, oxygen, hydrogen, nitrogen) can also be determined. The P-5 run data is used as an example.

- Section E.3: Determining other emission parameters. The calculation methodology of several emissions parameters, other than the emission factors, are displayed in this annexure. These parameters include α, CO: CO_2 ratio, ε_{O_2}, $\bar{v}_{chim}$, and several other which are given and discussed in Chapter 5.

4.3 THERMAL DATA PROCESSING

The thermal data processing methodology was developed to determine both the energy losses through the stack, as well as the energy losses to the environment via the surfaces of the stove. The first step to evaluating the surface energy flux is understanding the energy transfer mechanism. In the semi-continuous coal stove, the energy gets transferred from the hot combustion fluid to the internal surface area via convection. For the sake of this study, it was assumed that a homogeneous fluid temperature was present surrounding internal thermocouple measurements. In other words, the temperatures measured at the centre of each stove area were assumed to be similar to the temperature at the surface front where the hot fluid and the stove surface interface. Thereafter, the energy gets transferred via conduction through the layered material of the stove surface, where it finally encounters the air outside the stove. Here, the primary energy transfer mechanisms are convection and radiation. Since there was no intentional draft over the surfaces of the stove, it was assumed that only natural convection and radiation took place and that the conduction via the stove legs was negligible.

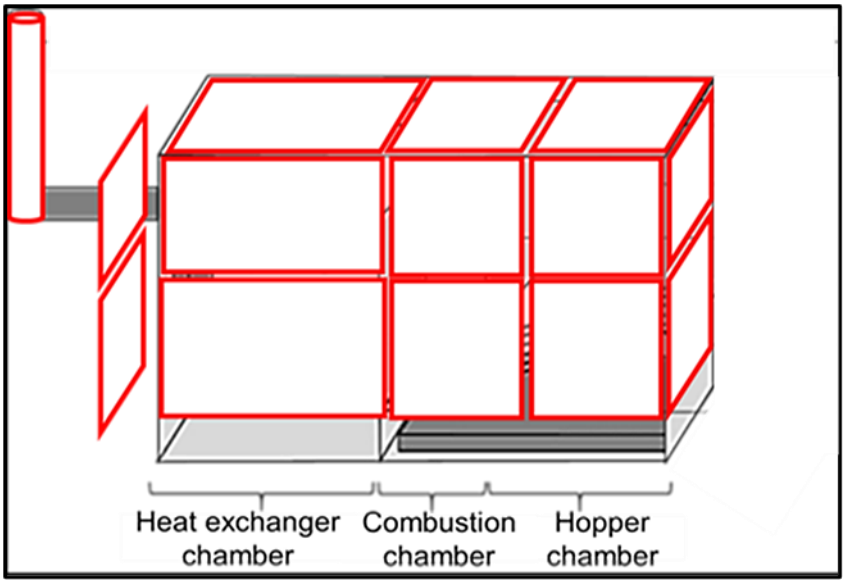

Figure 4-6: Stove external surface area division.

Next, the stove's external surfaces were divided into 14 segments as shown in Figure 4-6. To determine the total energy flux over the surfaces of the stove, and thus the total energy delivered, the radiation and free convection equations were applied to all these segments. Stove surface temperatures were taken throughout the run in 30-minute intervals for each of these surface segments. Furthermore, it was assumed that both vertical sides of the stove would produce the same energy output and that the energy lost through the underneath surfaces of the stove is

negligible. The equations used to calculate the total energy delivered are shown below and include free convection calculations(Equation 4-12 to 4-23), and radiation calculations (Equation 4-24).

$$\dot{Q} = h\,A\,(T_s - T_\infty) \quad \text{4-12}$$

$$h = Nu_L \frac{k}{L_C} \quad \text{4-13}$$

$$A = L_W L_H \;\; OR \;\; A = 2\pi r L_H \quad \text{4-14}$$

Where:

$\dot{Q}$	is the rate of heat transfer out of the body (convection) *(W).*
h	is the heat transfer coefficient *(W/m^{2}K).*
A	is the heat transfer surface area (stove segments) *(m^2).*
T_s	is the stove surface temperature *(K).*
T_∞	Is the environment temperature *(K)?*
Nu_L	is the Nusselt number *(-).*
k	is the thermal conductivity *(W/m·K).*
L_C	is the characteristic length *(m).*
L_W	is the width of the stove segment *(m).*
L_H	is the length of the stove segment *(m).*
r	is the radius of the stove chimney *(m).*

The first step in calculating the free convection heat transfer is by applying Newton's law of cooling (Equation 4-12). To apply this equation, the heat transfer coefficient must be known. The heat transfer coefficient (Equation 4-13) is however dependent on the flow regime of the air surrounding the stove. For free convection at the vertical heated surfaces (such as the side areas of the stove), the surrounding air is gradually heated and rises due to buoyancy and the reduced pressure gradient. Once enough energy is transferred to the hot air, a large enough pressure gradient forms to force the airflow into the turbulent regime, increasing the rate at which heat transfer takes place. Therefore, it is important to understand the flow regime of air next to the stove surfaces. The flow type can be identified using the Rayleigh number which is commonly known as a dimensionless number related to buoyancy-driven flow. To approximate the Rayleigh number, both the Grashof and Prandtl numbers must be known first.

$$Ra_L = Gr_L\,Pr \quad \text{4-15}$$

Laminar flow: $10^4 \leq Ra_L \leq 10^9\,;\; Nu_L = 0.59\,Ra_L^{0.25}$ 4-16

Turbulent flow: $10^9 \leq Ra_L \leq 10^{13}\,;\; Nu_L = 0.1\,Ra_L^{0.33}$ 4-17

Where:

Ra_L	is the Rayleigh number *(-).*
Gr_L	is the Grashof number *(-).*
Pr	is the Prandtl number *(-).*

The Rayleigh number approximation is given by Equation 4-15. The criteria for laminar and turbulent flow are also given by Equations 4-16 & 4-17, where the Rayleigh-Nusselt correlations are provided for both flow regimes. For the semi-continuous coal stove application, the Rayleigh number that was calculated for the vertical surfaces was always in the laminar flow regime ($10^4 \leq Ra_L \leq 10^9$) and therefore Equation 4-16 was mainly applied. The only exception was the chimney section. Due to the heigh of the vertical hot surface interface (height 3 meters), turbulent flow was calculated, and thus it was the only segment where Equation 4-17 was applied.

$$Pr = \frac{C_p\,\mu}{k} = \frac{v}{\alpha} \qquad 4\text{-}18$$

Where:

C_p is the specific heat *(J/kg·K).*
μ is the dynamic viscosity *(kg/m·s).*
v Is the kinematic viscosity *(m^2/s).*
α Is the thermal diffusivity *(m^2/s).*

The calculation of the Prandtl & Grashoff number is given in Equation 4-18 and Equation 4-19 respectively. Both these numbers were used in Equation 4-15 to determine the Raleigh number for free convection. The characteristic length of the heat transfer surface area is also given in Equations 4-20 & 4-21, where different characteristic length criteria are used based on the orientation of the hot surface area. In addition, the calculation of the film temperature is also given in Equation 4-23. The film temperature was used in determining the fluid properties such as the dynamic and kinematic viscosity.

$$Gr_L = \frac{g.\beta.(T_s - T_\infty).{L_C}^3}{v^2} \qquad 4\text{-}19$$

Vertical hot surface: $$Lc = L \qquad 4\text{-}20$$

Horizontal hot surface: $$Lc = \frac{A}{p} \qquad 4\text{-}21$$

$$\beta = \frac{1}{T_f} \qquad 4\text{-}22$$

$$T_f = \frac{T_s + T_\infty}{2} \qquad 4\text{-}23$$

Where:

g is the gravitational acceleration *(m/s^2).*
β is the coefficient of volume expansion *(1/K).*
L is the vertical length where buoyancy occurs *(m).*
p is the perimeter of the heat transfer surface (stove segments) *(m).*
T_f is the film temperature *(K).*

The calculation of the radiation heat transfer rate is given by Equation 4-24. For this equation, a thermal emissivity of 0.95 was used as the hot surface areas of the stove were coated with black thermal paint, to increase the efficiency of living space heating.

$$\dot{Q} = \sigma \varepsilon A \left(T_s^4 - T_\infty^4\right) \quad \text{4-24}$$

Where:

$\dot{Q}$ is the rate of heat transfer out of the body (radiation) *(W).*
σ is the Stefan-Boltzmann constant *(W/m^2K^4).*
ε is the thermal emissivity *(-).*

Finally, to complete the energy balance, a calculation of the stack losses is required. The stack losses consist of both energy losses from dry and wet gases. The dry gases are species such as carbon dioxide, nitrogen, oxygen, SO_X, NO_X, etc., while the wet gas is mainly water vapour that is present in the stack gas due to inlet air moisture, inherent fuel moisture, and H_2O formation during combustion. Both losses were considered for the overall stack loss calculation as given by Equation 4-27. The total stack loss efficiency is also calculated as shown in Equation 4-28, and is compared to the stack loss efficiency as calculated using the British standard for stack loss calculations (BS 845) [89]

$$Q = m_i C_{p\,i} \left(T - T_{ref}\right) \quad \text{4-25}$$

$$Q_{H2O} = m_{H2O\,(g)} C_{p\,H2O\,(l)} \left(T_{BP} - T_{ref}\right) + m_{H2O\,(g)} C_{p\,H2O\,(g)} \left(T - T_{BP}\right) + m_{H2O\,(l)} \Delta H_{Vap} \quad \text{4-26}$$

$$Q_{SL} = \Sigma\, m_i C_{p\,i} \left(T - T_{ref}\right) + Q_{H2O} \quad \text{4-27}$$

$$\eta_{SL} = \frac{(\Delta m\, CV_{corr} - \ Q_{SL})}{\Delta m\, CV_{corr}} \times 100 \quad \text{4-28}$$

Where:

Q is the total heat loss due to the specific heat of dry gases *(kJ).*
m_i is the total mass of pollutant species i emitted *(kg).*
$C_{p\,i}$ is the specific heat capacity of pollutant species i *(kJ/kg.K).*
T is the stack outlet temperature *(K).*
T_{ref} is the reference temperature (ambient) *(K).*
Q_{H2O} is the total heat loss due to moisture in stack emissions *(kJ).*
$m_{H2O\,(l)}$ is the total mass of liquid water (inherent fuel moisture) *(kg).*
$C_{p\,H2O\,(l)}$ is the specific heat capacity of water in the liquid phase *(kJ/kg.K).*
T_{BP} is the boiling point of water *(K).*
$m_{H2O\,(g)}$ is the total mass water vapour emitted *(kg).*
$C_{p\,H2O\,(g)}$ is the specific heat capacity of water in the gas phase *(kJ/kg.K).*
ΔH_{Vap} is the heat of vaporisation of water *(kJ/kg).*
Q_{SL} is the total stack heat loss due to both dry gases and moisture *(kJ).*
η_{SL} is the stack loss efficiency *(%).*
Δm is the mass of fuel combusted (a.f.b.) *(kg).*
CV_{corr} is the calorific value corrected for ash yield *(MJ/kg).*

To conclude the thermal data processing methodology, an overall energy balance of the stove is developed (Equation 4-29). The energy that is generated through combustion is accounted for through the stack losses, radiation, convection, and an error term. The error term was normally less than 10% of the total energy generation and is used to group several unaccounted energy losses that were not included in the calculations for simplicity's sake. These losses included energy transfer to the fuel, energy transfer to the stove material, energy loss through the bottom surfaces of the stove, energy losses through the dust and particulate matter in the stack, energy losses through the water boiling test, etc.

$$\mathrm{Q}_F = Q_{SL} + Q_{Con} + Q_{Rad} + Q_{Error} \qquad 4\text{-}29$$

Where:

Q_F	is the energy generated through combustion *(kJ).*
Q_{Con}	is the energy losses through free convection *(kJ).*
Q_{Rad}	is the energy losses through radiation *(kJ).*
Q_{Error}	is the unaccounted energy losses and error *(kJ).*

In addition to the main thermal data processing methodology shown above, further supporting calculations and information can be found in ANNEXURE E:

- Section E.4: Determining energy transfer rates. The thermal data processing methodology shown in Equation 4-12 to Equation 4-28 is applied to the P-5 run as an example calculation.

- Section E.5: Determining the stove energy balance. Using Equation 4-29, the energy balance of each stove-fuel combination can also be calculated. The P-5 run data is used as an example.

- Section E.6: Determining other thermal parameters. The calculation methodology of several other thermal parameters, other than the heat transfer rates, are displayed in this annexure. These parameters include P_F, P_D, η_D, η_{tot}, and several other which are given and discussed in Chapter 5.

4.4 EXPERIMENTAL REPEATABILITY

In this section, the repeatability of the semi-continuous coal stove using coal pellets is examined. For this purpose, the P-5 pellet batch was chosen to determine the accuracy, repeatability, and confidence of this fuel performance in the semi-continuous coal stove. The repeatability is indicated using a 95% confidence interval and a percentage error of the deviation on the magnitude of the values. The methodology used to determine these statistical values is shown in Annexure E.7.

Table 4-4: Repeatability and uncertainty of combustion parameters.

	Initial mass	**Run length**	**Grate shakes**	**Time between shakes**	**Average combustion rate**	**Combustion efficiency**
	kg	*hr*	-	*hr*	*kg/hr*	-
P-5	6.54	4.94	6	0.82	0.89	0.89
Repeat 1	6.22	4.96	8	0.62	0.83	0.89
Repeat 2	6.18	4.88	9	0.54	0.84	0.90
Repeat 3	6.32	4.71	7	0.67	0.86	0.86
Repeat 4	6.29	5.00	9	0.56	0.84	0.90
± 95% CI	0.17	0.14	2	0.14	0.03	0.02
± % ϵ	2.8	2.9	20.8	21.6	3.5	2.3
$\bar{x}$ ± 95% CI	6.31 ± 0.17	4.9 ± 0.14	8 ± 2	0.64 ± 0.14	0.85 ± 0.03	0.89 ± 0.02

In Table 4-4, a summary of the combustion parameters of the 5 identical runs is given. The largest uncertainty was calculated for the number of grate shakes and the average time between grate shakes. This is primarily due to unavoidable disturbances such as user input. Even though an attempt was made to standardise the grate shake procedure based on the criteria given in Section 4.1, it is left to the stove user's judgment under abnormal conditions when grate shakes should be conducted, and the severity thereof. This was dependent on the magnitude of ash formation, dead zones, channelling, and clinkers which also varied between runs. This non-homogeneous input therefore leads to a high standard deviation, error, and uncertainty. Despite these two parameters, the remaining combustion values are relatively similar and uncertainties of less than 5% are observed.

Table 4-5: Repeatability and uncertainty of the average internal temperatures of the semi-continuous coal stove.

	Hopper bottom	CC bottom	CC middle	HX middle	Chimney
	°C	*°C*	*°C*	*°C*	*°C*
P-5	870	730	700	260	160
Repeat 1	870	700	710	260	170
Repeat 2	940	670	730	260	170
Repeat 3	900	680	710	250	170
Repeat 4	820	680	730	260	170
± 95% CI	55	30	17	6	6
± % ϵ	6.2	4.3	2.3	2.2	3.3
$\bar{x}$ ± 95% CI	880 ± 50	690 ± 30	720 ± 20	260 ± 10	170 ± 10

In Table 4-5 a summary of the averaged stove internal temperatures is given for the 5 identical runs. Although most of the temperature results are relatively similar throughout the runs, the hopper bottom and the combustion chamber bottom temperatures displayed the most variability from run to run. The temperatures of these areas are typically representative of the combustion zone, and therefore any disturbance in the combustion zone such as grate shakes, clinkering or dead zones will carry over to the temperature profiles. Therefore, in Table 4-5 the largest area of uncertainty is the hopper and combustion chamber bottom temperature. It is also observed that the error magnitude and standard deviation decreased for results that were obtained closer to the stove exit. It is believed that due to the mixing and internal circulation, the effect of disturbances on the fluid temperature post combustion zone is reduced through dispersion and mixing. This can be seen in Table 4-5 where the temperature results for the heat exchanger chamber and chimney are almost identical between the 5 runs.

Table 4-6: Repeatability and uncertainty of water boiling test results.

	Cooking power	Cooking efficiency
	kW	*%*
P-5	0.59	8.3
Repeat 1	0.64	6.3
Repeat 2	0.59	7.6
Repeat 3	0.43	6.9
Repeat 4	0.54	8.1
± 95% CI	0.10	1.0
± % ϵ	17.8	13.9
$\bar{x}$ ± 95% CI	0.56 ± 0.10	7.4 ± 1.0

The water boiling test results of the 5 identical runs are displayed in Table 4-6. Both parameters displayed a significant uncertainty with a deviation error of greater than 10%. The poor repeatability of these parameters is mainly due to the application of the water boiling test. To standardise the water boiling test for the semi-continuous coal stove, it was decided to commence the test after the first grate shake which would indicate the end of the ignition phase. Due to the short duration of the water boiling test, it is possible that the temperature profile of that specific duration (±20 minutes) in which the test is conducted is not representative of the temperature profile during the remaining 4 hours of the run. The combustion energy produced during the water boiling test is also strongly dependent on the magnitude of the first grate shake, and how it affects the combustion zone. Perhaps for future studies, multiple water boiling tests can be performed during the run to minimise these effects on the test results.

Table 4-7: Repeatability and uncertainty of thermal performance parameters.

	P_F	P_D	η_{SL}	η_D	η_{tot}	$\overline{V}_{chim}$
	kW	*kW*	*%*	*%*	*%*	*m^3/hr*
P-5	6.7	5.5	89.6	82.7	73.8	15.5
Repeat 1	6.3	5.3	88.2	83.9	74.5	16.7
Repeat 2	6.4	5.8	88.8	90.5	81.1	15.7
Repeat 3	6.5	5.5	88.7	84.1	72.3	16.3
Repeat 4	6.4	5.5	88.3	86.2	77.9	16.8
± 95% CI	0.2	0.2	0.7	3.8	4.4	0.7
± % ϵ	2.9	4.0	0.8	4.5	5.8	4.5
x̄ ± 95% CI	6.5 ± 0.2	5.5 ± 0.2	89 ± 0.7	85 ± 3.8	76 ± 4.4	16 ± 0.7

In Table 4-7, a summary of the thermal performance parameters is given for the P-5 run and the respective repeat runs. All the parameters shown in Table 4-7 have a relatively low uncertainty margin and presented satisfactory repeatability with a confidence interval error of less than 5%. The parameter with the largest uncertainty is the stove total efficiency, which presented the largest deviation error compared to the other parameter in Table 4-7. The results of several calculation sets are used to determine the total energy efficiency, including combustion efficiency, stack losses, energy delivered, etc. In doing so, the uncertainty of all these calculation sets adds up and consequently results in a larger uncertainty for higher hierarchy calculations such as the total efficiency shown in Table 4-7. Even though this may be the case, the repeatability of this parameter is still satisfactory for the aim of this study.

Table 4-8: Repeatability and uncertainty of various emission parameters.

	α	$CO{:}CO_2$	ε_{O_2}	$\overline{v}_{chim}$	$\bar{\lambda}$	$y_{d/w}$	V_{H_2O}
	-	%	%	m/s	-	-	ml
P-5	0.982	1.9	2.3	0.5	1.81	0.947	34
Repeat 1	0.990	1.05	0.85	0.6	1.94	0.952	44
Repeat 2	0.994	0.67	0.79	0.6	1.83	0.951	43
Repeat 3	0.980	1.82	2.22	0.6	1.94	0.947	43
Repeat 4	0.993	0.74	1.07	0.6	1.94	0.953	45
± 95% CI	0.008	0.73	0.93	0.1	0.08	0.004	6
± % ϵ	0.8	59.1	64.5	9.6	4.3	0.4	13.2
x̄ ± 95% CI	0.988 ± 0.008	1.24 ± 0.73	1.45 ± 0.93	0.6 ± 0.1	1.89 ± 0.08	0.950 ± 0.004	42 ± 6

Various emission parameters calculated for the P-5 run and the respective repeats are given in Table 4-8 and Table 4-9. The largest uncertainty was calculated for the CO:CO_2 ratio, the oxygen balance error, and the PM & VOC concentration results. All these parameters are directly correlated to the combustion mechanisms in the semi-continuous coal stove and are therefore susceptible to the influence of disturbances on the combustion zone. It was also found that disturbances such as grate shakes can have significant effects on PM and CO levels depending on the frequency and severity thereof. It was also shown in Table 4-4 that the grate shakes of the 5 runs, and the frequency thereof, were not-repeatable and displayed a high level of uncertainty. Therefore, emission (O_2, CO, PM, VOC) related parameters are directly influenced by these disturbances and will consequently also show a high level of uncertainty and a low repeatability. Furthermore, the DustTrak(II) data is used in combination with both the A (Horiba PG "A") and B (Horiba PG "B") gas analyser data, to determine the true particulate matter emissions. It was found that if the residence time of any one of these gas analysers is slightly inconsistent with the rest, it could result in a false higher/lower PM emission result, which increases the level of uncertainty and reduces the repeatability of PM calculation parameters.

Table 4-9: Repeatability and uncertainty of PM and VOC stack gas concentrations.

	$[PM_{DT}]$	$[PM_T]$	$[VOC]$
	mg/m³	*mg/m³*	*mg/m³*
P-5	21.2	12.8	110
Repeat 1	22.6	26.9	130
Repeat 2	9.6	18.9	110
Repeat 3	30.1	26.1	130
Repeat 4	14.1	19.3	230
± 95% CI	9.9	7.2	62.3
± % ϵ	50.5	34.7	43.9
x̄ ± 95% CI	19.5 ± 9.9	20.8 ± 7.2	140 ± 60

The PM thimble results in Table 4-9 also show high levels of uncertainty. It was found that in some cases the thimble material would melt to the sides of the thimble holder (usually high-power runs with high temperature stack emissions), while in some cases moisture can condense in the thimble (low-power runs with low temperature stack gas). For both these scenarios, the initial versus final mass measurement will be impacted, resulting in a higher level of uncertainty and decreased repeatability. Finally, the VOC emissions also displayed a high level of uncertainty and a significant confidence interval error. It should be noted that the VOC data point of "Repeat run 4" is an outlier and was possibly caused by an experimental error. If this outlier was omitted from the data set, the data average with 95% CI would be 120 ± 10, decreasing the level of uncertainty by more than 80% and significantly increasing the confidence level and repeatability of this parameter.

Table 4-10: Repeatability and uncertainty of the sulphur balance.

	$m_{S\ Fuel}$	$m_{S\ Stack}$	OF_S
	g	*g*	-
P-5	47.7	21.0	0.44
Repeat 1	45.3	20.0	0.44
Repeat 2	45.1	21.6	0.48
Repeat 3	46.1	20.7	0.45
Repeat 4	45.9	21.2	0.46
± 95% CI	1.3	0.7	0.02
± % ϵ	2.8	3.6	4.6
x̄ ± 95% CI	46.0 ± 1.3	20.9 ± 0.7	0.45 ± 0.02

The mass sulphur emitted and the oxidation factors of the five runs are presented in Table 4-10. All three parameters displayed acceptable repeatability with a small margin of uncertainty and a confidence interval error of less than 5%. It was observed that the oxidation of sulphur is minimally influenced by combustion mechanisms, therefore most of the combustion zone disturbances such as grate shakes, clinkering, etc., had little effect on the sulphur emissions.

Table 4-11: Repeatability and uncertainty of emission factors.

	EF_{CO_2}	EF_{CO}	EF_{NO_x}	EF_{SO_x}	EF_{PM}	EF_{VOC}
	g/MJ	*g/MJ*	*mg/MJ*	*g/MJ*	*mg/MJ*	*mg/MJ*
P-5	94 ± 5	1.10 ± 0.04	83 ± 3	0.35 ± 0.01	15 ± 1	70
Repeat 1	95 ± 5	0.63 ± 0.03	95 ± 5	0.36 ± 0.02	19 ± 1	90
Repeat 2	96 ± 6	0.39 ± 0.02	96 ± 5	0.38 ± 0.02	7 ± 1	80
Repeat 3	94 ± 4	1.20 ± 0.04	92 ± 3	0.37 ± 0.01	23 ± 1	90
Repeat 4	96 ± 6	0.42 ± 0.02	99 ± 5	0.37 ± 0.02	11 ± 1	170
95% CI	1.0	0.47	8.0	0.01	8.0	50
% ϵ	1.3	63.1	8.2	3.9	52.4	49.7
$\bar{x}$ ± 95% CI	95 ± 1.0	0.75 ± 0.47	93 ± 8.0	0.37 ± 0.01	15 ± 8.0	100 ± 50

The emission factor summary of the five identical runs is exhibited in Table 4-11. Comparable to the results of Table 4-8, the CO, PM, and VOC emission factors displayed the largest level of uncertainty, with a confidence interval error of approximately 50% and higher. As discussed previously, these parameters are directly influenced by combustion zone disturbances and combustion mechanisms, which are highly non-homogeneous and differ from one run to another. The NO_X and SO_X emissions showed satisfactory repeatability for the aim of this study. Finally, the VOC emissions also displayed a relatively large uncertainty due to the single outlier of the "Repeat run 4" results. Again, if this data point is omitted from the set, an average with 95% CI of 80 ± 10 would be obtained, which greatly increases the repeatability and confidence level of this parameter.

CHAPTER 5 – RESULTS AND DISCUSSION

Chapter 5 presents the results obtained from the experimental setup and data processing detailed in Chapter 4. This chapter is structured into two main sections: Section 5.1 and Section 5.2.

Section 5.1 discusses general observations of typical stove operations, including clinkering, ignition, and grate shakes. One experiment is referenced in this section (P-5 run) to illustrate these observations, which are generally applicable to all runs unless specified otherwise. Despite standardising stove operation, data variability persisted and is also highlighted in this section.

Section 5.2 examines the influence of fuel type and characteristics, fuel PSD, and stove power settings. This section is divided into three parts:

- Section 5.2.1 compares fuel characteristics, including fuel type, binding agent presence and quantity, and waterproofing agent addition.

- Section 5.2.2 contrasts experiments conducted at low-power stove settings, with reference to the high-power variations.

- Section 5.2.3 explores the impact of fuel PSD on the measured parameters, averaged data, and calculation results.

In each subsection a discussion of combustion performance, thermal performance, and emission levels are included. Given the study's primary aim to evaluate coal pellets as an alternative to lump coal, Section 5.2.1 provides a comprehensive discussion, while Sections 5.2.2 and 5.2.3 offer brief summaries. Detailed discussions on the impact of stove power setting and fuel PSD are available in ANNEXURE C and ANNEXURE D, respectively. Throughout Chapter 5, comparisons with literature are attempted, though limited due to the unique operation and performance characteristics of the semi-continuous coal stove burning coal pellets. Performance parameters such as emission factors and thermal efficiencies are compared where possible.

5.1 GENERAL OBSERVATIONS AND TRENDS

To describe the influence of typical stove operation on combustion, emissions and the thermal performance, a single stove run (high-power, pellets: P-5, +13.2 mm to -19 mm fuel size) was selected.

The semi-continuous coal stove is intended to operate for long periods with minimal user input. However, it was found that the ash did not exhibit the “self-settling” ability that the stove was designed for. This meant that frequent grate shakes were necessary to ensure that the ash settled through the grate and deposited on the ash tray. The impact of grate shakes can be seen throughout most of the experimental data since it disrupts the combustion zone and influences both thermal and especially emission profiles. The mass data for the selected run can be seen in Figure 5-1. The grate shake instances are displayed on the x-axis as red dots. This convention to indicate grate shakes will be used throughout Chapter 5.

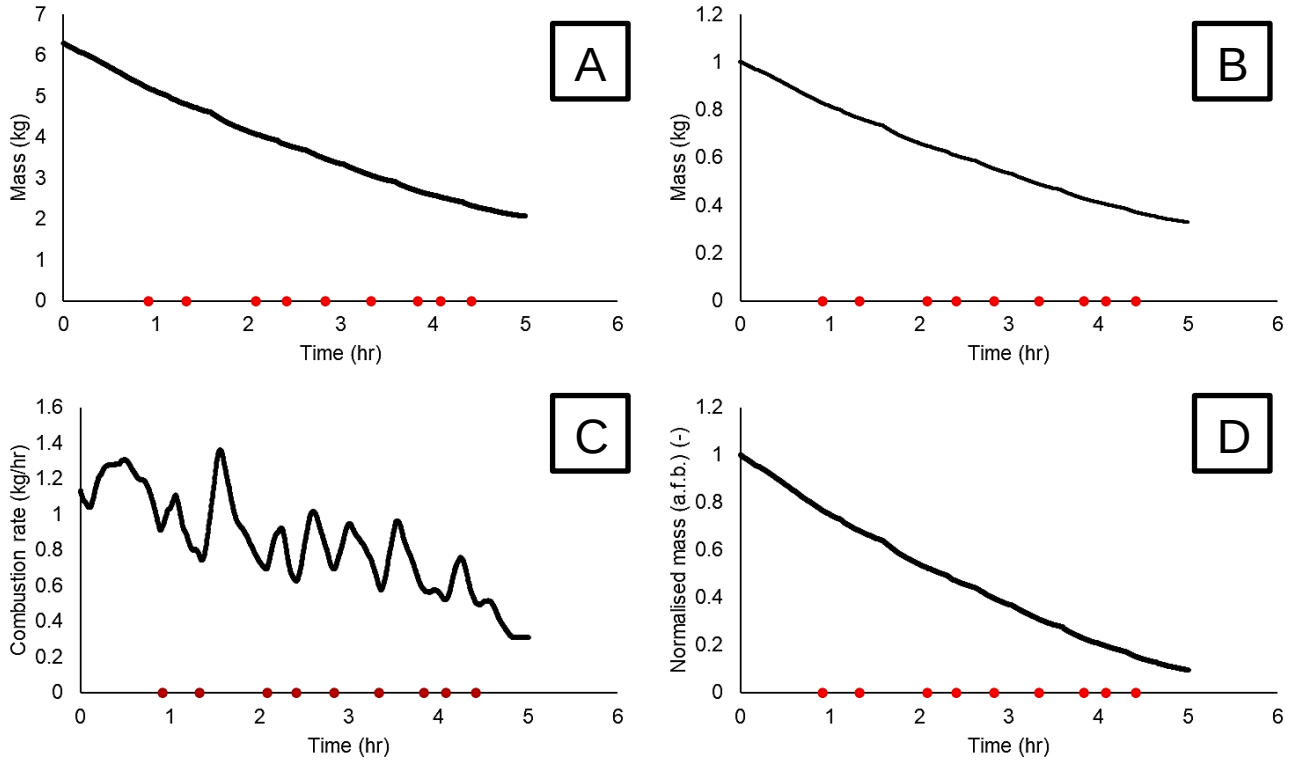

Figure 5-1: P-5 High-power +13.2 mm to -19 mm mass results: A) mass loss over run time, B) normalised mass loss, C) average combustion rate, and D) normalised mass loss on an ash free basis.

In Figure 5-1 A, the reported fuel mass over time is displayed. During experimental runs, the starting mass loaded into the hopper varied between 6.0 kg – 7.5 kg. Furthermore, when the normalised data in Figure 5-1 B is considered, the mass loss rate was found to be linear after removing the outliers caused by stove operation. The slight deviations that remained after smoothing was due to grate shakes and a visible reduction in combustion rate at the end of the run. The remaining mass fraction at the end of the run as shown in Figure 5-1 A & B is indicative of the material left within the stove after combustion, which includes the ash and inert material, and unburnt fuel. The ash free mass loss rate can be seen in Figure 5-1 D. The ash free mass fraction at the end of the run relates to the combustion efficiency, which is further discussed in Section 5.2. Experimental runs with more grate shakes, such as low-power runs, resulted in a larger ash free mass fraction at the end due to grate bypass of fuel and fines.

In Figure 5-1 C the transient combustion rate throughout the run is illustrated. Even though the average mass loss rate is reflected as relatively linear (Figure 5-1 A, B & D), it can be seen in Figure 5-1 C that the transient combustion rate is non-homogeneous and is significantly impacted by the grate shakes. The grate shakes result in ash segregation from the burning char particles, which results in a larger combustion rate. Conversely, the ash formation in the combustion zone acts as a combustion inhibitor and heat insulator, reducing the transient combustion rate. The combination of ash formation and grate shakes are the main factors resulting in combustion rate peaks and valleys during operation. Large peaks are present when more severe grate shakes are performed, and more ash is removed from the combustion zone. In contrast, the magnitude of the valleys depends on the amount of ash that accumulates in between grate shakes. It can be seen that the average gradient of Figure 5-1 C decreases as the run continues, similar to that in Figure 5-1 A, B & D. Larger valleys in the combustion rate graph generally depict dead zone formation where little combustion occurs. Throughout Section 5.2, such dead zones are highlighted for the respective runs. The influence of operator decision regarding grate shakes also contributed to the non-homogeneous nature of the combustion rate graph seen in Figure 5-1 C.

A fluctuation in the combustion rate caused by grate shakes directly translates to the energy output and consequently the temperature profiles within the stove. These temperature fluctuations can be seen in Figure 5-2. In Figure 5-2 A, the temperature profile of the combustion chamber can be seen. This is the main area of combustion and is the section of the stove with the largest temperature fluctuations. Initially, the highest temperature is observed at the bottom of the combustion chamber where the first combustion zone is established before the air inlet is opened. Once the fuel in this zone is depleted (in Figure 5-2 A after 1.5 hours) and mainly ash is left on the grate, the CC bottom temperature decreases. It is at this point whereafter the grate shake cycles begin.

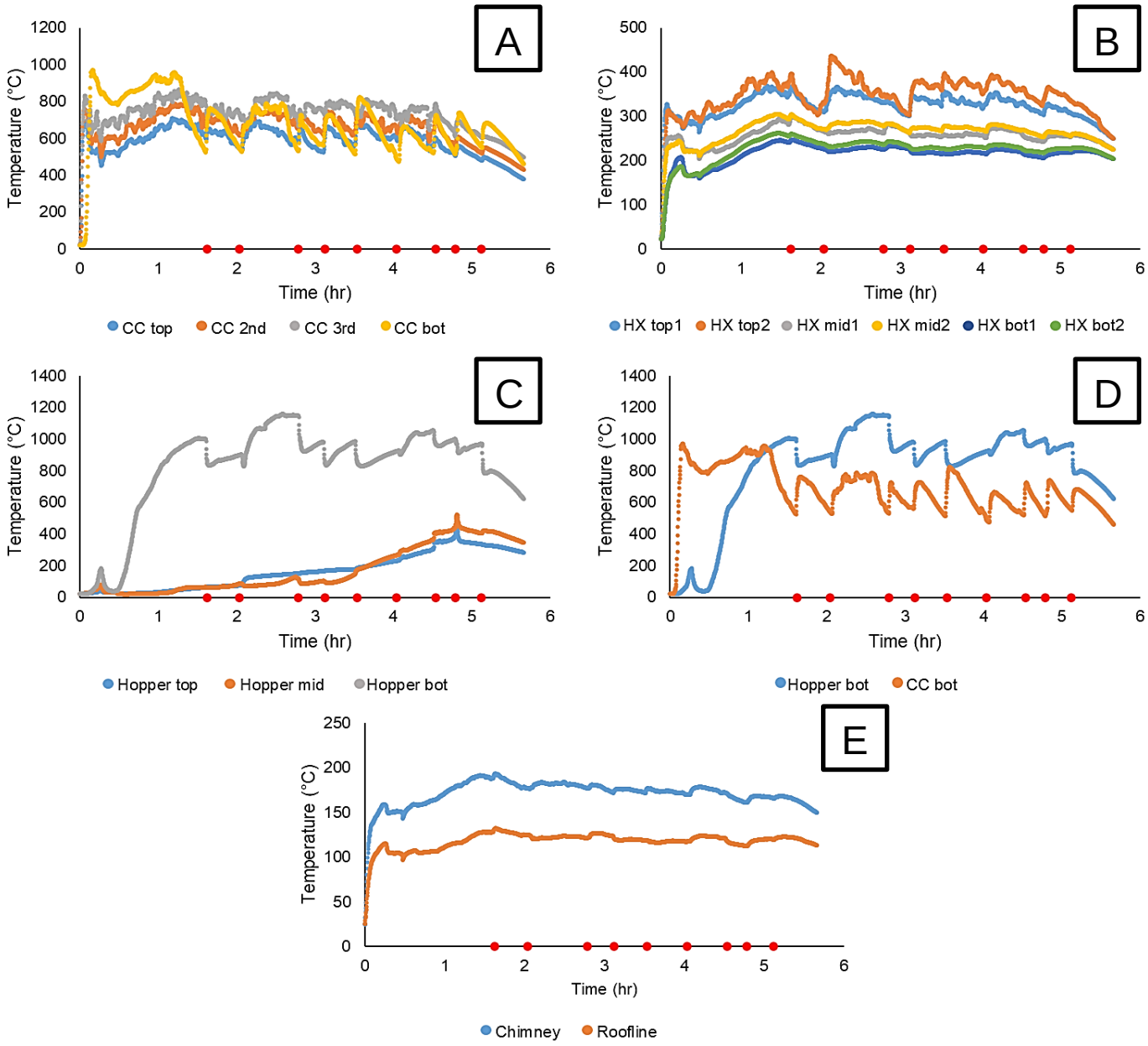

Figure 5-2: Stove temperature profile in: A) the combustion chamber (CC), B) the heat exchanger chamber (HX), C) the hopper chamber, D) the combustion zone, and E) the chimney.

Through experimental trial and error, it was found that establishing a proper initial combustion zone (as shown in Figure 5-3) is critical to minimise emissions once the ignition phase is over. This is further referred to in Section 5.2. In Figure 5-2 A it can also be seen that for the remainder of the run, the combustion chamber middle temperature (CC 3rd) exceeded the combustion chamber bottom temperature. This phenomenon can be attributed to the gas phase combustion of gasification and pyrolysis products, VOCs, and carbonaceous particulate matter. This occurs in the middle and top region of the combustion chamber and a bright flame can be observed here. This supports the 2-phase combustion mechanism that the stove was designed for.

In Figure 5-2 B & E, the temperature profiles of the heat exchanger chamber and the chimney (flue gas vent) can be seen respectively. It can be observed that the heat exchanger top temperatures also fluctuate due to grate shakes but to a lesser extent than the combustion chamber temperatures. The remainder of the heat exchanger and chimney temperatures shown in Figure 5-2 B & E are relatively linear and exhibit little fluctuations during the grate shake cycles. This is mainly due to the mixing and dispersion that occurs within these chambers, which homogenises the temperature profiles. In Figure 5-2 A & E it can also be seen that the difference between the inlet of the heat exchanger chamber (CC top – blue trend) and the chimney outlet (roofline temperature – orange trend) is approximately ± 500 °C for this specific run. In addition, the outlet temperature of the chimney was also relatively low. These findings highlight the heat exchange capability of the semi-continuous coal stove as a result of the internal circulation and the outlet baffle.

The hopper chamber temperature profile can be seen in Figure 5-2 C. The post ignition phase temperature at the bottom of the hopper is significantly higher than the rest of the stove since this is the propagation area of the active burning combustion zone. Between the hopper bottom area and the hopper mid area, pyrolysis, gasification, and cracking occur as described in Chapter 4.1. The hopper's middle and top sections are significantly colder than the that of the bottom since it contains the cold uncombusted fuel. This in combination with the surrounding refractory material provides the ideal conditions for the condensation and deposit of tars, volatiles, and other pyrolysis products. As the run progresses the hopper mid and top temperatures increase. This is a result of the decreasing hopper fuel level which removes the insulating fuel barrier between the bottom and the top sections of this chamber. Therefore, the hopper mid and top temperatures peak at the end of the run when little fuel is left in the hopper. Finally, the effect of grate shakes has little impact on the middle and top hopper temperatures. In Figure 5-2 D, the temperatures that are representative of primary combustion zone are displayed over the course of the run. The hopper bottom temperature is significantly higher than the combustion chamber temperature at all times apart from the first hour of the run. This is a result of the ignition procedure where is initial combustion zone is formed at the bottom of the combustion chamber.

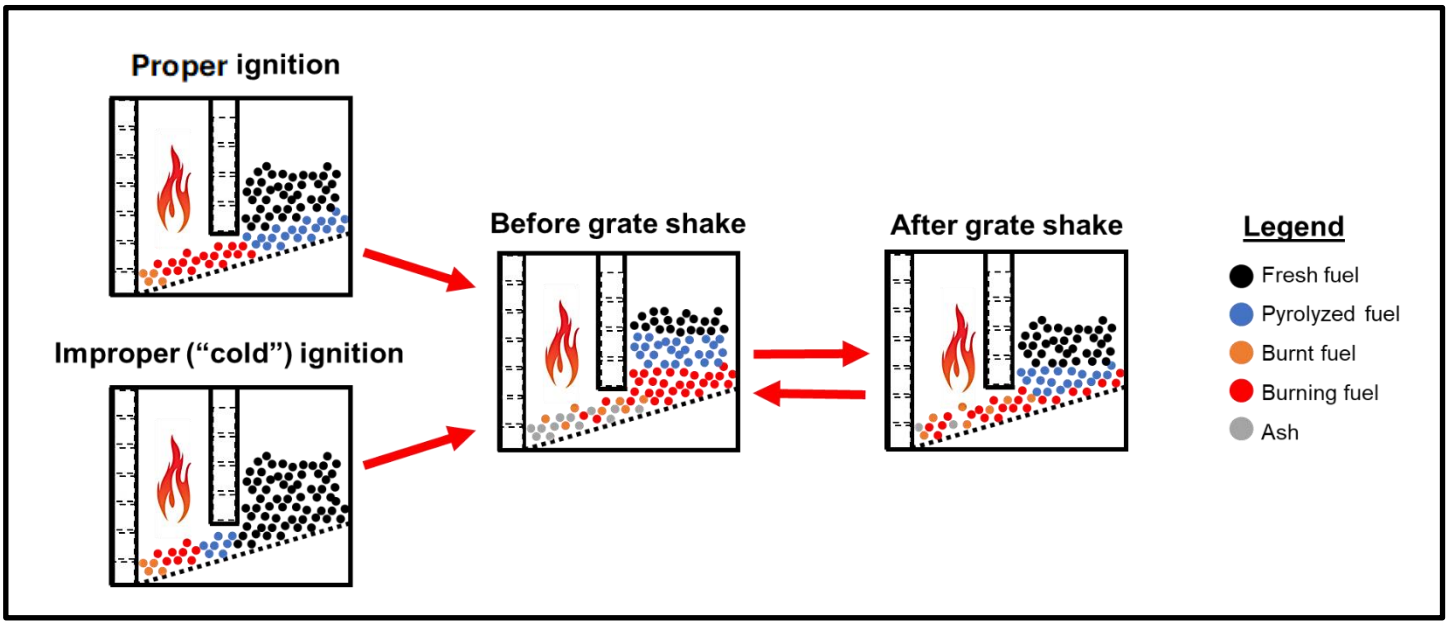

Figure 5-3: Combustion zone propagation diagram.

Due to the stove design, the propagation of the combustion zone occurred towards the hopper section which consequently formed the area with the highest temperature. It was found that the combustion zone formation follows the diagram displayed in Figure 5-3. As the run progresses, the CC bottom temperature decreases due to ash formation and the hopper bottom temperature increases as the combustion zone propagates to this area. This phenomenon repeats after each grate shake cycle as illustrated in Figure 5-3 and Figure 5-2 D. Finally, it can be seen in Figure 5-2 C & D that the combustion zone temperature exceeds 1100 °C at some instances in the run (e.g., at 2.5 hours). Runs where these high combustion zone temperatures occur, exhibit ash fusion (also known as "ash slag" or "clinkers") which significantly influences the stove operation and performance. These clinkers are shown in Figure 5-4, where moderate and severe ash fusion products are shown. It is also shown in Figure 5-4 that these clinkers can occupy and block most of the grate area at the bottom of the combustion chamber. The large clinker on the right of Figure 5-4 restricts fuel flow from the hopper chamber, resulting in air flow channelling and cooling of the cooking area.

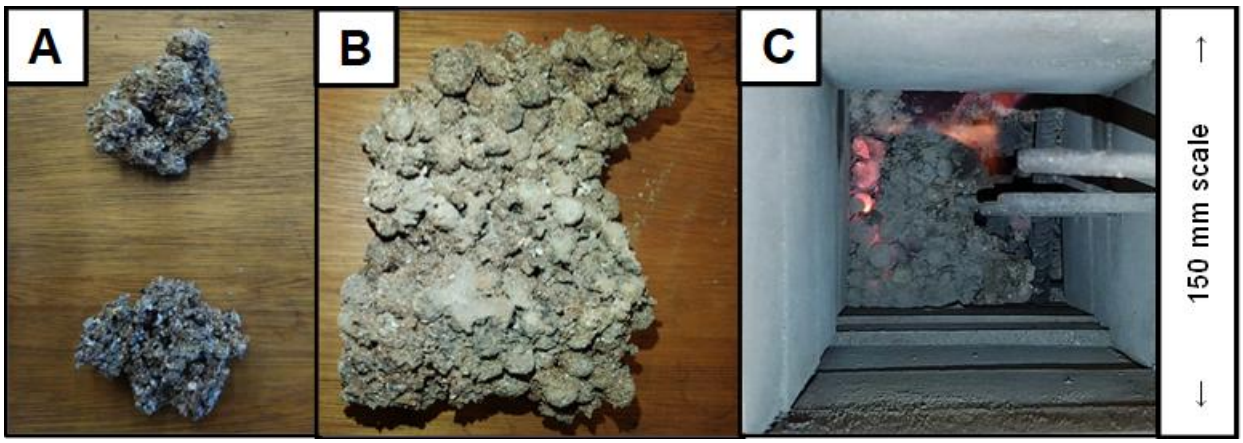

Figure 5-4: Ash fusion and clinker formation. A) moderate clinkering, B) severe clinkering, and C) channelling consequent to severe clinker formation in the CC.

In Figure 5-5 the emission levels in the chimney are reported, and grate shakes are displayed as red dots on the x-axis. The grate shakes caused noticeable spikes in pollutant concentrations when performed. In Figure 5-5 A, the carbon monoxide concentration, as reported by the gas analyser (dry basis), is shown. Two major areas of high carbon monoxide levels occur. Firstly, during non-steady state operation (at start and end of the run), and secondly after each respective grate shake. The relatively high carbon monoxide levels after grate shakes can be attributed to the increased combustion rates when most of the ash is rapidly removed. This can also be seen in Figure 5-5 C where the carbon monoxide, carbon dioxide and oxygen concentration are shown. The increased combustion rate increases the rate at which the main carbonaceous combustion products (CO_2 and CO) form. It also results in a temporary oxygen deficiency which leads to a decrease in the stoichiometric α value, (i.e., increased carbon monoxide formation relative to carbon dioxide). This can be seen in Figure 5-5 C at 2 hours when a large grate shake was performed. At this point, the excess oxygen levels in the fuel gas were reported to be between 0.0 – 0.5 vol.% O_2.

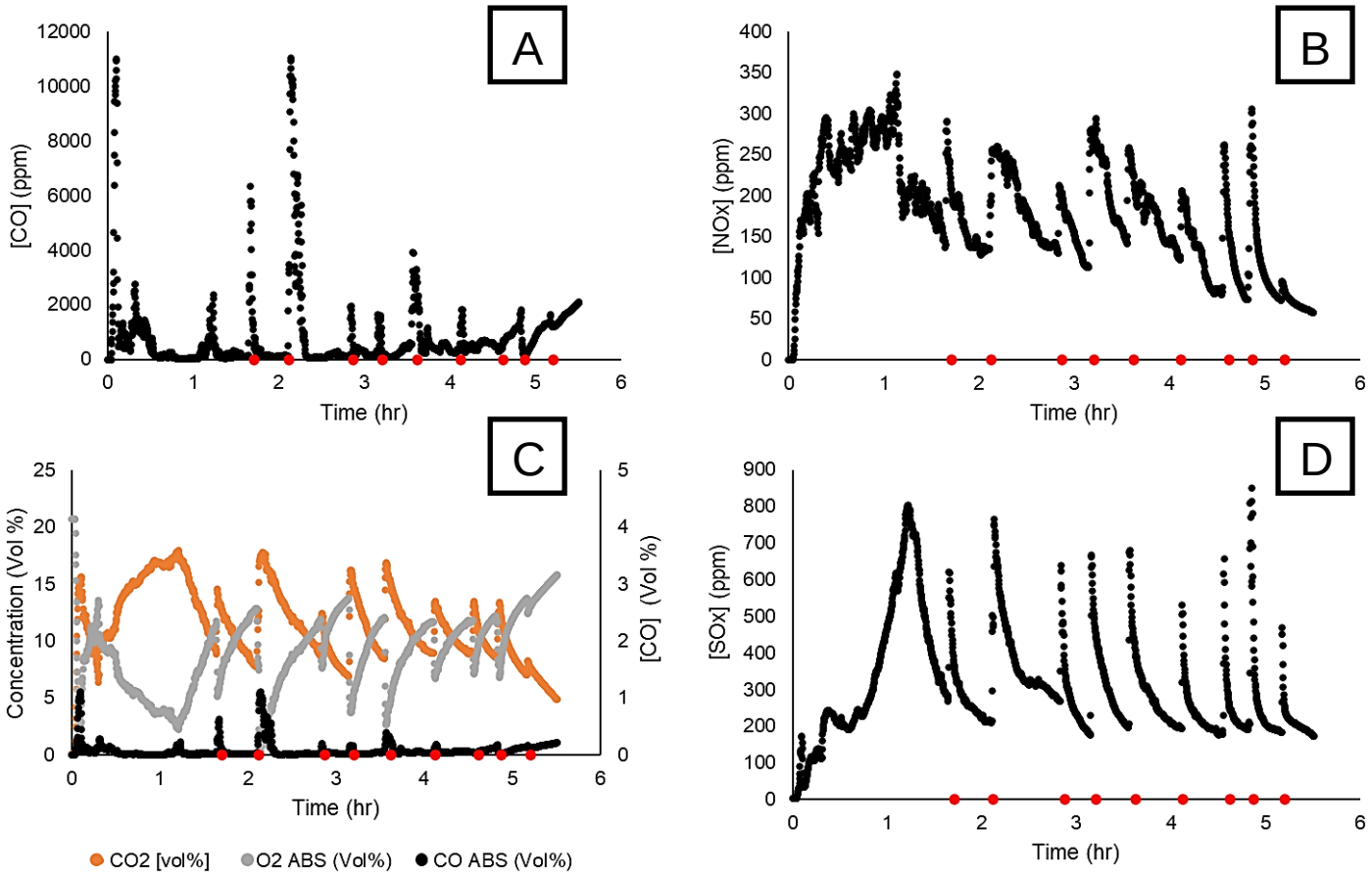

Figure 5-5: Flue gas concentration of species: A) carbon monoxide, B) Nitrogen oxides (NO_x), C) carbon monoxide, carbon dioxide & oxygen, and D) sulphur oxides (SO_x).

It was observed during the experiments that once the excess O_2 decreases below 0.5% the stack gas became visible, and a white plume of emissions and smoke could be seen exiting the chimney. This is a result of incomplete combustion of PM and CO emissions due to the low oxygen availability. As the combustion rate increases, more oxygen gets consumed by the solid fuel combustion and less oxygen permeates through the fuel bed. This limits combustion in the gas phase and results in higher levels of carbon monoxide in the flue gas. The CO levels instantaneously decrease as the excess oxygen increases above 0.5 vol.% O_2 and gas phase combustion is improved. This phenomenon can also apply to the latter part of the ignition phase (> 30 min after ignition) when the hopper lid is closed, and the air inlet is opened. Since the air inlet area is smaller than that of the hopper lid, this change can reduce the air supply which may cause a temporary oxygen deficiency. This can be seen in Figure 5-5 C at 0.5 hours when the hopper lid was closed.

To prevent a temporary oxygen deficiency during ignition, it is necessary to ensure that a proper initial combustion zone is formed before the hopper lid is closed (as shown in the top left of Figure 5-3). If the lid is open during ignition, a larger airflow is present, and complete combustion will occur in both phases. This results in lower carbon monoxide levels in the flue gas which was the case for the P-5 run shown in Figure 5-5. The consequence of an improper initial combustion zone, as shown in the bottom left of Figure 5-3 is greater pollutant levels at the start of the run and this will be discussed in Section 5.2.

Regardless of the ignition procedure, higher carbon monoxide levels are always present at the start and end of the run. This is due to the smouldering combustion mechanism of the fuel [90]. At the start of the run, the energy supply is not sufficient to cross the critical heat transfer threshold, which would result in the onset of oxidation. This leads to incomplete combustion and the SOP in Section 4.1.5 aims to minimise the duration of smouldering combustion by making use of both wood kindling and paraffin. The gradual increase of CO_2 and decrease of O_2 after ignition is a result of the propagation of the combustion zone, which stabilises approximately 1 hour after ignition. It is also at this point that the water boiling test is commenced. At the end of the run, smouldering is also present when the energy released by the fuel can no longer sustain complete combustion [90].

In Figure 5-5 B & D, the nitrogen oxides (NO_x) and sulphur oxides (SO_x) concentrations in the flue gas are displayed. The largest quantity of these emissions form during the first 2 hours of the run. During this period, no grate shakes were performed. These graphs follow the mechanism as described in literature [41], [56], where a large initial peak of NO_x and SO_x forms due to the volatilisation and combustion of organic compounds that contain sulphur and nitrogen. This correlates with the formation of the initial combustion zone where most of the pyrolysis and devolatilisation takes place. After the initial peak, the pollutant levels decrease together with the average combustion rate, as seen in Figure 5-1 C.

Throughout the run, grate shakes and the transient combustion rate influences the pollutant levels. After the initial peaks, NO_x and SO_x form due to the oxidation and combustion of organic compounds containing sulphur and nitrogen in the char. However, NO_x and SO_x spikes can also form due to the direct oxidation of inorganic species (e.g., pyrite) in the fuel [91]. Grate shakes entrain ash and inorganic compounds in the flue gas which increases the available area for oxidation [91]. This can be seen in Figure 5-5 B & D at approximately 5 hours into the run when a large spike of pollutant levels is seen at the end of the run at low combustion rates. In literature, reference to NO_x reduction in pulverised coal boilers is made where a reductive environment is created by applying staged combustion. In this case excess fuel is injected after the primary combustion zone, and a reductive atmosphere is created. This converts the nitrogen containing

compounds in the fuel to primarily N_2, which leads to reduced oxidation rates to NO_X species [92]. Furthermore, a positive correlation was identified between NO_X and excess air levels, while an inversely proportional correlation was found between CO and NO_X levels during pulverised coal combustion [93]. Similarly, based on the two staged combustion in the semi-continuous coal stove, lower NO_X levels are reported and a correlation between the NO_X, CO, and excess air levels are observed.

In Figure 5-6, the total particulate matter concentration levels in the flue gas are displayed. Figure 5-6 B contains the same data as Figure 5-6 A, but on a smaller scale (0 – 100 mg/m^3) to evaluate the results at low PM levels. The highest levels of PM were reported during the start of the run at ignition conditions. High concentration spikes also occurred during the first and second grate shakes in Figure 5-6, whereas smaller spikes formed after the remaining grate shakes. These occurrences can be explained by the following mechanisms:

- As discussed previously, smouldering takes place during the initial ignition phase. During this phase, most of the pyrolysis and devolatilisation occurs. Large quantities of carbonaceous particulate matter are volatilised and released into the gas flow. In the absence of complete gas phase combustion, these particulates are vented to the atmosphere instead of being combusted. When considering Figure 5-2 and Figure 5-6, the PM levels decrease as soon as the combustion chamber temperatures reach 500 °C which indicates proper gas phase combustion.

- During the second grate shake an oxygen deficiency occurs, and incomplete gas phase combustion occurs. Once again, carbonaceous particulates get vented to the atmosphere. As soon as the excess oxygen increases above 0.5 vol% O_2, the PM levels start decreasing.

- Due to the mechanical action of grate shakes, ash is segregated from the char particles and entrained in the gas flow. This is observed by the relatively smaller PM spikes that occurred after the 2nd grate shake in Figure 5-6. The entrainment of inert materials like dust, grit, and fly ash occurs, which is not influenced by the gas phase combustion mechanism.

Due to its reliance on complete combustion, the PM and CO concentrations have a similar relationship with oxygen availability. This is also supported by the remaining grate shake instances where the magnitude of the PM spikes in Figure 5-6, are indirectly proportional to the excess oxygen levels after grate shakes. The 5th grate shake between 3 and 4 hours in

Figure 5-6 also illustrates a large PM spike (> 10 mg/m^3) which correlates with low excess oxygen levels which is indicated in Figure 5-5 C.

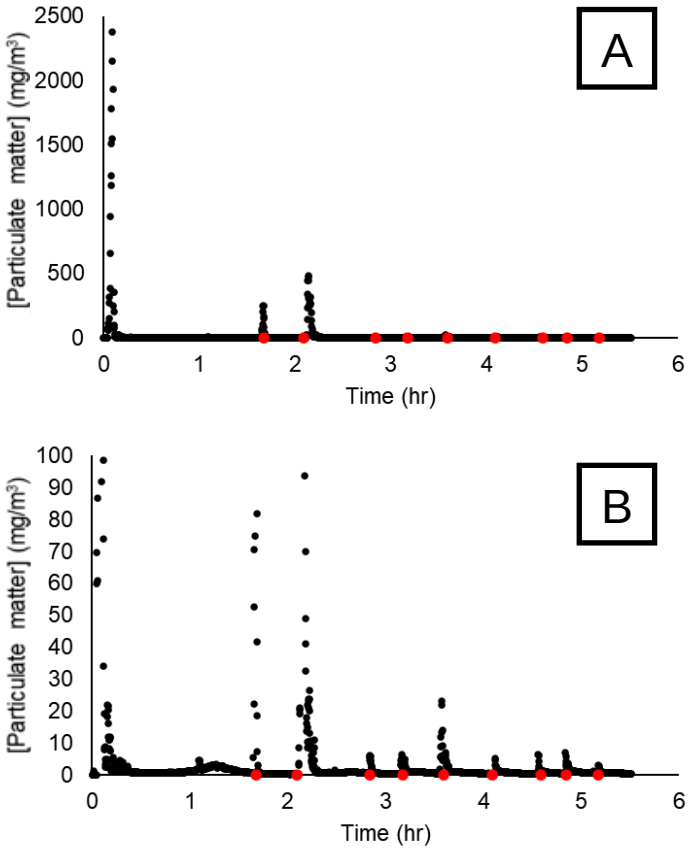

Figure 5-6: Particulate matter concentration in the chimney: A) 0 – max mg/m^3, and B) 0 - 100 mg/m^3

As discussed in Section 4.1.2, most of the inert solids settles out in bottom of the heat exchanger chamber. This dampens the effect of mechanical agitation on the PM emissions. Finally, between the grate shake instances where no disturbances occur, the PM levels emitted through the flue gas are lower than 10 mg/m^3 which is significantly lower than what is reported in the literature [21].

In Figure 5-7, the temperature profiles of the external stove surface areas are shown for the duration of the P-5 run. In this graph, the y-axis depicts the surface temperatures, the x-axis depicts the respective stove area segments, and the z-axis depicts the continuous 30-minute time intervals (where "#" refers to the 30-minute interval number) during which the surface temperature measurements were taken. The areas of the stove that displayed the highest surface temperatures are the front bottom area, the combustion chamber surfaces, and the heat

exchanger chamber lid. The high surface temperatures and thus high energy output directly correlate with the stove's internal temperatures and combustion rates.

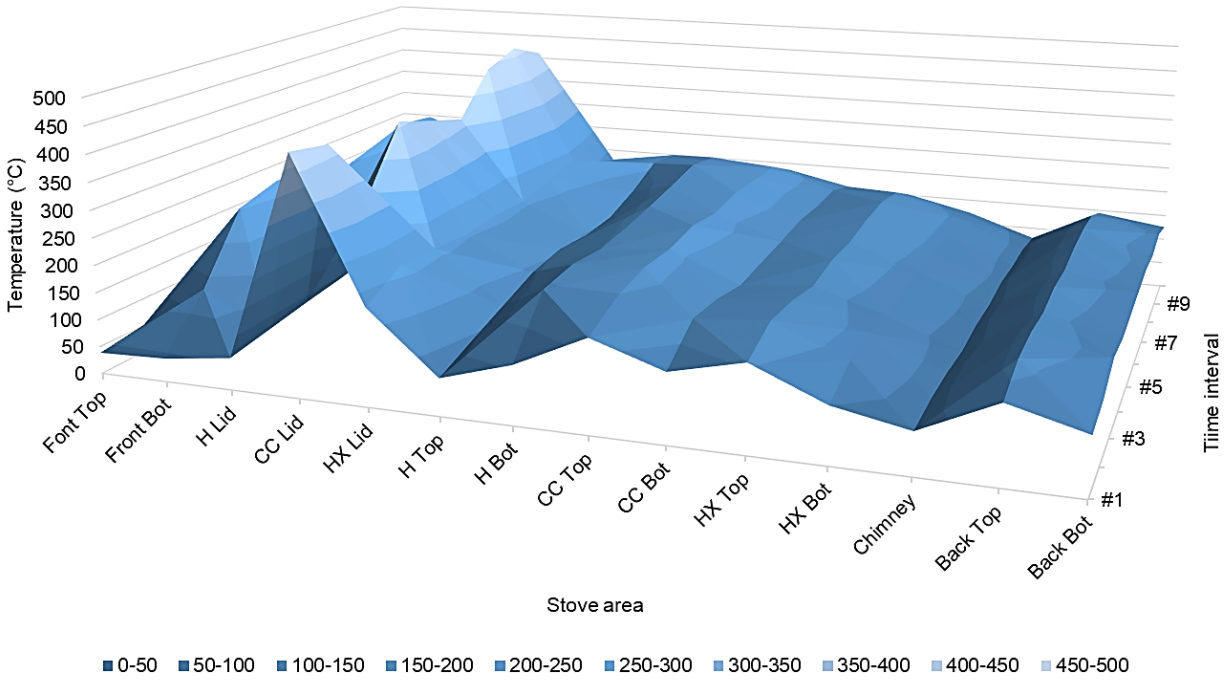

Figure 5-7: Pyrometer temperature results for different stove external surface areas.

The largest temperatures were reported for the combustion chamber lid, followed by the heat exchanger lid. This is the intent of the coal stove since these areas are used for cooking and simmering respectively. Furthermore, the high surface temperatures reported for the front of the stove, in contrast with the hopper bottom and combustion chamber bottom areas, are mainly due to the absence of refractory material around the air inlet region and where the grate handle is located. This results in high surface temperatures directly where the combustion zone propagation occurs. The high surface temperature in this area is only beneficial for living space heating and can potentially provide a hazard for the stove user. Finally, the surface temperatures for the hopper top and lid areas increase as the run progresses, while the total combustion energy output decreases. This is due to the hopper's internal temperature that increases as the hopper empties, in contrast with the decreasing combustion rate that impacts the energy output of the other stove areas.

5.2 THE INFLUENCE OF FUEL TYPE, PSD, AND POWER SETTING.

This section examines the influence of fuel characteristics, PSD, and stove power settings. Key measured parameters, processed data, and selected calculation results are provided and compared across runs. The observations and performance findings from Section 5.1 remain valid for all stove-fuel combinations and are not reiterated here. Instead, comparisons are made between different experiments, referencing these observations and characteristics.

5.2.1 Performance comparison of fuel characteristics

5.2.1.1 Combustion performance

The mass loss rates and normalised combustion rates on an ash free basis (a.f.b.) of the high-power runs using fuel of size range -19 mm +13.2 mm are displayed in Figure 5-8. The averaged combustion related parameters, including the averaged time between grate shakes, are illustrated in Table 5-1.

The initial mass of the runs, seen in Figure 5-8 A (y-axis intersect) and Table 5-1, varies based on packing density. The P-5-W run displayed the highest initial starting mass. This is due to fuel's high bed density as per the discussion in ANNEXURE B. The same is true for lump coal run, which also displayed a high packing density when compared to the other fuels. A higher initial mass was further found when a large volume of coal fines was present in the fuel. This was the case for the binderless pellets as indicated in Table 5-1. Due to the absence of a binding agent in this fuel, more fines formed during handling and loading, and therefore a significantly higher initial mass was obtained. This correlates with the poor combustion efficiency seen in Table 5-1, which was the lowest out of all 6 runs. This poor combustion efficiency is also visually displayed by the ash free mass fraction at the end of the run in Figure 5-8 B. The low combustion efficiency was caused by fines bypassing the grate and settling on the ash tray without combusting. Finally, the initial mass of the experiments was also impacted by the effectiveness of the ignition phase. If a poor ignition occurred, more unburnt wood kindling was present by the time the hopper was loaded. Since wood has a lower density than coal, the initial mass was found to be lower than expected.

Table 5-1: Combustion parameters of high-power runs with fuel size -19 mm +13.2 mm.

	Initial mass	Run length	Grate shakes	Time between shakes	Average combustion rate	Combustion efficiency
	kg	*hr*	-	*hr*	*kg/hr*	-
C	6.69	4.62	11	0.42	0.96	0.84
P-B	6.77	7.39	8	0.92	0.55	0.81
P-2.5	6.38	4.64	6	0.77	0.91	0.91
P-2.5-W	6.42	5.57	6	0.93	0.77	0.91
P-5	6.54	4.94	6	0.82	0.89	0.89
P-5-W	6.83	4.50	7	0.64	0.82	0.89

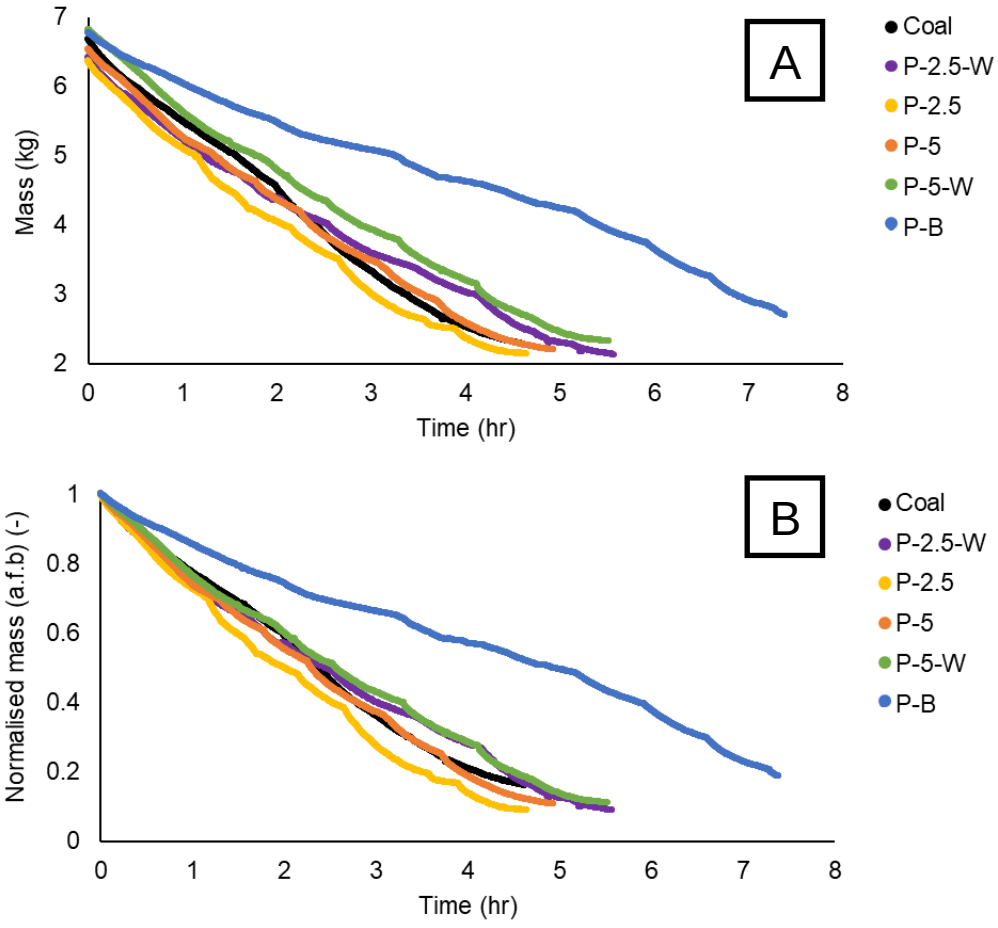

Figure 5-8: Combustion mass loss per time of high-power runs with fuel size -19 mm +13.2 mm: (A) as measured and (B) normalised & ash free basis.

The run length, which can be seen on the x-axis of Figure 5-8 as well as in the second column of Table 5-1, directly correlates with the combustion rate of the respective runs. In addition, the gradient of the graphs in Figure 5-8 A relates to the overall combustion rate displayed in Table 5-1. The binderless pellets exhibited the longest run length, as well as the lowest combustion rate when compared to the other fuel batches. This is mainly attributed to the absence of a binding agent. Normally binding agents improve the structural integrity of coal agglomerates, leading to more efficient and uniform combustion [81]. This finding correlates with literature where it was found that PVA binders improved the ignition and combustion of agglomerates, and accelerated combustion rates [56].

The combustion rate is not only dependent on the intrinsic characteristics of the fuel but also on the extent of grate shakes. When considering the steep slope of the yellow trend (P-2.5 mass loss) in Figure 5-8 A, the P-2.5 run exhibited the highest transient combustion rate. However, according to the average combustion rates displayed in Table 5-1, the lump coal showed the highest overall combustion rate. This is attributed to the lump coal displayed the worst ash settling ability and needed 60% – 80% more grate shakes than the agglomerated fuel as seen in Table 5-1. The grate shakes also cause unburnt fuel to settle onto the ash tray. Therefore, more grate shakes usually result in lower combustion efficiencies as unburn fuel bypasses the grate. This explains the higher average combustion rate and lower combustion efficiency of the lump coal when compared to the PVA binder pellets. This is further supported in Figure 5-8 A, where the lump coal and P-2.5 pellets showed similar final masses despite the lump coal run that started with approximately 300 grams more fuel.

The pellet batches without waterproofing (P-2.5 & P-5) displayed similar combustion rates to the lump coal run. These runs also exhibited a better ash settling ability and consequently fewer grate shakes were required. No significant correlation is observed between the amount of binder in the fuel and the respective combustion rates. However, the batches without a waterproofing agent displayed higher combustion rates than the fuel with a waterproofing agent. The clear distinction between the waterproofed pellets, and non-waterproofed fuel is visible in Figure 5-8. Since little is known about the chemical properties of the waterproofing agent, it can be possible that these chemicals act as an ignition retardant or contribute to the surface diffusion and mass transfer limitation of the combustion reaction.

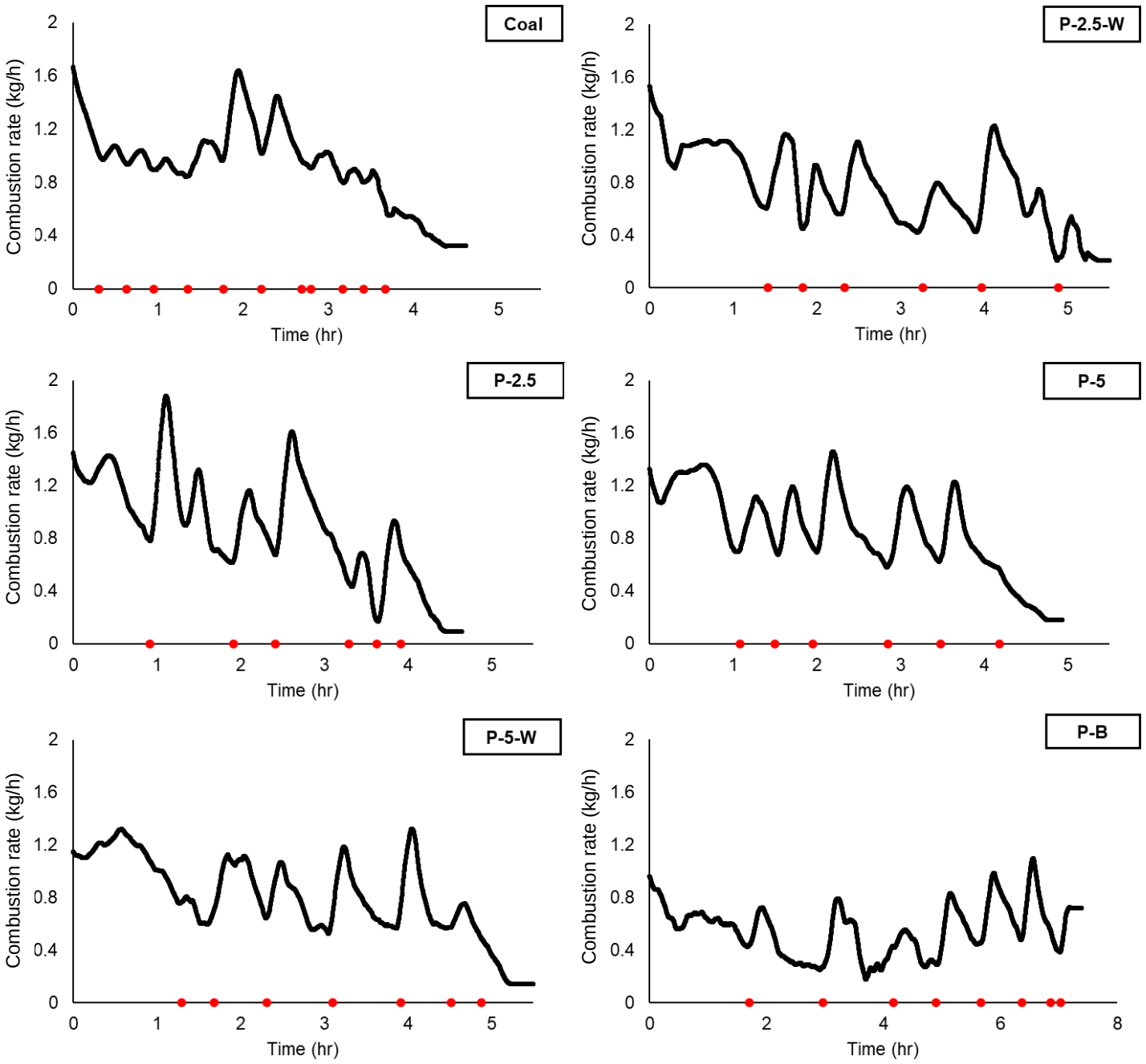

Figure 5-9: Combustion rates of high-power runs with fuel size -19 mm +13.2 mm.

The transient combustion rate for the different fuel batches during the high-power runs is displayed in Figure 5-9. The magnitude of the combustion rate spikes after grate shakes indicate the extent of the ash formation during combustion. Clinkers and dead zones can be removed using grate shakes with greater force, but the increased severity of these shakes increases the degree of ash segregation and therefore results in a steep combustion rate increase. Severe spikes as seen for the P-2.5 run suggests the presence of ash slag or clinkers in the combustion zone. After the P-2.5 run ended, large clinkers were found at the bottom of the hopper chamber

and underneath the stove bridge. These clinkers are disadvantageous to the operation of the coal stove since it prevents ash settling through the grate and hinders the flow of fuel from the hopper to the combustion chamber. In addition, these clinkers prevented the last remaining fuel from combusting and therefore contributed to the combustion inefficiency of this run. In Figure 5-9 it is further illustrated that the P-2.5 run exhibited the highest combustion rate variability compared to the other runs, which is a direct result of the clinker formation. In contrast, the lump coal exhibited the least combustion rate fluctuations compared to the other fuel batches.

The frequent grate shakes performed during the lump coal run resulted in a more stable combustion rate since the effect of ash holdup was reduced. As previously mentioned, the lump coal run also exhibited poor ash settling. This is due to the structure and high mechanical strength of the remaining material on the grate, post combustion. Consequently, the combustion rate of the coal immediately and rapidly decreased after ignition and a grate shake was required in the first 20 minutes after the hopper was filled. In contrast, the pellet fuel showed an improved ash settling ability and maintained stable combustion rates for 1 – 2 hours after the hopper was loaded. After 1 – 2 hours, dead zones formed on top of the grate which necessitated grate shakes.

In Figure 5-9 it can be seen that the lump coal showed the highest average combustion rate while the binderless pellets showed the lowest. This agrees with the discussion following Table 5-1. The binderless pellet run maintained a linear transient combustion rate, unlike the decreasing trend observed in the other five runs. It also exhibited the highest final combustion rate. The absence of a binder led to excess fines and easier fuel fragmentation, causing some fuel to bypass the grate during operation. This bypassed fuel likely combusted in the ash tray at the end of the run. At the end of the run, minimal combustion occurred on top of the grate, and ash transfer to the ash tray was reduced compared to during operation. This lack of ash settling allowed the top layer of unburnt fines to combust, resulting in a high combustion rate at end-of-run conditions. In Figure 5-9 it can also be seen that the final grate shake of a run usually does not influence the combustion rate, since little combustible fuel is left on the grate. However, clinkers can create an obstruction between remaining combustible fuel and the main combustion zone. When the final grate shake is conducted, this obstructed is removed and the last portion of fuel can therefore be reintroduced to the combustion zone, increasing the temperatures and the end of run combustion rate. This is apparent at the end of the P-2.5-W run when a small combustion rate spike is observed after the final grate shake. No significant correlation could be identified between the amount of PVA added to the pellet batches and the respective transient combustion rates in Figure 5-9.

5.2.1.2 Thermal performance

The thermal data of the experiments are collected by the stove internal thermocouples (TT 301-315). In Table 5-2, stove internal temperatures are displayed for high-power runs using fuel of size range -19 mm +13.2 mm. A key temperature of each chamber is displayed based on the significance thereof. The following areas and corresponding temperatures were chosen:

- The primary solid phase combustion zone. These are observed as the hopper bottom (TT305) and combustion chamber (CC) bottom (TT305) temperatures.
- The secondary gas phase combustion zone. This temperature is observed as the combustion chamber middle temperature (TT307).
- The heat transfer area. This temperature is observed as the heat exchanger (HX) middle temperature (TT311).
- The stove outlet. This temperature is observed as the chimney temperature (TT301).

Table 5-2: Average internal temperatures of the semi-continuous coal stove during high-power runs with fuel size -19 mm +13.2 mm.

	Hopper bottom *TT305*	**CC bottom** *TT309*	**CC middle** *TT307*	**HX middle** *TT311*	**Chimney** *TT301*
	°C	*°C*	*°C*	*°C*	*°C*
C	760	760	800	300	180
P-B	940	630	630	200	120
P-2.5	950	750	700	270	170
P-2.5-W	920	650	670	240	150
P-5	870	730	700	260	160
P-5-W	900	750	700	260	160

From Table 5-2, it is seen that the lump coal displayed the lowest average hopper chamber bottom temperature, and the highest CC bottom temperature in contrast with the coal pellets. This observation highlights the fundamental difference in combustion between the lump coal and the coal pellets. The lump coal combustion occurs mainly in the combustion chamber area, whereas the coal pellet combustion mainly occurs in the hopper chamber area. This might be attributed to various factors including grate shakes, ash settling ability, clinker formation, combustion zone propagation rate, bed permeability, etc. It is possible that the clinkers, which only formed during pellet runs, hindered combustion in the combustion chamber area. It is also possible that the high number of grate shakes for the lump coal run maintained the combustion at the bottom of the combustion chamber for longer time periods as illustrated in Figure 5-3.

The poor ash settling ability of the lump coal increases the labour required to operate the stove, when compared to the agglomerated fuel. However, the resulting low combustion zone propagation rate ensures that more oxygen is available for gas phase combustion which aids emission reduction. The improved gas phase combustion is evident from the high temperature reported in Table 5-1 for the combustion chamber middle temperature of the lump coal run. However, in Section 3.3.1 it was reported that the lump coal contained the highest amount of volatile matter. The combustion of these volatiles may also have contributed to the high combustion chamber middle temperature. The binderless pellets exhibited both the lowest CC bottom and CC middle temperatures, while also having the second highest average hopper bottom temperature. This indicates that combustion mainly took place in the hopper instead of in the combustion chamber, which is not ideal for cooking and heating. No significant correlation could be observed between the average combustion zone temperatures and the quantity of binder added to the fuel or the addition of waterproofing. Finally, the chimney temperature can also be seen in Table 5-2. The lump coal run exhibited the highest chimney temperature. This implies higher stack losses compared to the other runs. In contrast, the lowest chimney temperature was reported for the binderless pellets. All four PVA binder fuel batches showed a stack temperature of approximately 155 ± 10 °C, which indicates that no significant correlation between the amount of binder or the addition of waterproofing and the respective chimney temperatures could be found. The stack temperatures reported in Table 5-1 are also comparable to literature cited values of 150 °C to 200 °C [21].

In Figure 5-10, the hopper bottom and combustion chamber bottom temperatures that represent the combustion zone are displayed. The combustion zone ignition time is described in the literature as the time taken for the core temperature of the fuel bed (TT305 and TT309) to reach 500 °C [21]. In Figure 5-10, both lump coal and coal pellets ignite within the first 30 minutes after the start of the run. The lump coal bed reached 500 °C approximately 20 minutes into the run, while the coal pellets reached this temperature within 10 to 15 minutes. The only exception was the P-2.5-W run, which required approximately 25 minutes to reach this temperature. Both the lump coal and coal pellets' ignition times are significantly faster than what is reported in literature. Ignition times of approximately 25 to 50 minutes for lump coal and 25 to 30 minutes for LSF, using LPG as an ignition source was reported [21], [39]. The significantly faster ignition times shown in Figure 5-10 are primarily due to the effective ignition SOP discussed in Chapter 4.1, which was developed from extensive trial and error during preliminary stove testing. Additionally, the packing density and increased packing factor of the pellet batches likely improved the combustion zone propagation rate, thereby reducing the ignition time compared to lump coal. It is also proposed by Sumbane-Prinsloo [21] that increased porosity results in the possible increased absorption of O_2 which might explain the fast ignition of coal pellets.

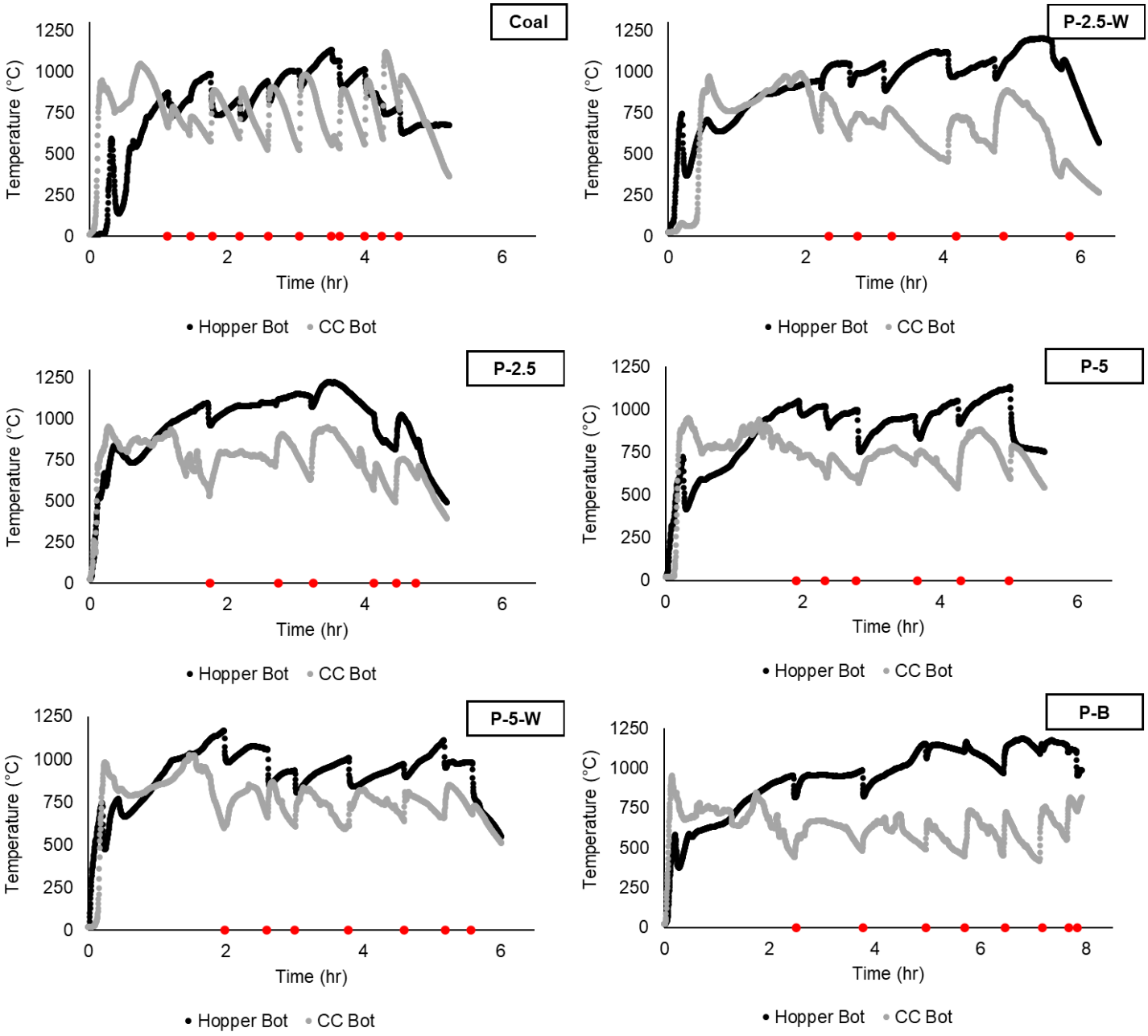

Figure 5-10: Combustion zone temperatures of high-power runs with fuel size -19 mm +13.2 mm.

The extent of ash formation can be seen by the variability of the combustion zone temperatures. The lump coal run displayed the largest temperature fluctuations in Figure 5-10 despite having a stable transient combustion rate as indicated in Figure 5-9. When comparing the temperature fluctuations with the transient combustion rate fluctuations (Figure 5-9), a relatively small change

in combustion rate results in large temperature fluctuation. The main reason for this phenomenon is the calorific value of the lump coal. The lump coal had the highest energy content of all the fuel batches, therefore a fluctuation in its combustion rate will have a greater impact on the combustion zone temperatures. The effect of clinkering and dead zone formation can also be seen in Figure 5-10 by the magnitude of the gradient declines between temperature spikes. Such a dead zone was present during the P-2.5-W run at 4 hours. The stable temperatures of the pellet baches prior to the first grate shake supports its improved ash settling ability relative to lump coal. The binderless pellet run showed the largest difference between its two combustion zone temperature profiles when compared to the other runs in Figure 5-10. This might be attributed to pellet fragmentation during the run and the resulting increased contact area for combustion zone propagation. When the hopper bottom temperatures of the pellet batches are considered, multiple instances occurred where the temperatures exceeded 1100 °C. This is significantly higher than what is reported in literature, where a peak combustion temperature of 761 °C and 836 °C are reported for a domestic stove burning lump coal and LSF respectively [21], and 900 °C for a BLDD clean burning coal stove [75]. These instances are likely where the ash fusion temperature is reached and clinkers form.

After the first grate shake was performed, a water boiling test was conducted for each run. The results of this test can be seen in Table 5-3 for all the for high-power runs using fuel size -19 mm +13.2 mm. From Table 5-3, the time to boil as well as the combustion energy generated can be seen. These parameters translate to the cooking power and the cooking efficiency, which is also displayed in the table.

Table 5-3: Water boiling test results for high-power runs with fuel size -19 mm +13.2 mm.

	Time to boil	**Cooking power**	**Cooking efficiency**
	min	*kW*	*%*
C	18	0.64	5.5
P-B	83	0.13	3.4
P-2.5	17	0.57	4.5
P-2.5-W	26	0.38	4.6
P-5	17	0.59	8.3
P-5-W	23	0.44	4.2

The lump coal run displayed a similar time to boil than the PVA pellet runs without waterproofing. The lump coal run also displayed the highest cooking power compared to the other runs. In addition, the lump coal run displayed the second highest cooking efficiency, where approximately 5.5% of the energy generated by combustion was transferred to the water pot during the test. Both the higher cooking power and cooking efficiency is likely caused by the location of the lump

coal combustion zone, which was directly underneath the cooking area in contrast to the pellet runs. The lump coal run displayed the highest average combustion chamber middle temperature (as seen in Table 5-2), so more energy was transferred from the hot flue gas to the upper cooking surface. This facilitated a high energy transfer rate from the cooking surface to the water pot as later shown in Figure 5-12. In contrast, the water boiling test for the binderless pellet run had the longest time to boil, the lowest cooking power and the lowest cooking efficiency. This is due to the low combustion rate during this run, as well as the location of the combustion zone. Since the binderless pellets mainly combusted at the bottom of the hopper, greater energy losses to the front and sides of the hopper occurred. This is evident by the lower combustion chamber middle and bottom temperatures of the binderless pellet run displayed in Table 5-2. When the PVA binder pellet runs are considered, it can be seen that the experiments using pellets without waterproofing (P-2.5 & P-5) displayed a greater cooking power than runs with waterproofing (P-2.5-W & P-5-W). This directly correlates with the combustion performance and temperature profiles of these runs, as discussed previously. In addition, the water boiling test during the P-5 run required 40% less energy than the other PVA binder pellet runs. Therefore, this run exhibited the highest cooking efficiency as 8.3% of the energy generated during the test was transferred to the water pot. Similar to the lump coal, this is due to the respective combustion mechanisms and the primary location of the combustion zone. At the time of the water boiling test, both the char combustion zone and gas phase combustion zones were well established, which aided the efficient transfer of energy to the cooking surface. Finally, when compared to a typical domestic coal stove burning lump coal, it was found that the stove-fuel combinations exhibited similar cooking power values. However, a maximum cooking efficiency of 2.58% was reported for the Dover™ domestic stove burning lump coal [21], which is significantly lower than that reported in Table 5-3.

Thermal performance parameters for the different runs are displayed in Table 5-4. In this table the following results are displayed: The stove power ratings are given as fired power (P_F) and as delivered power (P_D) via radiation and free convection. This is followed by the stack loss efficiency (η_{SL}), the energy delivered efficiency (η_D), and finally the stove overall thermal efficiencies (η_{tot_1} and η_{tot_2}). These overall thermal efficiencies are calculated from 1) the delivered energy and 2) the overall energy losses as per Equations E-26 and E-27 respectively. The calculated average chimney flow rate ($\bar{V}_{chim}$) is also included in this table to correlate the stack loss efficiency with. All the parameters shown in Table 5-4 are defined and elaborated on in Annexure E.6.

Table 5-4: Thermal performance parameters for high-power runs with fuel size -19 mm +13.2 mm.

	P_F	P_D	η_{SL}	η_D	η_{tot_1}	η_{tot_2}	$\overline{V}_{chim}$
	kW	*kW*	*%*	*%*	*%*	*%*	*m^3/hr*
C	8.0	6.6	87.8	82.4	69.2	73.1	20.1
P-B	4.2	3.5	92.0	82.5	67.1	61.7	9.2
P-2.5	6.9	5.8	89.6	84.1	76.6	78.3	16.0
P-2.5-W	5.9	4.7	89.6	79.2	72.1	77.6	15.4
P-5	6.7	5.5	89.6	82.7	73.8	77.7	15.5
P-5-W	6.2	4.8	90.3	77.6	69.0	76.7	14.0

η_{tot_1} *is calculated using the energy delivered via conduction and radiation approach (Equation E-26).*

η_{tot_2} *is calculated using the stack loss approach (Equation E-27).*

The lump coal run exhibited the highest power rating when compared to the coal pellets. This is partly due to its higher calorific value, combustion rate, and the formation and location of the combustion zones. The power rating of the lump coal run correlates with the cooking power presented in Table 5-3. In contrast with the lump coal, the binderless pellet run exhibited the lowest power rating. This is mainly due to the low overall combustion rate. Since the combustion rate is correspondent to the combustion energy release rate, a lower power rating for the binderless pellets is observed. When considering the PVA binder pellet runs, the stove power rating was higher when no waterproofing agent was present in the fuel. This corresponds to the cooking power results given in Table 5-3. The fired power output of the stove-fuel combinations reported in Table 5-4 is similar to that reported for the TJ4.0 (semi-continuous) cross-draft cookstove. Altanzul [40] reported a fired power of 3.5 kW to 6.5 kW with similar combustion rates and fuel CVs as shown in this study. A fired power rating of 6.5 kW to 8.0 kW was also reported for a household *Imbaula* stove [94], and 4 kW for a BLDD clean burning stove. Therefore, the reported power output of the stove-fuel combinations in Table 5-4 is on par with both traditional and improved combustion appliances.

When considering the thermal efficiencies in Table 5-4, the lump coal run did not display greater efficiencies that the pellet runs. Even though the largest power rating was obtained for the lump coal run, the thermal efficiencies are normalised for fuel calorific value, and therefore comparable between runs. The binderless pellet run showed a greater stack loss efficiency, while the PVA binder pellet runs displayed greater delivered and total efficiencies than the lump coal run. The lump coal run exhibited higher gas temperatures compared to the other fuels. The higher

temperature resulted in a greater thermal buoyancy which increased the pressure gradient between the inlet and outlet of the stove. This increased the natural draft of the stove during the lump coal run which is evident from the high chimney flow rate in Table 5-4. The higher natural draft ensures oxygen availability and complete combustion, but results in a lower stack loss efficiency as seen for the lump coal experiment. Hence, a trade-off between emissions performance and thermal efficiency was identified. The low combustion efficiency of the lump coal run as shown in Table 5-1 also contributed to the relatively lower overall thermal efficiency. The energy losses due to combustible matter is the ash was greater for the lump coal than the PVA binder pellet runs. Therefore, the combination of the stack losses and combustion losses resulted in the lower overall thermal efficiency.

The binderless pellets' run exhibited the lowest chimney flow rates and flue gas temperatures (Table 5-2). This relates to lower stack losses, and therefore the binderless pellet run exhibited the highest stack loss efficiency. Similar to what was found for the lump coal run, due to the low combustion efficiency the binderless pellet run displayed the lowest overall energy efficiency. The pellets with waterproofing displayed a higher stack loss efficiency than the pellets without waterproofing. These losses correlate with the average chimney flow rate where the P-2.5 and P-5 runs showed higher flow rates than their counterparts. The lower flowrates observed for the waterproofed fuel are likely a result of the effect of the waterproofing agent on the combustion mechanism and temperatures as discussed previously. This is further observed when both the delivered efficiency and overall thermal efficiency values are considered. Higher efficiencies were calculated for the non-waterproofed fuel runs, than the experiments where waterproofed fuel was used. This again highlights that that the waterproofing agent negatively impacted the stove thermal performance. When compared to literature, it was found the results reported for the stove-fuel combinations in Table 5-4 are comparable to that of the TJ4.0 cross-draft stove. Stack loss efficiencies of 90.7% to 93.1% was reported for lump coal and semi-coked coal briquettes respectively [40]. Finally, the delivered and overall efficiency results suggest a correlation between the quantity of binder added and the performance of the stove-fuel combination. The 2.5% PVA binder displayed higher efficiency values than the 5% PVA binder fuel, irrespective of waterproofing. In comparison with the other runs, the P-2.5 run exhibited the highest delivered efficiency and overall stove efficiency, while maintaining the lowest stack loss efficiency.

The stove energy produced, energy delivered, and heating efficiency are displayed in Figure 5-11 for each 30-minute measurement interval as determined from the surface temperature measurements during the runs.

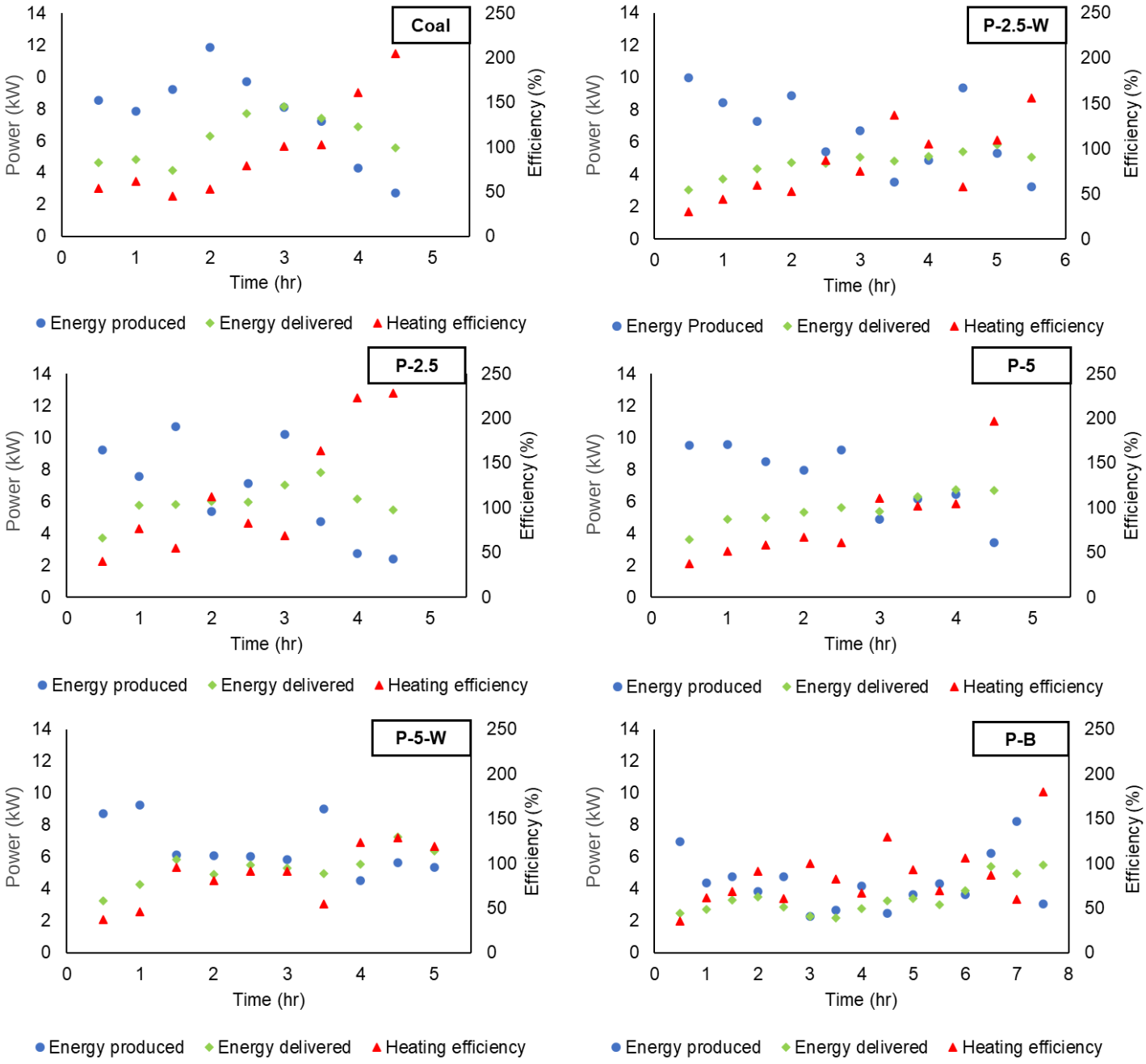

Figure 5-11: Energy produced, energy delivered, and heating efficiency for high-power runs with fuel size -19 mm +13.2 mm.

The lump coal run demonstrated an increase in heating efficiency over the course of the run which eventually exceeded 100%. At the start of the run the combustion energy is used for pyrolysis and to heat the fuel and cold surfaces of the stove. Therefore, the delivered energy is lower during this phase. Later in the run, the energy efficiency exceeds 100% since the energy delivered exceeds the energy produced. At this point, the combustion rate declines but heat from the

surfaces of the stove continuously dissipates to the environment. In Figure 5-11, the P-2.5 and P-2.5-W runs had the largest variability in thermal performance. This is due to the larger variance of the 2.5% PVA pellet combustion rates and the clinkering as discussed previously. Conversely the P-5 and P-5-W runs displayed less variability which is favourable for cooking purposes.

The total energy delivered by the semi-continuous coal stove, as displayed in Figure 5-11, can be further investigated by evaluating the different stove surfaces. The energy delivered by each respective stove surface area is displayed in Figure 5-12, according to the area division given in Section 4.3. The data points shown in this figure are 30 minutes apart correlating with the surface temperature measurements taken during the experiments. In Figure 5-12 it is shown that the combustion chamber lid undergoes the largest energy flux variability. This is caused by its proximity to the combustion zone and combustion products. A slight change in combustion rate or combustion temperature will directly impact the energy delivered by the combustion chamber lid surface. The chimney is the second highest area of energy flux, followed by the front bottom area of the stove. Despite the high energy output of the chimney its internal temperature is the lowest of the entire stove profile. The large energy output is mainly due to the surface area of this part of the stove, which is approximately a factor of 10 larger than the second largest area. The chimney surface area is larger than both sides of the stove combined. In addition, the lack of any refractory or insulating material in the chimney also adds to the relatively higher energy output. For most of the vertical stove surfaces the natural convection remains in the laminar region. This is, however, not true for the chimney since the free convection flow regime is directly proportional to the distance the fluid travels in the vertical axis. As the chimney is approximately three meters tall, the free convection enters the turbulent regime where increased energy transfer occurs.

The lump coal run displayed the highest energy delivered via the chimney which correlates with the stove temperatures give in Table 5-2. The lump coal run also displayed the highest energy delivered for the majority of the stove surfaces in contrast with the binderless pellets that presented the lowest overall energy delivered. The only exception is the areas at the front of the stove, surrounding the air inlet.

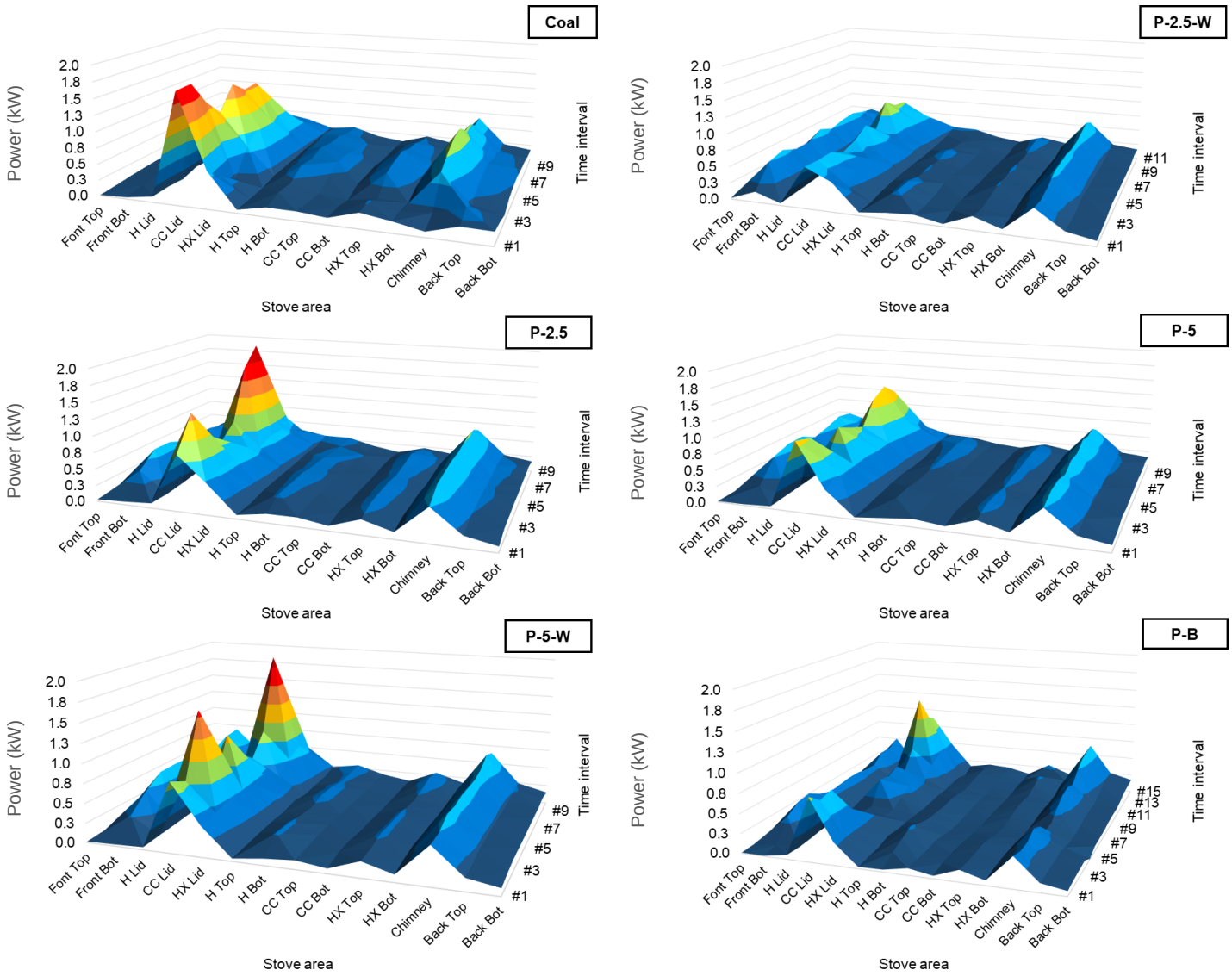

Figure 5-12: Total energy delivered (radiation & convection) from the stove surfaces for high-power runs with fuel size -19 mm +13.2 mm.

The lump coal run displayed the lowest front surface temperature, whereas these are seen to be higher for the pellet runs. This is a result of the lump coal combustion zone that was mainly located in the combustion chamber, unlike the pellet runs which was mainly located at the bottom of the hopper. The high surface energy flux associated with the front of the stove does not contribute to cooking energy, but rather presents a hazard to the stove user when operating the grate. Therefore, the lump coal run displayed favourable behaviour in this regard. The lump coal run, followed by the P-2.5 and P-5 pellet runs exhibited the highest energy delivered from the sides of the stove. Furthermore, the lump coal and P-2.5 runs showed the greatest combustion chamber and heat exchanger lid energy delivered. When considering the lump coal energy profile, it can be seen that the energy delivered from the combustion chamber lid during the water boiling test

period was the highest compared to the other runs. This is reflected in the cooking power of the lump coal as discussed previously.

5.2.1.3 Emission levels

The pollutant levels of the high-power runs using fuel with a size range of -19 mm +13.2 mm are given and discussed in this section. The interdependencies between the CO_2, O_2 and CO levels can also be seen in Figure 5-13.

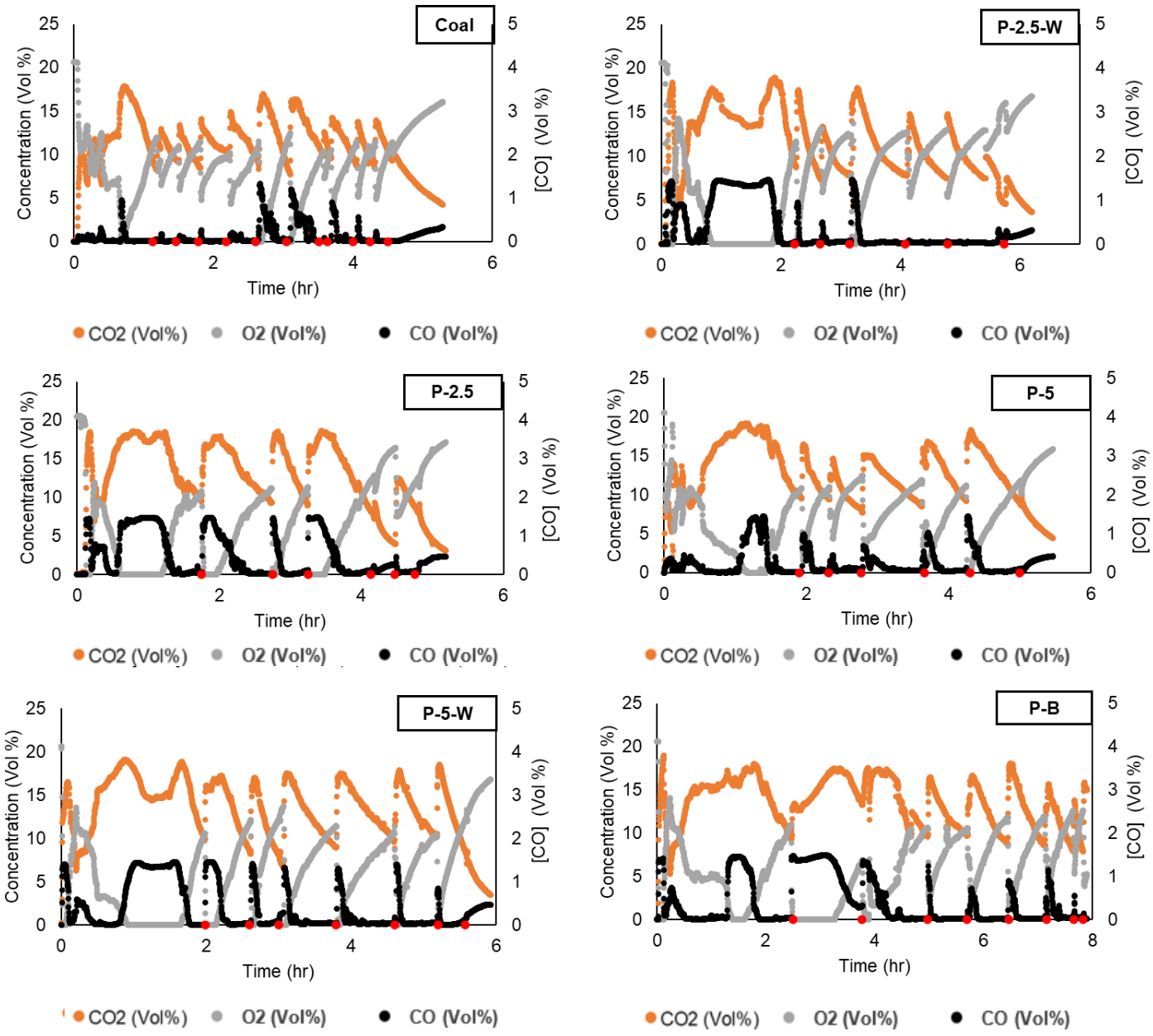

Figure 5-13: Carbon oxides and oxygen concentrations in the flue gas of high-power runs using fuel size -19 mm +13.2 mm.

Due to the primary combustion reaction of fuel, there exists a direct correlation between the oxygen and carbon dioxide levels. The proportionality of this correlation is described by the stoichiometric constants in the combustion reaction, which is 1:1. Therefore, in Figure 5-13 it can be seen that the change in O_2 levels is mirrored by the change in CO_2 levels. The high O_2 and low CO_2 levels at the end of the respective runs are due to the incomplete combustion caused by smouldering. The only exception is the binderless pellet run in Figure 5-13 that still exhibited high CO_2 levels at the end of the run. This is due to the high combustion rate of the P-B pellets at end-of-run conditions as discussed at the end of Section 5.2.1.1.

The initial CO_2, O_2 and CO trends of all runs in Figure 5-13 indicate the propagation of the combustion zone post ignition as per the discussion below Figure 5-5 in Section 5.1. This occurrence led to an extended period of oxygen deficiency for the pellet runs. In addition, the CO_2 trend of the fuel with waterproofing (P-2.5-W and P-5-W) exhibited an irregular “M” shape before the first grate shake. Since the waterproofing agent may be acting as a combustion and ignition retardant, it can cause a cold ignition phase as shown in Figure 5-3. The “M” shape of the CO_2 concentration seen in these runs are indicative of oxygen limitation resulting in combustion rate limitation and a decline in stoichiometric α value.

As described in Chapter 5.1, an important component of the CO_2 and O_2 interaction is the formation of CO. To compare the CO emission levels of the respective high-power runs, the mass flow rate of this pollutant is displayed in Figure 5-15. The proximity of grate shakes to the CO emission spikes is indicated in Figure 5-15. It is seen that waterproofed pellets displayed larger initial CO spikes, before the first grate shake when compared to the non-waterproofed pellets. In addition, the 2.5% PVA pellets showed larger initial CO spikes than the 5% PVA pellet batches. The CO spikes of the P-2.5 run after grate shakes also remained for longer durations. Hence, the CO emission spikes scaled with the amount of binder added to the fuel, and the addition of waterproofing. The lump coal run exhibited the lowest average CO levels followed by the P-5 run and P-B run. Furthermore, the increasing chimney CO mass flow rate at the end of the runs in Figure 5-14 can be attributed to the smouldering combustion regime.

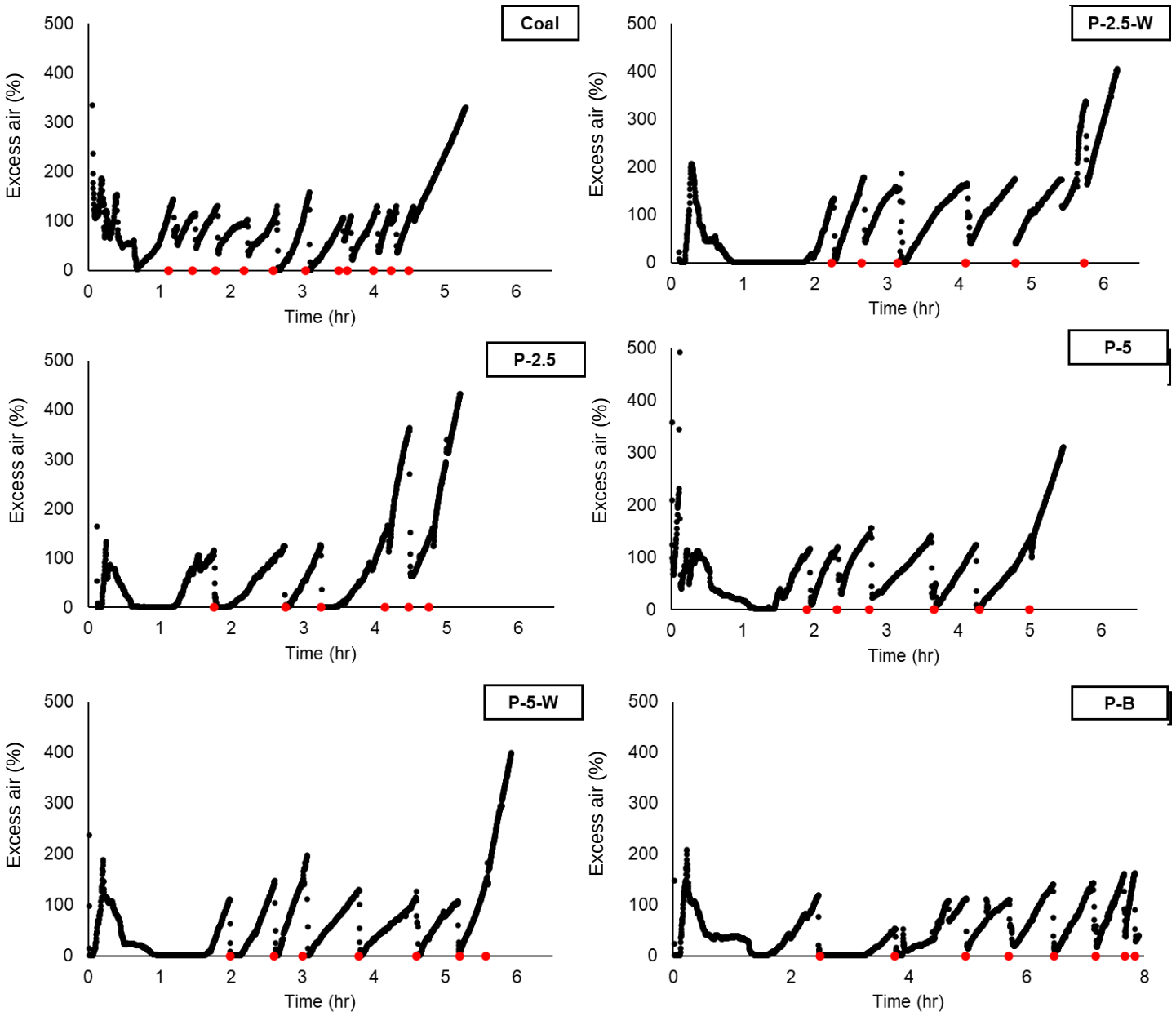

Figure 5-14: Excess air in the flue gas of high-power runs using fuel size -19 mm +13.2 mm.

Based on the previous discussion it was found that excess air is one of the most critical parameters to monitor in the pursuit of low emission levels. The calculated excess air levels of the respective runs can be seen in Figure 5-14. The operation of grate shakes was difficult to standardise due to the trade-off between the ash and dead zone removal, and the lower limit of the excess oxygen levels. Vigorous grate shakes caused excess air drops to the point of oxygen starvation which increased some pollutant levels.

The excess air after the grate shakes during the lump coal run remains above 0.5% which ensures sufficient oxygen availability for both phases of combustion. The lump coal and P-5 pellet runs exhibited the smallest excess air decrease before the first grate shake. Most of the pellet runs exhibit excess air levels close to the 0% mark after grate shakes, which contributes to the high emissions levels. It was also found that the excess air was negative at some instances, where insufficient oxygen was available for complete combustion to CO_2. These instances correlate with the “M" shape of the CO_2 graph in Figure 5-13. The P-B pellet run showed several low excess air instances and remained at 0% for an extended period after the first grate shake as well. The low excess air levels after grate shakes during the PVA pellet runs are likely due to the increased ignition and combustion propagation rates of the pellets. In addition, at approximately 220 °C the PVA binder decomposes [95]. The resulting mechanical brittleness decreased the combustion bed voidage, resulting in less air and O_2 permeation for gas phase combustion. This is supported by the observations made during the P-2.5-W run, where moderate clinker formation assisted combustion, instead of negatively impacting the stove performance. As discussed in Section 5.2.1.2, the P-2.5-W run in Figure 5-14 displayed symptoms of ash fusion and clinkering 3 - 4 hours after ignition. A large grate shake at exactly 4 hours resulted in the break-up of ash formations and allowed fuel to once again flow from the hopper to the combustion chamber. Thereafter, it can be seen in Figure 5-14 that the excess air after grate shakes did not drop below 50 vol.% for the remainder of the run, which improved the thermal performance and emissions levels after 4 hours. Furthermore, the moderate clinkers that were still present in the combustion zone after the grate shake increased the bed voidage at the bottom of the combustion chamber and lessened the active combustion zone ensuring air permeation. Upon visual inspection, a large flame was confirmed above the combustion zone for the remainder of the run, which indicates complete gas-phase combustion. The previous phenomena highlight the roll of oxygen availability, bed permeability and voidage, and the combustion zone propagation rate in the pursuit of lower emission levels. The double excess air spikes at the end of the P-2.5 and P-2.5-W runs are symptoms of clinkering. Clinkers prevent a portion of fuel from combusting, which mimics end-of-run conditions but after a severe grate shake the last fuel is freed and combustion continues.

An emissions parameter summary is given in Table 5-5. The summary includes the fraction of carbon that oxidises to CO_2 (α), the average carbon monoxide to carbon dioxide ratio ($CO{:}\,CO_2$), the oxygen balance error (ε_{O_2}), the average chimney velocity ($\bar{v}_{chim}$), the average oxygen correction factor ($\bar{\lambda}$), the dry to wet gas correction factor ($y_{d/w}$), and the volume of water collected from the water traps (V_{H_2O}). The calculation and definition of these parameters can be found in ANNEXURE E.

Table 5-5: Emission parameter summary of high-power runs using fuel of size -19 mm +13.2 mm.

	α	$CO:CO_2$	ε_{O_2}	$\bar{v}_{chim}$	$\bar{\lambda}$	$y_{d/w}$	V_{H_2O}
	-	%	%	m/s	-	-	ml
C	0.989	1.2	3.3	0.7	1.99	0.946	32
P-B	0.973	2.7	5.2	0.3	1.57	0.941	30
P-2.5	0.963	3.8	3.6	0.6	1.87	0.949	38
P-2.5-W	0.969	3.1	5.4	0.5	2.04	0.952	40
P-5	0.982	1.9	2.3	0.5	1.81	0.947	34
P-5-W	0.973	2.9	5.0	0.5	1.71	0.947	38

When considering the α value and the CO:CO_2 ratio, it can be seen that the lump coal run displayed a higher α value and a lower CO:CO_2 ratio than the coal pellets. This corresponds to the data on the carbon monoxide concentration graphs displayed in Figure 5-15. Furthermore, the addition of PVA binder to the fuel did not influence the α value or the CO:CO_2 ratio. When considering the PVA binder pellets, it can be seen that the 5% PVA pellet runs showed a greater α value and a lower CO:CO_2 ratio than the 2.5% PVA pellet run variants. Furthermore, no significant correlation between these parameters and the addition of a waterproofing agent, could be identified. Compared to the CO:CO_2 ratios reported in literature for the TJ4.0 semi-continuous coal stove [40], only the lump coal run exhibited a lower ratio. The other stove-fuel combinations exhibited similar ratios of between 1.9% to 2.9%, while the 2.5 wt.% PVA pellet runs produced significantly higher CO:CO_2 ratios [40]. It was also noted in literature that the lump coal in the TJ4.0 produced a lower CO:CO_2 ratio that the semi-coked coal agglomerates [40], similar to what is shown in Table 5-5. The lump coal and P-5 runs also reported lower CO:CO_2 ratios than what is typically reported for paraffin appliances (ratios of ±2%) [75] When considering the oxygen mass balance error, it can be seen that the P-B, P-2.5-W, and P-5-W runs displayed error values greater or equal to 5%. When considering the excess air levels in the stove as displayed in Figure 5-14, it can be seen that these three runs had the longest periods of oxygen deficiency during combustion. Under oxygen deficient conditions, other combustion products (such as COS) may have been formed. These compounds contribute to the oxygen error since it is not measured for in the stack gas (according to Section 1.3.1).

The average chimney velocity of the high-power runs is also displayed in Table 5-5. The lump coal run showed the highest chimney velocity which correlates with its higher combustion rates and temperature profiles as discussed earlier. In accordance to this, the binderless pellet run exhibited the lowest chimney velocity. All the PVA binder pellet runs exhibited similar chimney velocities. As mentioned in 5.2.1.2, the chimney velocity is linked to the respective thermal profiles in the stove. The average excess air correction factor can also be seen in Table 5-5. An inversely

proportional relationship between the CO:CO_2 ratio and the excess air correction factor was expected since carbon monoxide forms in oxygen-deficient conditions. However, this is not the case. When considering the P-2.5-W run, it displayed the second-highest CO:CO_2 ratio as well as the highest excess air correction factor. Therefore, no significant correlation could be made between the displayed average excess air correction factor, the CO:CO_2 results, and the different fuel characteristics.

The stack gas moisture content and water collected is also shown in Table 5-5. All the reported results are relatively similar, and no significant relationship could be observed between the moisture content of the respective runs. The water vapour fraction of stack gas is a function of the hydrogen and oxygen content of the fuel, in addition to the inherent moisture. Since these parameters were mainly similar between the fuel batches, it can possibly explain why no significant variation in moisture content was observed. Therefore, the addition of PVA binder and the quantity thereof, the addition of waterproofing, and the fuel type showed no influence on the moisture content of the stack gas. The sulphur balance of the respective high-power runs is displayed in Table 5-6. The mass sulphur in the fuel ($m_{S\ Fuel}$), in the ash ($m_{S\ Ash}$) and emitted via the stack gas ($m_{S\ Stack}$) can be seen. The oxidation factor of sulphur to SO_x is also displayed (OF_S), as well as the percentage undetected sulphur species. The calculation methodology and description of these parameters are given in Annexure E-3.

Table 5-6: Sulphur balance for high-power runs using fuel size -19 mm +13.2 mm.

	$m_{S\ Fuel}$	$m_{S\ Ash}$	$m_{S\ Stack}$	OF_S	$Undetected$
	g	*g*	*g*	-	*%*
C	32.7	3.4	23.6	0.72	17.6
P-B	50.8	32.9	17.6	0.35	0.5
P-2.5	49.1	25.7	21.5	0.44	3.7
P-2.5-W	49.4	24.9	19.8	0.40	9.5
P-5	47.7	25.1	21.0	0.44	3.4
P-5-W	47.8	25.6	21.6	0.47	1.2

The lump coal contained the lowest inherent sulphur, while the coal pellets reported similar sulphur levels. When considering the sulphur oxidation factors, the lump coal run emitted the most sulphur, despite starting with the least amount of sulphur in the fuel. This is further supported by the small amount of sulphur that was experimentally found in the ash after the lump coal run, when compared to that of the coal pellets. The order of magnitude difference in total sulphur species between the ash of the lump coal and the pellets may have been due to several reasons:

- The origin of the fuel. Since the lump coal and coal fines originated from different sources, the quantity of sulphur containing organic and inorganic compounds in these fuels may differ. Organic sulphur is more volatile and unstable than inorganic sulphur as indicated in literature [56]. It is therefore possible that the lump coal contained more organic sulphur than the coal fines resulting in a higher oxidation factor.
- The number of grate shakes. The lump coal run was subject to eleven grate shakes whereas only seven or less grate shakes were performed during the coal pellet runs. The higher number of grate shakes may have resulted in inorganic sulphur entrainment in the flue gas, creating large areas for oxidation to occur. Consequently, higher sulphur emissions would be observed.
- The post combustion agglomerate structure. Inorganic sulphur oxidation can occur during combustion and the rate thereof is proportional to the available surface area [91]. It is therefore possible that the physical structure of the coal pellets post combustion, especially the ash fusion products, limits the available area for oxidation of inorganic sulphur (e.g. pyrite) to occur.

The largest percentage of undetected sulphur was determined for the lump coal, followed by the P-2.5-W run. This can be attributed to either the accumulation of measurement errors or to the formation of miscellaneous sulphur species. Some species such COS or H_2S are not analysed for in the stack gas but can form during experimental conditions. Finally, no significant correlation can be made between the results displayed in Table 5-6, and the use of PVA binder, the quantity thereof, or the addition of waterproofing.

The SO_X mass flow rate in the stack for all six high-power runs can be seen in Figure 5-16. It is shown that the lump coal run exhibited a large initial spike of SO_x after ignition. However, the majority of the pellet batches did not exhibit this high initial spike. This once again suggests that the lump coal contained more organic sulphur species than the coal pellets, which oxidised during the devolatilisation phase at the start of the run. This could also be due to the high initial combustion rate of the lump coal run after ignition as discussed earlier. The lump coal run further exhibited the highest average SO_X mass flow rate throughout the run which also agrees with the higher average combustion rate of this run. It is shown in Figure 5-16 that significant SO_x spikes are formed after each grate shake, which only lasts for a few minutes. This can be attributed to the temporary entrainment of inorganic sulphur species in the gas flow, and consequently the direct oxidation thereof [91]. Finally, due to the non-uniform nature of the SO_X flow rate graphs caused by the grate shakes, no significant correlation can be made between these results and the PVA binder pellet batches.

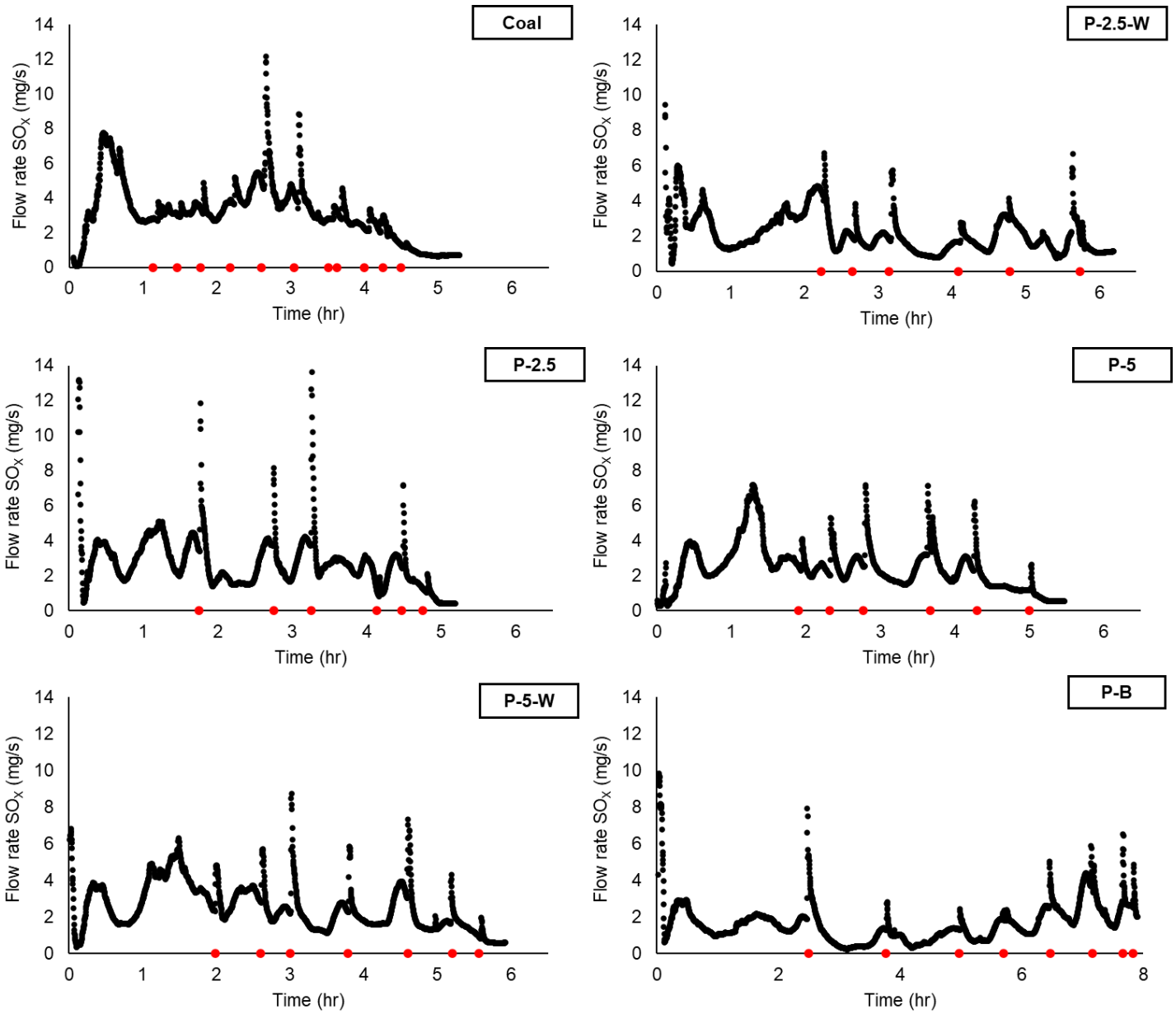

Figure 5-16: Mass flow rate of SOx emissions in the flue gas of high-power runs using fuel size -19 mm +13.2 mm.

The NO_X mass flow rate in the stack gas for all six high-power runs using fuel size -19 mm +13.2 mm can be seen in Figure 5-17. It is shown that all the runs exhibited a large NO_X emission spike at the start of the run. This correlates with the discussion in Section 2.3.4, which highlights the NO_X emissions observed during the initial volatilisation phase. The lump coal run exhibited the largest NO_X emission spike at the start of the run, as well as the largest overall NO_X emission levels throughout the run. This is once again attributed to the higher combustion rate of the lump coal.

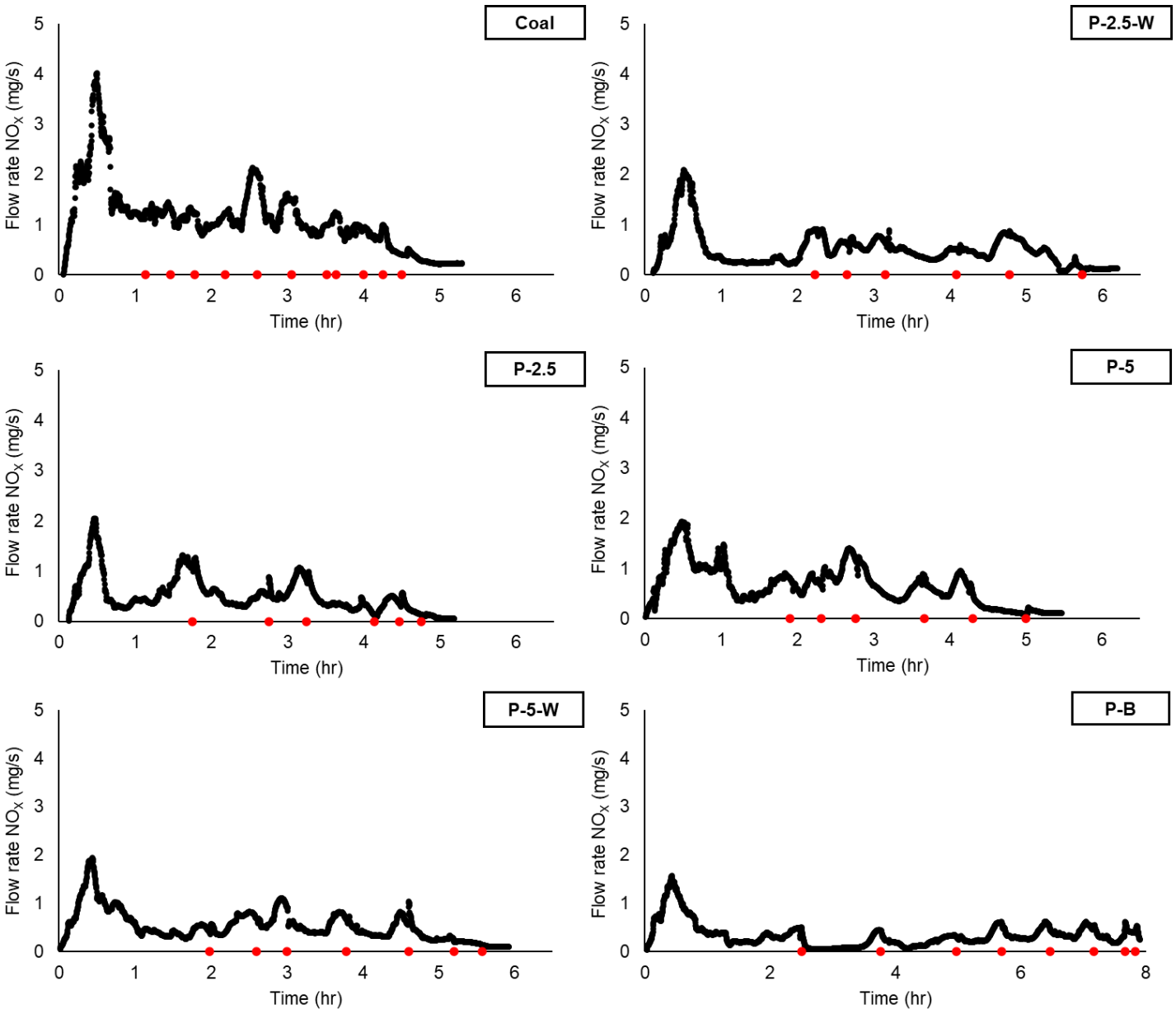

Figure 5-17: Mass flow rate of NOx emissions in the flue gas of high-power runs using fuel size -19 mm +13.2 mm.

In Figure 5-17 it is further shown that the binderless pellet run showed the lowest initial NO_X spike, and this pollutant flow rate remained below 1 mg/s for the rest of the experiment. This is consistent with the previous argument, given that the P-B run exhibited the lowest combustion rate. The effect of the grate shakes can be seen when correlating the shake instances with the peaks of the NO_X emission spikes. The main difference between the impact of grate shakes on the NO_X and SO_X emission levels is the magnitude of the emission spikes after these grate shakes. The NO_X emissions do not spike as significantly as SOx, CO, or PM when these shakes are performed. In addition, the SO_X emissions showed a few minutes of large vertical emission spikes which is not seen in Figure 5-17. All these observations indicate that organic nitrogen is converted during

the increased transient combustion and devolatilisation mechanisms as opposed to the oxidation of inorganic nitrogen. Finally, the addition of PVA or waterproofing agent did not have an impact on the occurrence of NO_X emissions. The PM mass flow rate in the stack gas for high-power runs using a fuel size of -19 mm +13.2 mm can be seen in Figure 5-18.

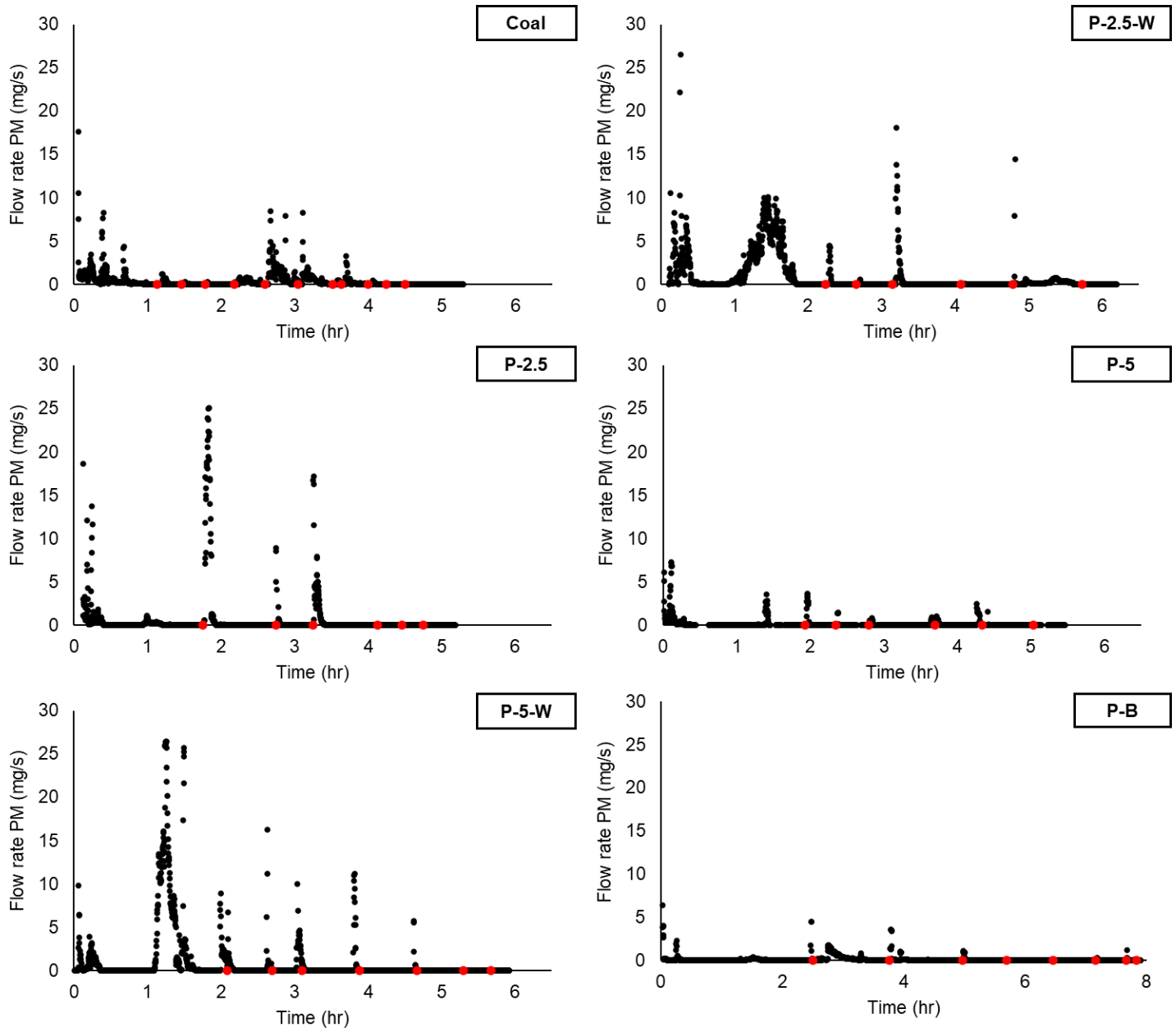

Figure 5-18: Mass flow rate of PM emissions in the flue gas of high-power runs using fuel size -19 mm +13.2 mm.

In Figure 5-18 it can be seen that some grate shakes resulted in major PM spikes. During the instances when no grate shakes were performed, the PM mass flow rate for most pellet runs was less than 1 mg/s. It was observed that vigorous grate shakes resulted in higher PM spikes during the P-2.5 and P-2.5-W runs, where extreme grate shakes were needed to forcefully break large clinkers that formed during the run. This is supported by the P-B run that displayed minimal PM spikes after the grate shakes. During this run, gentle grate shakes were performed due to the brittle nature of the P-B pellets. In addition, the low combustion rate and combustion zone temperatures resulted in minimal ash fusion and clinkers, which improved the ash settling ability. When considering Figure 5-15 and Figure 5-18, it is observed that the PM spikes before the first grate shake during the P-2.5 and P-2.5-W runs correlate with the oxygen deficiency instances. During an oxygen deficiency instances, incomplete gas phase combustion is present which results in the emission of carbonaceous PM. Similar to the CO emission results, the PM emissions decreased once the excess O_2 levels increased above 0.5 vol% post oxygen starvation. Therefore, the magnitude of the PM spikes is not only related to the severity of the grate shakes but also the excess air levels. The lump coal run displayed high PM levels even between grate shakes (as seen 2.5 – 3.5 hours into this run). This can be attributed to the high combustion rate of the lump coal at this point in the run, in combination with the high volatile matter content of the lump coal compared to the other fuel batches. The P-2.5 pellet run displayed higher PM emissions than the P-5 run, however, the opposite is true for the waterproofed pellets. Therefore, no significant correlation can be made between the quantity of PVA binder added and the PM emission level of the respective runs.

The average PM and VOC stack gas concentrations in the flue gas are displayed in Table 5-7. The calculation if these concentrations can be found in ANNEXURE E.

Table 5-7: PM and VOC flue gas concentrations of high-power runs using fuel of size -19 mm +13.2 mm.

	$[PM_{DT}]$	$[VOC]$
	mg/m³	*mg/m³*
C	50	440
P-B	40	170
P-2.5	100	140
P-2.5-W	140	150
P-5	20	110
P-5-W	170	140

The waterproofed fuel runs exhibited the highest average PM emission concentration of all six runs. This might be due to the addition of the waterproofing agent that affected combustion mechanisms as discussed previously. The four remaining runs displayed similar average PM concentrations exiting the chimney. Finally, the average VOC concentration in the stack gas of the respective runs is also shown in Table 5-7. It can be seen that the VOC concentration of the lump coal run was significantly higher than compared to the other stove runs. This can be attributed to the higher volatile matter content of the lump coal, compared to the coal pellets. Among the pellet runs, the binderless pellets displayed the highest average VOC concentration and the P-5 run displayed the lowest. As indicated in literature [40], VOC emissions scale inversely with combustion zone temperature, which supports this finding.

The emission factors for the respective runs are displayed in Table 5-8. In this table, the emission factors for carbon dioxide (EF_{CO_2}), carbon monoxide (EF_{CO}), nitrogen oxides (EF_{NO_x}), sulphur oxides (EF_{SO_x}), particulate matter (EF_{PM}), and volatile organic compounds (EF_{VOC}) are displayed.

Table 5-8: Emission factor summary for high-power runs using fuel size -19 mm +13.2 mm.

	EF_{CO_2}	EF_{CO}	EF_{NO_x}	EF_{SO_x}	EF_{PM}	EF_{VOC}
	g/MJ	*g/MJ*	*mg/MJ*	*g/MJ*	*mg/MJ*	*mg/MJ*
C	93 ± 5	0.67 ± 0.04	120 ± 6	0.36 ± 0.02	37 ± 2	310
P-B	91 ± 4	1.70 ± 0.01	62 ± 1	0.31 ± 0.01	30 ± 1	100
P-2.5	95 ± 4	2.40 ± 0.08	65 ± 2	0.37 ± 0.01	78 ± 3	90
P-2.5-W	94 ± 4	2.00 ± 0.04	72 ± 1	0.33 ± 0.01	120 ± 2	110
P-5	94 ± 5	1.10 ± 0.04	83 ± 3	0.35 ± 0.01	15 ± 1	70
P-5-W	93 ± 5	1.70 ± 0.01	72 ± 1	0.37 ± 0.01	120 ± 1	90

The carbon dioxide emission factors for all the runs are all similar. Since the composition of the fuels is similar, and carbon reacts predominantly to CO_2, a linear relationship exists between the formation of CO_2 and the combustion energy. Only the formation of CO can lower the α value and therefore the CO_2 emission factor . The carbon monoxide emission factor for the lump coal was the lowest of all the batches, followed by the P-5 pellet run. Most pellet runs displayed carbon monoxide emission factors more than double that of the lump coal run. The low carbon monoxide pollutant levels of lump coal are mainly due to the combustion mechanism of this fuel, and the minimisation of oxygen deficiency in the stove during this run. For runs where secondary gas phase combustion is prolonged (P-5 and lump coal), lower CO emission factors can be seen. The highest carbon monoxide emission factor was calculated for the P-2.5 run. This was due to the significant amount of oxygen-deficient combustion instances during this run. Furthermore, the 5%

PVA binder pellets displayed lower carbon monoxide emission factors compared to the 2.5% PVA binder pellets. No significant correlation can be made between the carbon monoxide emission factors and the addition of a binder or waterproofing to pellets.

In contrast to the carbon monoxide emission factors, the lump coal presented the highest nitrogen oxide emission factor when compared to the coal pellets. The effects of NO_X reduction through combustion in a reductive environment, as described in Section 5.1, supports the lower emission factor results reported in Table 5-8. This is facilitated by oxygen deficient conditions and higher CO emission levels, with fuel rich (secondary) gas phase combustion [92]. The NO_X emission factors are directly proportional to the oxygen availability during combustion and indirectly proportional to the residence time and combustion zone temperatures in the stove. In this case, the residence time is related to the natural draft flow rate in the stove. As discussed previously, the lump coal run exhibited high oxygen availability, the highest natural draft flow rate and the lowest hopper bottom temperatures when compared to the coal pellets. Therefore, this run showed the highest NO_X emission factor compared to the other runs. Furthermore, the binderless pellet run presented the lowest NO_X emission levels. During the P-B run, the lowest natural draft flow rate was determined together with elevated combustion zone (hopper bot) temperatures and frequent oxygen deficient periods. Finally, the P-5 run showed the highest NO_X emission factor amongst the pellet batches. This run exhibited a low combustion zone temperature together with sufficient oxygen during combustion, as can be seen in Figure 5-14. However, no significant correlation could be observed between the NO_X emission factors and the quantity of PVA binder present in the fuel, or the addition of waterproofing to pellets.

Despite the high oxidation rate of the sulphur during the lump coal run, the SO_X emission factor remains comparable to the other fuel batches as shown in Table 5-8. This can be attributed to the higher energy delivered by the lump coal when compared to the coal pellets. However, when the emission factors of these batches are considered on a *g/kg* basis (neglecting thermal performance), the lump coal displayed significantly higher SO_X levels than the other runs as discussed previously. In accordance with the previous statement, the binderless pellet run exhibited the lowest SO_X emission factors. No significant correlation can be made between the SO_X emission factors and the quantity of binder added to the fuel, or the presence of a waterproofing agent.

From Table 5-8 no significant correlation between the type of fuel and PM emissions could be identified. The P-5 run exhibited the lowest particulate matter emission levels when compared to all the other fuel batches. In contrast, the P-2.5-W and P-5-W runs displayed the highest particulate emission levels relative to the other high-power runs. This indicates that the addition of a waterproofing agent increased the particulate matter emissions by approximately 400% when

compared to the lump coal and binderless pellets. Since little information is known about the nature of the waterproofing agent, no conclusion was made in this regard.

The lump coal run exhibited the highest VOC emission factor when compared to the other fuel batches as shown in Table 5-8. This can be attributed to the higher volatile matter of the lump coal. All the pellet batches displayed relatively similar VOC emission factors, with the P-5 run exhibiting the lowest. In contrast, the P-2.5-W run displayed the highest VOC emission factor. Similar to the PM emission factors, the waterproofed pellets showed on average a higher VOC emission level than their counterparts. This is mainly due to the combustion temperatures of the respective runs, where the VOC emissions are inversely proportional to the combustion zone temperature as found in literature [40]. No significant correlation can be made between the addition of PVA binder to the agglomerates, the quantity thereof, and the VOC emission factors. The results in Table 5-8 can be compared to literature in which lump coal and low smoke fuel (LSF) was combusted in a domestic *Dover*^{TM} coal stove [38]. When considering the CO emission factors, the results reported in this study are significantly lower than what was reported in literature [38]. Both the SO_X and NO_X emission factors in Table 5-8 is roughly one order of magnitude lower than what was reported for lump coal and LSF combustion in the traditional domestic coal stove. The PM emission factors reported in Table 5-8 is a maximum of one order of magnitude lower than that reported for LSF, and two orders of magnitude lower than that reported for the lump coal [38]. This is mainly due to the operating principal of the semi-continuous coal stove, where separate combustion of char and volatiles occur.

5.2.2 Stove power setting

In Section 5.2.1, the high-power runs were discussed in detail, and a comparison between the performance of the fuel characteristics are made. In this section however, the focus is placed on the comparison between the high- and low-power runs as the differences are highlighted, discussed and explained. This section also provides the main results regarding the influence of stove power setting on the combustion, thermal, and emission performance of the selected stove-fuel combinations. The detailed discussion of the low-power runs in comparison to high-power runs is given in ANNEXURE C for reference. An attempt was made to compare the low-power runs' findings to literature, however limited information is available since literature focus is predominantly on emissions reduction without variance in stove power output.

5.2.2.1 Combustion performance

In Table 5-9, a summary of the combustion parameters for the low-power runs using can be found. The relative difference between the high- and low-power runs' combustion parameters are also indicated in brackets.

Table 5-9: Combustion parameters of low-power runs with fuel size -19 mm +13.2 mm.

	Run length	**Grate shakes**	**Time between shakes**	**Average combustion rate**	**Combustion efficiency**
	hr	-	*hr*	*kg/hr*	-
C	8.43 (+82%)	12 (+1)	0.7 (+67%)	0.54 (-44%)	0.83 (-1%)
P-B	11.95 (+62%)	8 (-)	1.49 (+62%)	0.27 (-51%)	0.62 (-23%)
P-2.5	8.72 (+88%)	8 (+2)	1.09 (+42%)	0.47 (-48%)	0.9 (-1%)
P-2.5-W	9.93 (+78%)	7 (+1)	1.42 (+53%)	0.4 (-48%)	0.83 (-9%)
P-5	7.35 (+49%)	8 (+2)	0.92 (+12%)	0.57 (-36%)	0.88 (-1%)
P-5-W	11.39 (+153%)	7 (-)	1.63 (+155%)	0.36 (-56%)	0.82 (-8%)

A greater distinction between combustion performance of the respective low-power runs can be seen, when compared to the high-power runs. The low-power runs lasted for approximately 50% - 150% longer than the high-power runs. This is mainly consequent to limiting the natural draft flow rate through the stove by closing the air controller, resulting in lower combustion rates. Similar to the high-power runs, the waterproofed fuel runs displayed significantly longer run lengths than the non-waterproofed fuel runs, and lower overall combustion rates. The P-5-W run was affected by an improper combustion zone (as displayed in Figure 5-3) that formed during the ignition phase. This greatly impacted the combustion performance, thermal performance and emission

levels of this runs and again highlighted the importance of forming a proper combustion zone during the ignition phase. For this reason, the P-5-W run displayed the greatest relative difference in run length, time between grate shakes, and combustion rate when comparing the low- and high-power runs. It was also observed that all the low-power runs showed increased run lengths, number of grate shakes, and average time between grate shakes compared to the high-power runs. In addition, all the low-power runs displayed lower average combustion rates and lower combustion efficiencies compared to the high-power run variants. All low-power runs required 0 – 2 grate shakes more than the high-power runs, with the lump coal run still requiring the most. In addition, it was observed that the lower combustion rates of the low-power runs reduced the clinker formation during the pellet runs since lower combustion zone temperatures were reached. Therefore, a greater ash-settling ability was observed which led to a fewer number of grate shakes needed, and less frequent. Similar to the high-power runs, the lump coal displayed the worst ash-settling ability and therefore needed the most grate shakes.

The binderless pellets showed the lowest combustion efficiency and the largest relative difference between high- and low-power run results. Similarly, the waterproofed pellets also showed lower combustion efficiencies compared with the high-power runs. However, the lump coal and non-waterproofed pellets' combustion efficiency remained relatively constant. The decline in P-B, P-2.5-W and P-5-W runs' combustion efficiencies can be attributed to the smouldering combustion mechanism. The temperature profiles of these runs were significantly lower compared to the non-waterproofed fuel and the lump coal runs. Lower combustion zone temperatures result in an earlier onset of smouldering combustion since less heat transfer is available for complete combustion. Once smouldering combustion takes place, premature end-of-run conditions are reached, and ultimately the runs are ended with unburnt fuel left in the stove. This combustion mechanism was only observed during low-power runs, and only for these specific three runs. Finally, when reflecting on the stability of the transient combustion rate graphs, the variance of this parameters (spikes and dips) was much smaller than for high-power runs. The lower variability is attributed to lower combustion temperatures and ash formation rates. This reduces the effect of dead zone formation and clinkering while improving the ash-settling ability relative to the high-power runs. The binderless pellet run showed the most linear transient combustion rate in contrast with the high-power run results.

5.2.2.2 Thermal performance

Averaged stove temperatures of each chamber are given in Table 5-10 for low-power runs using fuel with a size range of -19 mm +13.2 mm.

Table 5-10: Average internal temperatures of the semi-continuous coal stove during low-power runs with fuel size -19 mm +13.2 mm.

	Hopper bottom *TT305*	**CC bottom** *TT309*	**CC middle** *TT307*	**HX middle** *TT311*	**Chimney** *TT301*
	°C	*°C*	*°C*	*°C*	*°C*
C	650 (-14%)	790 (+4%)	720 (-10%)	230 (-23%)	130 (-28%)
P-B	680 (-28%)	540 (-14%)	380 (-40%)	100 (-50%)	50 (-58%)
P-2.5	730 (-23%)	700 (-7%)	590 (-16%)	180 (-33%)	110 (-35%)
P-2.5-W	840 (-9%)	650 (-)	550 (-18%)	160 (-33%)	90 (-40%)
P-5	830 (-5%)	730 (-)	650 (-7%)	200 (-23%)	110 (-31%)
P-5-W	680 (-24%)	620 (-17%)	470 (-33%)	130 (-50%)	70 (-56%)

It was found that all the low-power runs' temperatures are significantly lower than the high-power run variants, as a result of reducing the natural draft flowrate. In correlation with the high-power variants, the lump coal run exhibited the highest temperatures across the stove profile (excluding the hopper bottom temperature) while the P-B run displayed the lowest. The lump coal run showed a similar temperature profile to the high-power variant, where a relatively high combustion chamber temperature is observed in parallel with a lower hopper bottom temperature. In contrast, all the pellet batches showed significantly higher combustion zone temperatures at the bottom of the hopper in comparison to the combustion chamber bottom. This agrees with the high-power runs' results and was attributed to the combustion mechanism that was fundamentally different between the two fuel types.

For low-power runs, specifically the P-B, P-2.5-W and P-5-W runs, an average chimney temperature below 100 °C was observed which led to liquid formation in the chimney. It was found that a tar-like liquid flowed from the chimney back into the heat exchanger chamber and settled at the bottom of the stove. This influenced the stove performance by:

1. Lower stack losses were found for these runs as the wet gas losses are limited, which normally account for a large portion of the stack losses. This energy is transferred to the stove surfaces, instead of losses via chimney emission.

2. The tar liquid that settled at the bottom of the heat exchanger chamber acted as an insulator and decreased the conduction losses at the bottom of the stove.

3. It was found that these tar liquids can build up in the chimney elbow as it flows down and solidifies around the outlet baffle. This impacts the formation and flow of the natural draft during operation which was observed for the three aforementioned runs. The lower draft flow rates of the respective runs can be seen in Table 5-12.

The water boiling test results for low-power runs using fuel with a size range of -19 mm +13.2 mm are displayed in Table 5-11.

Table 5-11: Water boiling test results for low-power runs with fuel size -19 mm +13.2 mm.

	Time to boil	**Cooking power**	**Cooking efficiency**
	min	*kW*	*%*
C	23 (+28%)	0.5 (-22%)	10.8 (+96%)
P-B	214 (N/A) **	0.04 (-69%)	1.9 (-44%)
P-2.5	61 (+259%)	0.17 (-70%)	3.4 (-24%)
P-2.5-W	74 (+185%)	0.13 (-66%)	2.8 (-39%)
P-5	53 (+212%)	0.21 (-64%)	4.4 (-47%)
P-5-W	184 (+700%)	0.05 (-89%)	1.9 (-55%)

*** P-B did not boil and reached a max temperature of 90 °C.*

Similar to the high-power runs, the lump coal and P-5 runs could reach boiling point the fastest. However, in contrast with the high-power runs, the binderless pellet run could not reach boiling point and only heat the water to a maximum temperature of 90 °C during the entire run. For the P-5-W run, the rate of combustion energy transfer to the water pot is slightly greater than the energy losses of the water pot. This is reflected through the relatively low cooking power calculated for this run and the slow increase in water temperature observed. For the P-B run, the thermal losses of the water pot were greater than the energy transferred from the cooking surface to the water pot via conduction, convection and radiation. In other words, the energy losses of the water pot were approximately 0.04 kW at 90 °C, which the P-B run could not overcome. That is consequently why the water could not reach boiling point. This is supported through the P-B and P-5-W runs which exhibited the lowest cooking power and efficiencies out of all the high- and low-power runs.

It was found that the time required to boil the water during the lump coal run, was comparable to that of the high-power run variant. Due to the high combustion chamber middle temperature, and effectiveness of the gas phase combustion, more energy was transferred to the cooking area

relative to the other stove surfaces during this run. This also resulted in a much greater cooking efficiency, as approximately 10% of the combustion energy was transferred to the water pot. This cooking efficiency for the lump coal run is the highest efficiency calculated for all low- and high-power runs. Similar to the high-power runs, the fuel without waterproofing exhibited improved boiling times, cooking power, and cooking efficiencies than the fuel with waterproofing added.

In Table 5-12, a summary of the main thermal parameters is displayed, including the power rating of the stove-fuel combinations, and the respective thermal efficiencies.

Table 5-12: Thermal performance parameters for high-power runs with fuel size -19 mm +13.2 mm.

	P_F	P_D	η_{SL}	η_D	η_{tot_1}	η_{tot_2}	$\overline{V}_{chim}$
	kW	*kW*	*%*	*%*	*%*	*%*	*m^3/hr*
C	4.5 (-44%)	4 (-39%)	91 (+4%)	89.4 (+8%)	74.4 (+8%)	64.6 (-12%)	10.1 (-50%)
P-B	2.1 (-50%)	1.6 (-54%)	95.1 (+3%)	77.8 (-6%)	58.4 (-13%)	54.4 (-12%)	4.8 (-48%)
P-2.5	3.6 (-48%)	2.9 (-50%)	92.9 (+4%)	81.2 (-3%)	73 (-5%)	71.8 (-8%)	7.8 (-51%)
P-2.5-W	3 (-49%)	2.5 (-47%)	93.1 (+4%)	82.1 (+4%)	68.2 (-5%)	67.1 (-14%)	6.6 (-57%)
P-5	4.3 (-36%)	3.8 (-31%)	91.3 (+2%)	87.3 (+6%)	77.1 (+4%)	72.2 (-7%)	9 (-42%)
P-5-W	2.7 (-56%)	2 (-58%)	94.6 (+5%)	75.2 (-3%)	61.8 (-10%)	58.2 (-24%)	5.8 (-59%)

η_{tot_1} is calculated using the energy delivered via conduction and radiation approach (Equation E-26).
η_{tot_2} is calculated using the stack loss approach (Equation E-27).

The low-power runs displayed significantly lower power ratings than the high-power runs. These runs maintained a power output of 2 kW – 4.5 kW for more than 7 hours. The average chimney flow rates were approximately half of what was found for high-power runs. Despite this significant reduction in chimney flow rate and lower chimney temperatures, the stack loss efficiency of the low-power runs only increased between 2% - 5%. This is due to the prolonged run lengths of the low-power runs where the instantaneous stack losses are reduced, but the accumulated (total) stack losses remain relatively constant. In agreement with the high-power runs, the P-B run displayed the lowest stack temperature and average flow rate, and thus the greatest stack loss efficiency.

The effects of smouldering combustion during low-power runs can be seen for all the thermal parameters displayed in Table 5-12. The degree and duration thereof (P-B > P-5-W > P-2.5-W) is inversely proportional to the magnitude of power output and energy efficiency values of the

respective low-power runs. The only exception is the stack loss efficiency, which increases with an increase in duration of smouldering combustion as seen for the three indicated runs. Even though the thermal stack loss efficiency is increased, the delivered and overall (total) efficiencies are significantly reduced. This is attributed to the increased amount of combustible matter (CO, VOCs, carbonaceous PMs, hydrocarbon gases, etc.) that was emitted as a result of smouldering combustion, instead of complete combustion. Therefore, the energy generated per mass fuel consumed, was less for the P-B and P-5-W runs than for the other runs, resulting in reduced delivered and overall energy efficiencies.

5.2.2.3 Emission levels

The emission levels for low-power runs are obtained and discussed similar to that of Section 5.2.1. The carbon oxides and the excess oxygen levels recorded in the chimney for low-power runs using fuel of a size range of -19 mm +13.2 mm are displayed in Figure 5-19.

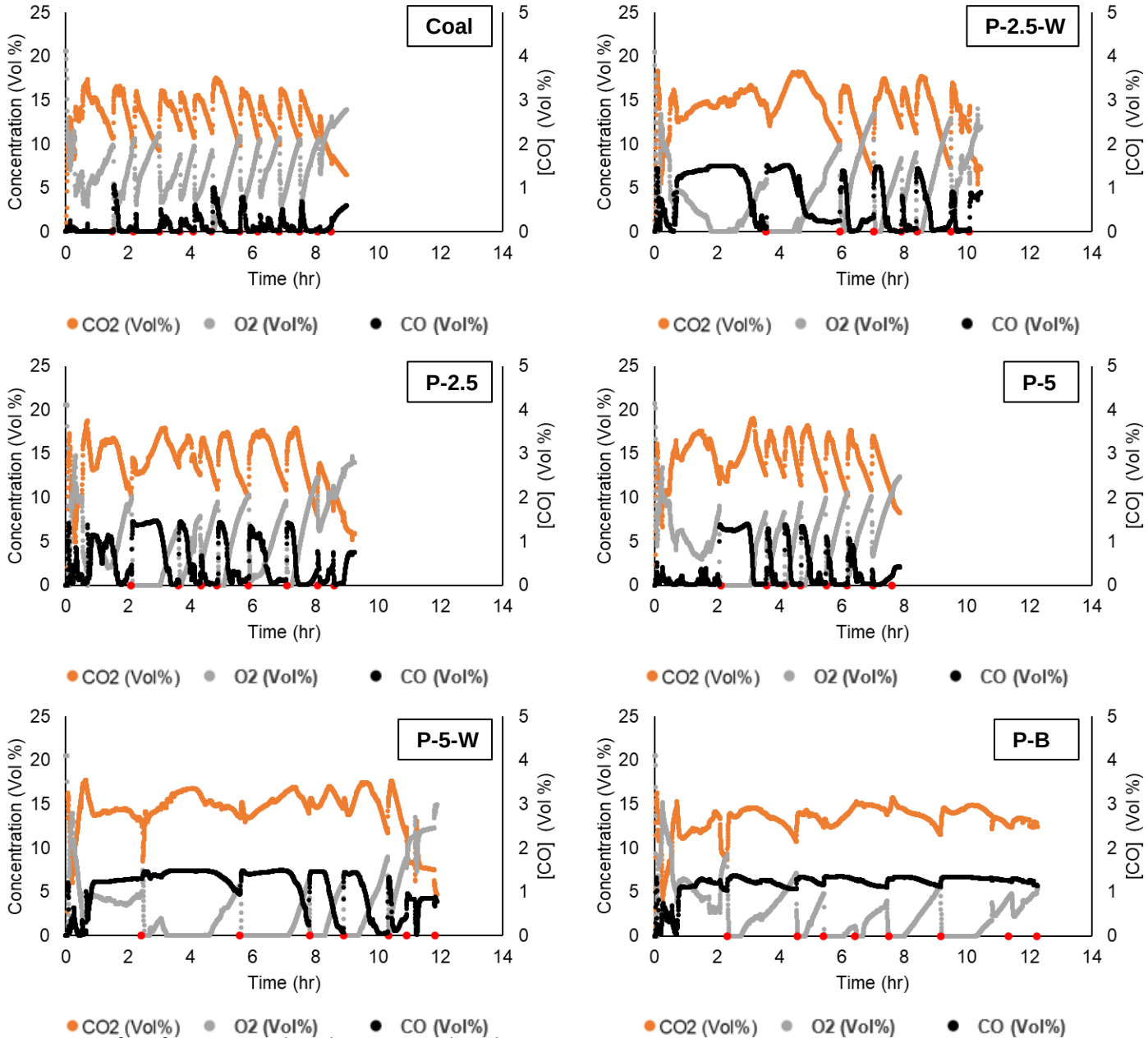

Figure 5-19: Carbon oxides and oxygen concentrations in the flue gas of low-power runs using fuel size -19 mm +13.2 mm.

During the low-power experiments, it was found that two mechanisms exist which limits combustion and increased emission levels:

1. Proper combustion zone, high combustion and propagation rate. The combustion reaction is restricted due to reagent availability (oxygen limited).
2. Improper (cold) combustion zone, slow propagation rate. The combustion reaction limited due to insufficient energy transfer for onset of combustion (smouldering).

It was found that the ideal operating point for low-power runs were “between” these mechanisms where sufficient energy transfer is available for complete combustion, but the combustion, ignition and propagation rates are low enough to prevent oxygen deficiency. The lump coal run was the only low-power experiment to display this behaviour where complete gas phase combustion occurred, and low CO and PM emission levels were observed. The P-5 run also operated with a similar mechanism, but with higher combustion and propagation rates as seen by the CO emission spikes after 2 hours into this run. It was also found that large transient combustion rate spikes resulted in an increased oxygen consumption rate while the airflow is limited for low-power runs. Therefore, the emission levels observed during low-power runs are more susceptible to transient combustion rate variations as a result of the O_2 limitation than compared to high-power runs.

It was found that the averaged CO_2 levels for low-power runs are lower than for the high-power runs. This is attributed to the increased formation of CO during low-power runs compared to high-power runs. In addition, some low-power runs (P-B and P-2.5-W) displayed non-typical consistently high CO levels where excess oxygen measure in the chimney rarely exceeded 7 vol.%. For these runs, grate shakes were initiated based on ash formation and dead zones despite low oxygen levels in the chimney. It can also be seen that the CO_2 and CO levels for these runs remained relatively constant for prolonged periods in contrast to the high-power run results. The low-power runs displayed significantly lower excess air levels on average than the high-power runs, as expected. Similar to what was observed for the high-power runs, the excess air levels of the lump coal run rarely decreased to 0% or lower.

A summary of the emission factors for the low-power runs is illustrated in Table 5-13.

Table 5-13: Emission factor summary for low-power runs using fuel size -19 mm +13.2 mm.

	EF_{CO_2}	EF_{CO}	EF_{NO_x}	EF_{SO_x}	EF_{PM}	EF_{VOC}
	g/MJ	*g/MJ*	*mg/MJ*	*g/MJ*	*mg/MJ*	*mg/MJ*
C	91 (-2%)	0.59 (-12%)	100 (-17%)	0.34 (-6%)	23 (-38%)	40 (-87%)
P-B	93 (+2%)	5.2 (+206%)	24 (-61%)	0.17 (-45%)	983 (+3177%)	110 (+10%)
P-2.5	93 (-2%)	2.3 (-4%)	49 (-25%)	0.3 (-19%)	68 (-13%)	100 (+11%)
P-2.5-W	91 (-3%)	2.9 (+45%)	49 (-32%)	0.25 (-24%)	51 (-58%)	80 (-27%)
P-5	93 (-1%)	1.4 (+27%)	60 (-28%)	0.31 (-11%)	33 (+120%)	120 (+71%)
P-5-W	94 (+1%)	4.3 (+153%)	29 (-60%)	0.2 (-46%)	270 (+125%)	100 (+11%)

The lump coal is the only run that showed an improved CO emission factor compared to the high-power runs, while the CO emission factor of all the other pellet batches increased with a factor of 2 – 3 compared to the high-power variants. This significant increase can be attributed to prolonged combustion under oxygen-deficient conditions, which was not the case for the lump coal run. The P-B run, followed by the P-5-W run showed the highest CO emission factors, which can be attributed to the respective combustion mechanisms observed during the runs. The lump coal run followed by the P-5 run showed the lowest CO emission factors, which was also observed for the high-power run results.

The lump coal low-power run exhibited the highest NO_X emission factors, with the P-B the lowest. This agrees with the observations made for high-power runs. As discussed in Section 5.1 combustion in a reductive environment can lead to reduced NO_X emission levels [92]. This mechanism applies to both high-power and low-power NO_X emissions. The runs with the highest natural draft flow rate, as well as minimal instances of oxygen deficiency, resulted in higher NO_X emission factors as is the case of the P-5 and lump coal runs. The opposite is also true where low draft flow rates, high combustion temperatures, and more instances of oxygen deficiency resulted in relatively low NO_X emission factors. This was seen for the P-B and P-5-W runs. However, a key difference between the low- and high-power runs are the magnitude of the difference between lump coal and pellet runs' NO_X emission factors. The low-power lump coal run exhibited NO_X emission factors 2 - 4 times higher than most pellet runs, where this difference was significantly less for high-power runs. In addition, the P-5 run displayed the closest experimental conditions to the lump coal run, in terms of natural draft flow rate, oxygen availability, and temperature profile, but consequently only reported a NO_X emission factor of 60 mg/MJ which is 40% lower than the lump coal run. Therefore, it must be considered that more than just operating conditions influence NO_X emissions. It is possible that other factors influence NO_X emissions including type of nitrogen species in the fuel and the structure or properties of the ash.

The lump coal run, followed by the P-5 and P-2.5 runs all showed similar SO_X emission factors, which is also comparable to the magnitude of SO_X emission factors of the high-power runs. In contrast, however, the P-B and P-5-W runs displayed the lowest SO_X emission factors. Considering the combustion parameters, it was found that the SO_X emission factors directly correlate with the combustion efficiency of the respective runs. The total mass sulphur emitted as SO_X in the stack gas during low-power runs can be seen to be significantly less than for the high-power runs. The only exception to this observation was the lump coal run. All the pellet batches exhibited a decrease in mass sulphur emitted, 10% – 30% lower compared to the high-power counterparts. However, the lump coal run did not display a significant reduction sulphur species emissions. This is supported by the sulphur oxidation factors. All pellet batches showed a significant decrease in sulphur oxidation when compared to the high-power runs, except the lump coal run. The main contributing factor for this observation is unknown. It is possibe that the type of sulpher species in the fuel had a greater impact on sulphur emissions that the change in combustion rate. Further perimentation and analyses will be needed for a deeper insight into this phenomenon.

The PM emission factors remained relatively comparable to the high-power runs, except for the P-B and P-5-W runs. It is shown that the PM emission levels for these runs significantly increased when compared to the high-power variants. This agrees with literature findings [40]. This can be attributed to prolonged exposure to oxygen-deficient conditions, where incomplete complete combustion occurred as a result of the smouldering combustion mechanism. The P-B run showed the highest PM levels for all experimental runs. The difference between the high-power P-B and low-power P-B runs' emission factors is roughly a factor of 30. The lump coal and P-5 run exhibited the lowest PM emission factors. Both these runs displayed typical oxygen levels for low-power runs, high CC middle temperatures, and typical combustion conditions. This consequently resulted in the low CO and PM emissions compared to the other runs. The VOC emission factor results of the low-power runs are in dissimilarity with the high-power run results, as well as literature findings. The lump coal run displayed the lowest VOC emission factor even though this fuel had the highest volatile matter content relative to the other fuels. Furthermore, as stated in the literature, a high combustion temperature usually correlates with low VOC emission factors. While this may be true for the lump coal, this phenomenon is not visible for the coal pellets runs' results. The experimental repeatability of this parameters was acceptable for high-power runs, however it is possible that larger variability occurs as the experiment length increases where more non-VOC matter builds up in the activated carbon filters. Improvements to experimental methodology should be considered for future low-power experiments.

5.2.3 Fuel size and packing

In Section 5.2.1 the combustion, thermal, and emission parameters of the respective high-power runs using a single fuel PSD (-19 mm + 13.2 mm), were given and discussed. In this section however, high-power runs using fuel of various PSDs are compared and discussed. This section highlights the main findings with regards to the influence of fuel PSD and packing characteristics on the combustion, thermal, and emission performance of the selected stove-fuel combinations. The detailed discussion pertaining to high-power run using various fuel size ranges is given in ANNEXURE D for reference. No literature references could be found that indicates the impact of fuel packing and PSD on the performance of a cookstove performance.

A key to the 6 batches that was used for fuel PSD experiments can be seen in Table 5-14. Each fuel batch and corresponding experiment was labelled based on the packing characteristics of the fuel.

Table 5-14: Key to fuel batches and runs which used different size range pellets.

Batch Key	Description	Packing characteristic	Size range
P-2.5 L	2.5 wt.% PVA pellets; no waterproofing	Low density; High bed voidage; Low surface area per volume; Low surface area per mass	-19 mm +13.2 mm
P-2.5 M	2.5 wt.% PVA pellets; no waterproofing	Medium density; Medium bed voidage; Medium surface area per volume; Medium surface area per mass	-19 mm +9.5 mm
P-2.5 H	2.5 wt.% PVA pellets; no waterproofing	High density; Low bed voidage; High surface area per volume; High surface area per mass	-13.2 mm +6.7 mm
P-2.5-W L	2.5 wt.% PVA pellets; waterproofing added	Low density; High bed voidage; Low surface area per volume; Low surface area per mass	-19 mm +13.2 mm
P-2.5-W M	2.5 wt.% PVA pellets; waterproofing added	Medium density; Medium bed voidage; Medium surface area per volume; Medium surface area per mass	-19 mm +9.5 mm
P-2.5-W H	2.5 wt.% PVA pellets; waterproofing added	High density; Low bed voidage; High surface area per volume; High surface area per mass	-13.2 mm +6.7 mm

5.2.3.1 Combustion performance

A combustion parameter summary of the 2.5 wt.% PVA pellet runs using fuel of various size ranges, is given in Table 5-15.

Table 5-15: Combustion parameters of high-power 2.5 wt.% PVA pellet runs using fuel of various size ranges.

	Initial mass	Run length	Grate shakes	Time between shakes	Average combustion rate	Combustion efficiency
	kg	*hr*	-	*hr*	*kg/hr*	-
P-2.5 L	6.38	4.64	6	0.77	0.91	0.91
P-2.5 M	6.59	4.32	4	1.08	0.90	0.81
P-2.5 H	6.94	5.91	8	0.74	0.70	0.82
P-2.5-W L	6.42	5.57	6	0.93	0.77	0.91
P-2.5-W M	6.94	5.85	5	1.17	0.76	0.87
P-2.5-W H	6.61	5.92	5	1.18	0.63	0.77

The smaller size range pellet runs started with a higher initial mass than the larger size range pellet runs. These mass values correlate with the packing density of the respective fuel size ranges since a similar volume of fuel is loaded into the stove. When considering the number of grate shakes required for each run, and the average time between these respective grate shakes, no significant correlation was observed between these parameters and the packing characteristics. Therefore, the fuel PSD had little influence on the ash-settling ability of the fuel. This is in contrast with initial test runs (Annexure A) where it was found that a smaller size range fuel might result in improved ash setting. Instead, it was observed that the smaller size range pellets (“H” runs) were more likely to form clinkers and ash fusion areas than compared to the larger size range pellet runs (“L” runs). This had the opposite effect on ash settling ability and caused ash holdup which resulted in the need for more severe grate shakes. This is also reflected in the combustion efficiency of the respective runs, where the lowest combustion efficiency is reported for the high-density smaller size pellet runs.

The influence of combustion zone disturbances such as dead zones, grate shakes, and clinkers was prominent for all runs irrespective of fuel packing characteristics or size range. No significant difference in combustion rate can be observed between the different size range runs as initially believed. Furthermore, all of the runs displayed a similar magnitude of combustion rate peaks and valleys throughout the runs.

5.2.3.2 Thermal performance

Key averaged stove temperatures of each chamber are given in Table 5-16 for high-power runs using 2.5 wt.% PVA binder fuel with various size ranges.

Table 5-16: Average internal temperatures of the semi-continuous coal stove during high-power runs with various fuel PSDs.

	Hopper bottom *TT305*	**CC bottom** *TT309*	**CC middle** *TT307*	**HX middle** *TT311*	**Chimney** *TT301*
	°C	*°C*	*°C*	*°C*	*°C*
P-2.5 L	950	750	700	270	170
P-2.5 M	820	720	700	260	170
P-2.5 H	840	660	630	220	150
P-2.5-W L	920	650	670	240	150
P-2.5-W M	890	720	660	230	140
P-2.5-W H	750	680	590	210	130

All the size range runs displayed higher hopper bottom temperatures than the combustion chamber temperatures. This difference was greater for the “L” runs which showed the highest average combustion zone temperature compared to the other size ranges. Since the “L” runs exhibited reduced clinkering compared to the other runs, they also displayed higher average combustion zone temperatures as seen for the hopper bottom and combustion chamber bottom temperatures compared to the other runs. From the combustion chamber middle temperatures, “L” runs using larger size range pellets with increased voidage and lower surface area to volume exhibited higher gas phase combustion temperatures, and therefore more complete combustion. In addition, the high-density fuel runs exhibited the lowest average combustion chamber middle temperature indicative of incomplete gas phase combustion when compared to the other runs.

The hopper bottom temperatures of the larger size pellets (“L” runs) were on average greater than those of the other pellet runs. The effects of severe clinkering and dead zone formations during the high-density fuel runs were observed at ≥ 3 hours into these runs. As a result, deep valleys were observed in the combustion zone temperature results, where severe grate shakes were required to amend the combustion zone and improve stove operation. No clear indication of a faster propagation rate can be seen for the smaller size range pellet batches. The rate at which the combustion zone temperatures increase before the first grate shake is similar for all the runs. It is possible that the onset of ash fusion and clinkering occurs in the middle of the combustion zone, underneath the stove bridge where no thermocouple measurement is available.

The cooking power and cooking efficiency of the respective runs could be correlated with packing parameters. The higher cooking power values correlated with the “M” size fuel runs, while a low

cooking power correlates with the “H” fuel runs. This was attributed to the time in the run when the water boiling test was conducted. Even though an overall higher gas phase temperature was observed for the “H” runs, during the ±30 min of the water boiling test the immediate combustion chamber temperatures were slightly higher for the “M” runs than compared to the “H” runs. It was also observed that the cooking efficiency increased with an increase in packing density and a decrease in voidage. This is likely due to the increased clinker and ash formations at the bottom of the hopper for the smaller size pellet runs, which formed an ash insulation layer reducing the energy losses to the front and bottom parts of the stove. Therefore, the “L” runs which exhibited less clinkering and ash fusion, experienced higher hopper temperatures, higher energy losses during the water boiling test, and therefore lower cooking efficiencies compared to the other runs.

In Table 5-17, a summary of the main thermal parameters is displayed, including the power rating of the stove-fuel combinations, and the respective thermal efficiencies.

Table 5-17: Thermal performance parameters for high-power runs with fuel size -19 mm +13.2 mm.

	P_F	P_D	η_{SL}	η_D	η_{tot_1}	η_{tot_2}	$\bar{V}_{chim}$
	kW	*kW*	*%*	*%*	*%*	*%*	*m^3/hr*
P-2.5 L	6.9	5.8	89.6	84.1	76.6	78.3	16.0
P-2.5 M	6.8	5.3	88.7	78.1	63.2	68.8	17.2
P-2.5 H	5.3	4.1	88.4	77.5	63.8	65.7	16.0
P-2.5-W L	5.9	4.7	89.6	79.2	72.1	77.6	15.4
P-2.5-W M	5.8	4.7	91.2	81.9	71.2	74.2	12.4
P-2.5-W H	4.8	3.6	90.2	73.7	56.8	58.0	13.2

η_{tot_1} is calculated using the energy delivered via conduction and radiation approach (Equation E-26).

η_{tot_2} is calculated using the stack loss approach (Equation E-27).

The fired and delivered power output of the stove decreases with an increase in fuel packing density. For the stack loss efficiency values, the results are similar between runs irrespective of fuel packing or size range. Similarly, the average chimney flow rate and stack outlet temperature can be correlated with packing parameters and fuel size. The difference between these parameters however is not significant enough to result in a visible correlation between stack losses and fuel packing characteristics. Both the delivered energy efficiency and the total stove energy efficiency scales with the packing parameters and PSD. It was found that the low-density pellet runs exhibited higher energy efficiency than the other runs. The improved thermal parameters of these -19 mm +13.2 mm PSD runs are a direct result of increased oxygen availability for gas phase combustion, reduced clinkering, and lower energy losses through uncombusted gases.

5.2.3.3 Emissions levels

The emission levels for high-power runs using various fuel PSDs are obtained and discussed similar to that of Section 5.2.1. The carbon oxides and the excess oxygen levels recorded in the chimney during these runs are displayed in Figure 5-19.

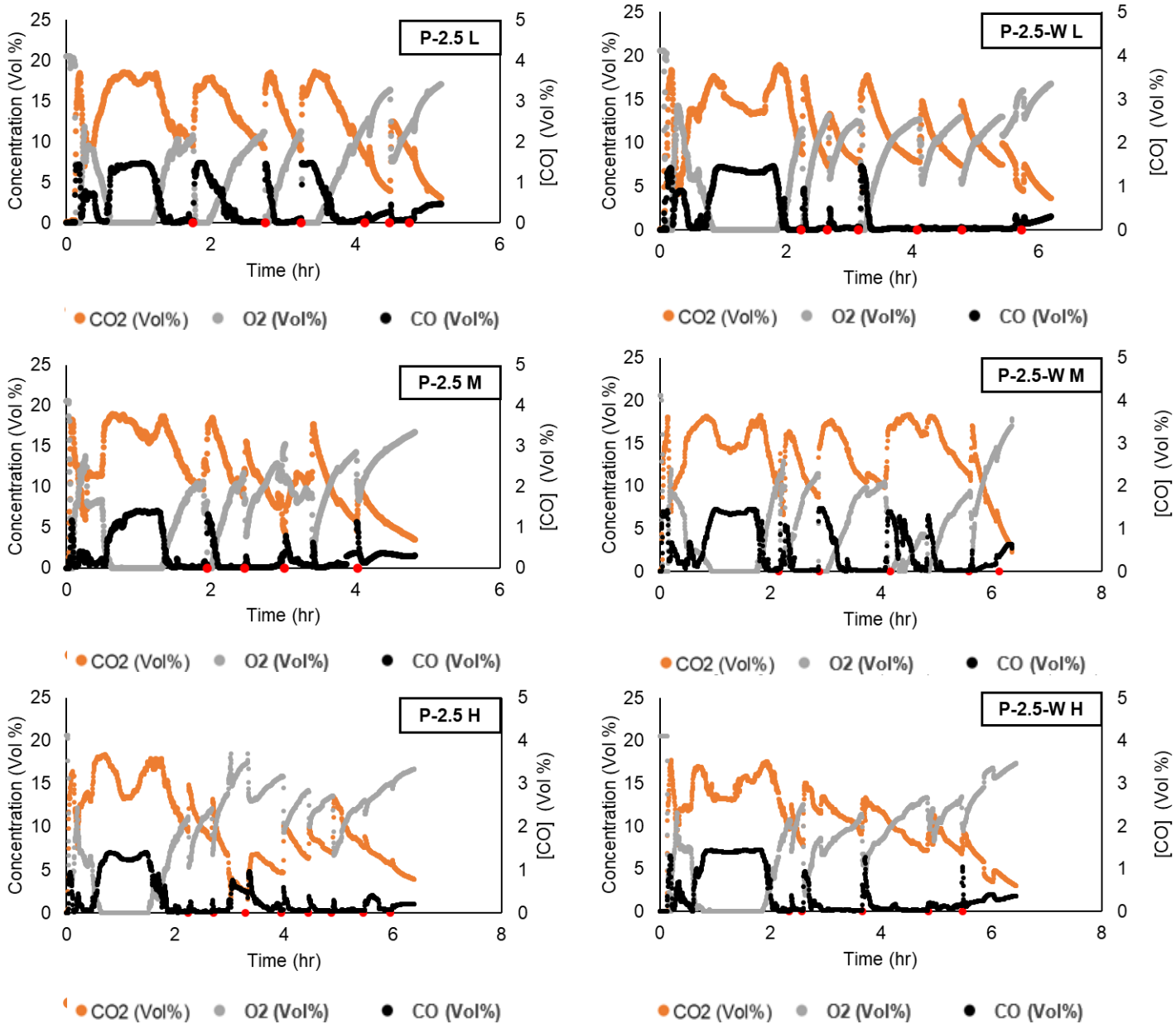

Figure 5-20: Carbon oxides and oxygen concentrations in the flue gas of high-power runs using fuel of various size ranges.

Non-typical behaviour was observed during multiple runs where the CO_2 decreases and the O_2 increases after the grate shake. This interaction is the opposite of what was shown in Section 5.1. This abnormal behaviour can be attributed to severe clinkering. These conditions were observed for the “H” and “M” runs, especially the P-2.5 H run where a substantial part of the run was conducted at low CO_2 and high O_2 concentrations. The severe clinkering that occurred during these runs resulted in ash-solid layering, which caused channelling through the combustion bed. This increased the excess oxygen and reduced the available combustion zone area. This also correlates with a lower combustion chamber middle temperature as shown for the “H” runs.

All the runs experienced CO emission spikes after grate shakes, with long periods of high CO levels in the stack gas before the first grate shake. These high levels of CO were observed for all the runs irrespective of fuel size or packing characteristics. The magnitude of the CO spikes and the length of elevated CO levels were less for the “H” runs compared to the other variants. This was attributed to increased excess oxygen availability for complete combustion as provided by the air channelling through the char bed. The length of the oxygen deficiency periods after the ignition phase was found to scale with a change in fuel size. Longer periods of oxygen deficiency were observed for the “H” pellet runs after the ignition phase. This is due to the increased duration required for a full combustion zone to form when a dense packed char bed is present.

Both the α value as well as the averaged $CO:CO_2$ ratio of the P-2.5-W runs scale with the fuel size range. Higher $CO:CO_2$ ratios and lower α values are obtained for the runs with a higher packing density. This is caused by the reduced oxygen availability that is associated with a higher density char bed, and therefore incomplete combustion. The total mass sulphur emitted, as well as the overall sulphur oxidation factors scale down with an increase in packing density. The main factors that influenced the total sulphur emissions are the combustion efficiencies and combustion rates of the respective runs. The P-2.5-W H run showed both the lowest combustion efficiency and combustion rate, and displayed the lowest total sulphur emitted compared to the other runs. The magnitude and length of the NO_X spikes after each grate shake remain relatively constant throughout the different runs. No significant correlation was observed between the NO_X emissions and the packing characteristics of the fuel. All the parameters that influence NO_X emissions, such as natural draft flow rate, combustion zone temperature, etc., remaining relatively constant for all the various runs. The PM emissions are relatively similar for all the various runs.

A summary of the emission factors of the 2.5 wt.% PVA pellet runs using fuel of various size ranges, is given in Table 5-18.

Table 5-18: Emission factor summary for high-power runs using fuel of different size ranges.

	EF_{CO_2}	EF_{CO}	EF_{NO_x}	EF_{SO_x}	EF_{PM}	EF_{VOC}
	g/MJ	*g/MJ*	*mg/MJ*	*g/MJ*	*mg/MJ*	*mg/MJ*
P-2.5 L	95 ± 4	2.4 ± 0.1	65 ± 2	0.37 ± 0.01	78 ± 3	90
P-2.5 M	95 ± 4	1.8 ± 0.1	89 ± 3	0.34 ± 0.01	25 ± 1	90
P-2.5 H	94 ± 3	2.1 ± 0.0	81 ± 1	0.34 ± 0.01	100 ± 2	110
P-2.5-W L	94 ± 4	2.0 ± 0.0	72 ± 1	0.33 ± 0.01	120 ± 2	110
P-2.5-W M	92 ± 5	2.1 ± 0.0	66 ± 1	0.32 ± 0.01	57 ± 1	90
P-2.5-W H	93 ± 4	2.3 ± 0.0	72 ± 1	0.29 ± 0.01	41 ± 1	50

From the emission factor results presented in Table 5-18 , the “L” runs with increased bed voidage, and permeability did not exhibit lower CO, PM, and VOC emission factors as initially expected. Both the CO and PM emission factors show no significant correlation with changes in fuel PSD. The same is true for the NO_X emissions. However, the SO_X emission factors scale with fuel PSD due to the combustion performance of the respective runs. The lack of correlation between the emission results and fuel size range in Table 5-18 might be attributed to the effect of disturbances on the combustion characteristics. Even though the higher bed voidage of the -19 mm +13.2 mm pellet runs improved the gas phase combustion, other parameters such as clinkering, grate shakes, and user error had a greater impact on the emission factors and skewed the correlation between emission factors and packing characteristics.

CHAPTER 6 – CONCLUSION AND RECOMMENDATIONS

6.1 CONCLUSION

This study aimed to evaluate the thermal and emissions performance of a semi-continuous coal stove using coal pellets as an alternative fuel source. Six fuel batches were tested: lump coal (C), binderless pellets, and four variations of PVA binder pellets, both with and without waterproofing. Testing was conducted using the semi-continuous coal stove developed by New Dawn Engineering in collaboration with North-West University. The main parameters of interest included the type of fuel, the fuel characteristics, fuel PSD, and performance during low- and high-power stove settings. It was found that the combustion behaviour differed significantly between lump coal and coal pellets. While lump coal demonstrated a combustion zone primarily in the combustion chamber, coal pellets showed a combustion zone largely in the hopper chamber, leading to variations in stove power output. The lump coal exhibited the highest power rating, while the binderless pellets had the lowest. Additionally, fuel without a waterproofing agent produced a greater power output compared to the waterproofed agglomerates, while the amount of PVA binder did not significantly affect the power rating. It was found that the waterproofing agent significantly impacted the stove-fuel combinations' thermal performance, however the same was not found for the emissions parameters. When compared to a traditional Dover^{TM} household cookstove, the stove-fuel combinations presented similar cooking power values and power ratings, but with significantly greater thermal efficiencies. These values are similar to those reported for the TJ4.0, a semi-continuous cross-draft stove with a nearly identical design.

In terms of emissions, the lump coal showed the lowest CO emission factor, while most pellet runs, particularly P-2.5, produced CO emissions more than double that of lump coal. The high CO emission factors of the coal pellets was mainly caused by combustion in oxygen deficient conditions, which was not observed during the lump coal experiments. NO_X emissions were influenced by oxygen availability, natural draft flowrate and combustion zone temperatures, with lump coal producing the highest NO_X emission factor and P-B the lowest. Variations in NO_x emissions was mainly attributed to combustion in a reductive environment. The SO_X emission factors remained relatively comparable between the different fuel batched, however the oxidation of sulphur during the lump coal run was significant higher compared to the other fuel batches. Particulate matter emissions showed no significant correlation with fuel type. The P-5 run produced the lowest PM levels, while the waterproofed pellets significantly increased particulate emissions by approximately 400%. VOC emissions were highest during the lump coal run, with waterproofed pellet runs generally showing higher VOC levels than non-waterproofed pellet runs.

The quantity of binder or the addition of a waterproofing did not significantly affect the emission factors.

Overall, the lump coal and 5 wt.% PVA binder pellets (P-5) demonstrated an acceptable thermal performance and lower emission levels across both power settings, using a -19 mm +13.2 mm fuel PSD. A summary can be made regarding the stove's key advantages utilising either lump coal or pellets. As excess oxygen is preheated when it permeates through the combusting char bed, an increase in combustion efficiency of vapours and volatiles was found. The separation of the two combustion phases leads to reduced CO, PM and VOC emissions, which was clearly observed during experimentation. In addition, the stove's cross-draft design with horizontal combustion zone aids in NOx reduction. This is achieved by creating reductive combustion conditions below the formation temperature of thermal NO_x. A disadvantage was also identified during the experimental phase. Since oxygen gets consumed by char combustion before permeating through the combustion bed, oxygen deficient combustion is possible. This was especially prominent for coal pellet runs. Oxygen deficient conditions resulted in incomplete combustion and increased emission of combustible gases and volatile matter. As a result, a significant increase of CO, VOC and PM emissions was observed during these periods. However, these emission levels, and the overall emission factors, were still well below that reported in literature for domestic coal stoves. In conclusion, the lump coal and P-5 stove-fuel combinations exhibited superior performance relative to the other combinations evaluated across both low- and high-power settings. The P-5 pellets is therefore identified as a suitable alternative fuel for the semi-continuous coal stove and can be implemented for household use.

6.2 RECOMMENDATIONS

When considering the stove set-up and methodology, multiple water boiling tests should be performed during the run to minimise the effects of combustion disturbances on the test results. Furthermore, additional measures should be taken to prevent the deposit of moisture or PM in the activated carbon tube (for VOC emissions) during low-power runs. The methodology with regards to PM emission calculations should also be reconsidered since correlating three sets of gas analyser results, each with a different residence time, significantly increases the uncertainty and error margin of online PM measurements. It is further recommended that a XRD and XRF analyses of the ash are performed in future work to improve the explanation of phenomenon such as ash fusion or clinkering.

For future study the need for grate shakes should be minimised if possible. The repeatability and uncertainty of both the thermal performance data and emission levels were significantly impacted by combustion disturbances such as grate shakes, dead zones, and ash fusion (clinkers). A fuel with a lower ash yield could eliminate the need for grate shakes by improving the ash settling rate, ash hold-up, and consequently further improve the thermal and emissions quality of combustion in the semi-continuous coal stove.

6.3 IMPLEMENTATION AND PROSPECTS

This section contains an evaluation of the ease of operation of the semi-continuous coal stove using either lump coal or coal pellets as fuel. The main domestic purpose of a cookstove is to provide energy for cooking and living space heating. For cooking, the high-power setting is recommended. The semi-continuous coal stove using lump coal provided the highest power output and energy delivered. This stove-fuel combination could also boil the water the fastest. As an alternative, the P-5 fuel displayed similar results with less grate shakes needed which significantly increases the ease of operation.

For living space heating, a low and steady combustion rate is required where the stove can operate for extended periods with minimal user input (grate shakes) required. The low-power P-B run displayed a desirable linear combustion rate and steady operation with continuous ash settling. This resulted in long periods between grate shakes which indicates reduced user input. However, tar liquid build-up was observed in the chimney elbow due to the low stack temperatures displayed by this stove fuel combination. This can block the stove exit and impact the internal cross-draft required for stove operation. In a severe case, it was observed that a reverse draft formed, and emissions seeped out the stove apertures around the air inlet and ash tray. Therefore, the use of a stove-fuel combination with minimal grate shakes and a greater stack temperature during low-power runs is recommended. The lump coal delivered the highest energy output during its low-power runs and showed the best emissions performance (low-power) out of all fuel batches. However, the higher number of grate shakes that are associated with these runs is a drawback. When considering the remaining pellet batches for space heating, the P-5 fuel would be the most optimal choice. Despite is lower thermal output and emissions performance when compared to lump coal, it required less grate shakes over the run duration. In addition, its heat output was still sufficient for the purpose of domestic heating and its thermal efficiency was greater than that of the other pellet batches. Although the P-2.5 pellets also adhered to the requirements of space heating, it is not recommended due to its high clinker formation. Another factor that affects the application feasibility of the semi-continuous coal stove is the handling and storage of the fuel before operation. The fuel has to remain intact during handling and should remain intact after prolonged exposure to water. In this regard, the lump coal and P-5 pellets are the most suitable options. Although the other waterproofed pellets were also suitable from a handling and storage perspective, the waterproofing agent negatively impacted the thermal performance and emission levels during operation.

Clinkering increases the required user input during stove operation and is challenging to remove from the combustion zone to the ash tray during operation. It was found that all pellet runs produced clinkers and dead zones, and the severity thereof was less during low-power runs when

compared to the high-power runs. The P-5 pellets exhibited the lowest clinker formation of all the pellet runs while no clinkers were observed during the lump coal runs. Furthermore, the smaller size range pellet runs were associated with more severe clinkering, and it is therefore recommended to use a PSD of -19 mm +13.2 mm to minimise this phenomenon when pellets are used. Finally, the lump coal run displayed the lowest front surface temperature of all fuel batches as discussed in Section 5.2.1. The high surface temperature at the front of the stove does not contribute to cooking energy, but rather presents a hazard to the stove user when operating the grate handle and air inlet controller.

The P-5 pellets is the most suitable alternative to lump coal based on the data discussed in this work. However, lump coal remains the most suitable fuel for the semi-continuous coal stove since the appliance was designed for it. This is evident when considering the lump coal's handling and storage characteristics, optimal cooking and heating performance, no observable clinker formation and lower burn risk when compared to the pellet batches. In order to improve the feasibility of the P-5 pellets, design changes to the semi-continuous coal stove should be considered. It is recommended that changes be made to the grate in order to manipulate the combustion mechanism that was observed when using pellets. The first improvement to consider is covering the section of the grate directly below the hopper chamber. This will redirect the airflow to the bottom of the combustion chamber and maintain a complete char and gas phase combustion zone in this area. This also reduces oxygen consumption at the bottom of the hopper, and therefore minimises clinker formation. The second improvement to consider is a revaluation of the grate angle and the open area underneath the stove bridge. This should be designed to cater for the physical properties associated with coal pellets instead of lump coal. The fuel flow and combustion bed dimensions can then be optimised for pellets instead. Finally, a closable opening can be added to the stove elbow to easier clean the chimney and allow liquid draining after low-power runs.

BIBLIOGRAPHY

[1] South African Department of Energy, “Coal Resources.” Accessed: Mar. 27, 2020. [Online]. Available: http://www.energy.gov.za/files/coal_frame.html

[2] K. Ratshomo and R. Nembahe, “South African Coal Sector Report Directorate : Energy Data Collection , Management and Analysis”, *Department of Energy*, pp. 1–34, 2016.

[3] M. Balmer, “Household coal use in an urban township in South Africa”, *Journal of Energy in Southern Africa*, vol. 18, no. 3, pp. 27–32, 2007, doi: 10.17159/2413-3051/2007/v18i3a3382.

[4] E. Nel, L. Marais, and Z. Mqotyana, “The regional implications of just transition in the world’s most coal-dependent economy: The case of Mpumalanga, South Africa”, *Frontiers in sustainable cities*, pp. 1–16, 2023, doi: 10.3389/frsc.2022.1059312.

[5] H. R. Bohlmann, J. M. Horridge, R. Inglesi-Lotz, E. L. Roos, and L. Stander, “Regional employment and economic growth effects of South Africa’s transition to low-carbon energy supply mix”, *Energy Policy*, vol. 128, no. 5, pp. 830–837, 2019, doi: 10.1016/j.enpol.2019.01.065.

[6] C. C. de Saxe, J. van Eeden, L. Kemp, A. Steenkamp, and J. Cowper, “High-capacity coal trucks to reduce costs and emissions at South Africa’s power utility”, *Research in Transportation Business and Management*, vol. 48, pp. 1–12, 2023, doi: 10.1016/j.rtbm.2022.100898.

[7] IEA, IRENA, UNSD, World Bank, and WHO, “Tracking SDG 7: The Energy Progress Report.”, Accessed: Apr. 20, 2024. [Online]. Available: https://trackingsdg7.esmap.org/downloads.

[8] W. M. Champion, *et al*., “Mutagenicity- and pollutant-emission factors of pellet-fueled gasifier cookstoves: Comparison with other combustion sources”, *Science of the Total Environment*, vol. 739, no. 1, p. 39-48, 2020, doi: 10.1016/j.scitotenv.2020.139488.

[9] S. Bonjour, *et al.*, “Solid fuel use for household cooking: Country and regional estimates for 1980-2010”, *Environ Health Perspect*, vol. 121, no. 7, pp. 784–790, 2013, doi: 10.1289/ehp.1205987.

[10] Stats SA, “General household survey - 2013”, Accessed: Apr. 15, 2021. [Online]. Available: https://www.statssa.gov.za/publications/P0318/P03182013.pdf

[11] M. M. Adane, G. D. Alene, and S. T. Mereta, “Biomass-fuelled improved cookstove intervention to prevent household air pollution in Northwest Ethiopia: a cluster randomized controlled trial”, *Environ Health Prev Med*, vol. 26, no. 1, pp. 1–15, 2021, doi: 10.1186/s12199-020-00923-z.

[12] K. R. Smith, *et al.*, “Energy and human health”, *Annu Rev Public Health*, vol. 34, pp. 159–188, 2013, doi: 10.1146/annurev-publhealth-031912-114404.

[13] I. Onah, A. Nyong, and K. H. Ayuba, “A case study of improved cookstoves and clean fuel use by selected Nigerian Households”, *World Dev*, vol. 142, p. 105-416, 2021, doi: 10.1016/j.worlddev.2021.105416.

[14] M. Chambwera and H. Folmer, “Fuel switching in Harare: An almost ideal demand system approach”, *Energy Policy*, vol. 35, no. 4, pp. 2538–2548, 2007, doi: 10.1016/j.enpol.2006.09.010.

[15] C. Muller and H. Yan, “Household fuel use in developing countries: Review of theory and evidence”, *Energy Econ*, vol. 70, pp. 429–439, 2018, doi: 10.1016/j.eneco.2018.01.024.

[16] Trading Economics, “South Africa Unemployment Rate.” Accessed: Apr. 28, 2020. [Online]. Available: https://tradingeconomics.com/south-africa/unemployment-rate

[17] J. Ludwig, L. T. Marufu, B. Huber, M. O. Andreae, and G. Helas, “Domestic combustion of biomass fuels in developing countries: A major source of atmospheric pollutants”, *J Atmos Chem*, vol. 44, no. 1, pp. 23–37, 2003, doi: 10.1023/A:1022159910667.

[18] A. O. Fayiga, “Environmental pollution in Africa”, *Env Dev Sust*, vol. 20, no. 1, pp. 41-73, 2018, doi: 10.1007/s10668-016-9894-4.

[19] Clean Cooking Alliance, “Clean Cooking Catalog”, Accessed: Jun. 09, 2023. [Online]. Available: http://catalog.cleancookstoves.org/

[20] The World Bank, “Clean and Improved Cooking in Sub-Saharan Africa”, Accessed: May. 19, 2023. [Online]. Available: https://documents1.worldbank.org/curated/en/164241468178757464/pdf/98664-REVISED-WP-P146621-PUBLIC-Box393185B.pdf

[21] L. P. Sumbane-Prinsloo, “The effect of particle size on the performance of low-smoke fuels in coal stoves”, M.Eng. dissertation, North-West University, 2017.

[22] K. Ravindra, M. Kaur-Sidhu, and S. Mor, “Transition to Clean Household Energy through an Application of Integrated Model: Ensuring Sustainability for Better Health and Environment”, *Science of The Total Environment*, vol. 775, p. 145-657, 2021, doi: 10.1016/j.scitotenv.2021.145657.

[23] World Health Organisation, “Mortality from household air pollution.” Accessed: Apr. 03, 2020. [Online]. Available: https://www.who.int/gho/phe/indoor_air_pollution/burden/en/

[24] E. Gakidou *et al.*, “Global, regional, and national comparative risk assessment of 84 behavioural, environmental and occupational, and metabolic risks or clusters of risks, 1990-2016: A systematic analysis for the Global Burden of Disease Study 2016”, *The Lancet*, vol. 390, no. 10100, pp. 1345–1422, 2017, doi: 10.1016/S0140-6736(17)32366-8.

[25] P. Hystad *et al.*, “Health effects of household solid fuel use: Findings from 11 countries within the prospective urban and rural epidemiology study”, *Environ Health Perspect*, vol. 127, no. 5, pp. 1–11, 2019, doi: 10.1289/EHP3915.

[26] P. S. B. Gordon, *et al.* “Europe PMC Funders Group Respiratory risks from household air pollution in low and middle income countries”, *The Lancet Resp Med*, vol. 2, no. 10, pp. 823–860, 2016, doi: 10.1016/S2213-2600(14)70168-7.

[27] J. Grigg, “Particulate Matter Exposure in Children Relevance to Chronic Obstructive Pulmonary Disease”, *Proceedings of the American Thoracic Society*, vol. 6, pp. 564–569, 2009, doi: 10.1513/pats.200905-026RM.

[28] M. N. Khan, C. Z. B. Nurs, M. M. Islam, M. R. Islam, and M. M. Rahman, “Household air pollution from cooking and risk of adverse health and birth outcomes in Bangladesh: A nationwide population-based study”, *Environ Health*, vol. 16, no. 1, pp. 1–8, 2017, doi: 10.1186/s12940-017-0272-y.

[29] CoalTech, “Market overview.” Accessed: May. 13, 2020. [Online]. Available: https://www.coaltechenergy.com/market-overview/

[30] E. Muzenda, “Potential uses of South African Coal fines: A review”, *3rd international conference on Mechanical,Electronics and Mechatronics engineering*, pp. 37–39, 2014.

[31] J. F. Reddick, H. Von Blottnitz, and B. Kothuis, “A cleaner production assessment of the ultra-fine coal waste generated in South Africa”, *J South Afr Inst Min Metall*, vol. 107, no. 12, pp. 811–816, 2007.

[32] D. Taulbee, R. Hodgen, and N. Aden, “Co-briquetting of coal and biomass”, *29th Annual International Pittsburgh Coal Conference 2012, PCC 2012*, vol. 1, no. 1, pp. 122–147, 2012.

[33] J. E. Mills, “Binders for Coal Briquets”, *United States Geological Survey*, vol. 343, pp. 1–56, 1908.

[34] A. A. Botha, J. R. Bunt, H. W. J. P. Neomagus, and F. B. Waanders, “Reactivity study of fine discard coal agglomerates”, *J Anal Appl Pyrolysis*, vol. 113, pp. 723–728, 2015, doi: 10.1016/j.jaap.2015.03.001.

[35] FEECO International, “The Agglomeration Handbook”, Accessed: Jan. 21, 2020. [Online]. Available: https://feeco.com/wp-content/uploads/2022/07/The-FEECO-Agglomeration-Handbook.pdf

[36] R. D. Perlack, G. G. Stevenson, and R. B. Shelton, “Prospects for Coal Briquettes as a Substitute Fuel for Wood and Charcoal in U.S. Agency for International Developement Assisted Countries”, Technical Report, Oak Ridge National Laboratory, 1986.

[37] New Dawn Engineering, “Coal Stove”, Accessed: Sep. 03, 2024. [Online]. Available: https://www.newdawnengineering.com/website/opening.php

[38] L. P. Sumbane, S. J. Piketh, J. R. Bunt, and H. W. J. P. Neomagus, “Evaluating the performance and emission reductions of a coal-derived low-smoke fuel in a conventional household stove”, *Proceedings of the 25th Conference on the Domestic Use of Energy, DUE 2017*, pp. 44–50, 2017, doi: 10.23919/DUE.2017.7931823.

[39] T. Kühn, J. R. Bunt, H. W. J. P. Neomagus, S. J. Piketh, R. C. Everson, and S. Coetzee, “Coal-derived low smoke fuel assessment through coal stove combustion testing”, *J Anal Appl Pyrolysis*, vol. 126, no. 1, pp. 158–168, 2017, doi: 10.1016/j.jaap.2017.06.012.

[40] J. Altanzul, “Research on the Structural Optimization and Emissions Performance of a New Model Household Heating Stove”, Masters dissertation, China Agricultural University, 2017.

[41] A. Bueno-López and A. García-García, “Combined SO2 and NOx removal at moderate temperature by a dual bed of potassium-containing coal-pellets and calcium-containing pellets”, *Fuel Processing Technology*, vol. 86, no. 16, pp. 1745–1759, 2005, doi: 10.1016/j.fuproc.2004.11.010.

[42] P. J. Hancox and A. E. Gotz, “South Africa ’ s coalfields – a 2014 perspective”, Accessed: Aug. 06, 2024. [Online]. Available: https://repository.up.ac.za/bitstream/handle/2263/58453/Hancox_South_2014.pdf

[43] P. Fecko, B. Tora, and M. Tod, “Coal waste: handling, pollution impacts and utilization”, *The Coal Handbook: Towards Cleaner Production*, vol 2, pp. 63–84, 2013.

[44] L. D. Michaud, “911 Metallurgist: Coal Beneficiation Process Diagram.” Accessed: Mar. 28, 2021. [Online]. Available: https://www.911metallurgist.com/blog/coal-beneficiation-process-diagram

[45] H. C. Voges, “Tests on the beneficiation. of coal fines*”, *Journal of the Southern African Institute of Mining and Metallurg*, vol. 91, no. 2, pp. 41–51, 1991.

[46] Department of Minerals and Energy, “National Inventory Discard and Duff Coal – 2001 Summary Report”, *Energy*, pp. 1–31, 2001.

[47] CoalTech, “Coal fines waste pelletising technology launched”, Accessed: Nov. 10, 2020, [Online]. Available: https://www.miningreview.com/top-stories/coal-fines-waste-pelletising-technology-launched/

[48] R. R. Maake and C. J. Grobbelaar, “Re-evaluation of the South African Coal resource/reserves – methodology and UN-ECE classification and characterization framework in the South African context.”, *Proceedings from the 3rd Indaba on coal science and technology, Fossil Fuel Foundation of South Africa*, 1997.

[49] C. J. Grobbelaar, A. S. Surridge, and J. K. Asamoah, “Strategy for the management and utilization of discard coal and fines. Colloquium on coal processing, utilization and control of emissions.”, *South African Institute of Mining and Metallurgy (SAIMM)*, 1995.

[50] N. J. Wagner, “The characterization of weathered discard coals and their behaviour during combustion”, *Fuel*, vol. 87, no. 8–9, pp. 1687–1697, 2008, doi: 10.1016/j.fuel.2007.09.009.

[51] T. England, “A Review of Past and Present Work both Locally and Internationally: The Economic Agglomeration of Fine Coal for Industrial And Commercial Use”, Technical Report, CoalTech, 2000.

[52] S. J. Mangena and G. J. De Korte, “Development of a Process for Producing Low Smoke Fuels from Coal Discards, Report”, Technical Report, Division of Mining Technology, CSIR, 2005.

[53] G. J. De Korte, “C.S.I.R. Contribution to Coaltech 2020”, Technical Report, Division of Mining Technology, CSIR, 1999.

[54] N. E. Altun, C. Hicyilmaz, and A. S. Bagci, “Combustion Characteristics of Coal Briquettes . 1 . Thermal Features”, *Energy & Fuels*, vol. 17, no. 5, pp. 1266–1276, 2003.

[55] A. Garcia-Maraver and M. Carpio, “Factors Affecting Pellet Quality”, *Transactions on State of the Art in Science and Engineering*, vol. 85, pp. 21–35, 2015, doi: 10.2495/978-1-84566-062-8/002.

[56] W. J. Li, S. Y. Lu, R. P. Wang, C. Q. Lin, X. D. Li, and J. H. Yan, “Combustion and Emission Characteristics of Coal Logs with Different Binders for Transportation in a Hydraulic Pipeline”, *Energy and Fuels*, vol. 30, no. 2, pp. 1335–1340, 2016, doi: 10.1021/acs.energyfuels.5b02075.

[57] M. Sedighi and H. Salarian, “A comprehensive review of technical aspects of biomass cookstoves”, *Renewable and Sustainable Energy Reviews*, vol. 70, no. May 2018, pp. 656–665, 2017, doi: 10.1016/j.rser.2016.11.175.

[58] R. Quansah *et al.*, “Effectiveness of interventions to reduce household air pollution and / or improve health in homes using solid fuel in low-and-middle income countries : A systematic review and meta-analysis”, *Environ Int*, vol. 103, pp. 73–90, 2017, doi: 10.1016/j.envint.2017.03.010.

[59] W. Du *et al.*, “Emissions of particulate PAHs from solid fuel combustion in indoor cookstoves”, *Science of the Total Environment*, vol. 771, p. 145-411, 2021, doi: 10.1016/j.scitotenv.2021.145411.

[60] M. M. Adane, G. D. Alene, S. T. Mereta, and K. L. Wanyonyi, “Effect of improved cookstove intervention on childhood acute lower respiratory infection in Northwest Ethiopia: a cluster-randomized controlled trial”, *BMC Pediatr*, vol. 21, no. 1, pp. 1–13, 2021, doi: 10.1186/s12887-020-02459-1.

[61] M. A. Kirby *et al.*, “Effects of a large-scale distribution of water filters and natural draft rocket-style cookstoves on diarrhea and acute respiratory infection : A cluster-randomized

controlled trial in Western Province , Rwanda", *PLOS Medicine*, vol.16, no. 6, pp. 1–24, 2019.

[62] E. Puzzolo, D. Pope, D. Stanistreet, E. A. Rehfuess, and N. G. Bruce, "Clean fuels for resource-poor settings : A systematic review of barriers and enablers to adoption and sustained use", *Environ Res*, vol. 146, pp. 218–234, 2016, doi: 10.1016/j.envres.2016.01.002.

[63] W. Pailman, J. De Groot, M. Clifford, S. Jewitt, and C. Ray, "Experiences with improved cookstoves in Southern Africa", vol. 29, no. 4, pp. 13–26, 2018.

[64] K. Ekouevi, "Household Energy for Cooking Project Design Principles", Accessed: Aug. 24, 2020. [Online]. Available: https://documents1.worldbank.org/curated/en/320081468183548304/pdf/902740NWP0Hous0Box0385285B00PUBLIC0.pdf

[65] D. Sweeney, M. Hegde, K. Leith, and A. Smith, "Handbook for Biomass Cookstove Research, Design, And Development: A Practical Guide to Implementing Recent Advances." Accessed: Aug. 25, 2020. [Online]. Available: https://cleancooking.org/wp-content/uploads/2021/07/517-1.pdf

[66] S. Patel, A. Leavey, S. He, J. Fang, K. O. Malley, and P. Biswas, "Characterization of gaseous and particulate pollutants from gasification-based improved cookstoves", *Energy for Sustainable Development*, vol. 32, pp. 130–139, 2016, doi: 10.1016/j.esd.2016.02.005.

[67] N. J. Wagner and B. Hlatshwayo, "The occurrence of potentially hazardous trace elements in five Highveld coals, South Africa", *Int J Coal Geol*, vol. 63, no. 3–4, pp. 228–246, 2005, doi: 10.1016/j.coal.2005.02.014.

[68] W. H. Calkins, "Determination of Organic Sulfur-Containing Structures in Coal by Flash Pyrolysis Experiments.", *ACS Division of Fuel Chemistry, Preprints*, vol. 30, no. 4, pp. 450–465, 1985.

[69] G. Shen *et al.*, "Emission factors of particulate matter and elemental carbon for crop residues and coals burned in typical household stoves in China", *Environ Sci Technol*, vol. 44, no. 18, pp. 7157–7162, 2010, doi: 10.1021/es101313y.

[70] Y. Chen *et al.*, “Measurements of black and organic carbon emission factors for household coal combustion in China: Implication for emission reduction”, *Environ Sci Technol*, vol. 43, no. 24, pp. 9495–9500, 2009, doi: 10.1021/es9021766.

[71] G. Zhi, C. Peng, Y. Chen, D. Liu, G. Sheng, and J. Fu, “Deployment of coal briquettes and improved stoves: Possibly an option for both environment and climate”, *Environ Sci Technol*, vol. 43, no. 15, pp. 5586–5591, 2009, doi: 10.1021/es802955d.

[72] M. M. Islam, R. Wathore, H. Zerriffi, J. D. Marshall, R. Bailis, and A. P. Grieshop, “In-use emissions from biomass and LPG stoves measured during a large, multi-year cookstove intervention study in rural India”, *Science of The Total Environment*, vol. 758, p. 1-40, 2020, doi: 10.1016/j.scitotenv.2020.143698.

[73] Y. Chen *et al.*, “Measurements of emission factors for primary carbonaceous particles from residential raw-coal combustion in China”, *Geophys Res Lett*, vol. 33, no. 20, pp. 2–5, 2006, doi: 10.1029/2006GL026966.

[74] G. Zhi, C. Peng, Y. Chen, D. Liu, G. Sheng, and J. Fu, “Deployment of coal briquettes and improved stoves: Possibly an option for both environment and climate”, *Environ Sci Technol*, vol. 43, no. 15, pp. 5586–5591, 2009, doi: 10.1021/es802955d.

[75] M. Ibraimo, H. J. Annegarn, and C. Pemberton-Pigott, “Modelling of bottom-lit down-draft (BLDD) clean-burning coal stove”, *Proceedings of the 22nd Conference on the Domestic Use of Energy*, 2014, doi: 10.1109/DUE.2014.6827754.

[76] B. Dan-Asabe, S. A. Yaro, D. S. Yawas, B. Dan-Asabe, D. S. Yawas, and S. Y. Aku, “Water Displacement and Bulk Density-Relation Methods of Finding Density of Powered Materials”, *International Journal of Innovative Research in Science, Engineering and Technology*, vol. 2, no. 9, pp. 5561 – 5566, 2007.

[77] C. W. Meyer, “Structural characterisation of a coke particle packed bed”, Technical Report, North-West University, 2019.

[78] M. Temmerman, F. Rabier, P. D. Jensen, H. Hartmann, and T. Böhm, “Comparative study of durability test methods for pellets and briquettes”, *Biomass Bioenergy*, vol. 30, no. 11, pp. 964–972, 2006, doi: 10.1016/j.biombioe.2006.06.008.

[79] N. T. Leokaoke, J. R. Bunt, H. W. J. P. Neomagus, F. B. Waanders, C. A. Strydom, and T. S. Mthombo, “Manufacturing and testing of briquettes from inertinite-rich low-grade

coal fines using various binders", *J South Afr Inst Min Metall*, vol. 118, no. 1, pp. 83–88, 2018, doi: 10.17159/2411-9717/2018/v118n1a10.

[80] S. J. Mangena, G. J. de Korte, R. U. McCrindle, and D. L. Morgan, "The amenability of some Witbank bituminous ultra fine coals to binderless briquetting.", *Fuel Processing Technology,* vol. 85, no. 15, pp. 1647–1662, 2004.

[81] D. L. Botha and W. J. P. Neomagus, "Evaluation of binders in briquetting of coal fines for application in combustion processes", M.Eng. dissertation, North-West University, 2019.

[82] N. T. Modiri, "An evaluation of coal briquettes using various binders for application in fixed-bed gasification", M.Eng. dissertation, North-West University, 2016.

[83] IPC Coal, "South African Coal", Accessed: Apr. 22, 2023. [Online]. Available: http://www.ipcafrica.co.za/products_coal.htm

[84] M. Steyn and R. C. A. Minnitt, "Thermal coal products in South Africa", *The Southern African Institute of Mining and Metallurgy*, vol. 110, no. 10, pp. 593-599, 2010.

[85] S.-L. Weeber, B. Cairncross, and R. M. S. Falcon, "Mineralogical, petrographic and geological controls on coal ash fusion temperature", *The South African Institute of Mining and Metallurgy.*, vol. 100, no. 3, pp. 181–190, 2000.

[86] S. R. Richards, "Physical Testing of Fuel Briquettes", *Fuel Processing Technology*, vol. 25, no. 1, pp. 89–100, 1990.

[87] D. L. Botha, N. T. Leokaoke, J. R. Bunt, and H. W. J. P. Neomagus, "Evaluation of polymer binders in briquetting of coal fines for combustion applications", *The Journal of the Southern African Institute of Mining and Metallurgy*, vol. 121, no. 3, pp. 113-118, 2021, doi: 10.17159/2411.

[88] T. Makonese, "Systematic Investigation of Smoke Emissions from Packed-bed Residential Coal Combustion Devices", PhD Thesis, University of Johannesburg, 2015.

[89] British Standards Institution, *BS 845-1 : 1987 Methods for assessing thermal performance of boilers for steam, hot water and high temperature heat transfer fluids. Part 1 : Concise procedure.* BSI, 1987.

[90] G. Rein, "Smouldering Combustion Phenomena in Science and Technology", *International Review of Chemical Engineering*, vol. 1, no. 1, pp. 3-18, 2009.

[91] G. Hu, K. Dam-Johansen, S. Wedel, and J. P. Hansen, “Decomposition and oxidation of pyrite”, *Progress in Energy and Combustion Science*, vol. 32, no. 3, pp. 295-314, 2006. doi: 10.1016/j.pecs.2005.11.004.

[92] B. Zhu, B. Shang, X. Guo, C. Wu, X. Chen, and L. Zhao, “Study on Combustion Characteristics and NOx Formation in 600 MW Coal-Fired Boiler Based on Numerical Simulation”, *Energies (Basel)*, vol. 16, no. 1, 2023, doi: 10.3390/en16010262.

[93] J. Cai, D. Li, D. Chen, and Z. Li, “NOx and H_2S formation in the reductive zone of air-staged combustion of pulverized blended coals”, *Frontiers in Energy*, vol. 15, no. 1, pp. 4–13, 2021, doi: 10.1007/s11708-020-0804-y.

[94] T. Makonese, D. M. Masekameni, and H. J. Annegarn, “Influence of coal properties on the performance of fixedbed coal-burning braziers”, *Journal of Energy in Southern Africa*, vol. 28, no. 2, pp. 40–51, 2017, doi: 10.17159/2413-3051/2017/v28i2a1374.

[95] Z. He, Z. Xia, J. Hu, L. Ma, and Y. Li, “Thermodynamic properties of polyvinyl alcohol binder of electrically controlled solid propellant”, *Journal of Polymer Research*, vol. 26, no. 9, 2019, doi: 10.1007/s10965-019-1894-2.

ANNEXURE A – FUEL AND BINDER SELECTION

This section focuses on the selection of the ideal fuel composition and binder that would present suitable results to achieve the study aim. The section focuses on the findings of preliminary tests and experimental runs that was used to base the fuel selection decisions on and stands separate of the main study experiments as discussed in Chapter 4 & 5.

A.1 SELECTION METHODOLOGY

For the fuel selection experiments, three batches of coal pellets containing different binders and one batch of standard D grade lump coal was used to investigate the influence of the pellet properties on combustion. These pellets with different properties were prepared by an external company *(CoalTech PTY.LTD).* The binders used for these pellets include polyvinyl alcohol (PVA), starch, and water (also referred to as binderless pellets). All pellet batches were in a size range of between 19 mm and 6.7 mm. The experimental setup, equipment and combustion appliance used for these preliminary tests is identical to the setup that is discussed in Chapter 4 in detail. The composition of the different fuel batches can be seen in the table below.

Table A1: Fuel batch composition from proximate analyses (air dried basis).

Lump coal (D grade)		**Binderless Pellets**	
Moisture content *(%)*	4.0	Moisture content *(%)*	5.8
Ash yield *(%)*	21.4	Ash yield *(%)*	26.0
Volatile matter *(%)*	24.5	Volatile matter *(%)*	21.5
Fixed carbon *(%)*	50.1	Fixed carbon *(%)*	46.7
Calorific value *(MJ/kg)*	23.6	Calorific value *(MJ/kg)*	20.5
Starch Binder Pellets		**PVA Binder Pellets**	
Moisture content *(%)*	8.6	Moisture content *(%)*	6.0
Ash yield *(%)*	12.2	Ash yield *(%)*	25.7
Volatile matter *(%)*	19.2	Volatile matter *(%)*	22.9
Fixed carbon *(%)*	60.0	Fixed carbon *(%)*	45.4
Calorific value *(MJ/kg)*	25.1	Calorific value *(MJ/kg)*	20.3

The starch binder pellets are classified as C grade, whereas the other three fuel batches are classified as D grade, based on their calorific value and composition. These classifications represent the fuel quality currently used in South African low-income communities. The binderless and PVA binder pellets have identical compositions since they were prepared from the same coal fines. Hence, the addition of PVA binder did not significantly influence the fuel composition. The relative low ash yield of the starch binder pellets can be attributed to the origin of the fines, which were likely procured from a local coal wash plant.

A.2 FUEL SELECTION FINDINGS

During experiments, the following observations were made:

- The pellet batches displayed ideal pre-combustion packing and handling behaviour, including minimal handling and breakage losses during fuel loading and efficient packing on the stove grate. These observations increase the technical feasibility of implementing coal pellets as an alternative fuel in rural environments.

- The binderless pellets and PVA binder pellets displayed minimal ash fusion during combustion, while the starch pellets formed “clinkers” (metallic slag formation) underneath the stove bridge. This characteristic is detrimental to the stove's operation since these formations blocked the fuel from reaching the combustion zone. The formation of these clinkers might be credited to the fuel composition or a possible fluxing compound within the binder, which lowered the ash fusion temperature during combustion.

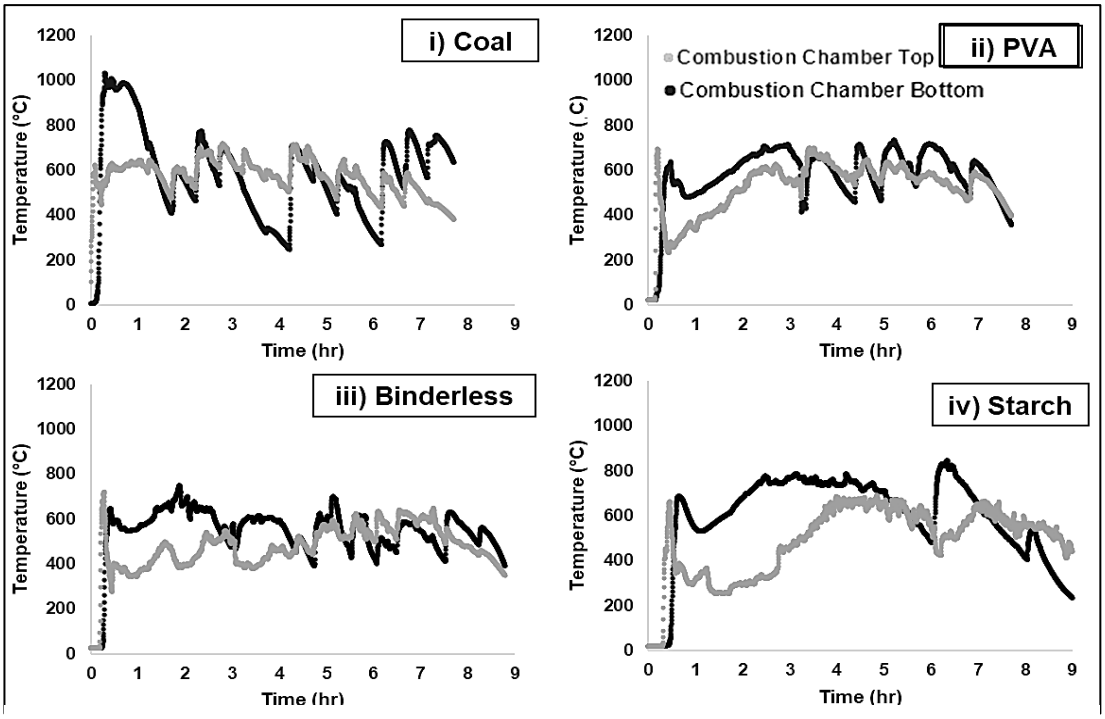

Figure A1: Combustion chamber temperatures of preliminary test runs.

In Figure A1, the time sequences of combustion chamber temperatures are presented for each binder type. The temperature fluctuations and influence of the grate shake on the combustion zone can be seen. The lump coal and the binderless pellets required a similar number of grate shakes, while the starch binder pellets required the least. This might be due to the low ash yield or the increased ash settling rate after combustion. Furthermore, the combustion duration of the starch and binderless pellets exceeded that of the PVA binder pellets and lump coal. This is in accordance with literature which reported that the addition of PVA binder makes agglomerates more prone to being ignited and increases the combustion rate of the fuel [56]. Finally, the lump coal data displayed a large temperature increase during the ignition phase of the experiments (the first hour after fuel ignition). In contrast, the coal pellets remained at a lower temperature during this phase. The starch binder pellets showed the largest average combustion zone temperature compared to the other fuel batches. Finally, it was also found that the lump coal showed the largest temperature fluctuations after grates shakes were performed. These fluctuations correlate with ash formation (ash acts as a combustion inhibitor and insulates the combustion zone) and indicate dead zones, as shown in Figure A1 (i) at 4 and 6 hours after ignition.

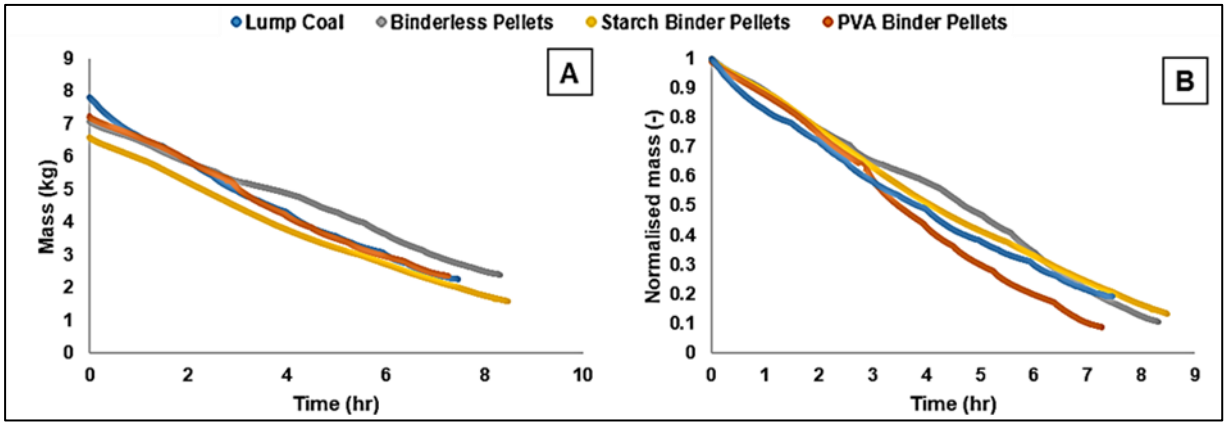

Figure A2: Fuel combustion mass loss rate (A) and normalised mass fraction (B).

In Figure A2, the combustion mass loss rate (A), as well as the normalised mass fraction (ash-free basis) (B), are displayed. The combustion rate is directly proportional to the mass-loss rate (the gradient of the curve in Figure A2 (A) and the combustion temperatures in Figure A1. This correlation can be observed for the high ignition temperature of lump coal (Figure A1) and the relatively steep gradient of the lump coal graph (Figure A2), between 0 – 2 hours after ignition.

Both observations indicate an increased initial combustion rate when compared to the other fuel batches. Furthermore, the PVA binder pellets displayed the highest mass loss rate, and therefore combustion rate, followed by the lump coal. The starch binder pellets and binderless pellets showed similar overall combustion mass-loss rates. The residual ash-free mass fractions are indicated in Figure A2 (B) by the final values at the end of the combustion sequence. This is representative of the overall combustion efficiency for each of the respective runs. It was found that the PVA binder pellets showed the highest combustion efficiency, and the lowest fraction of unburnt carbon left in the ashtray. All pellet batches displayed improved combustion efficiency compared to lump coal, which might be due to the geometry and packing of the fuel. In addition to the temperature and mass loss data, emissions data was also captured to calculate overall emission factors. These factors can be calculated using the flue gas flow rate and assuming the ideal gas law to determine the quantity of each pollutant emitted. However, the data presented in this section were determined using an overall mass balance calculation due to the limitations faced with flue gas measurements. The emission factors are displayed in dimensions [g/MJ], which conveys the amount of a certain pollutant emitted per energy delivered by the stove. These factors were calculated as follows:

Table A2: Emission factors of coal stove and fuel combinations.

Fuel	Emission factors *(g/MJ)*			
	CO_2	CO	NO_x	SO_x
PVA binder pellets	87.8	1.05	0.07	0.34
Binderless pellets	87.0	1.78	0.07	0.32
Starch binder pellets	90.3	2.78	0.02	0.27
Grade D lump coal	89.1	0.51	0.15	0.35
Low-smoke fuels in domestic stove [38]	89	4.8	0.4	4.1
Lump coal in domestic stove [38]	98	3.4	0.3	1.2

The emission factors presented in Table A2 represent the four fuel batches. They are compared to the emission factor results obtained in literature by combusting lump coal and low smoke fuel (LSF) in a domestic DoverTM coal stove [38]. In Table A2, the pellet batches displayed higher levels of CO than lump coal, possibly due to the size and packing of the fuel. The spherical nature of the coal pellets increases the propagation of the combustion zone from the combustion chamber to the hopper. Since the airflow rate is kept constant, the availability of oxygen cannot satisfy the increasing stoichiometric oxygen demand, and therefore higher levels of carbon monoxide are observed.

Furthermore, the NO_x emission factors of all the coal pellets are significantly lower than for lump coal. This might be due to the average combustion bed temperature during the experiments. An indirect proportional correlation can be made between the average combustion bed temperatures (Figure A1) and the NO_x emission factors. A possible explanation might be that the NO_x molecules thermally decompose to N_2 and O_2 at elevated combustion bed temperatures (but still below thermal NO_x formation temperatures). From Table A2, it can also be seen that the SO_x emissions remain relatively constant for all fuel types combusted in the semi-continuous coal stove. This can be attributed to sulphur, which is primarily an inherent or extraneous compound of coal and is not significantly influenced by combustion or fuel geometry. The addition of a PVA binder to the coal fines did not influence the NO_x or SO_x emission levels, as can be seen when the emission factors of PVA binder pellets and binderless pellets in Table A2 are compared. Finally, it is observed that all fuel batches in combination with the improved semi-continuous coal stove display significantly lower emission levels than both low smoke fuel and lump coal when burnt in a domestic coal stove.

A.3 FUEL SELECTION CONCLUSION

Three coal pellet batches and one lump coal batch was combusted in the semi-continuous coal stove. All the fuel batches required grate shakes to increase the ash settling rate and decrease dead zone formation. However, the starch binder pellets required the least grate shakes and exhibited the best ash settling rate. Furthermore, the PVA binder pellets exhibited the highest combustion rate and combustion efficiency. It was found that all the pellet batches produced higher levels of CO when compared to lump coal, with the PVA binder pellets producing the least. The addition of a PVA binder did not influence NO_x or SO_x emissions of coal pellets. For a domestic fuel application, using a PVA binder could be advantageous, since it does not contribute to the emission levels of coal combustion and increases the combustion rate of coal fines (which is ideal for cooking purposes). The PVA binder also increases the durability of the agglomerates and contains no fluxing compounds. Finally, it was found that all the fuel batches in combination with the improved semi-continuous coal stove delivered significantly lower NO_x, SO_x, and CO emission levels than when compared to a domestic *Dover*^{TM} coal stove burning lump coal and LSF. The semi-continuous coal stove coupled with lump coal or coal pellets are suitable for domestic use but should be further evaluated. Using a PVA binder for further investigation should be considered. A fuel sample with a wide size range should also be investigated to determine the influence of particle size, particle geometry and fuel packing on combustion. The effect of coal pellets' ash yield and composition should also be investigated to determine the influence on coal pellet combustion parameters.

ANNEXURE B – PACKED BED CHARACTERISATION

B.1 PACKED BED PROPERTIES

The packing of fuel directly correlates with packed bed characteristics such as bulk density, bed voidage, air permeability, effective surface area, etc. These parameters could be correlated with combustion performance and emission levels but have not been done in literature for cookstoves before. Thus, study also aims to correlate these fuel packing parameters with the combustion performance of the respective batches. In other words, since packed beds with homogenous particles, composed of different particle size ranges, will be used to test the combustion performance in this study, a unique opportunity exists to correlate packing parameters with combustion performance. To do so, a significant difference in packing parameter with the variance of particle size range is needed to adequately describe the influence of packing on combustion. For this reason, several packed bed parameters are determined and calculated in this section for means of comparison in Chapter 5.2.3.

Table B1: Bed density of binderless pellet mixtures (in kg/L).

	50% mixtures		
Size range	**- 26.5mm + 19mm**	**- 19mm + 13.2mm**	**- 13.2mm + 11.2mm**
- 26.5mm + 19mm	0.71	0.73	0.74
- 19mm + 13.2mm	0.73	0.72	0.77
- 13.2mm + 11.2mm	0.74	0.77	0.77
- 11.2mm + 9.5mm	0.76	0.78	0.79
- 9.5mm + 6.7mm	0.79	0.77	0.8
- 6.7mm + 5.6mm	0.79	0.80	0.81
- 5.6mm + 4.75mm	0.82	0.81	0.81
	Other mixtures		
- 26.5mm + 9.5mm	25% mixture		0.77
- 19mm + 9.5mm	33.33% mixture		0.76

Based on the similar circularity factors (from image analysis software) and material density of the different pellet batches, it was assumed that the bulk density results of a single pellet batch would be an accurate representation of all the batches, irrespective of the binder or water proofing agent.

The difference in mixture density when varying the size ranges would be similar for all the pellet batches. This only holds true when comparing identical size ranges. For this reason, only one pellet batch was used to evaluate the bed density at different size range mixtures. The binderless pellets were randomly selected and the results are displayed in Table B1.

While considering the ideal size range criteria as stated in Chapter 3, 50% mixtures were the main focus of this characterisation test. Two special mixtures were also included into the fuel characterisation to represent equivalent (by volume) mixtures with more than two size ranges. These two mixtures were a 33.3 vol.% mixture and a 25 vol.% mixture. From Table B1, it can be seen that the bed density decreases as the size range increases, and vice versa. However, no significant difference can be seen between the different mixtures when considering bed density solely. In order to obtain a quantifiable change in packing as the size range is varied, other parameters were investigated such as: void fraction, surface area to volume ratio, and surface area per fuel mass. These packing parameters are displayed in Table B2 – Table B4.

Table B2: Bed voidage fraction of binderless pellet mixtures.

Number	**Size range**	***50% mixtures***		
		- 26.5mm + 19mm	**- 19mm + 13.2mm**	**- 13.2mm + 11.2mm**
1	- 26.5mm + 19mm	0.53	0.52	0.51
2	- 19mm + 13.2mm	0.52	0.52	0.49
3	- 13.2mm + 11.2mm	0.51	0.49	0.49
4	- 11.2mm + 9.5mm	0.49	0.49	0.48
5	- 9.5mm + 6.7mm	0.47	0.49	0.46
6	- 6.7mm + 5.6mm	0.47	0.47	0.46
7	- 5.6mm + 4.75mm	0.46	0.46	0.46
		Other mixtures		
1+2+3+4	- 26.5mm + 9.5mm	25% mixture		0.49
2+3+4	- 19mm + 9.5mm	33.33% mixture		0.49

The average bed void fraction of the pellet batch was calculated using Equation A-1.

$$\varepsilon_{avg} = 1 - \frac{\rho_b}{\rho_p} \quad \text{A-1}$$

Where:

ε_{avg} is the average void fraction of the fuel packed bed.

ρ_b is the packed bed / bulk density as displayed in **Table B1**.

ρ_p is the particle / material density as displayed in Table 3-5.

It can be seen that the void fraction of the packed bed produces a greater variance with change in size range when compared to the bed density, however not significant enough to correlate the packing parameter with the combustion performance of the fuel batch.

Table B3: Surface area to volume of 50% mixtures (mm^2/mm^3)

	50% mixtures		
Size range	**- 26.5mm + 19mm**	**- 19mm + 13.2mm**	**- 13.2mm + 11.2mm**
- 26.5mm + 19mm	0.26	0.32	0.38
- 19mm + 13.2mm	0.32	0.37	0.43
- 13.2mm + 11.2mm	0.38	0.43	0.49
- 11.2mm + 9.5mm	0.42	0.48	0.54
- 9.5mm + 6.7mm	0.50	0.56	0.62
- 6.7mm + 5.6mm	0.62	0.67	0.73
- 5.6mm + 4.75mm	0.71	0.77	0.83
	Other mixtures		
- 26.5mm + 9.5mm	25% mixture		0.43
- 19mm + 9.5mm	33.33% mixture		0.48

Next the surface area to volume ratio of the packed bed was determined in an attempt to improve the variance of packing parameter between the bed mixtures. The surface area to volume ratio was determined using the surface area of equivalent diameter spheres that falls in the size range of the mixtures, and the volume of the particles data gained from the fluid submersion test. The results are displayed in Table B3. From the table it can be seen that the variance in packed bed parameter with change in size range is much more significant than the previous two packing parameters. The highest surface area to volume ratio was obtained for the small size range particles (bottom right corner of Table B3) whereas the least surface is to volume ratio was determined for the large size range particles (top left corner of Table B3). This correlates with literature findings and theoretical calculations for mixtures with spheres of different size ranges.

Table B4: Surface area per fuel mass of 50% mixtures (m^2/kg).

50% mixtures			
Size range	**- 26.5mm + 19mm**	**- 19mm + 13.2mm**	**- 13.2mm + 11.2mm**
- 26.5mm + 19mm	0.37	0.44	0.51
- 19mm + 13.2mm	0.44	0.52	0.56
- 13.2mm + 11.2mm	0.51	0.56	0.64
- 11.2mm + 9.5mm	0.55	0.62	0.68
- 9.5mm + 6.7mm	0.64	0.72	0.77
- 6.7mm + 5.6mm	0.78	0.85	0.91
- 5.6mm + 4.75mm	0.87	0.95	1.02
Other mixtures			
- 26.5mm + 9.5mm	25% mixture		0.56
- 19mm + 9.5mm	33.33% mixture		0.63

Finally, the surface area per fuel mass of 50% mixtures and two special mixtures were determined and displayed in Table B4. Once again, the surface area was determined using the surface area of equivalent diameter spheres, while the fuel mass was obtained from the results in Table 3-5. It can be seen that the surface area per fuel mass follow the same trend as the surface area to volume ratio as presented in Table B3. However, these results present a greater difference in packing parameters (when compared to the previous parameters) as the mixture size range is varied.

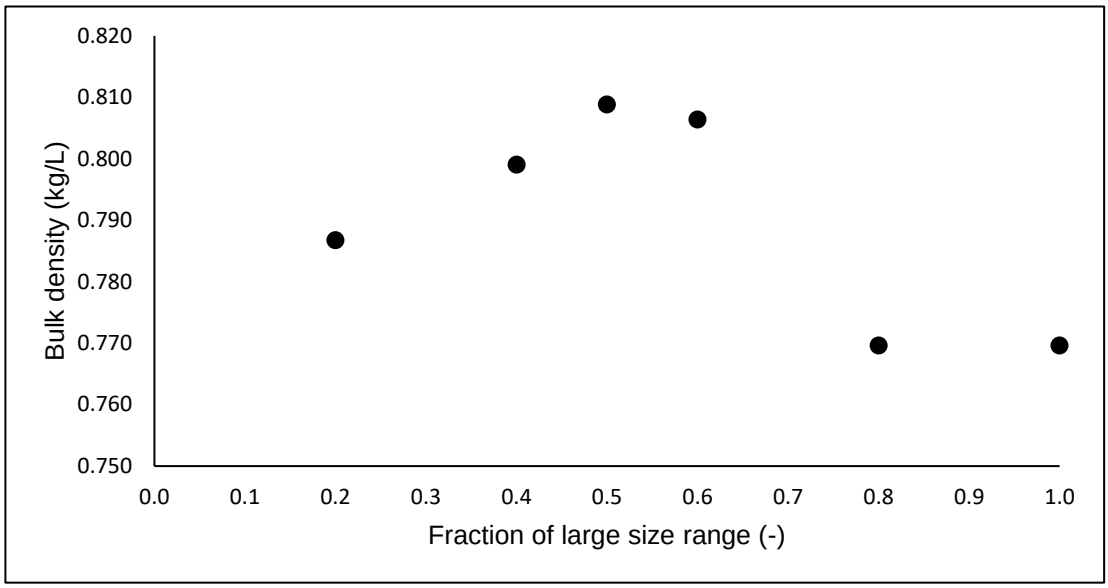

Figure B1: Bed density of binderless pellets' percentage mixtures.

To determine the effect of percentage mixtures on the packing density, a characterisation test was done using P-B pellets with two size ranges (-19 mm +13.2 mm & -9.5 mm +7.6 mm). The results of the percentage mixtures characterisation test can be seen in Figure B1. It was found that the mixture with a 1:1 volume ratio of large size range to small size ranges (50 vol% mixture) resulted in the highest density packing. Therefore, any other combination of mixing fraction would result in less fuel being loaded into the cookstove combustion chamber. The use of 50% mixtures in the determination of packing parameters are therefore recommended. In an attempt to validate whether the assumption of using only the binderless pellets for characterisation was accurate, the packed bed density, using the aforementioned size ranges, was experimentally determined for all the other pellet types. These results can be seen in Table B5.

Table B5: Density characterisation of the three chosen size ranges.

Size range	-19 mm +13.2 mm	-19 mm +9.5 mm	-13.2 mm +6.7 mm
C	-	0.76 ± 0.002	-
P-2.5	0.717 ± 0.006	0.722 ± 0.003	0.73 ± 0.007
P-2.5-W	0.707 ± 0.006	0.710 ± 0.003	0.716 ± 0.006
P-5	0.717 ± 0.006	0.726 ± 0.003	0.729 ± 0.003
P-5-W	0.737 ± 0.005	0.748 ± 0.009	0.754 ± 0.008

It can be seen that the bed density of the different pellet batches follows a similar trend when compared to the results obtained using only binderless pellets (Table B1). The difference in bulk density between the different pellet batches can mainly be attributed to the varying particle/material density of each fuel type. It can be seen that even though there is no significant correlation between the results of the different size ranges (considering the confidence intervals) the average mean density values can be divided into low, medium, and high-density packing. Therefore, as the packing volume increases, a significant difference in packing density between size ranges is possible. Finally, since the density results in Table B5 correlates with the results found using only P-B pellets, it can be concluded that the assumption of using only one pellet batch for characterisation was acceptable.

ANNEXURE C – INVESTIGATION OF STOVE POWER SETTING

The detailed discussion of the low-power runs in comparison to high-power runs follows. The results presented in this section was obtained by operating the semi-continuous coal stove on ingress air, with the inlet air controller completely closed. An attempt was made to compare the low-power runs' findings to literature, however limited information is available since literature focus is predominantly on emissions reduction without variance in stove power output.

C.1 COMBUSTION PERFORMANCE

The combustion performance results as recorded during the respective low-power runs can be seen in Figure C1. The mass loss data are shown for the duration of the run lengths. A summary of the combustion parameters for low-power runs using fuel of size range -19 mm +13.2 mm is also given in Table C1.

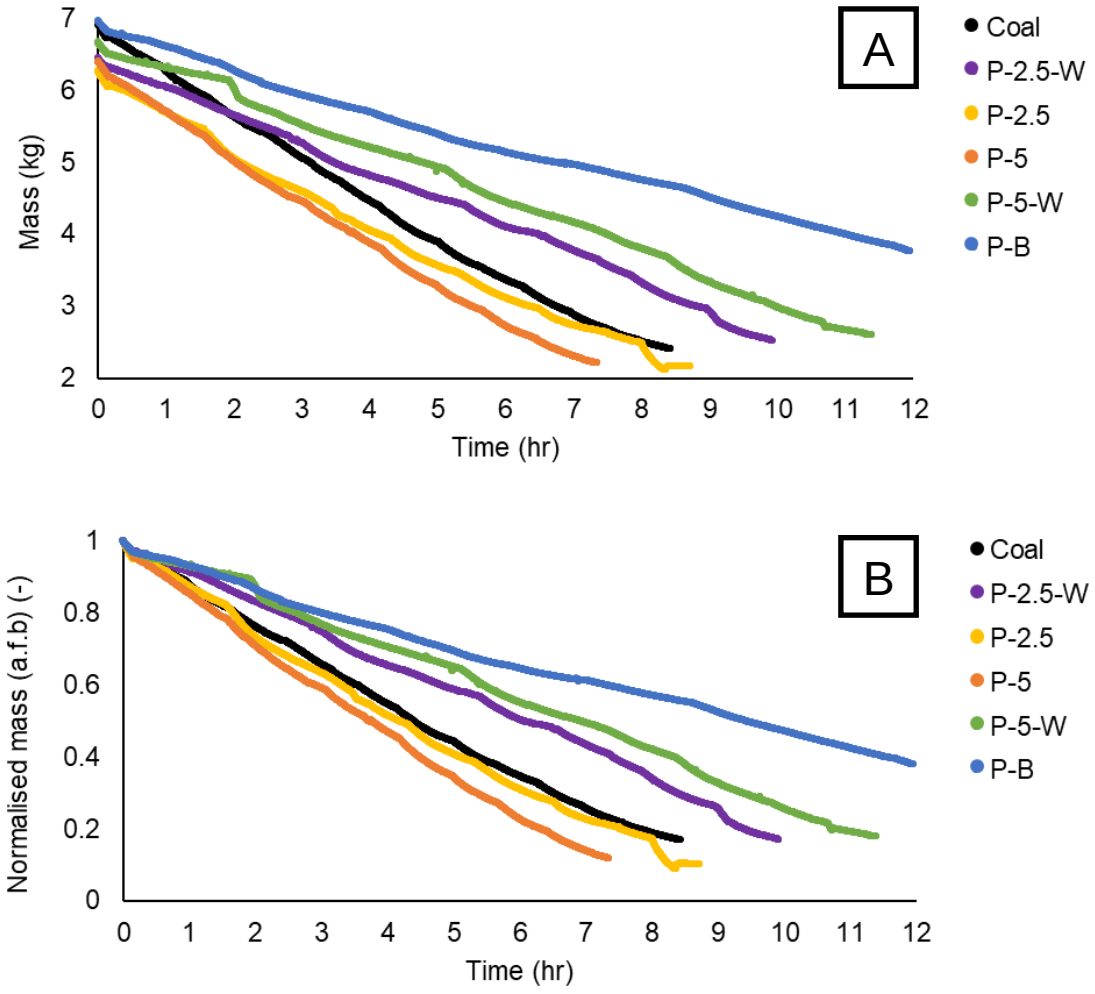

Figure C1: Mass loss of low-power runs with fuel size -19 mm +13.2 mm: (A) as measured and (B) normalised & ash free basis.

From the results illustrated in Figure C1, a greater distinction between the respective low-power runs can be seen, when compared to the high-power runs (Figure 5-8 and Table 5-1). The initial mass values of the low-power runs, as can be seen in both Figure C1 (A) and in Table C1, correlates with the observations made for the high-power runs. The binderless pellets exhibited the highest initial mass due to the excessive amount of fines, whereas the lump coal and P-5-W runs also displayed relatively high initial mass values due to the packing density of the respective fuels. The PVA pellet runs showed an increase in initial mass correlating with increased PVA binder content, whereas the waterproofed pellet runs also showed higher initial mass values than their non-waterproofed counterparts. This observation is further supported by the P-2.5 run that displayed the lowest initial mass, while the P-5-W run displayed the highest of all the PVA pellet runs, for both low- and high-power settings. This might be attributed to the amount of material (binder or waterproofing) added to the fuel during the production process.

Table C1: Combustion parameters of low-power runs with fuel size -19 mm +13.2 mm.

	Initial mass	**Run length**	**Grate shakes**	**Time between shakes**	**Average combustion rate**	**Combustion efficiency**
	kg	*hr*	-	*hr*	*kg/hr*	-
C	6.93	8.43	12	0.70	0.54	0.83
P-B	6.97	11.95	8	1.49	0.27	0.62
P-2.5	6.27	8.72	8	1.09	0.47	0.90
P-2.5-W	6.45	9.93	7	1.42	0.40	0.83
P-5	6.40	7.35	8	0.92	0.57	0.88
P-5-W	6.66	11.39	7	1.63	0.36	0.82

When considering the run length and combustion rate of the respective runs, it is shown that the low-power runs lasted for approximately 60% - 150% longer than the high-power runs. This is mainly consequent to limiting the natural draft flow rate through the stove, resulting in lower combustion rates. This is also illustrated in the average gradient of the mass loss data presented in Figure C1. The binderless pellets showed the longest run length and the lowest combustion rate. This is expected since similar behaviour was found for the high-power runs and was attributed to the lack of a binding agent. In contrast, the P-5 pellets had the shortest run length and highest combustion rate. Furthermore, when considering the waterproofed pellet runs' graphs in Figure C1, it is seen that these runs differ significantly from the non-waterproofed fuel variants. The waterproofed fuel runs displayed significantly longer run lengths than the non-waterproofed fuel runs, and lower overall combustion rates. This observation is similar than what was reported

for the high-power runs in Section 5.2, however the difference between these two fuels was more prominent during the low-power runs. When comparing the run lengths and combustion rates between low- and high-power runs, only one outlier can be seen. The P-5-W run showed low combustion rates and a significantly longer run length than the other PVA binder pellet batches. The magnitude difference in comparison with the other pellet batches does not correlate with the high-power runs. This is due to an improper combustion zone (as displayed in Figure 5-3) that formed during the ignition phase of the P-5-W run. The significant impact of an improper combustion zone during ignition can be seen in both the run length and combustion rate of the P-5-W experiment. When considering the shape of the graphs in Figure C1, several non-uniform areas in the P-5-W, P-2.5 and P-2.5-W graphs can be seen. This occurs at 2 hours, 8 hours, and 9 hours respectively. These severe changes in gradient and combustion rate are attributed to the influence of the grate shakes and clinker formations. The dead zones and clinkers results in a decrease in combustion rate, whereafter the use of severe grate shakes to break the ash formations usually results in combustion rate, temperature, and emission spikes. This results in a typical “irregularity” of the mass loss data as seen in Figure C1.

When considering the number of grate shakes performed, it is shown that all low-power runs required 1 – 2 grate shakes more than the high-power runs, with the lump coal still requiring the most. The similar amount of grate shakes needed between the low-power runs and the high-power runs are due to the lower average combustion rate and thus lower dead zone formation rates. In addition, it was observed that the lower combustion rates for the pellet runs also minimised the clinker formation since lower combustion zone temperatures were reached (as displayed in Section C.2). Therefore, a greater ash-settling ability of the pellets fuels was observed during low-power runs, which led to a lower number of shakes needed, and less frequent. The average time between grate shakes for the lump coal run was the lowest, in contrast with the P-5-W and P-B pellet batches. Similar to the high-power runs, the lump coal displayed the worst ash-settling ability and therefore needed the most amount of grate shake.

When considering the combustion efficiency of the respective runs, the binderless pellets showed the lowest combustion efficiency, far lower than what was reported for high-power runs. This is due to the high number of excess fines, as well as the formation of clinkers towards the end of this run. The clinkers prevented the last remaining fuel in the hopper from reaching the active combustion zone, therefore adding to the low combustion efficiency. The non-waterproofed pellets showed the highest combustion efficiencies, identical to the high-power runs. The decline in P-B, P-2.5-W & P-5-W combustion efficiencies can be attributed to the smouldering combustion mechanism. It is shown in Section C.2 that the temperature profile of these runs was much lower compared to the non-waterproofed fuel and the lump coal runs. Lower combustion zone

temperatures result in an earlier onset of smouldering combustion since minimal heat transfer is available for proper combustion. Once smouldering combustion takes place, premature end-of-run conditions are reached, and ultimately the runs are ended with greater amounts of unburnt fuel left in the stove.

The respective transient combustion rate graphs of the low-power runs using fuel size -19 mm +13.2 mm are displayed in Figure C2.

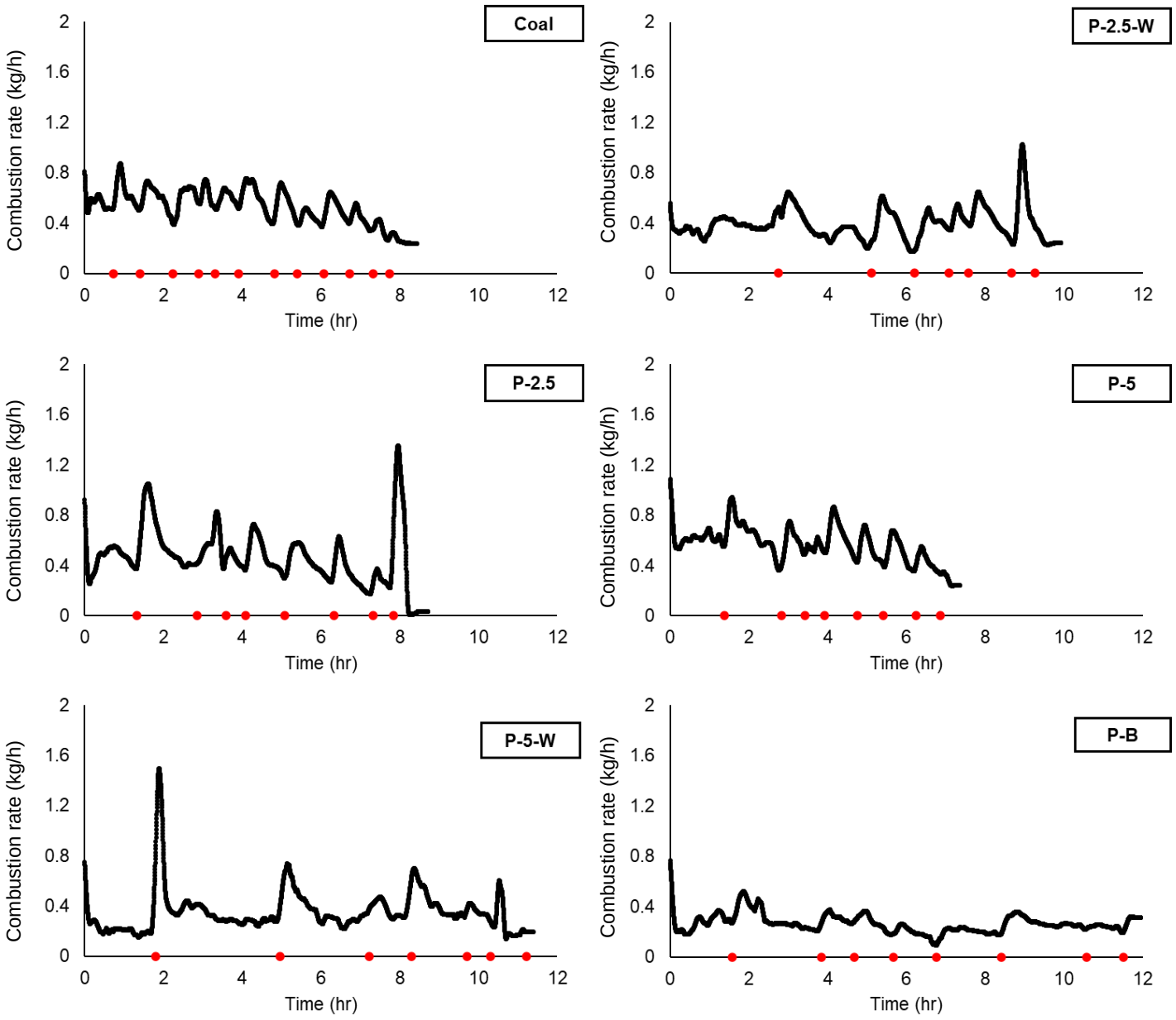

Figure C2: Combustion rates of low-power runs with fuel size -19 mm +13.2 mm.

It is shown that all the low-power runs had significantly lower combustion rates than the high-power runs, which is expected. Furthermore, it can be seen that the lump coal and P-5 pellet runs showed the highest combustion rate values compared to the other runs. In contrast, the P-B run displayed the lowest average transient combustion rate throughout the run and correlated with the overall combustion rate values displayed in Table C1. When reflecting on the stability of the transient combustion rate graphs, the magnitude of peaks and valleys displayed in Figure C2 is much smaller than for high-power runs. Furthermore, it can be noticed that the lump coal and P-5 pellet runs also displayed lower magnitude spikes, when compared to the other low-power runs. The lower variability of transient combustion rates is due to lower combustion temperatures and ash formation rates. This reduces the effect of dead zone formation and clinkering while improving the ash-settling ability relative to the high-power runs. The binderless pellet run showed the most favourable transient combustion rate for a low-power setting. The linear nature of the combustion rate graph for the P-B run correlates with the desired steady operation and continuous ash settling. This is supported by the long periods between grate shakes for the P-B run. This is also in alignment with the application of low-power runs since the goal of this power setting is to present a low, continuous, and steady combustion rate that delivers constant heating energy to the living environment over a long period, with minimal user input required.

The large combustion rate spikes at the end of the P-2.5 and P-2.5-W runs are mainly due to clinker formation as highlighted previously. This can be seen in Figure C2 as the combustion rate at the end of the run spikes severely, and proceeds by dropping to approximately 0 kg/hr. It was observed that the final amount of fuel was blocked by large clinkers underneath the stove bridge and was consequently liberated by performing severe grate shakes to break these clinkers and ensure fuel flow. It was found that all pellet runs produced clinkers and dead zones, however the severity and extent of these formations were much lower compared to the high-power runs.

C.2 THERMAL PERFORMANCE

Averaged stove temperatures of each chamber are given in Table C2 for low-power runs using fuel with a size range of -19 mm +13.2 mm.

Table C2: Average internal temperatures of the semi-continuous coal stove during low-power runs with fuel size -19 mm +13.2 mm.

	Hopper bottom *TT305*	**CC bottom** *TT309*	**CC middle** *TT307*	**HX middle** *TT311*	**Chimney** *TT301*
	°C	*°C*	*°C*	*°C*	*°C*
C	650	790	720	230	130
P-B	680	540	380	100	50
P-2.5	730	700	590	180	110
P-2.5-W	840	650	550	160	90
P-5	830	730	650	200	110
P-5-W	680	620	470	130	70

It is shown in Table C2 that all the low-power runs' temperatures are significantly lower than what was displayed for high-power runs in Table 5-2. This is due to the lower combustion rate and reduced natural draft flow rate in the stove. Furthermore, the lump coal run exhibited the highest temperatures across the stove profile (excluding the hopper bottom temperature) while the P-B run displayed the lowest. The lump coal run showed a similar temperature profile to the high-power variant, where a relatively high combustion chamber temperatures are observed in parallel with a lower hopper bottom temperature. In contrast, all the pellet batches showed significantly higher combustion zone temperatures at the bottom of the hopper in comparison to the combustion chamber bottom. This was also observed for high-power runs and accredited to the combustion mechanism that was fundamentally different between the two fuels. Similar to the high-power variants, the binderless pellet run showed the lowest combustion chamber temperatures. The lump coal low-power run displayed higher average CC bottom temperatures than the high-power run while still maintaining adequate gas phase combustion. This is however not the case for pellet runs. The lowest CC middle temperature, indicative of gas phase combustion, was reported for the P-B run followed by the P-5-W run. This correlates with low excess oxygen and high emission levels for these runs. The lump coal and P-5 runs showed the highest CC middle temperatures indicating the greater degree of gas phase combustion that occurred during these runs. This was also reflected in the temperature profile throughout the downstream sections of the stove. Like the high-power runs, the lump coal displayed the highest heat exchanger chamber temperatures and the largest temperature gradient from the combustion chamber to the chimney. This translates to a high heat transfer rate, in contrast to the relatively

low temperature gradient seen for the pellet runs. The lump coal run exhibited the highest chimney temperature, followed by the P-5 run. In contrast, the P-B, P-2.5-W and P-5-W runs showed average chimney temperatures below 100 °C, which led to liquid formation in the chimney. It was observed that a tar-like liquid flowed from the chimney back into the heat exchanger chamber and settled at the bottom of the stove. This influenced the stove performance by:

1. Lower stack losses were found for these runs as the wet gas losses are limited, which normally account for a large portion of the stack losses. This energy is transferred to the stove surfaces, instead of losses via chimney emission.

2. The tar liquid that settled at the bottom of the heat exchanger chamber acted as an insulator and decreased the conduction losses at the bottom of the stove.

3. It was found that these tar liquids can build up in the chimney elbow as it flows down and solidifies around the outlet baffle. After multiple stove runs it can result in the blockage of the stove exit. This negatively impacts the stove operation as it hinders the internal cross-draft required for stove operation. In a severe case, it was observed that a reverse draft forms and emissions seeped out the stove apertures around the air inlet and ash tray. This could potentially expose the stove user and people in the nearby living environment directly to the harmful combustion emissions.

The P-2.5-W low-power run displayed greater hopper temperatures than the P-2.5 run, but lower downstream temperatures in the rest of the stove sections. This supports the impact of clinkering which limits the char combustion to the hopper section of the stove. Furthermore, the P-5-W low-power run showed lower temperatures than all the other PVA pellet runs, and similar profiles to that of the P-B run. The main contributing factor for the low temperatures reported during the P-5-W runs was the improper (cold) initial combustion zone. Finally, similar to the high-power runs, no significant correlation could be observed between the amount of binder added to the fuel and the temperature profiles displayed in Table C2.

The combustion zone temperatures of the low-power runs using fuel with a size range of -19 mm +13.2 mm can be seen in Figure C3.

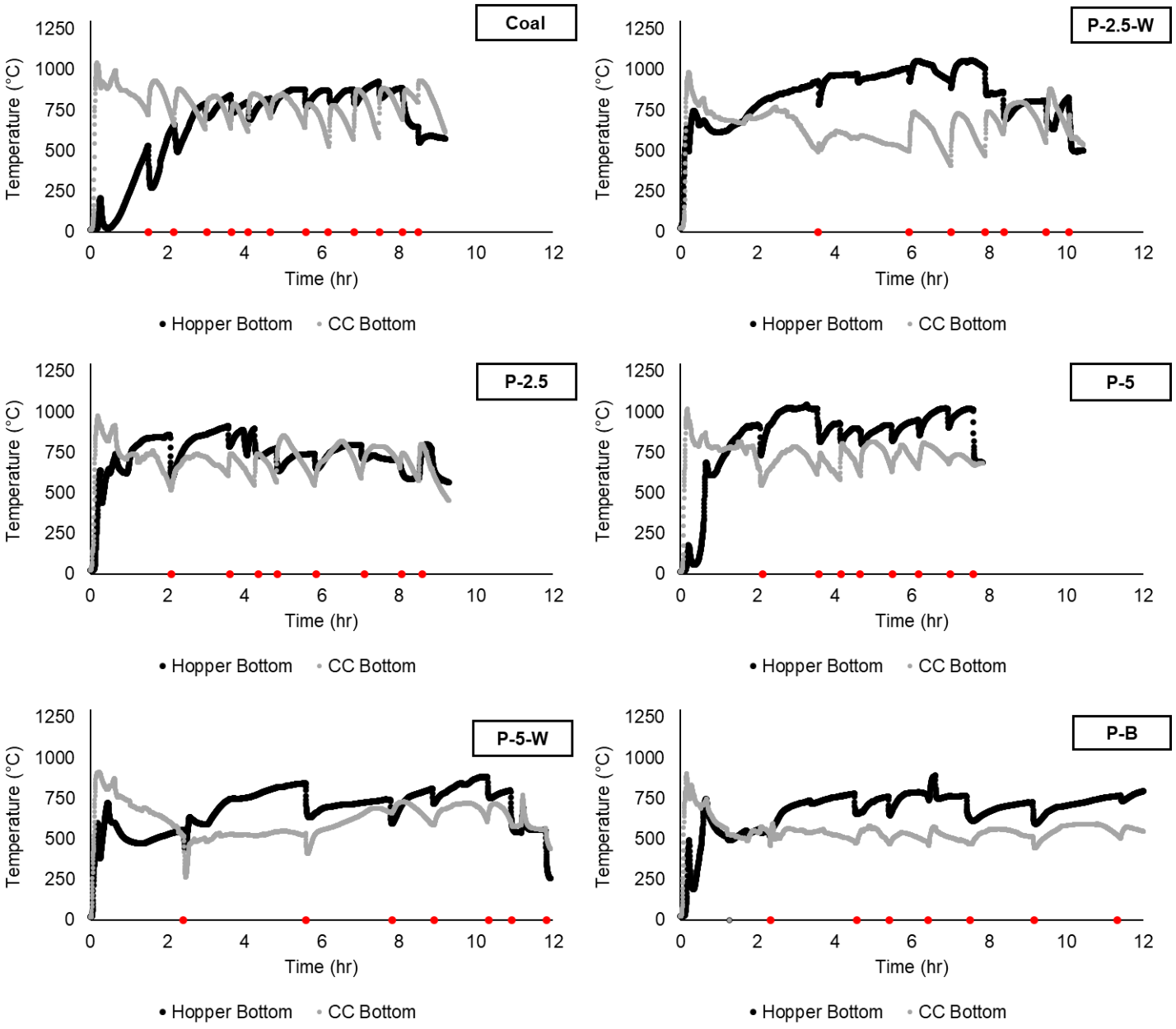

Figure C3: Combustion zone temperatures of low-power runs with fuel size -19 mm +13.2 mm.

In this figure, all the low-power runs exhibited lower combustion zone temperatures than the respective high-power run variants consequent to reducing the natural draft flow rate. The lump coal run displayed the highest combustion zone temperature, and the P-B run the lowest, which

was also observed for the high-power runs. The large temperature difference between the hopper bottom and combustion chamber bottom temperatures of the P-2.5-W run are a direct result of ash fusion and clinkering. It can be seen that this run presented the largest combustion zone temperature gradient, likely due to the clinkers underneath the stove bridge that acted as a fuel barrier, and heat insulator. Finally, the lump coal, P-2.5 and P-5 runs showed typical combustion zone temperature profiles for low-power runs, and thus no significant correlation could be observed between the amount of binder added to the fuel, and the respective combustion zone temperatures.

Table C3: Water boiling test results for low-power runs with fuel size -19 mm +13.2 mm.

	Time to boil	**Cooking power**	**Cooking efficiency**
	min	*kW*	*%*
C	23	0.50	10.8
P-B	214**	0.04	1.9
P-2.5	61	0.17	3.4
P-2.5-W	74	0.13	2.8
P-5	53	0.21	4.4
P-5-W	184	0.05	1.9

** P-B did not boil and reached a max temperature of 90 °C.

The water boiling test results for low-power runs using fuel with a size range of -19 mm +13.2 mm are displayed in Table C3. It is shown that the lump coal run, followed by the P-5 run took the shortest time to boil the water. This correlates with the combustion chamber middle (gas phase combustion) temperatures shown in Table C2. In contrast, the P-B run, followed by the P-5-W run took the longest time to boil. Furthermore, the binderless pellet run could only heat the water to a maximum temperature of 90 °C during the entire run. For the P-5-W run, the rate of combustion energy transfer to the water pot is slightly greater than the energy losses of the water pot. This is reflected through the relatively low cooking power calculated for this run and the slow increase in water temperature observed. For the P-B run, the thermal losses of the water pot were greater than the energy transferred from the cooking surface to the water pot via conduction, convection and radiation. In other words, the energy losses of the water pot were approximately 0.04 kW at 90 °C, which the P-B run could not overcome. That is consequently why the water could not reach boiling point. This is further observed through the P-B and P-5-W runs which exhibited the lowest cooking power and efficiencies out of all the high- and low-power runs. The low energy transfer rates are attributed to the low combustion rates observed for these runs, as well as the non-typical gas phase combustion and low combustion chamber temperatures.

It is shown in Table C3, that all runs took significantly longer to boil the water than the high-power runs. This is expected since low-power runs are intended to reduce energy output and prolong the duration of the stove operation without reloading fuel. The only exception to this observation is the lump coal run, which time to boil is comparable to that of the high-power run. Due to the unusual high combustion chamber middle temperature, and effectiveness of the gas phase combustion, more energy was transferred to the cooking area relative to the other stove surfaces during this run. This also resulted in a much greater cooking efficiency, as approximately 10% of the combustion energy was transferred to the water pot. This cooking efficiency for the lump coal run is the highest efficiency calculated for all low- and high-power runs.

Similar to the high-power runs, the fuel without waterproofing exhibited improved boiling times, cooking power, and cooking efficiencies than the fuel with waterproofing added. Similarly, this can be attributed to the respective combustion mechanisms and temperature profiles observed during the runs.

Table C4: Thermal performance parameters for low-power runs with fuel size -19 mm +13.2 mm.

	P_F	P_D	η_{SL}	η_D	η_{tot_1}	η_{tot_2}	$\bar{V}_{chim}$
	kW	*kW*	*%*	*%*	*%*	*%*	*m^3/hr*
C	4.5	4.0	91.0	89.4	74. 4	64.6	10.1
P-B	2.1	1.6	95.1	77.8	58.4	54.4	4.8
P-2.5	3.6	2.9	92.9	81.2	73.0	71.8	7.8
P-2.5-W	3.0	2.5	93.1	82.1	68.2	67.1	6.6
P-5	4.3	3.8	91.3	87.3	77.1	72.2	9.0
P-5-W	2.7	2.0	94.6	75.2	61.8	58.2	5.8

η_{tot_1} is calculated using the energy delivered via conduction and radiation approach (Equation E-26).

η_{tot_2} is calculated using the stack loss approach (Equation E-27).

A summary of the thermal performance parameters for low-power runs is displayed in Table C4. In this table, it is shown that the low-power runs displayed significantly lower power ratings than the high-power runs. The runs maintained a power output of 2 kW – 4.5 kW for more than 7 hours. The lump coal run, followed by the P-5 pellet run, showed the highest fired and delivered power. In contrast, the P-B run followed by the P-5-W run showed the lowest fired and delivered power. This is in correlation with the internal stove temperatures and combustion rates displayed previously. Similar to what was observed and discussed for the high-power runs, the non-waterproofed pellet runs exhibited higher fired and delivered power ratings.

When considering the average chimney flow rates, and the stack loss efficiency of the respective runs, it is noticed that the chimney flow rates were approximately half of what was shown for high-power runs. The stack loss efficiency however is still in the same range as what was displayed for the high-power runs. In correlation with the chimney outlet flow rates, and respective runs' temperature profiles shown in Table C2, the P-B run, and P-5-W run, had the lowest stack temperature and average flow rate, and thus the greatest stack loss efficiency. In contrast the P-5 and lump coal runs displayed the highest chimney temperatures and flow rates, thus resulting in the lowest stack loss efficiency compared to the other runs. The overall stack loss efficiency for the low-power runs is also higher than that calculated for the high-power runs. Following the higher temperature profiles and increased combustion performance of the non-waterproofed fuel, these runs exhibited higher stack losses than the waterproofed pellet runs.

The energy delivered efficiency for the low-power runs is significantly higher for the lump coal and P-5 runs, than for the rest of the low-power runs. These efficiencies are also higher than the values presented for the high-power runs, which is attributed to the reduction in stack flow rate, stack temperature, and thus reduced stack losses. The lowest delivered energy efficiency was reported for the P-B run followed by the P-5-W run. This is attributed to the energy losses through combustible matter and gases in the stack gas. Even though the stack losses were minimised for these runs, the amount of combustible matter (CO, VOCs, carbonaceous PM, etc.) that was emitted as a result of smouldering combustion, were far greater than for the other runs. Therefore, the actual combustion energy generated per mass fuel consumed, was less for the P-B and P-5-W runs than for the other runs, resulting in reduced delivered and overall energy efficiencies. Furthermore, the P-B run exhibited the lowest total energy efficiency of all the runs conducted in this study. The P-5 run showed the highest total energy efficiency followed by the lump coal run. The total energy efficiency of the non-waterproofed pellets was also found to be significantly higher than compared to the waterproofed pellets. Similar to what was reported for high-power runs, the thermal performance of the waterproofed fuel might have been influenced by the chemical properties of the waterproofing agent, correlating with the temperature and combustion parameters discussed previously.

The stove energy produced, energy delivered, and heating efficiency is displayed in Figure C4 for all low-power runs. Similar to the high-power runs, the lump coal displayed typical energy and efficiency trends. This was also observed for the P-5 low-power run where the combustion energy at the start of the run exceeds the delivered energy but decreases as the run progresses. At the end of these runs, a clear increase in heating energy efficiency can be seen as the surfaces of the stove slowly dissipate energy due to the specific heat capacity of the stove material, while the combustion energy is reduced. It can be debated the lump coal and P-5 low-power runs produced

typical energy efficiencies similar to that of high-power runs even though the stove power output was reduced.

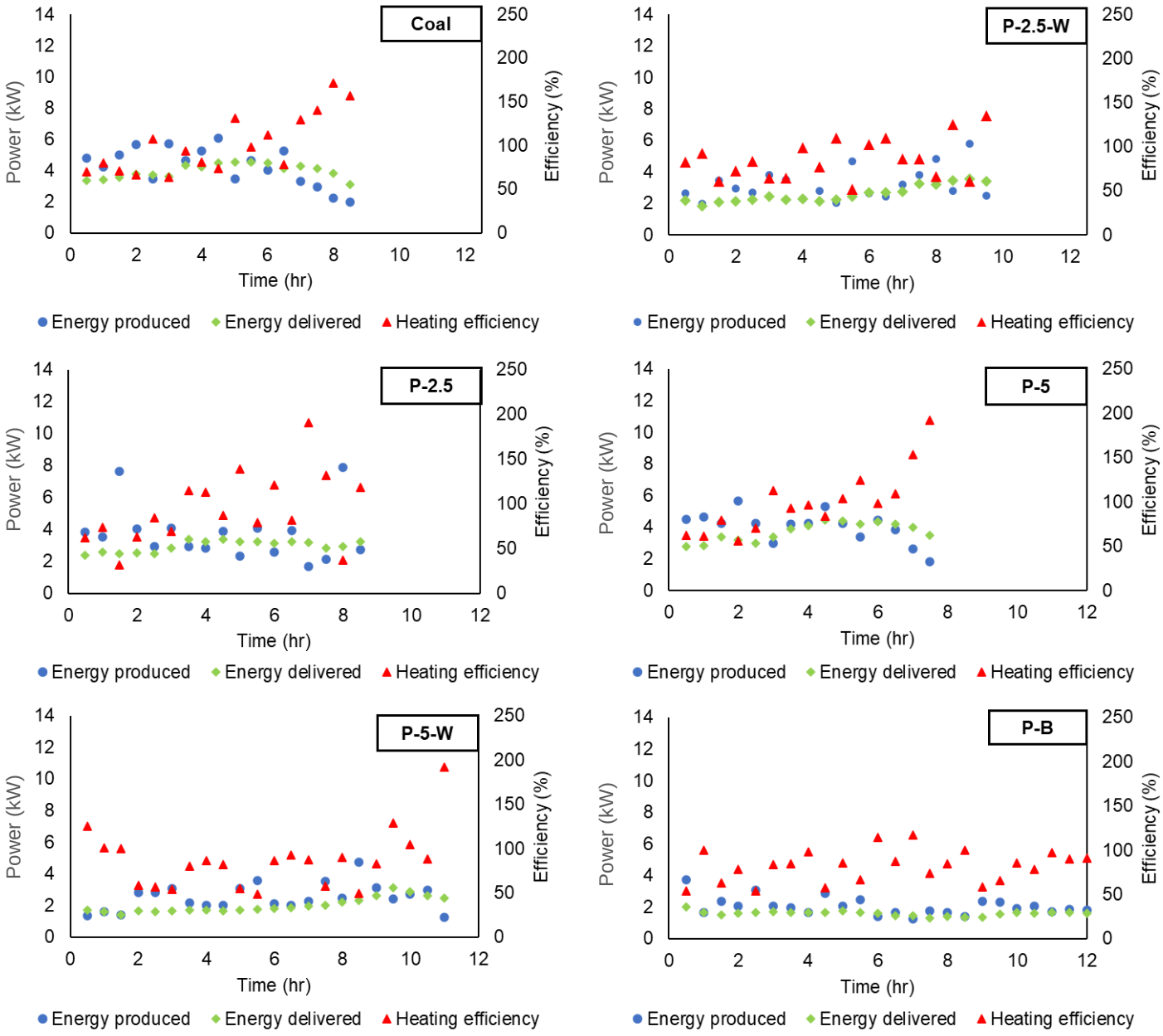

Figure C4: Energy produced, energy delivered, and heating efficiency for low-power runs using fuel of size -19 mm +13.2 mm.

Similar to the high-power run variants, the P-2.5 and P-2.5-W runs showed the largest variability in energy output during the run, while the P-B and P-5-W runs displayed relatively linear delivered energy and efficiency values. The linear nature of the P-B and P-5-W runs' energy profiles are favourable for low-power runs which are intended for continuous and steady living space heating over long periods. The high variability of the P-2.5 and P-2.5-W runs is likely caused by the effect

of clinkering and consequent severe grate shakes. Finally, the P-B low-power run showed the lowest energy delivered of all the runs while the lump coal displayed the highest energy delivered.

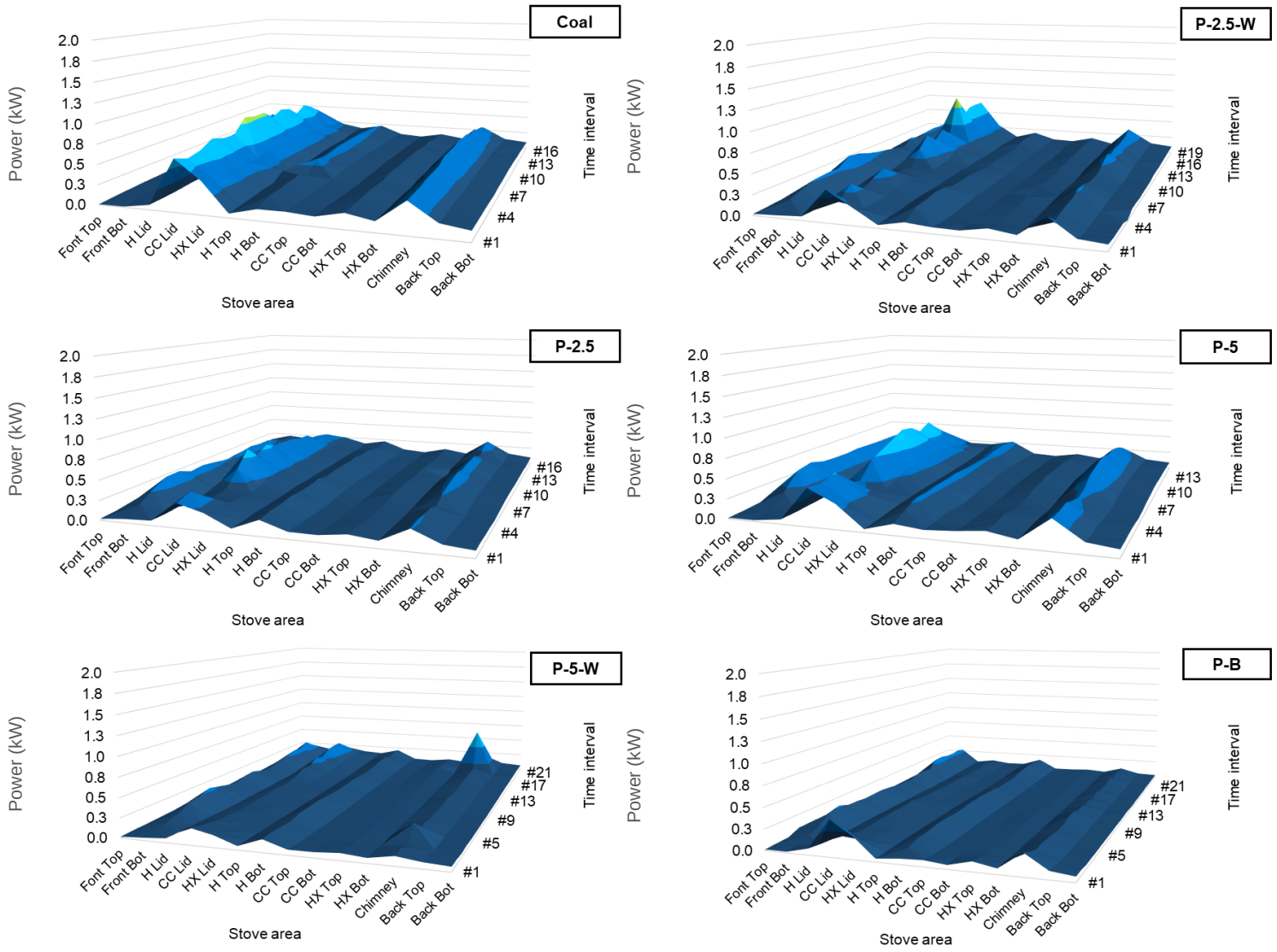

Figure C5: Total energy delivered (radiation & convection) from the stove surfaces for low-power runs with fuel size -19 mm +13.2 mm.

The average energy delivered by each respective stove surface area is displayed in Figure C5, according to the division discussed in Chapter 4. It is shown that for all the runs, the combustion chamber and heat exchanger chamber lids are the areas with the highest energy flux, as expected. Furthermore, all the low-power runs delivered significantly less energy from the surfaces of the stove than the high-power run variants, as intended. It can be seen that the lump coal and the P-5 low-power runs presented the highest energy output compared to the other low-

power runs. The main difference however is that for the lump coal run, minimal energy was delivered through the front surfaces of the stove as can be seen in Figure C5. The P-5 run, however, showed significant energy flux through the front bottom and top areas of the stove. In the context of high-power runs, this is a disadvantage since less energy is delivered through the cooking surface of the stove, but for a low-power run where the intention is living space heating, it can be argued that the P-5 run displayed a greater energy flux distribution through all surfaces of the stove and not predominantly through the cooking surface. This might be an advantageous characteristic of the P-5 low-power run when considering living space heating.

Similar to the high-power runs, the combustion chamber lid displayed the largest energy flux variability in most of the low-power runs. Only the P-5-W and P-B runs displayed constant, low variability energy flux throughout the run, which correlates with the results discussed previously. For these runs, similar energy flux profiles were calculated for all the areas of the stove as can be seen in Figure C5, due to the smouldering combustion that occurred in these runs. Finally, the low combustion temperatures and low draft flow rates reduced the chimney energy flux during the P-5-W and P-B runs in contrast to the other low-power runs.

C.3 EMISSION LEVELS

The carbon oxides and the excess oxygen levels recorded in the chimney for low-power runs using fuel of a size range of -19 mm +13.2 mm are displayed in Figure C6.

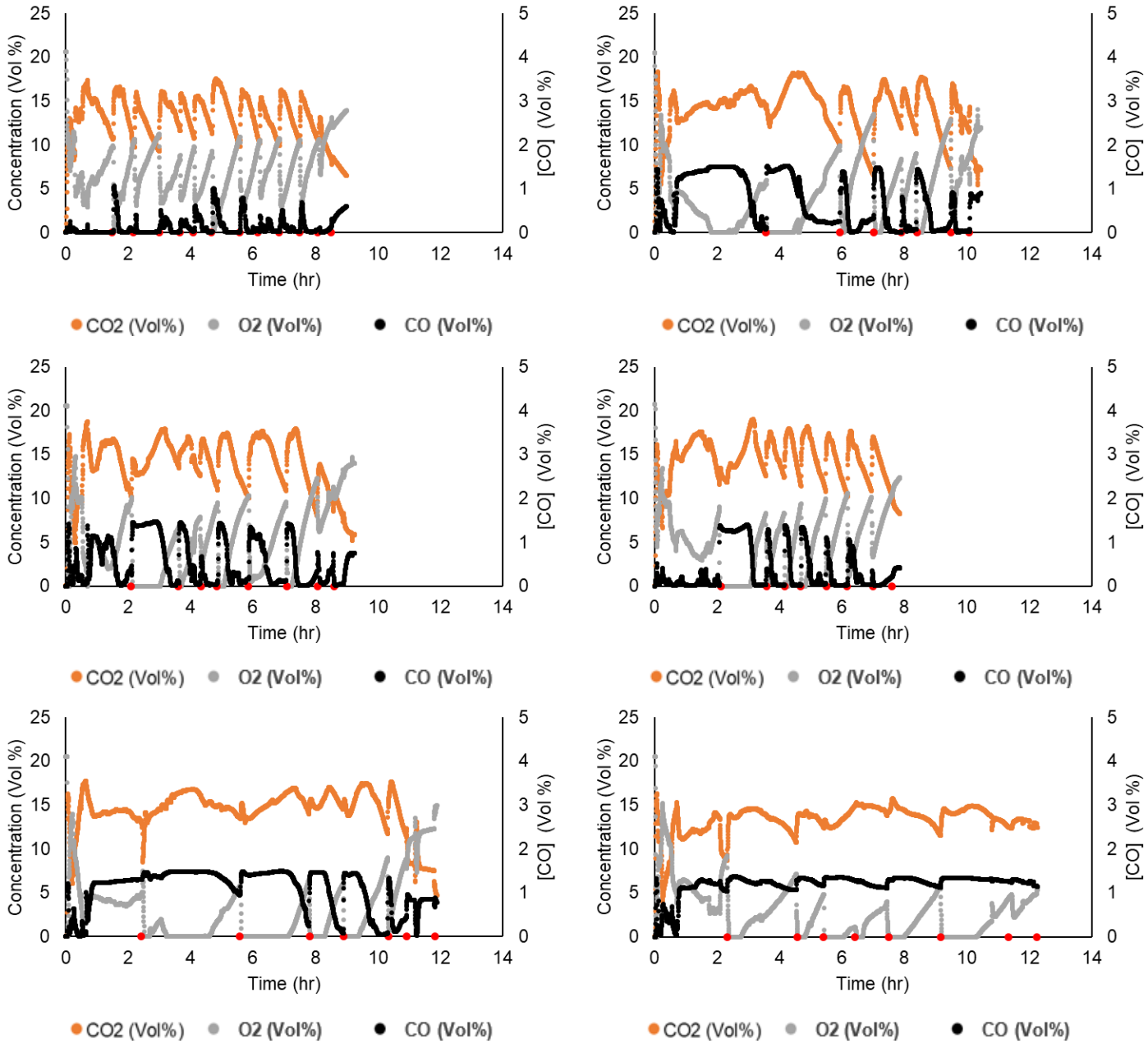

Figure C6: Carbon oxides and oxygen concentrations in the flue gas of low-power runs using fuel size -19 mm +13.2 mm.

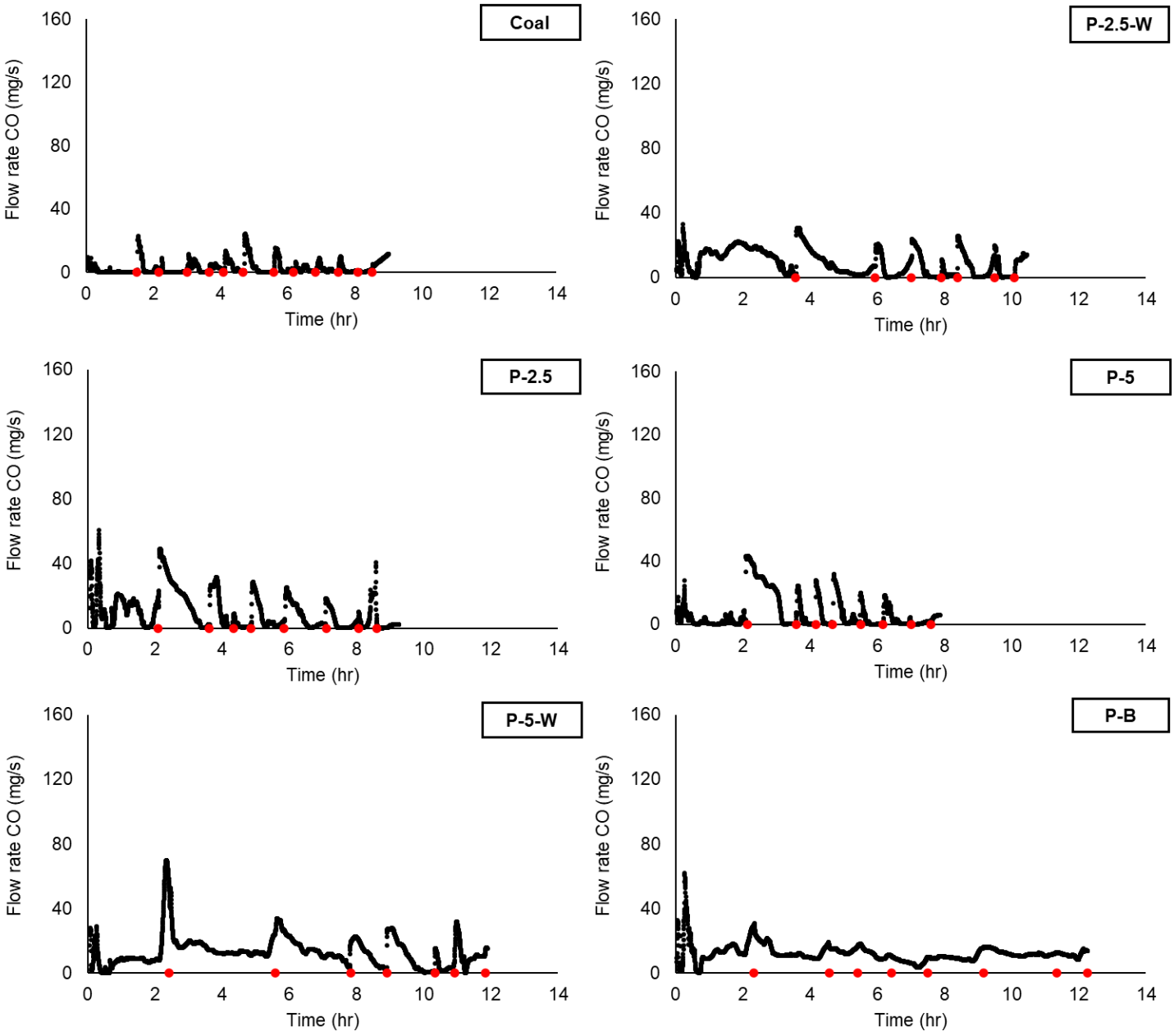

Figure C7: The carbon monoxide mass flow rate of low-power runs using fuel with a size range of -19 mm +13.2 mm.

The calculated CO mass flow rates exiting the chimney of respective low-power runs using fuel with a size range of -19 mm +13.2 mm are displayed in Figure C7. The main difference between the low-power runs and the high-power runs can be seen when considering the P-5-W and P-B runs in Figure C6 and Figure C7. These runs displayed consistently high CO levels where the excess oxygen in the chimney rarely exceeded 7 vol.%. These non-typical continuous high CO levels are also displayed in Figure C7. For these runs, grate shakes were initiated based on ash formation even when the oxygen levels in the chimney were still relatively low. It can also be seen that the CO_2 levels for these runs remained relatively linear in contrast to the other runs where the CO_2 and O_2 graphs form peaks and valleys throughout the run. When considering the excess

air levels in the stove, similar observations can be made. The calculated excess air levels of the respective low-power runs using fuel with a size range of -19 mm +13.2 mm are displayed in Figure C8. It is shown that the low-power runs have significantly lower excess air levels than what was obtained for the high-power runs. This is expected since the air levels are minimised by closing the inlet air controller, and effectively running the stove on ingress air. The lump coal and P-5 runs showed the fastest increase in excess air after grate shakes. This correlates with the relatively higher combustion rate when compared to the other low-power runs as previously discussed. The higher combustion rate translates to an increased ash formation rate and therefore a greater increase in excess oxygen levels after grate shakes.

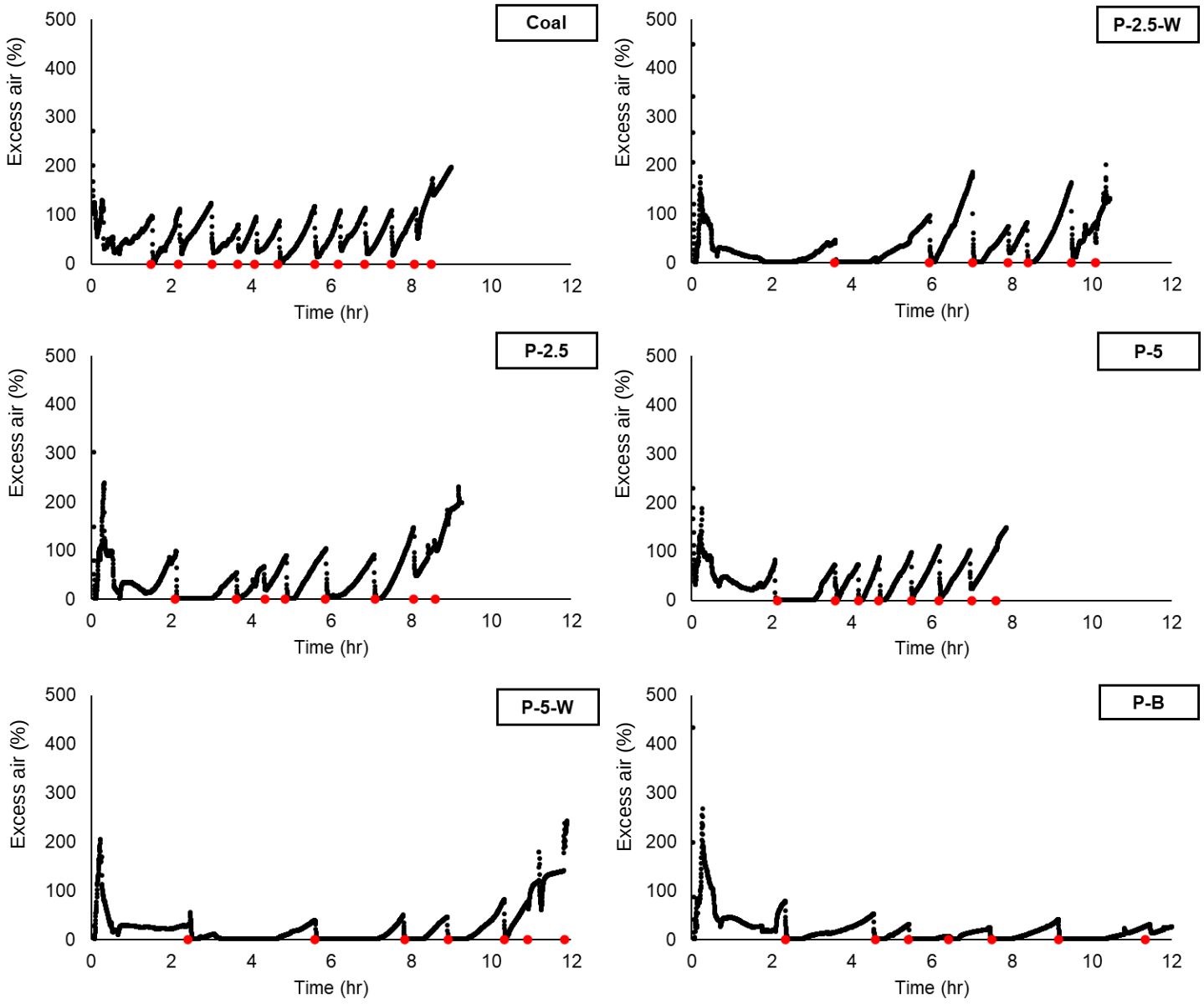

Figure C8: Excess air concentrations in the flue gas of low-power runs using fuel size -19 mm +13.2 mm.

Similar to what was observed for the high-power runs, the excess air levels of the lump coal run rarely decreased to 0% or lower. This was however not the case for pellet runs. The maintained excess air levels of the lump coal run after grate shakes result in improved combustion and emissions performance. It was found that the excess air, combustion rates, and emission levels are all dependent variables of the combustion mechanism. It is shown that the combustion mechanism can follow two extreme cases during low-power runs, depending on the propagation rate:

1. **Proper combustion zone, fast propagation rate.**
   A large combustion zone and fast propagation rate increases the natural draft flow rate in the stove through high heat transfer rates and pressure gradients. The higher draft in turn provides more oxygen to the combustion zone, however, the excess air is still limited since for low-power runs the air controller is closed, and the stove is run on ingress air. This means that the solid phase combustion expands and increases since most of the oxygen is consumed in this area. In the gas phase, however, minimal combustion takes place since little oxygen is available for reaction. This results in high PM and CO emissions. For most of the low-power runs, this condition cannot be altered or amended since an interaction between the combustion propagation rate, natural draft and excess air only increases with oxygen availability, which cannot be further reduced since the air inlet is already closed. Therefore, the combustion rate reaches an upper ceiling limit due to oxygen availability and only reduces at the end of the run when most of the char fuel is spent. Examples of the proper combustion zone, and fast propagation rate can typically be seen in Figure C6 to Figure C8 for the P-2.5 and P-2.5-W runs.

2. **Improper combustion zone, slow propagation rate.**
   The improper combustion zone and a slow propagation rate results in low combustion energy generation and therefore minimal heat transfer to the internal fluid. This results in a low natural draft since not enough energy is available to create a higher-pressure gradient. The low natural draft results in less air to the combustion zone, reducing the combustion, heat generation, and propagation rates. This consequently forms smouldering combustion where the entire combustion mechanism is limited by the heat transfer rate. During the smouldering combustion regime, continuous high CO and PM levels are observed despite sufficient oxygen availability for reaction. In contrast to the previously discussed mechanism, this forms a lower limit for the combustion rate and propagation rate and can only be amended by opening the air inlet and adding a combustion accelerant to the combustion zone. For experimental consistency, it was not

done in this study. Examples of the improper combustion zone and slow propagation rate can typically be seen in Figure C6 to Figure C8 for the P-5-W and P-B runs

It was found that the ideal operating conditions for low-power runs were in the middle between the proper combustion zone, fast propagation rate mechanism, and the improper combustion zone, slow propagation rate mechanism. The lump coal run operated seemingly in the middle of these limits, where sufficient energy was available to drive the natural flow rate. The combustion zone propagation rate was also not high enough to cause oxygen deficiency, which ensured proper gas phase combustion and low CO and PM emissions. The P-5 run also operated with a similar mechanism, but slightly towards the higher propagation rate mechanism as supported by the CO emissions after 2 hours into this run. It was also found that large transient combustion rate spikes during low-power runs are not preferable in terms of emission performance since it increases the oxygen consumption rate while the airflow is limited for low-power runs. Therefore, low-power are more sensitive to transient combustion rate variations than compared to high-power runs.

A summary of the main emission parameters as calculated for the various low-power runs, is displayed in Table C5.

Table C5: Emission parameter summary of low-power runs using fuel size -19 mm +13.2 mm.

	α	$CO{:}CO_2$	ε_{O_2}	$\overline{v}_{chim}$	$\bar{\lambda}$	$y_{d/w}$	V_{H_2O}
	-	%	%	m/s	-	-	ml
C	0.990	1.1	2.0	0.4	1.63	0.941	74
P-B	0.921	9.1	18.8	0.2	1.51	0.948	140
P-2.5	0.964	4.0	5.4	0.3	1.56	0.947	74
P-2.5-W	0.952	5.1	8.4	0.2	1.52	0.938	75
P-5	0.977	2.4	4.9	0.3	1.47	0.943	70
P-5-W	0.934	7.6	11.7	0.2	1.44	0.946	85

When considering the α value and the CO:CO_2 ratio, it was found that the P-B and the P-5-W runs displeased that lowest α value and the highest CO:CO_2 ratio. This is in correlation with the results discussed previously where these runs displayed continuous high CO emission levels. Furthermore, the oxygen error was also the greatest for the P-B and the P-5-W runs which correlate with the CO results. It can be seen that all the runs presented lower α values, higher CO:CO_2 ratios, and greater oxygen balance error values compared to the high-power runs. The

only exception is the lump coal run. The lump coal low-power run exhibited similar combustion behaviour that the high-power run variant and thus presented comparable emission results. The agglomerated fuel low-power runs, however, showed less favourable combustion behaviours compared to the high-power runs when reflecting on oxygen deficiency occurrences and pollutant levels. Thus, the lower α values, higher CO:CO_2 ratios, and greater oxygen balance error values compared to the high-power runs was expected. The correlation between the relatively high CO:CO_2 ratio and the high oxygen balance error values for the P-B and P-5-W runs can again be contributed to the formation of miscellaneous oxygen containing species (such as COS). The chimney velocity of the low-power runs is approximately 50% lower than the high-power run variants, which is expected since the natural draft flow rate was minimised.

Even though the P-B and P-5-W runs displayed prolong periods of oxygen deficiency, the averages correction factor remained relatively comparable for all the runs. When considering the amount of water collected from the stack gas, it was found that the all the low-power runs exhibited much higher moisture condensation rates compared to the high-power runs. The low-power runs accumulated roughly 50% more water during the run, which is mainly due to the decreased stack gas temperature and the increased run duration. One outlier can however be observed. The P-B run accumulated approximately double the amount of moisture compared to the other low-power runs, and roughly 5 times the amount of moisture than the high-power P-B variant run. This significant increase in moisture accumulation is due to the extreme low stack temperatures (near ambient), resulting in condensation and fluid back-flow into the stove. When the water and tar liquid returns to the heat exchanger chamber, it vaporises again and consequently forms a heating-cooling loop between the stove and chimney. This phenomenon resulted in severe accumulation of moisture in the experimental equipment and sampling lines, which ultimately lead to blockages and equipment failure. Extra care should be taken to prevent this from occurring during large scale implementation.

Table C6: Sulphur balance for low-power runs using fuel size -19 mm +13.2 mm.

	$m_{S\,Fuel}$	$m_{S\,Stack}$	OF_S
	g	*g*	-
C	33.9	23.3	0.69
P-B	52.2	7.6	0.15
P-2.5	48.2	16.5	0.34
P-2.5-W	49.7	13.3	0.27
P-5	46.7	17.8	0.29
P-5-W	46.6	11.0	0.24

The sulphur balance of the low-power runs using fuel size -19 mm +13.2 mm are displayed in Table C6. The total sulphur analyses that were done for the ash samples were only conducted for high-power runs, therefore no results for total sulphur in the ash, or the percentage of undetected sulphur species could be reported. From the results displayed in Table C6, it is shown that the initial sulphur that was present at the start of the run is identical to the initial values displayed for high-power runs. Furthermore, the mass sulphur emitted for the low-power runs can be seen to be significantly less than for the high-power runs. The only exception to this observation is the lump coal run. All the pellet batches exhibited a decrease in total mass sulphur emitted, 10% – 30% lower, compared to the high-power counterparts. Only the lump coal run did not display a significant reduction in total sulphur emitted. This can also be seen when considering the sulphur oxidation factors. All pellet batches showed a significant decrease in sulphur oxidation when compared to the high-power runs, except the lump coal run. The main contributing factor for this observation is not known yet, as stated previously. However, it can be reasoned that the change in combustion rate did not affect the total mass sulphur emitted by the lump coal run. Therefore, a more likely factor that influenced the sulphur emissions is the type of sulphur species present in the fuel, or the structure of the agglomerates during and post combustion. Again, no significant correlation or explanation can be given with certainty, and more experimentation and analyses will be needed for further insight into this phenomenon. From the results displayed in Table C6 it can further be seen that the waterproofed pellets exhibited lower sulphur emissions and lower oxidation factors than the non-waterproofed fuel. This is in correlation with the high-power run findings.

A summary of the SO_X emission graphs for low-power runs using fuel size -19 mm +13.2 mm is displayed in Figure C9. It is shown that the sulphur mass flow rate of the low-power runs is significantly lower than the high-power variants. This is in correlation with the SO_X emission results discussions previously for the results in Table C6 where the sulphur oxidation factors were observed to be lower than the high-power run variants. For the low-power runs it can also be seen that the SO_X mass flow rate is related to the combustion temperature, oxygen availability, combustion rate, and combustion efficiency. It is exhibited in Figure C9 that the runs with the lowest combustion temperature (P-B and P-5-W) showed the lowest mass flow rate of SO_X emission compared to the other runs. This can be attributed to the sulphates in the fuel that are commonly volatilised at temperatures higher than approximately 800 °C. These two runs not only operated below this 800 °C threshold but also exhibited extended periods of oxygen deficiency and low combustion rates. The P-B runs also displayed the worst combustion efficiency compared to the other runs. This all explains why the P-B and P-5-W runs reported the lowest overall SO_X mass flow rate, with the P-B run the lowest.

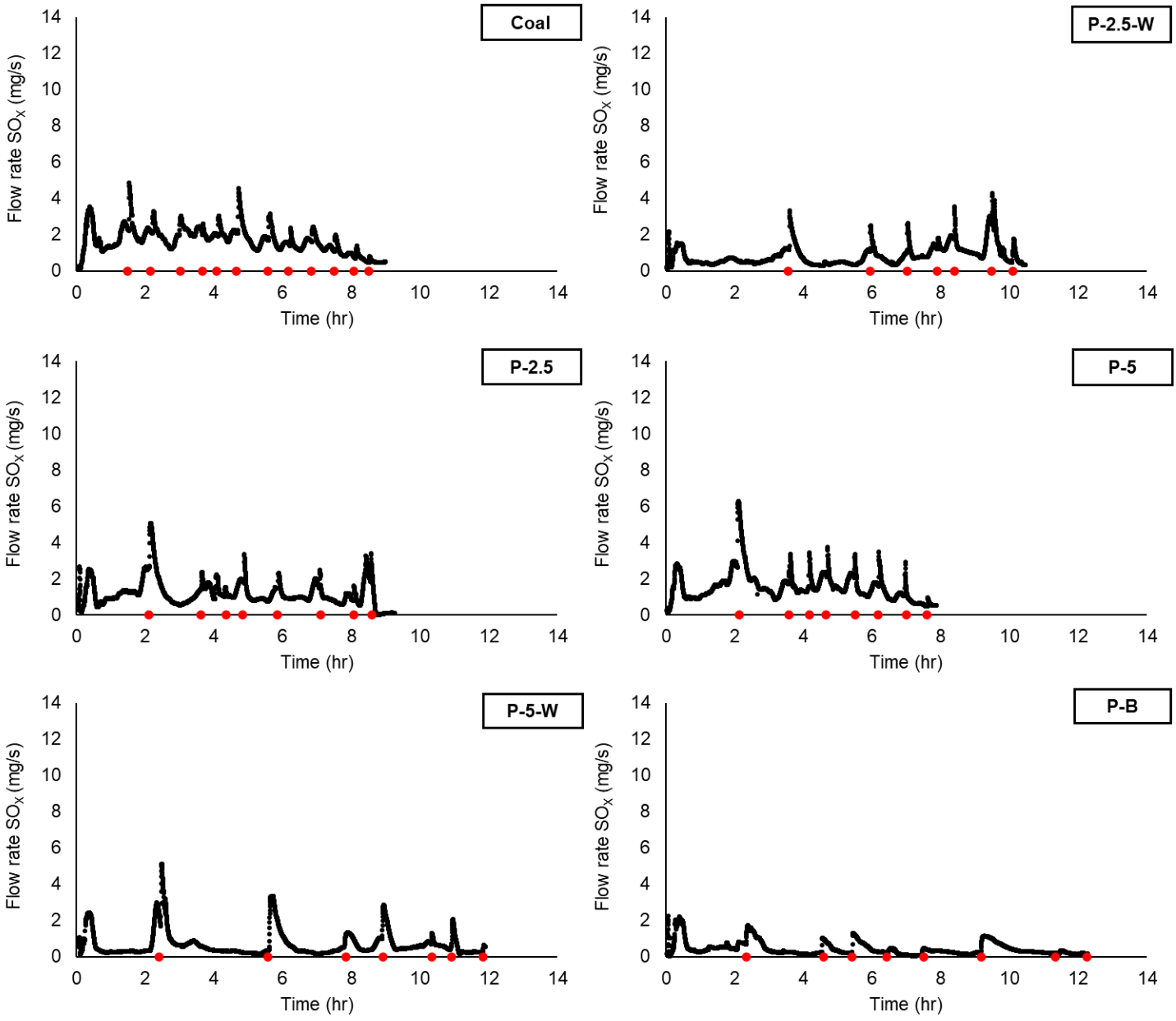

Figure C9: Mass flow rate of SOx emissions in the flue gas of low-power runs using fuel size -19 mm +13.2 mm.

When considering the grate shake intervals for the P-B run and P-5-W runs, it can be seen that these shakes resulted in concave SO_X mass flow rate spikes which were unique compared to the other stove runs. This observation might be attributed to the volatilisation of sulphates as the combustion temperature increases above 800 °C directly after these grate shakes. In contrast to the low SO_X mass flow rate of the P-B and P-5-W runs, the lump coal and P-5 runs displayed the highest overall SO_X mass flow rate as discussed in the results displayed in Table C6.

In Figure C10 the NO_X mass flow rate of the low-power runs using fuel of size -19 mm +13.2 mm are displayed.

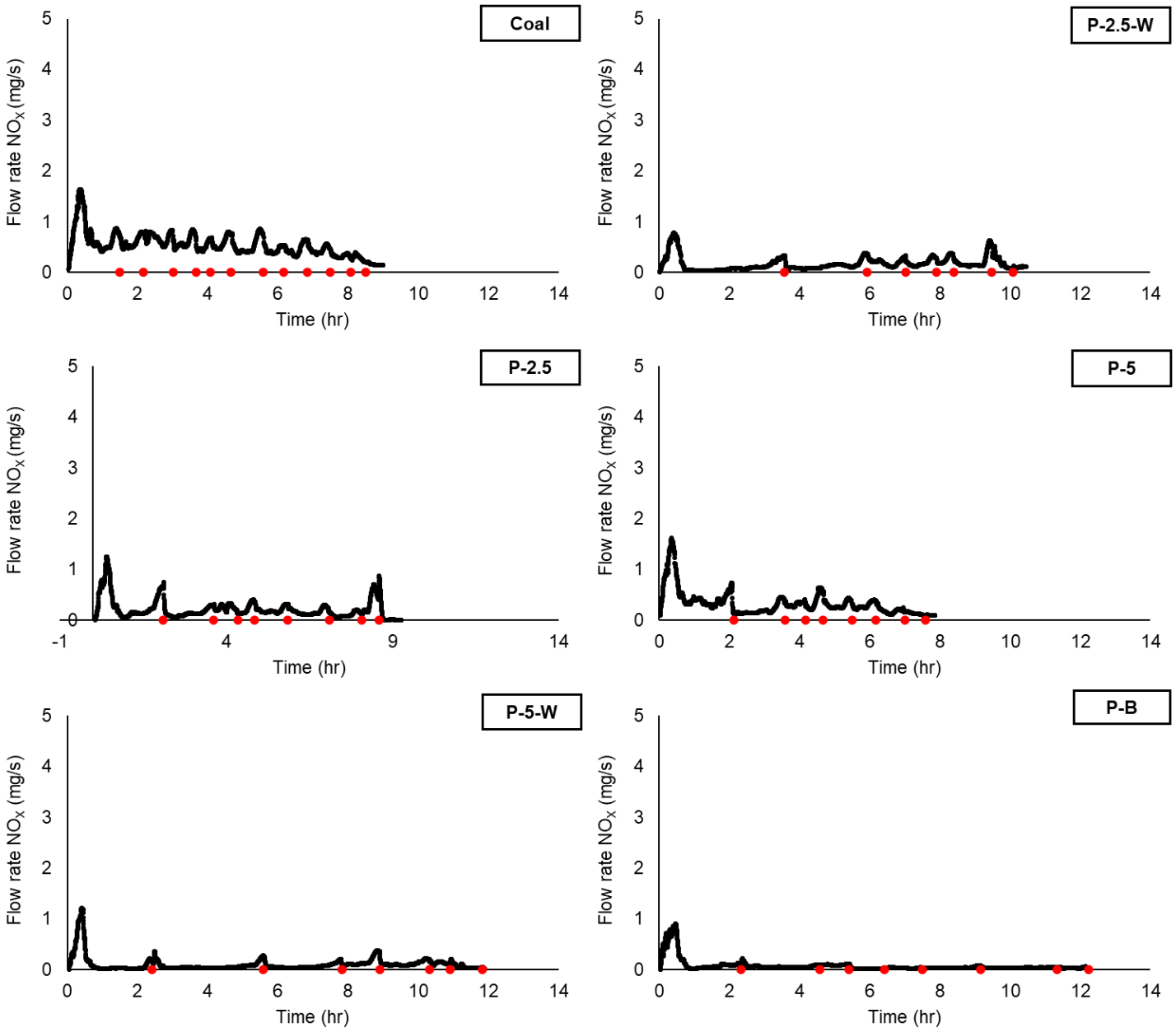

Figure C10: Mass flow rate of NOx emissions in the flue gas of low-power runs using fuel size -19 mm +13.2 mm.

It can be seen that the lump coal run displayed the highest overall NO_X emission levels compared to the coal pellet runs. This is mainly due to a combination of factors including the higher natural draft flow rate, a higher combustion rate, greater average excess oxygen concentration in the combustion zone, and lower residence time of NO_X emission in the combustion zone compared

to the pellet runs. Conversely, the P-5-W and P-B pellets showed the lowest NO_X emission mass flow rates of all the pellet batches which is also due to the aforementioned combination of factors but only on the opposite end of the scale. It can be seen in Figure C10 that all the NO_X emission levels are lower for the low-power run variants than the high-power run variants of the respective runs. This is due to a lower natural draft flow rate, lower combustion rate, less excess oxygen in the combustion zone, and greater residence time of NO_X emission in the combustion zone compared to the high-power pellet runs. It can also be seen in the figure that the initial spikes of the NO_X pollutant are similar to the high-power runs but at a significantly lower magnitude. Again, this is due to the volatilisation of the organic nitrogen species, however, the lower magnitude is likely due to the thermal decomposition of a portion thereof, and the lower volatilisation rate brought on by the lower combustion zone propagation rate. Furthermore, the magnitude of the NO_X flow rate spikes is also quite lower than for the high-power runs, which is likely due to the same reason. However, the NO_X mass flow rate spikes of the grate shake instances for the P-B and P-5-W runs were so low that it almost seems that the grate shake did not influence the pollutant flow rate, especially not in the detectable range. Similar behaviour was observed for the other emission species of the P-B run where the impact of grate shakes was far less severe than for the other runs. This can be attributed to the improved ash settling ability that was observed for the P-B and the P-5-W runs, as well as the combustion mechanisms related to smouldering combustion. Finally, all the pellet runs displayed NO_X emission mass flow rates lower than 1 mg/s which is ideal for the emissions reduction aim of the improved semi-continuous coal stove. No further significant comparison or correlation could be made between the NO_X emission flow rates, the quantity of PVA binder added to the pellets, or whether waterproofing was added to the pellets.

In Figure C11 the particulate matter mass flow rate of low-power runs using fuel of size -19 mm +13.2 mm are displayed. Immediately it can be seen that the lump coal and P-2.5-W low-power runs displayed much lower PM emission levels than the respective high-power variants. The PM mass flow rate of the P-2.5 and P-5 pellet runs were approximately similar to the high-power variants, while the P-5-W and P-B runs showed significantly higher PM emission levels and mass flow rates exiting the chimney. This is most likely due to the combustion mechanism of these runs. As already mentioned, the PM and CO emission levels both reflect the effectiveness of the gas phase combustion. Since the P-5-W run and P-B runs experience smouldering combustion, non-ideal gas phase combustion occurred especially after grate shakes.

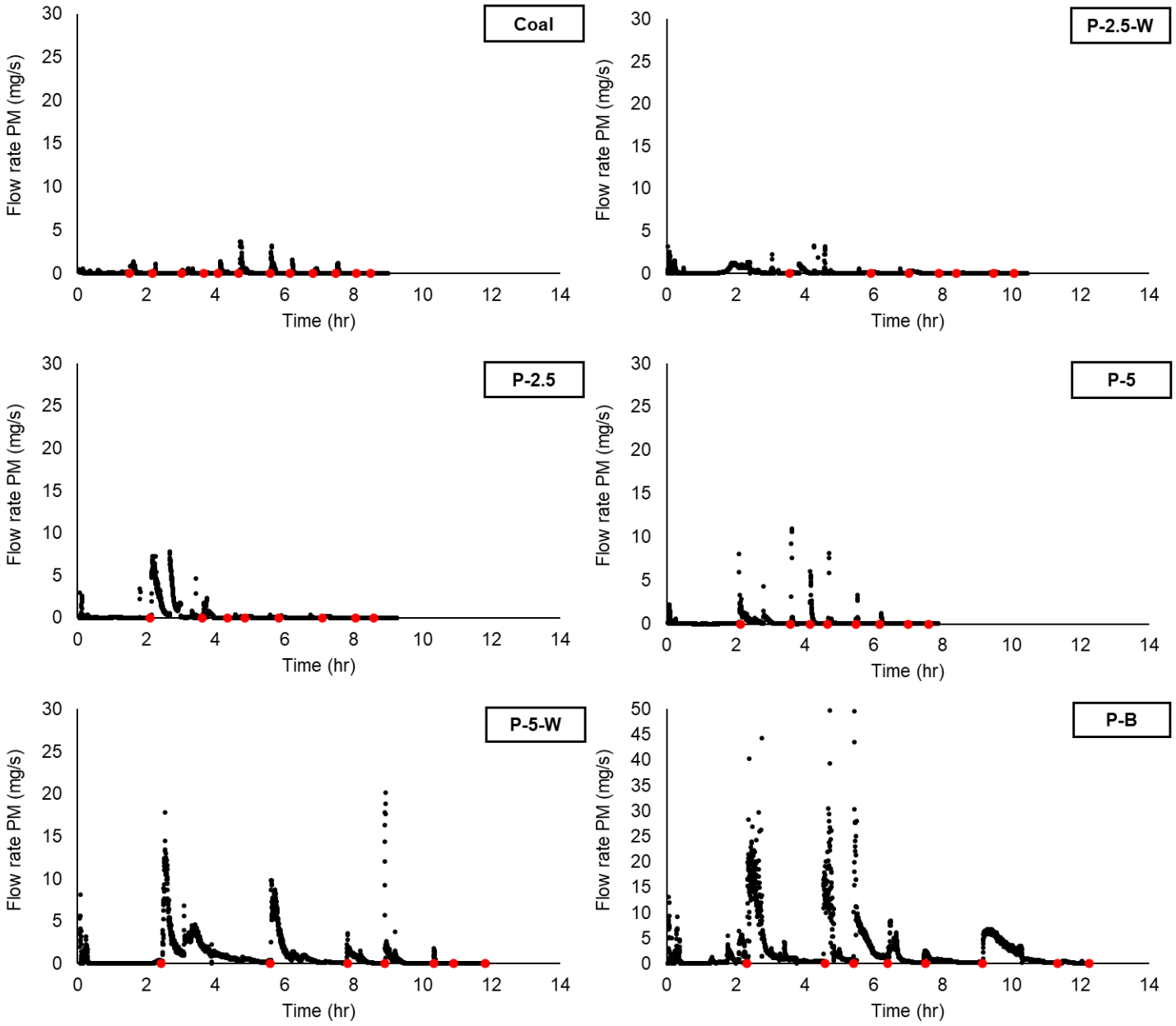

Figure C11: Mass flow rate of PM emissions in the flue gas of low-power runs using fuel size -19 mm +13.2 mm.

This is supported by the P-5-W run that exhibited improved combustion performance towards the end of the run, which correlated with a lower mass flow rate of PM emissions during this period. For all these low-power runs, the cause of the high PM levels is more related to the absence of the gas phase combustion and lower combustion zone temperatures, than the volatilisation of dust, grit, and inert particulate matter caused by grate shakes. This is reflected for the P-2.5-W run and the P-2.5 run (post 3 hours) as grate shakes seem to minimally impact the PM levels. This is because the low-power runs exhibited an improved ash-settling ability, resulting in less frequent grate shakes, and far less severe grate shakes. Another addition to this observation was

the minimal clinkers that formed during the low-power runs, which meant that only gentle grate shakes were performed, and little combustion zone disruption took place. Another observation that can be made for all low-power runs is the low PM emission flow rate of all the low-power runs prior to the first grate shake. A combination of the combustion zone disturbance and the onset of oxygen deficiency, results in the spike of PM emissions after the first grate shake for all the runs. This again motivates the importance of fuel ash settling ability, minimisation of grate shakes, and oxygen availability for gas phase combustion. Finally, no significant correlation could be made between the quantity of PVA binder added to the pellet runs or the addition of waterproofing, and the PM mass flow rate of the respective low-power runs.

The average PM and VOC stack gas concentrations in the flue gas of the respective low-power runs are displayed in Table C7.

Table C7: PM and VOC stack gas concentrations in the flue gas of low-power runs using fuel size -19 mm +13.2 mm.

	$[PM_{DT}]$	$[VOC]$
	mg/m³	*mg/m³*
C	30	70
P-B	1500	170
P-2.5	110	160
P-2.5-W	80	140
P-5	50	220
P-5-W	440	170

The P-B and P-5-W runs exhibited abnormally high PM emissions, compared to the other runs. This can again be attributed to the combustion mechanism and the absence of gas phase combustion. For the other four runs, the averaged PM concentration in the stack gas remained relatively comparable to the high-power variants of the respective runs. The calculated VOC emission concentrations are comparable to the results obtained for the high-power runs. The lump coal low-power run exhibited the lowest VOC emissions of all the low-power runs, even though the lump coal contained the highest fraction of volatile matter compared to the other fuel batches. Furthermore, the VOC concentration of the low-power runs does not correlate inversely proportional to the combustion temperature of the respective low-power runs. This is in contrast to literature findings, and what was displayed for high-power runs. It is possible that the increase in stack moisture or increased PM emissions could result in incorrect VOC measurements by effecting the final mass of the activated carbon tubes. This should be a consideration for any future experimentation on low-power stove runs.

The emission factor summary of the low-power runs is displayed in Table C8.

Table C8: Emission factor summary for low-power runs using fuel size -19 mm +13.2 mm.

	EF_{CO_2}	EF_{CO}	EF_{NO_x}	EF_{SO_x}	EF_{PM}	EF_{VOC}
	g/MJ	*g/MJ*	*mg/MJ*	*g/MJ*	*mg/MJ*	*mg/MJ*
C	91 ± 4	0.59 ± 0.01	100 ± 2	0.34 ± 0.01	23 ± 1	40
P-B	93 ± 6	5.20 ± 0.00	24. ± 0	0.17 ± 0.00	983 ± 1	110
P-2.5	93 ± 6	2.3 ± 0.03	49 ± 1	0.30 ± 0.00	68 ± 1	100
P-2.5-W	91 ± 3	2.9 ± 0.00	49 ± 0	0.25 ± 0.00	51 ± 1	80
P-5	93 ± 5	1.4 ± 0.01	60 ± 1	0.31 ± 0.00	33 ± 1	120
P-5-W	94 ± 7	4.3 ± 0.00	29 ± 1	0.20 ± 0.00	270 ± 1	100

The lump coal run exhibited the lowest CO emission factor compared to the other low-power runs. Furthermore, the lump coal is the only run that showed an improved CO emission factor compared to the high-power runs, while the CO emission factor of all the other pellet batches increased with a factor of 2 – 3 compared to the high-power variants. This significant increase can be attributed to prolonged combustion under oxygen-deficient conditions, which was not the case for the lump coal run. The P-B run, followed by the P-5-W run showed the highest CO emission factors, which can be attributed to the respective combustion mechanisms observed during the runs. The lump coal run followed by the P-5 run showed the lowest CO emission factors, which was also observed in the high-power run results. Non-waterproofed fuel showed lower CO emission factors than waterproofed fuel, which correlates with the combustion performance discussed previously.

It can be seen in Table C8 that the lump coal run exhibited the highest NO_X emission factors, with the P-B the lowest. A similar observation was made for the high-power runs. When considering combustion in a reductive environment, as discussed previously for NO_X emissions, it can be applied here as well. The runs with the highest natural draft flow rate, as well as minimal instances of oxygen deficiency, resulted in higher NO_X emission factors as is in the case of the P-5 and lump coal runs. The opposite is also true. Low draft flow rates, high combustion temperatures, and more instances of oxygen deficiency resulted in relatively low NO_X emission factors. This was seen for the P-B and P-5-W runs. However, a key difference between the low- and high-power runs' results are the magnitude of the difference between lump coal and pellet runs' NO_X emission factors. The low-power lump coal run exhibited NO_X emission factors 2 - 4 times higher than most pellet runs, where this difference was significantly less for high-power runs. In addition, the P-5 run displayed the closest experimental conditions to the lump coal run, in terms of natural draft flow rate, oxygen availability, and temperature profile, but consequently only reported a NO_X

emission factor of 60 mg/MJ which is 40% lower than the lump coal run. Therefore, it must be considered that more than just operating conditions influence NO_X emissions. It is possible that other factors can play a role in NO_X emissions as well including type of nitrogen species in the fuel, and the physical structure or properties of the fuel and ash.

The lump coal run, followed by the P-5 and P-2.5 runs all showed similar SO_X emission factors, which is also comparable to the magnitude of SO_X emission factors of the high-power runs. In contrast, however, the P-B run followed by the P-5-W runs displayed the lowest SO_X emission factors. Furthermore, considering the combustion parameters of the respective runs as displayed in Table C1, it can be seen that the SO_X emission factors directly correlate with the combustion efficiency of the respective runs. This also correlates with the relatively low oxidation factors of these runs displayed in Table C6.

The PM emission factors shown in Table C8 remained relatively comparable to the high-power runs, except for the P-B and P-5-W runs. It is shown that the PM emission levels for these runs significantly increased when compared to the high-power variants. This can be attributed to prolonged exposure to oxygen-deficient conditions. The P-B run showed the highest PM levels for all experimental runs conducted in this study. The difference between the high-power P-B and low-power P-B runs' emission factors is roughly a factor of 30. When considering the other runs, it is observed that the PM emission factor trend correlates with the trends highlighted for CO emissions. This is likely due to the presence of the gas phase combustion that influences both the emission of CO and PM. This can also be seen for the lump coal run, followed by the P-5 run, which exhibited the lowest PM emission factors similar to what was discussed for the CO emission factors. Both these runs displayed ideal oxygen levels for low-power runs, high CC middle temperatures, and typical combustion conditions. This consequently resulted in the low CO and PM emissions compared to the other runs.

The VOC emission factors for low-power runs are also shown in Table C8. These results are in dissimilarity with the high-power runs, as well as literature findings. The lump coal run displayed the lowest VOC emission factor even though this fuel had the highest volatile matter content relative to the other fuels. Furthermore, as stated in the literature, a high combustion temperature usually correlates with low VOC emission factors. While this may be true for the lump coal, when considering the PVA binder pellets it is shown that the P-5 run displayed the highest VOC emission factor out of all the low-power runs even though it showed improved combustion performance and higher temperatures. No scientific explanation can be given for this observation, and further experimentation on specifically VOC emissions is required to determine the exact cause of this phenomenon.

ANNEXURE D – INVESTIGATION OF FUEL SIZE AND PACKING

D.1 COMBUSTION PERFORMANCE

The influence of fuel PSD, and the corresponding packing parameters, on the stove combustion characteristics were evaluated using the 2.5 wt.% PVA binder pellets. The three size range variations that were chosen for this section is given and discussed in Chapters 3 & 4. The key to the fuel batch identification can be seen in Table D1.

Table D1: Key to fuel batches and runs which used different size range pellets.

Batch Key	Description	Packing characteristic	Size range
P-2.5 L	2.5 wt.% PVA pellets; no waterproofing	Low density; High bed voidage; Low surface area per volume; Low surface area per mass	-19 mm +13.2 mm
P-2.5 M	2.5 wt.% PVA pellets; no waterproofing	Medium density; Medium bed voidage; Medium surface area per volume; Medium surface area per mass	-19 mm +9.5 mm
P-2.5 H	2.5 wt.% PVA pellets; no waterproofing	High density; Low bed voidage; High surface area per volume; High surface area per mass	-13.2 mm +6.7 mm
P-2.5-W L	2.5 wt.% PVA pellets; waterproofing added	Low density; High bed voidage; Low surface area per volume; Low surface area per mass	-19 mm +13.2 mm
P-2.5-W M	2.5 wt.% PVA pellets; waterproofing added	Medium density; Medium bed voidage; Medium surface area per volume; Medium surface area per mass	-19 mm +9.5 mm
P-2.5-W H	2.5 wt.% PVA pellets; waterproofing added	High density; Low bed voidage; High surface area per volume; High surface area per mass	-13.2 mm +6.7 mm

The combustion mass loss rate of the runs using dissimilar fuel size ranges can be seen in Figure D1. The overall and averaged combustion parameters that correspond to the respective graphs are displayed in Table D2. The initial mass of the runs can be seen on the y-axis intersect of Figure D1 A, as well as in the second column of Table D2. The smaller size range pellet runs (“M” and “H” runs) started with a higher initial mass than the larger size range pellet runs. A similar observation is made when considering the initial mass of the respective runs displayed in Table D2. These mass values correlate with the packing density of the respective fuel size ranges as

given in Section B.1. The “L” (low density) runs showed the lowest initial mass, while the “H” runs displayed the highest initial mass. The only exception to this observation is the P-2.5-W M run which showed the highest mass of all the runs despite the size range of this run being associated with a “medium” packing density. This is possibly due to the higher amount of fines that were loaded with the fuel at the start of this run when compared to the other runs. This, however, it is not reflected in the combustion efficiency which is normally the case for runs with a high fines content.

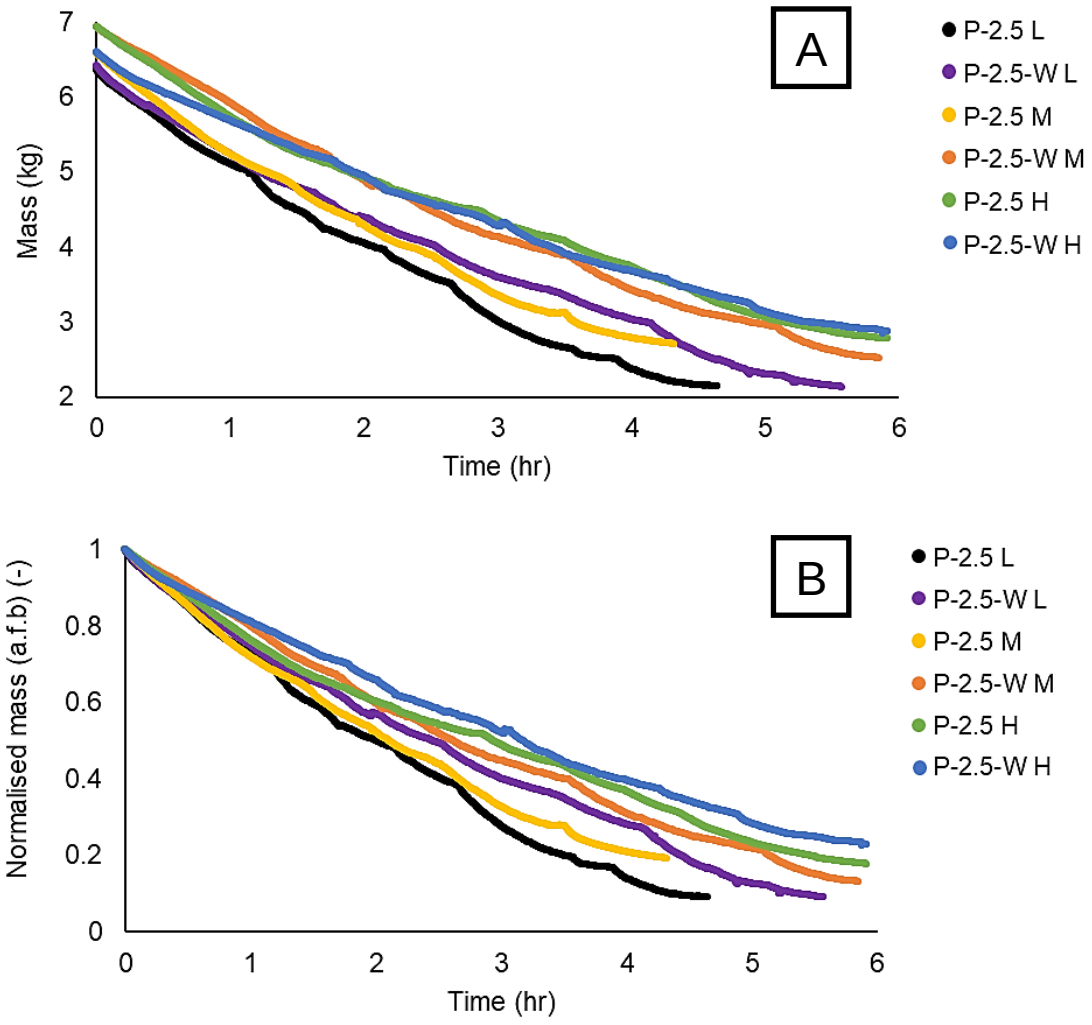

Figure D1: Combustion mass loss per time for high-power runs using different fuel sizes: (A) as measured and (B) normalised & ash free basis.

It can also be seen in Figure D1 (A) and Table D2 that the run lengths increase with packing density, since at a relatively similar combustion rate, a run with a higher mass will usually result in a longer run length if the influence of disturbances are minimised.

When considering the number of grate shakes required for each run, and the average time between the respective grate shakes, no significant correlation was observed between these parameters and the packing characteristics. In other words, the packing parameters showed little influence on the ash-settling ability of the fuel. This is in contrast with initial test runs (as given in Annexure A) that showed a smaller size range fuel might result in improved ash setting. Instead, it was observed during the runs that the smaller size range pellets ("H" runs) were more likely to form clinkers and ash fusion areas than compared to the larger size range pellet runs ("L" runs). This can also be seen in the unsteady nonhomogeneous combustion rate graphs exhibited in Figure D1. This had the opposite effect on ash settling ability and instead caused ash holdup resulting in the need for more severe grate shakes. This is also reflected in the combustion efficiency of the respective runs (ash-free mass fraction at the end of the run in Figure D1 (B), where the lowest combustion efficiency is reported for the high-density smaller size pellet runs.

Table D2: Combustion parameters of high-power 2.5 wt.% PVA pellet runs using fuel of various size ranges**.**

	Initial mass	**Run length**	**Grate shakes**	**Time between shakes**	**Average combustion rate**	**Combustion efficiency**
	kg	*hr*	-	*hr*	*kg/hr*	-
P-2.5 L	6.38	4.64	6	0.77	0.91	0.91
P-2.5 M	6.59	4.32	4	1.08	0.90	0.81
P-2.5 H	6.94	5.91	8	0.74	0.70	0.82
P-2.5-W L	6.42	5.57	6	0.93	0.77	0.91
P-2.5-W M	6.94	5.85	5	1.17	0.76	0.87
P-2.5-W H	6.61	5.92	5	1.18	0.63	0.77

It was expected that a greater packing density, and surface area to volume/mass packing characteristics increased the combustion zone propagation rate of the "H" pellet runs compared to the "L" runs. The rate at which the combustion zone spreads from one fuel particle to the next is directly proportional to the surface contact area of these pellets. Therefore, a size range with a higher surface area to volume/mass ratio will have an increased packing factor and will therefore experience an overall higher rate of combustion propagation and spread. This would result in high solid phase combustion temperatures which could approach the ash melting temperatures of the fuel and therefore result in clinker and ash lump formations. This consequently impacts the run by increasing the ash holdup on the grate, lowering the overall combustion rate of the run, and requiring more severe grate shakes to ensure ash settling. In turn, the severe grate shakes result in more fuel loss. This might explain why a smaller fuel size range fuel, such as the -13.2 mm +6.7 mm runs, displayed a low combustion efficiency ("H" runs in Table D2), and why the "L" runs displayed higher overall combustion rates than the other runs. However, the gradient of the

combustion rate graphs in Figure D1 at the start of the runs are relatively similar, which does not support the claim of a faster combustion zone propagation rate for “L” runs. When considering the transient combustion rates of the respective runs in Figure D2, a similar observation can be made.

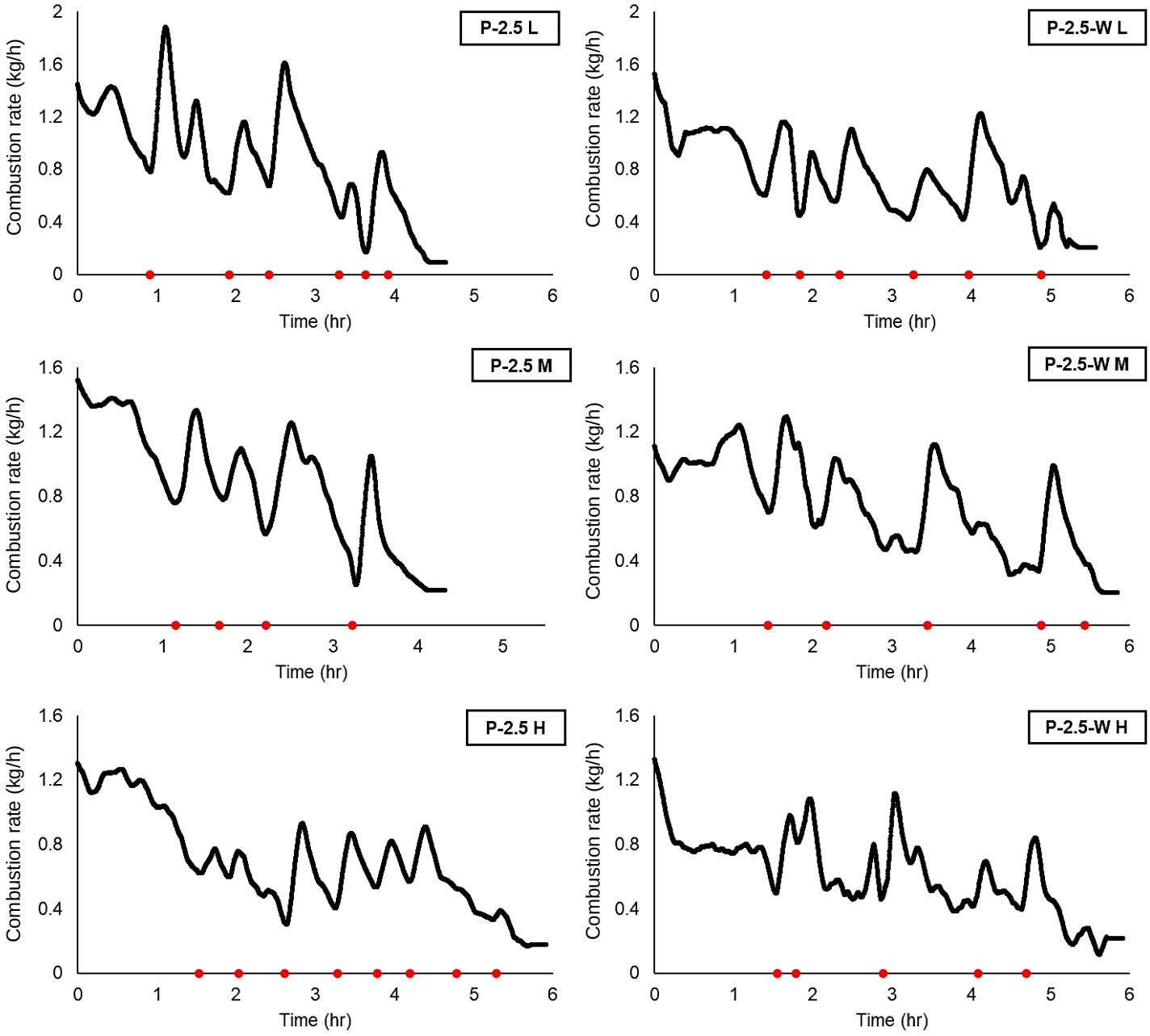

Figure D2: Combustion rates of high-power runs using fuel of different size ranges.

In Figure D2 the average combustion rates of the high-power runs using different fuel size ranges can be seen. The influence of combustion zone disturbances such as dead zones, grate shakes, and clinkers is prominent for all runs irrespective of fuel packing characteristics or size range. No significant difference in combustion rate can be observed between the different size range runs, especially not during the start of the run as proposed by the hypothesis mentioned previously. Instead, all of the runs display a similar magnitude of combustion rate peaks and valleys throughout the runs. The only observation that can be made is the increase of “noise” in the combustion rate graphs for the smaller size range pellet (“H”) runs. This is likely due to a portion of the fuel, which was smaller than the grate aperture, resulting in burning fuel dropping to the ash tray instead of remaining on the grate. This would increase the combustion inefficiency as was shown in Table D2. When this phenomenon occurs, clinkering and ash fusion can improve the combustion process by suspending the fuel between grate shakes. This can be seen for the P-2.5 H run before and after the 3rd grate shake, as the combustion rate “noise” reduces as a result of ash fusion.

D.2 THERMAL PREFORMANCE

Key averaged stove temperatures of each chamber are given in Table D3 for high-power runs using 2.5 wt.% PVA binder fuel with various size ranges.

Table D3: Average internal temperatures of the semi-continuous coal stove during high-power runs with various fuel PSDs.

	Hopper bottom *TT305*	**CC bottom** *TT309*	**CC middle** *TT307*	**HX middle** *TT311*	**Chimney** *TT301*
	°C	*°C*	*°C*	*°C*	*°C*
P-2.5 L	950	750	700	270	170
P-2.5 M	820	720	700	260	170
P-2.5 H	840	660	630	220	150
P-2.5-W L	920	650	670	240	150
P-2.5-W M	890	720	660	230	140
P-2.5-W H	750	680	590	210	130

All the size range runs displayed higher hopper bottom temperatures than the combustion chamber temperatures. This difference is greater for the “L” fuel which showed the highest average combustion zone temperature compared to the other size ranges. This correlates with the increased clinker formation and ash holdup observed for the “H” runs. Since the “L” runs exhibited minimal clinkering compared to the other runs, they also displayed higher average combustion zone temperatures as seen for the hopper bottom and combustion chamber bottom temperatures compared to the other runs displayed in Table D3. The only exception to this observation is the P-2.5-W L run that experienced a dead zone area at the bottom of the combustion chamber which could not be amended with grate shake attempts. As a result, this run reported the lowest combustion chamber bottom temperature compared to the other size range runs, while still maintaining the second highest hopper bottom temperature.

It was expected that the packing parameters will have a significant impact on the gas phase combustion since the packing of the fuel may impact the air availability by i) varying the combustion zone propagation rate and thus oxygen availability for gas phase combustion, and ii) varying bed voidage resulting in increased/decreased air permeability through the combustion zone bed, ensuring oxygen availability for gas phase combustion. When considering the combustion chamber middle temperatures, larger size pellets with increased voidage and lower surface area to volume did indeed exhibit increased gas phase combustion temperatures. In addition, the high-density pellets run exhibited the lowest average combustion chamber middle temperature and thus exhibited the worst gas phase combustion compared to the other runs. This is also supported by the temperature profiles of the heat exchanger chamber and chimney

section, where the overall fluid temperature decreases with an increase in fuel packing density and surface area to volume ratio. Therefore, when considering the temperature profiles of the stove during the respective runs, the hypothesis holds.

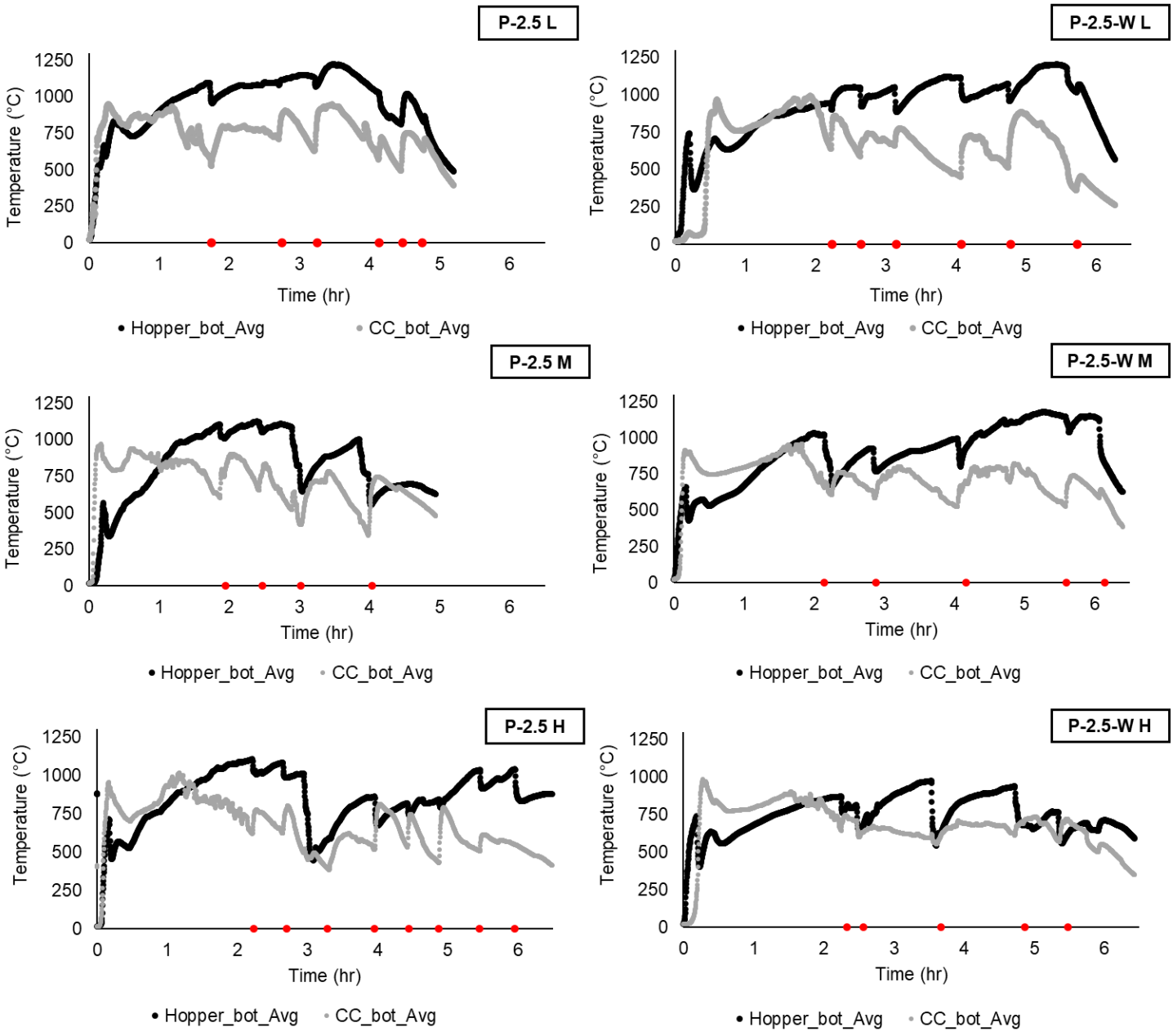

Figure D3: Combustion zone temperatures of high-power runs using fuel of different size ranges.

The combustion zone temperatures of the six respective runs are displayed in Figure D3. In correlation with the results shown in Table D3, the hopper bottom temperatures of the larger size pellets (“L” runs) were on average greater than those of the other pellet runs. The effects of severe clinkering and dead zone formations are prominent for the smaller pellet size, and high packing

density fuel batches at ≥ 3 hours into these runs. As a result, deep valleys can be seen in the combustion zone temperature results, where severe grate shakes were required to amend the combustion zone and stove operation. The magnitude of these valleys scale with increased packing density and surface area to volume/mass. However, no proof of a faster propagation rate can be seen for the smaller size range pellet batches. The rate at which the combustion zone temperatures increase before the first grate shake is similar for all the runs. It is possible that the onset of ash fusion and clinkering occurs in the middle of the combustion zone, underneath the stove bridge between the hopper and combustion chambers. No thermocouple measurement is available for these areas and should be considered for future experimentation.

The water boiling test results of the respective runs can be seen in Table D4.

Table D4: Water boiling test results for high-power runs with different fuel PSDs.

	Time to boil	**Cooking power**	**Cooking efficiency**
	min	*kW*	*%*
P-2.5 L	17	0.57	4.5
P-2.5 M	17	0.62	6.7
P-2.5 H	26	0.42	7.7
P-2.5-W L	26	0.38	4.6
P-2.5-W M	21	0.47	5.0
P-2.5-W H	38	0.27	5.0

When considering the water boiling test results, it is observed that the time required to boil the water did not scale with the packing parameters of the fuel. However, it is observed that the cooking power and cooking efficiency can be correlated with packing parameters. The higher cooking power values correlate with the “M” size fuel runs, while a low cooking power correlates with the “H” fuel runs. This is in contrast to the stove temperature profiles of the respective runs as previously discussed. Improved gas phase combustion and higher combustion chamber middle temperatures normally result in increased cooking power, which is not the case for the results shown in Table D4. Instead, the runs with “medium” packing parameters and relatively average combustion chamber temperatures displayed a high cooking power. This might be attributed to the time in the run when the water boiling test was conducted. Even though an overall higher gas phase temperature was observed for the “H” runs, it is possible that during the ±30 min of the water boiling test, the immediate combustion chamber temperatures were slightly higher for the “M” runs than compared to the “H” runs. This can be seen in Figure D3 where the P-2.5 M run displayed the highest combustion chamber temperature after the first grate shake (during the water boiling test) compared to the other run variants. The cooking efficiency values displayed in Table D4 can also be correlated to the respective packing parameters of the 2.5%

PVA pellets. It is observed that the cooking efficiency increased with an increase in packing density and a decrease in voidage. This is in correlation with previous findings where higher hopper bottom temperatures usually resulted in increased energy losses to the front surfaces of the stove and therefore lower cooking energy efficiencies. This is believed that the increased clinker and ash formations at the bottom of the hopper (for the smaller size pellet runs) formed an ash insulation layer reducing the energy losses to the front and bottom parts of the stove compared to the lower density fuel runs. Therefore, the "L" runs that exhibited less clinkering and ash fusion, experienced higher hopper temperatures, higher energy losses during the water boiling test, and therefore lower cooking efficiencies, compared to the other runs.

Table D5: Thermal performance parameters for high-power runs with different fuel PSDs.

	P_F	P_D	η_{SL}	η_D	η_{tot_1}	η_{tot_2}	$\bar{V}_{chim}$
	kW	*kW*	*%*	*%*	*%*	*%*	*m^3/hr*
P-2.5 L	6.9	5.8	89.6	84.1	76.6	78.3	16.0
P-2.5 M	6.8	5.3	88.7	78.1	63.2	68.8	17.2
P-2.5 H	5.3	4.1	88.4	77.5	63.8	65.7	16.0
P-2.5-W L	5.9	4.7	89.6	79.2	72.1	77.6	15.4
P-2.5-W M	5.8	4.7	91.2	81.9	71.2	74.2	12.4
P-2.5-W H	4.8	3.6	90.2	73.7	56.8	58.0	13.2

The thermal performance parameters of high-power runs using fuel of different size ranges can be seen in Table D5. When the power ratings of the stove-fuel combinations are reflected upon, it is observed that the fired and delivered power rating of the stove decreases with an increase in fuel packing density and surface area to volume/mass. This correlates with both the oxygen availability hypothesis, as well as the overall combustion rates displayed in Table D2. When considering the stack loss efficiency values, the results are similar between runs irrespective of fuel packing or size range. Even though the average chimney flow rate and average stack outlet temperature can be correlated with packing parameters and fuel size, the difference between these parameters is not significant enough to result in a visible correlation between stack losses and fuel packing characteristics. This is also the case for the average chimney velocity (Table D6) which normally correlates with stack losses and remained relatively constant during these runs. Finally, both the delivered energy efficiency and the total stove energy efficiency scales with the packing parameters and size range. It can be seen that the low density, low surface area to volume & mass pellet runs exhibited higher energy efficiency than the other runs, in contrast to the high density and high surface area to volume/mass pellet runs. This can be attributed to a combination of factors. The lower energy delivered efficiency for the "H" runs is mainly due to the

increased initial mass, increased run length, and decreased combustion rate as discussed previously. Even though the stack losses are relatively similar to the other runs, the amount of energy that is lost throughout the longer duration of the runs is significantly more for the “H” runs compared to the rest. In addition to these factors, the lower combustion efficiency of the high density (“H”) runs also contributed to the low total energy efficiency of the stove-fuel combinations.

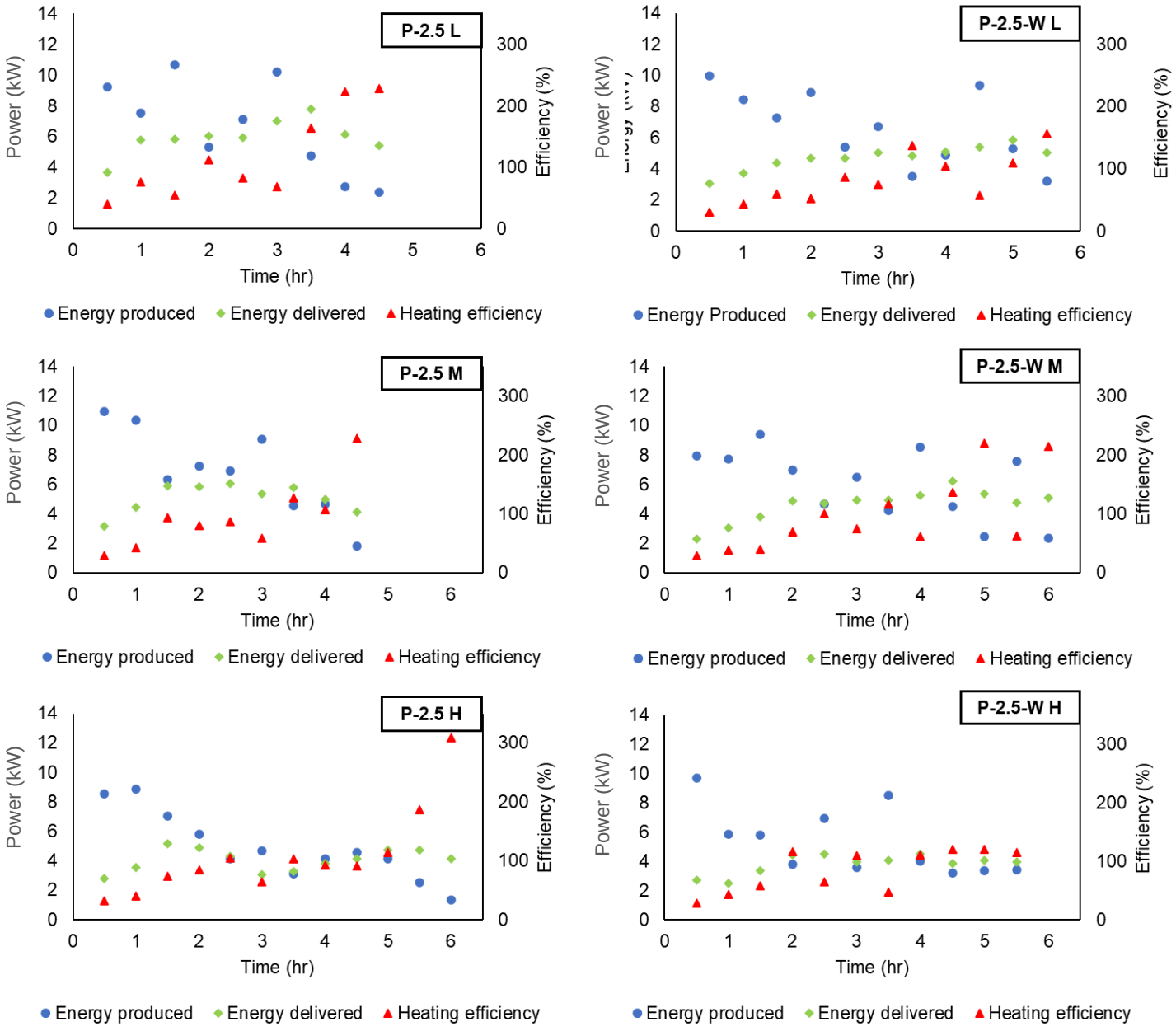

Figure D4: Energy produced, energy delivered, and heating efficiency for high-power runs using fuel of different size ranges.

In Figure D4 the energy produced, energy delivered, and heating efficiency for the runs with different size ranges can be seen. From the results displayed, it is observed that the energy distribution of all the runs is highly variable. The only run that displayed a relatively typical energy profile was the P-2.5 H run, which exhibited an exponential increase in energy efficiency at the end of the runs as expected. The high variability of the runs is directly related to the combustion zone disturbances, which explains why these runs do not exhibit linear energy profiles. Furthermore, it is observed that the larger size range fuel runs displayed higher overall energy outputs compared to the smaller size fuel runs. This is in correlation with the results displayed in Table D5 as well as the combustion rates and temperature profiles previously given.

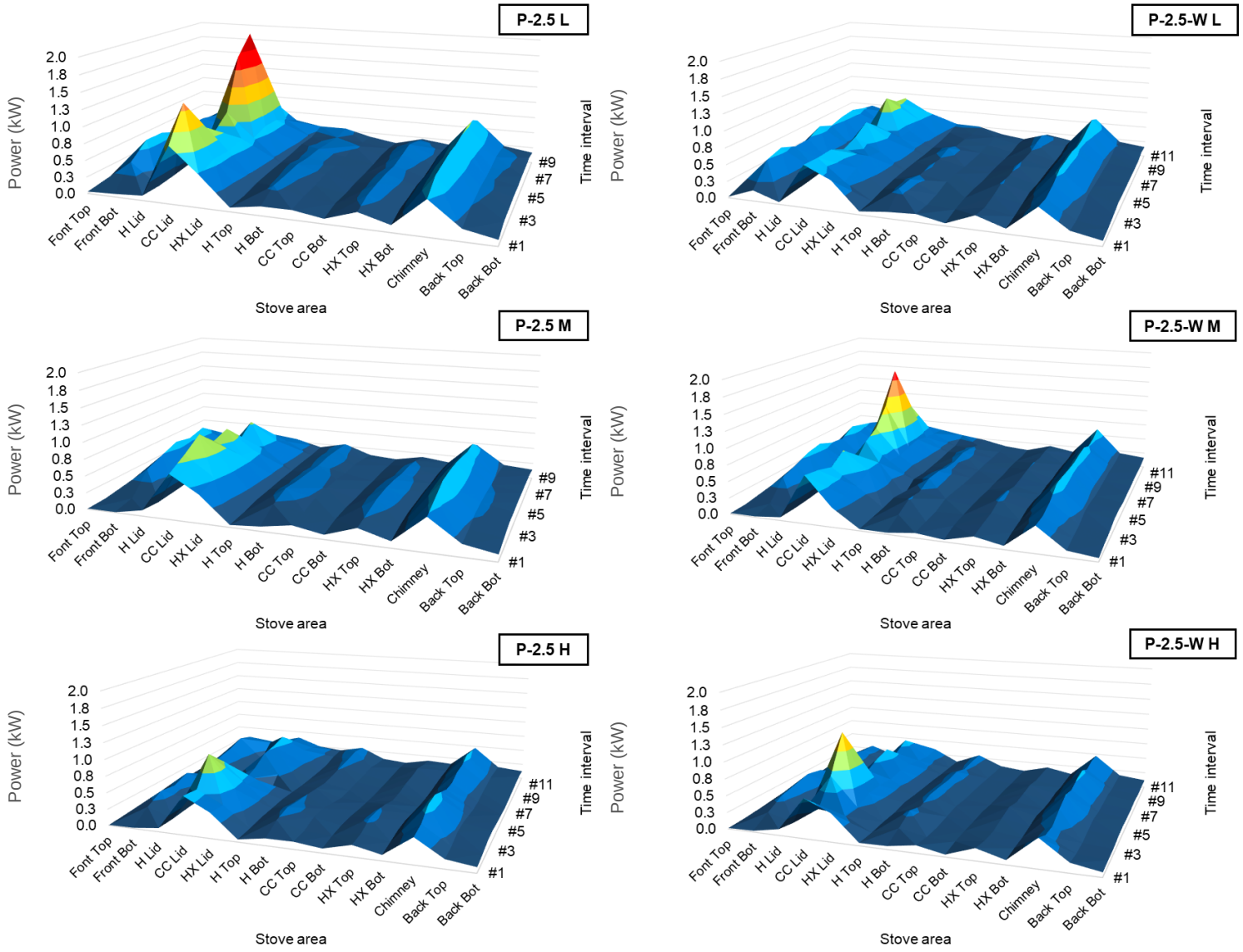

Figure D5: Total energy delivered (radiation & convection) from the stove surfaces for high-power runs using fuel of various size ranges.

The stove surface energy flux profiles are given in Figure D5 for the six respective runs. It can be seen that all the runs showed similar energy outputs across the different stove segments, except for the combustion chamber and heat exchanger lid areas. These areas were found to be the most susceptible to disturbances in the combustion zone, and therefore a large variability can be seen for all the runs. The magnitude of variability however does not increase/decrease with a change in fuel size or packing parameters which is visible for all the runs, similar to the results displayed in Table D5. The only clear distinction that can be between the different runs is the energy delivered by the front part of the stove. It can be observed in Figure D5 that the “L” runs using larger fuel sizes, exhibited the largest energy loss through the front area of the stove compared to the other smaller fuel size range runs. This energy losses scale with an increase in packing density and surface area/volume, and directly correlates with the hopper bottom temperatures displayed in Figure D3 and Table D3. As stated previously, this is likely due to the increased clinkering and ash fusion that resulted in an insulation barrier for this part of the stove. Finally, evidence of the combustion zone propagation rate can also be seen in Figure D5. Since the combustion zone starts at the bottom of the combustion chamber and underneath the stove bridge, the stove front temperature (“Front Bot” area), as well as the sides of the hopper (“H Bot” area) are approximately ambient temperature. As the combustion zone spreads to the bottom of the hopper section, the outside surface temperatures of the hopper chamber will also gradually increase. When considering the results displayed in Figure D5, it can be seen that the low-density large size pellet runs (“L”) exhibited a greater rate of temperature increase at the stove front and hopper side areas, compared to the other runs. Furthermore, this rate of temperature increases scales with changes in packing parameters. This observation supports the previous findings where a smaller size range and higher surface area to volume pellet batch do not necessarily increase the combustion zone propagation rate. This means that the amount of clinker formation and ash fusion observed for the “H” runs was not a result of the combustion zone propagation rate as originally thought, but perhaps by another mechanism such as packing density. It is possible that a densely packed combustion bed and low bed voidage may result in higher bed core temperatures, and thus due to the limited air permeation and cooling, the ash melting temperature is easier reached.

D.3 EMISSION LEVELS

The CO, CO_2 and O_2 concentrations in the stack gas of the respective runs are shown in Figure D6. The interaction and proportionality between these gases are also shown. From the results displayed it can be seen that the low density runs displayed typical combustion behaviour in terms of the CO, CO_2 and O_2 concentrations in the stack gas. The CO_2 and O_2 species form a direct correlation, while the CO concentration spikes when the O_2 concentration reduces below 0.5 vol%. Non-typical behaviour is seen for “M” runs, as shown in Figure D6 for the P-2.5 M run results

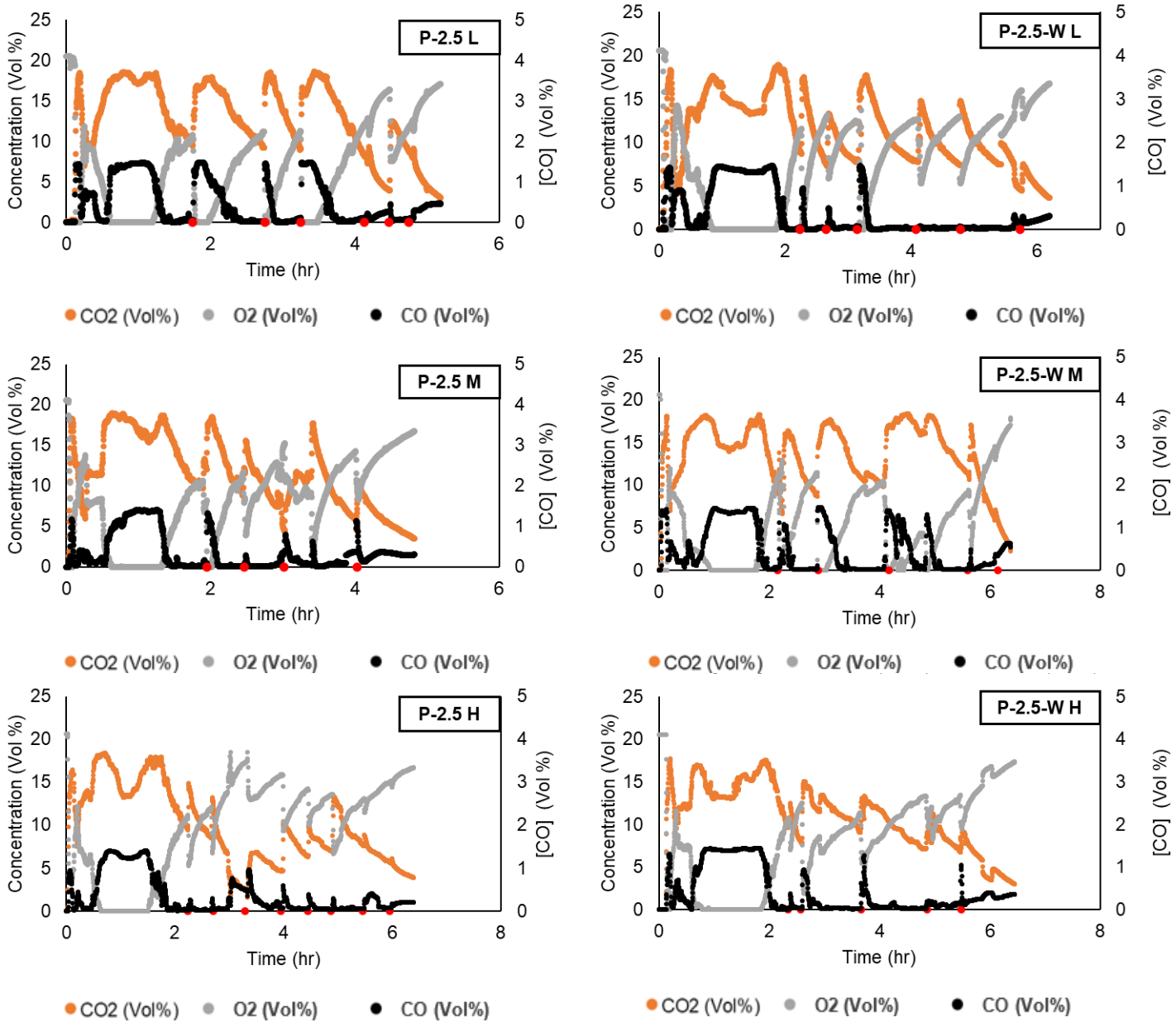

Figure D6: Carbon oxides and oxygen concentrations in the flue gas of high-power runs using fuel of various size ranges.

around the third grate shake (3 hours into the run). It was found that the CO_2 decreases and the O_2 increases after the grate shake.

This abnormal behaviour can be attributed to severe clinkering. Similar behaviour can be seen for the “H” runs, especially the P-2.5 H run where a substantial part of the run was conducted at low CO_2 and high O_2 concentrations without performing a grate shake. The severe clinkering that occurred during these runs resulted in ash-solid layering, which caused channelling through the combustion bed. This increased the excess oxygen and reduced the available combustion zone area. The “H” runs with significant clinkering were repeated but a similar outcome was observed. The increase in excess oxygen and reduction of the combustion zone area showed a significant

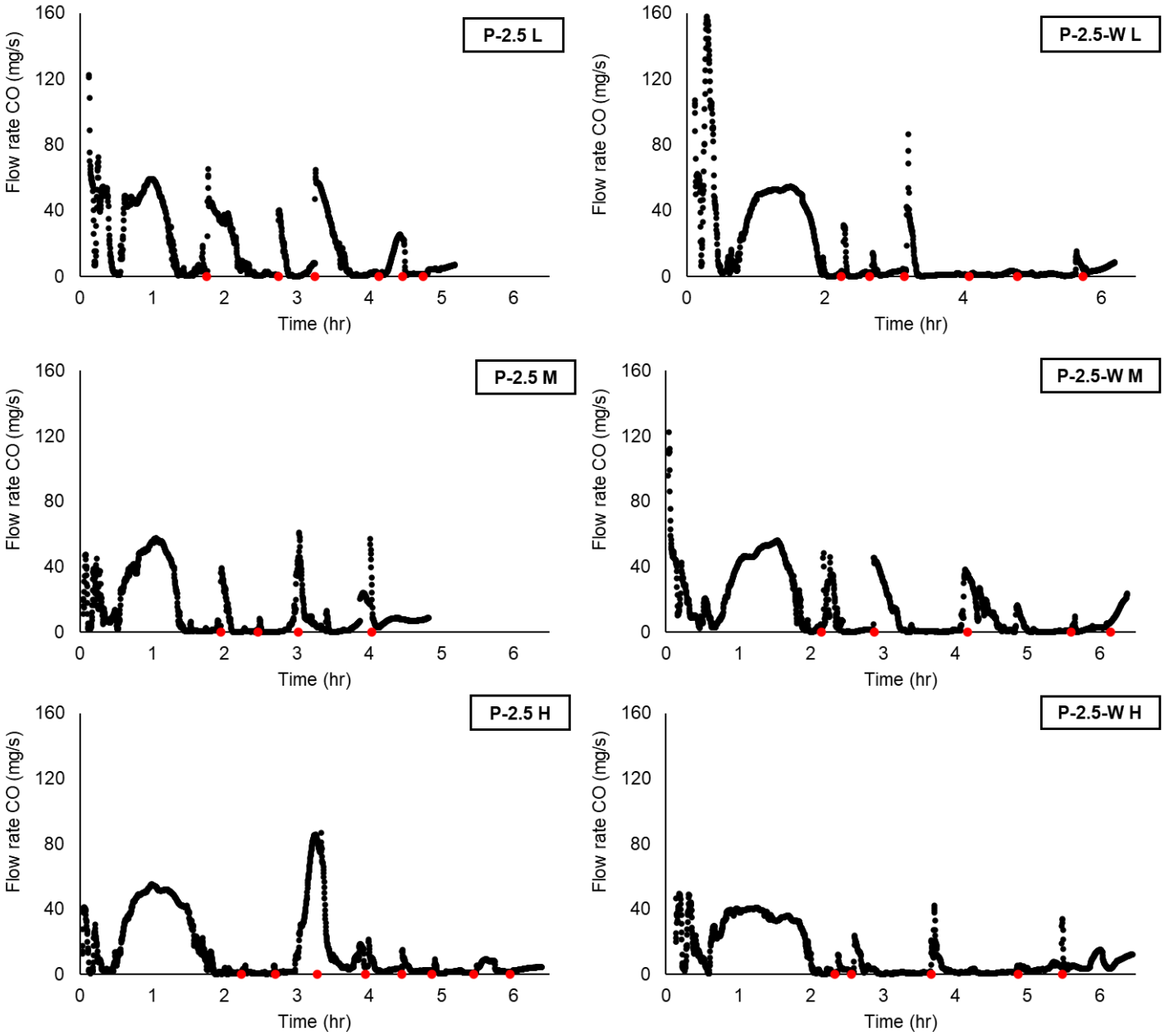

Figure D7: Carbon monoxide mass flow rate of high-power runs using fuel of various size ranges.

impact on the emission profile of the stove and resulted in low combustion rates and combustion temperatures as previously shown.

The carbon monoxide mass flow rate of the respective runs can be seen in Figure D7. All the runs experienced CO emission spikes after grate shakes, with long periods of high CO levels in the stack gas after the ignition phase and before the first grate shake. As discussed in Section 5.1, this is due to the oxygen deficiency in the combustion chamber. It can be observed that the high levels of CO are present irrespective of fuel size or packing characteristics. The magnitude of the spikes after most grate shakes, and the length of these elevated CO emission periods after grate

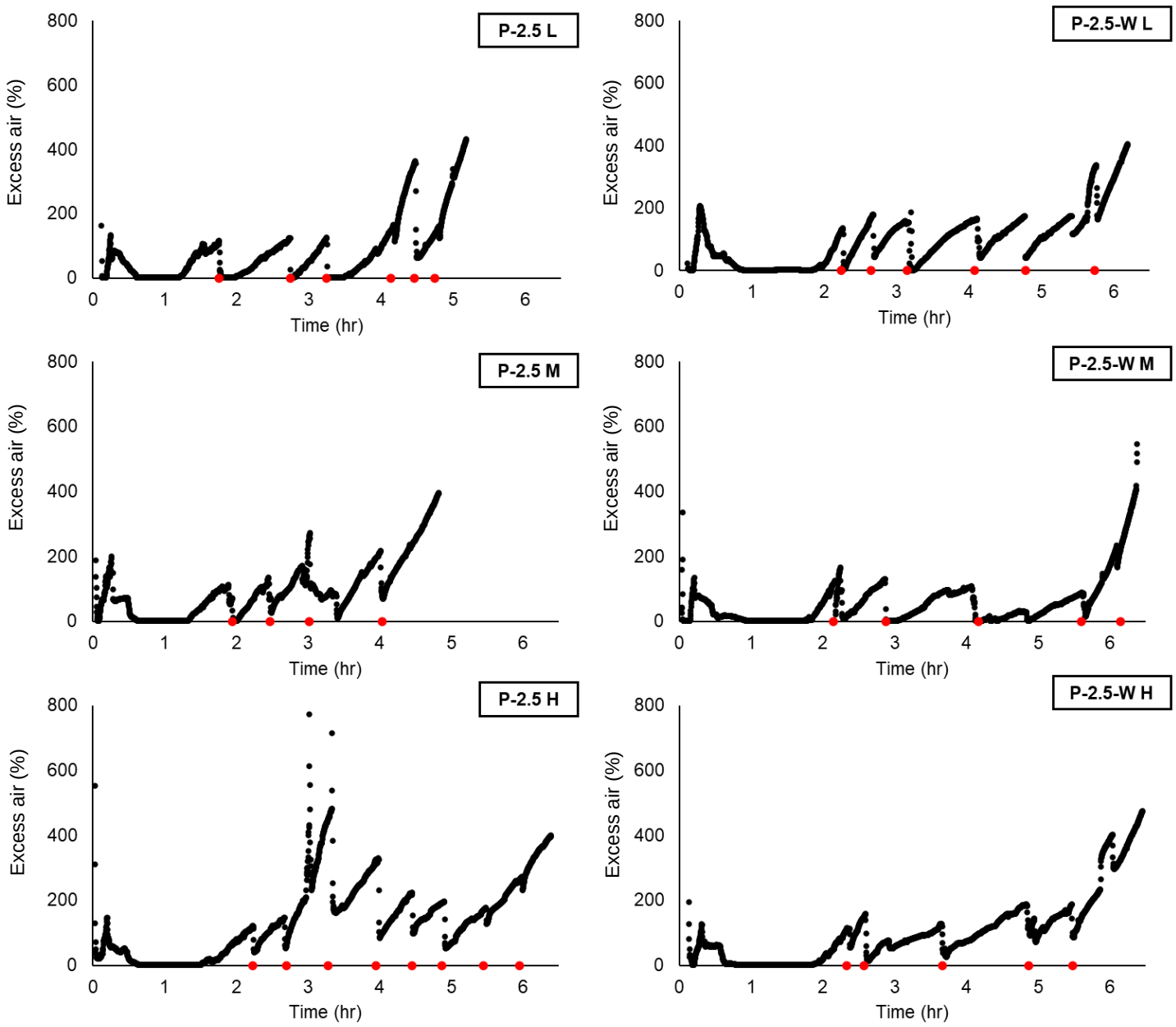

Figure D8: Excess air concentrations in the flue gas of high-power runs using fuel of various size ranges.

shakes, are less for the “H” runs compared to the other experiment variants. This is mainly due to the increased excess oxygen availability for complete combustion.

The severe clinkering and ash fusion during the small size range fuel runs resulted in air channelling through the combustion bed which increased the oxygen availability for combustion. This phenomenon can also be seen in Figure D8, where the excess oxygen levels in the stack gas are displayed for the respective runs. The high excess air levels caused by clinkering are especially prominent for the P-2.5 H and P-2.5 M run results. Furthermore, clinkering and air channelling can also improve combustion performance by preventing oxygen deficiency in the stove’s combustion chamber. This can be seen in Figure D8 for the small size range pellets, where the excess air levels remain above 10% after grate shakes. Finally, the length of the oxygen deficiency period after the ignition phase scales with a change in fuel size. The period of low excess air levels before the first grate shake increased for “H” pellet runs. This is attributed to the increased duration required for a full combustion zone to form when a dense char bed is present.

A summary of the emission factors of high-power runs using fuel of different size ranges is provided in Table D6.

Table D6: Emission parameter summary of high-power runs using fuel of various size ranges.

	α	$CO:CO_2$	ε_{O_2}	$\bar{v}_{chim}$	$\bar{\lambda}$	$y_{d/w}$	V_{H_2O}
	-	%	%	m/s	-	-	ml
P-2.5 L	0.963	3.8	3.6	0.6	1.87	0.949	38
P-2.5 M	0.970	3.1	3.6	0.6	2.07	0.950	49
P-2.5 H	0.966	3.8	4.1	0.6	2.56	0.953	44
P-2.5-W L	0.969	3.1	5.4	0.5	2.04	0.952	40
P-2.5-W M	0.967	3.7	6.3	0.4	1.68	0.943	41
P-2.5-W H	0.964	3.8	6.4	0.5	2.17	0.950	50

Both the α value as well as the averaged $CO:CO_2$ ratio of the P-2.5-W runs scale with the fuel size range. Higher $CO:CO_2$ ratios and lower α values are obtained for the runs with a higher packing density. This is caused by the increased oxygen availability that is associated with a lower density char bed. The same observation could not be made for the P-2.5 runs. When considering the other emission parameter sets displayed in Table D6, none could be correlated with packing characteristics. The magnitude of all the results presented in Table D6 are comparable to the previous high-power run results of -19 mm +13.2 mm fuel displayed in Section 5.2.1. The

increased clinkering of these runs likely skewed the results presented in Table D6, which may have resulted in the lack of correlation.

The sulphur balance results of high-power runs using fuel of different size ranges are shown in Table D7.

Table D7: Sulphur balance for high-power runs using fuel of various size ranges.

	$m_{S\ Fuel}$	$m_{S\ Stack}$	OF_S
	g	*g*	-
P-2.5 L	49.1	21.5	0.44
P-2.5 M	50.7	18.1	0.36
P-2.5 H	53.4	19.4	0.36
P-2.5-W L	49.4	19.8	0.40
P-2.5-W M	53.5	19.5	0.36
P-2.5-W H	50.9	15.1	0.30

The initial sulphur mass correlates with the initial mass of the run, where the high bed density runs showed the highest initial sulphur mass before combustion. When the stack emissions are considered, both the total mass sulphur emitted, as well as the overall sulphur oxidation factors scale down with an increase in packing density. The main factors that influenced the total sulphur emissions are the combustion efficiencies and combustion rates of the respective runs as displayed in Table D2. These parameters correlate with the total stack sulphur emitted and also scale with the respective packing parameters. This is especially seen for the P-2.5-W H run which showed both the lowest combustion efficiency and combustion rate, and displayed the lowest total sulphur emitted compared to the other runs. The only outlier to this observation is the P-2.5 M run which exhibited slightly lower sulphur emissions than the “L” and “H” variants and showed a similar oxidation factor than the other runs. This behaviour can be attributed to the number of grate shakes that were performed during this run. In Table D2 it can be seen that this run required the least number of grate shakes, which minimised the volatilisation instances of sulphur in the ash, dust and grit, and therefore exhibited approximately 5% less total sulphur emissions than the other runs displayed in Table D7.The mass flow of SO_X emissions can be seen in Figure D9. In correlation with the results shown in Table D7, the SO_X mass emitted can be seen varying with change in fuel size.

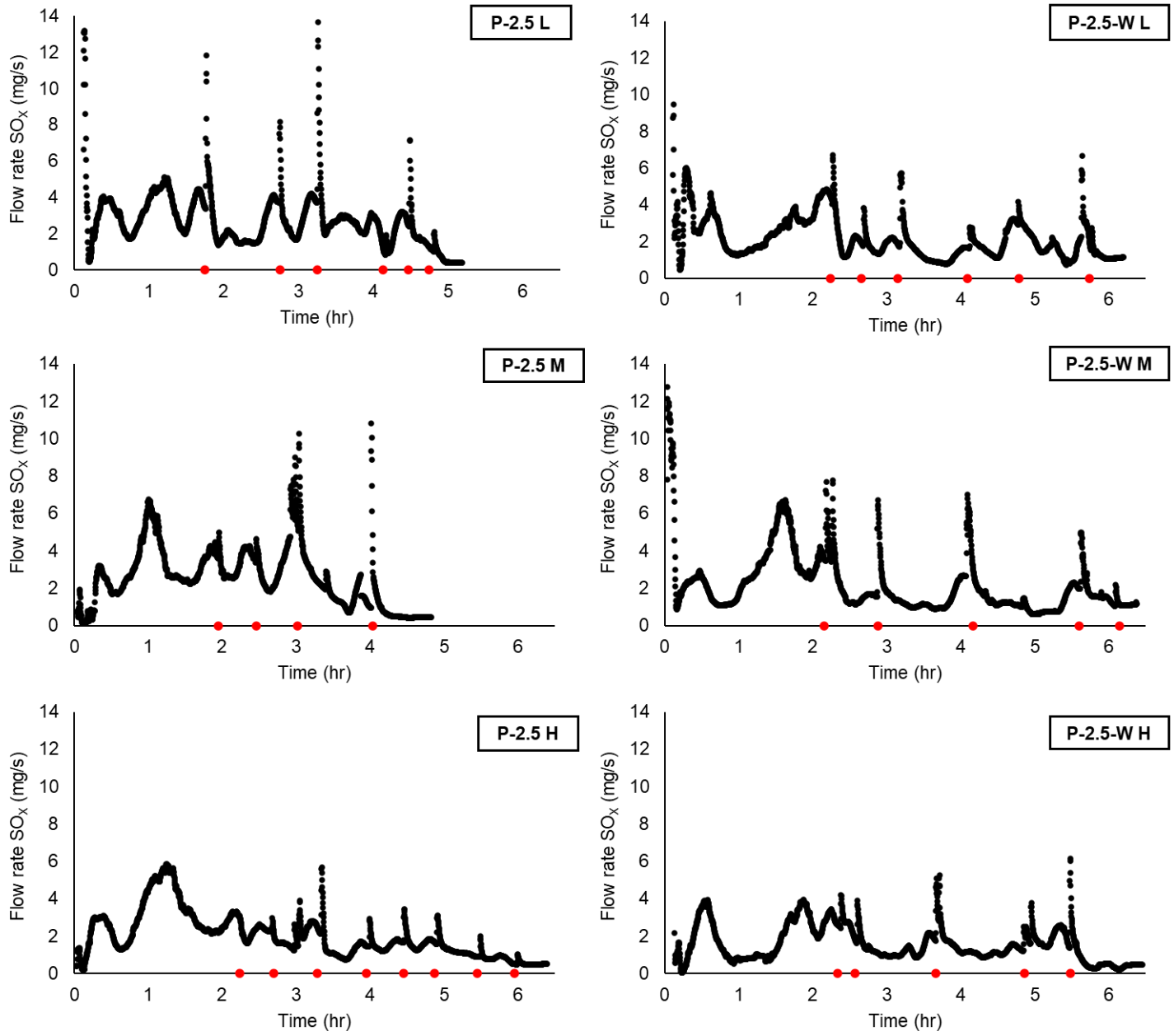

Figure D9: Mass flow rate of SOx emissions in the flue gas of high-power runs using fuel of various sizes.

The magnitude of the SO_X mass flow rate spikes after grate shakes, is less for the small size range fuel, compared to the larger fuel size “M" and “L” runs. This can be seen when comparing the P-2.5 L and P-2.5 H runs. It is possible that the clinkering and ash fusion mechanism bound most of the ash, dust, and inert material on top of the grate, reducing the volatilisation of sulphur-containing material and thus reducing the oxidation of sulphur to SO_X. In Figure D10 the mass flow rate of NO_X emissions emitted is displayed for the respective runs.

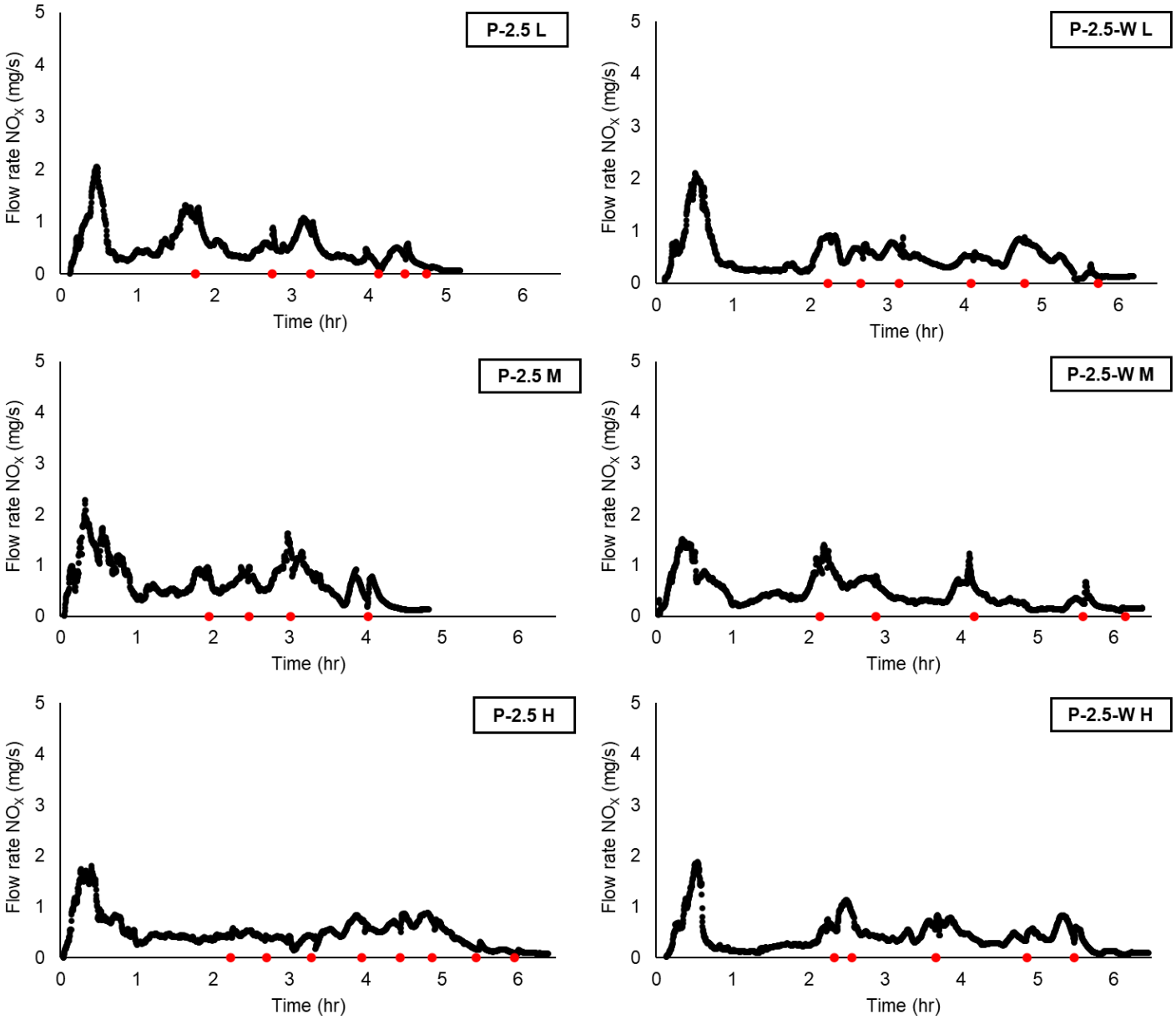

Figure D10: Mass flow rate of NOx emissions in the flue gas of high-power runs using fuel of various sizes.

All runs displayed similar NO_X emissions flow rates, with the magnitude of the initial NO_X spike during the ignition phase remaining consistent irrespective of fuel size or packing characteristics. The magnitude and length of the NO_X spikes after each grate shake remain relatively constant throughout the different runs. No significant correlation was observed between the NO_X emissions and the packing characteristics of the fuel. This is due to all the parameters that influence NO_X emissions, such as natural draft flow rate, combustion zone temperature, etc., remaining relatively constant for all the various runs. The mass flow rate of PM emissions for the respective runs can be seen in Figure D11.

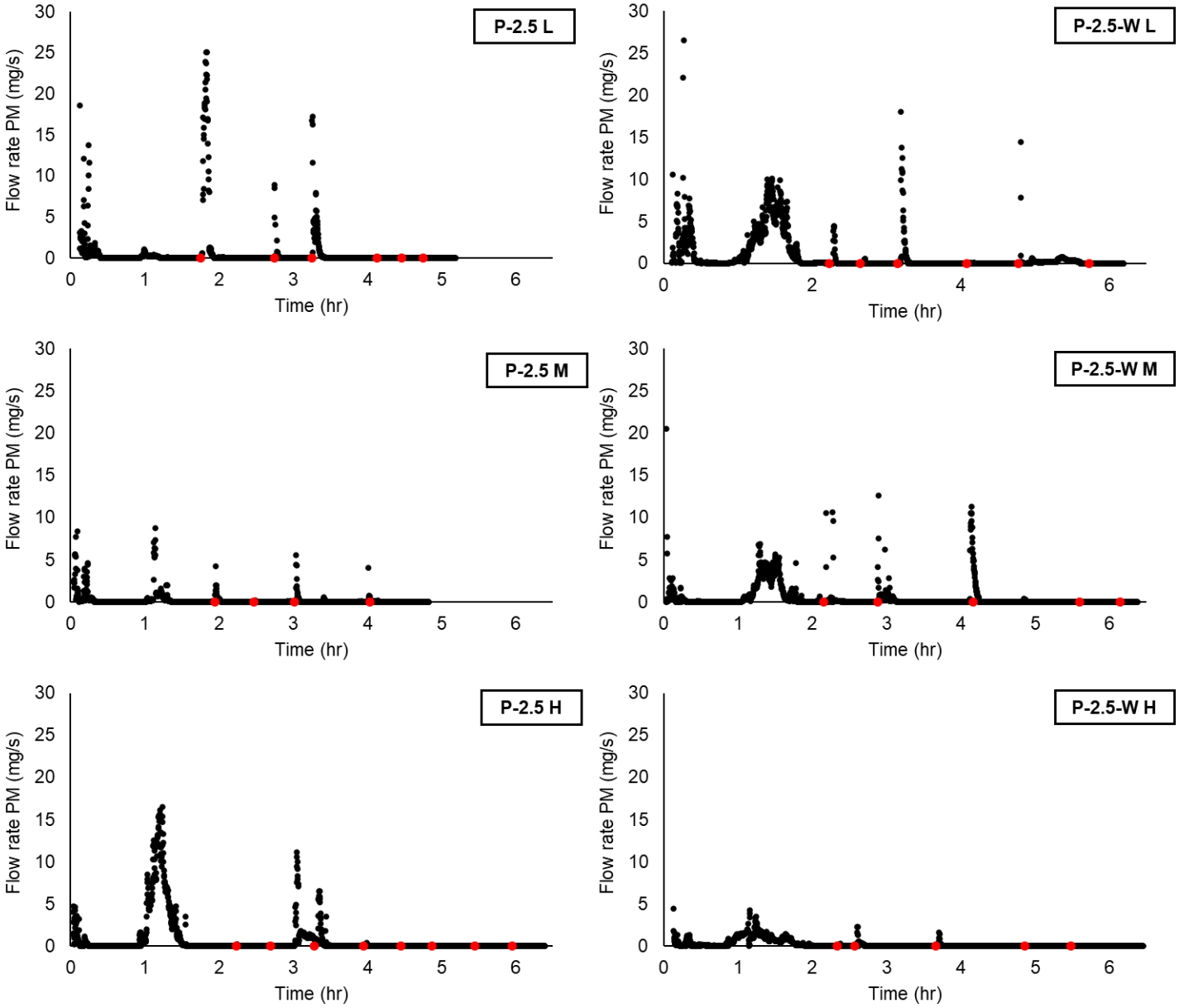

Figure D11: Mass flow rate of particulate matter emissions in the flue gas of high-power runs using fuel of various sizes.

The PM emissions are relatively similar for all the various runs. The initial PM spike during oxygen deficiency conditions is also observable for all the runs. However, the degree and magnitude of these PM spikes differ. For the P-2.5 runs, the CO emissions before the first grate shake increased as the packing density increases, whereas the opposite is seen for the P-2.5-W runs. It was believed that the decreased air permeability for high packing density fuel would cause poor gas phase combustion, and thus increased PM emission. However, this is observed for only the P-2.5 runs, but not for the P-2.5-W runs. More experimentation is required to better understand this observation. Finally, it can be seen that similar to the CO emissions, the magnitude of the PM

spikes after grate shakes was less than for the “H” compared to the “L” and “M” runs. This can also be attributed to the air channelling that was caused by the clinkering and the ash fusion. The PM and VOC stack gas concentration of the 2.5 wt.% PVA binder pellets of various size ranges, are shown in Figure D8.

Table D8: Emission parameter summary of high-power runs using fuel of various size ranges.

	$[PM_{DT}]$	$[VOC]$
	mg/m³	*mg/m³*
P-2.5 L	100	140
P-2.5 M	30	130
P-2.5 H	110	130
P-2.5-W L	140	150
P-2.5-W M	90	150
P-2.5-W H	50	70

The PM concentration of the P-2.5-W pellets decreased with an increase in packing density. Similar to the CO results, this can be attributed to the improved gas phase combustion cause by air channelling. However, for the P-2.5 runs no significant correlation could be observed between the PM concentration and the respective fuel size ranges. The VOC stack gas concentration remained relatively constant throughout the runs, and no significant correlation could be identified. These VOC results are also in contrast with literature findings since the average VOC concentration is not inversely proportional to the combustion chamber temperatures reported in Table D3. The P-2.5-W H run displayed both the lowest VOC concentration and the lowest CC middle temperature.

The emission factor summary of the high-power runs using different size ranges are presented in Table D9. All the emissions factors are of the same magnitude as those of the high-power runs displayed in Section 5.2.1.

Table D9: Emission factor summary for high-power runs using fuel of different size ranges.

	EF_{CO_2}	EF_{CO}	EF_{NO_x}	EF_{SO_x}	EF_{PM}	EF_{VOC}
	g/MJ	*g/MJ*	*mg/MJ*	*g/MJ*	*mg/MJ*	*mg/MJ*
P-2.5 L	95 ± 4	2.4 ± 0.1	65 ± 2	0.37 ± 0.01	78 ± 3	90
P-2.5 M	95 ± 4	1.8 ± 0.1	89 ± 3	0.34 ± 0.01	25 ± 1	90
P-2.5 H	94 ± 3	2.1 ± 0.0	81 ± 1	0.34 ± 0.01	100 ± 2	110
P-2.5-W L	94 ± 4	2.0 ± 0.0	72 ± 1	0.33 ± 0.01	120 ± 2	110
P-2.5-W M	92 ± 5	2.1 ± 0.0	66 ± 1	0.32 ± 0.01	57 ± 1	90
P-2.5-W H	93 ± 4	2.3 ± 0.0	72 ± 1	0.29 ± 0.01	41 ± 1	50

The “L” runs with increased bed voidage, and permeability did not exhibit lower CO, PM, and VOC emission factors compared to the other runs, as initially expected. Both the CO and PM emission factors show no significant correlation with changes in fuel size range. The same is true for the NO_X and PM emissions. The SO_X emission factors scale with fuel size range due to combustion performance of the respective runs. For P-2.5-W pellet runs, the high bed density runs exhibited higher CO emissions and vice versa. The lack of correlation between the other results and fuel size range might be due to the effect of disturbances on the combustion characteristics. Even though the higher bed voidage of the -19 mm +13.2 mm pellet runs improved the gas phase combustion effectiveness, other parameters, such as clinkering, grate shakes, and user error, might have had a larger impact on the emission factors. The use of fuel with an improved ash settling ability and a higher ash melting temperature might result in favourable homogeneous steady-state conditions.

ANNEXURE E – CALCULATIONS AND EXAMPLES

E.1 DETERMINING EMISSION FACTORS

In this section an example of the emissions calculations is given. Equations 4-1 to 4-11 is used to illustrate how emission factors and relevant emission parameters are determined. The first set of data is the mass loss data as obtained from the Sartorius platform scale. An example of such a data set can be seen in Figure E1.

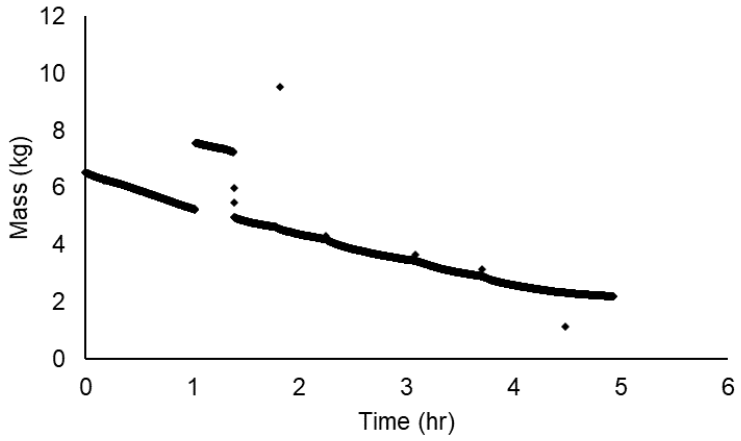

Figure E1: Fuel mass loss over time (P-5).

The outliers are removed from this data set using equation 4-1. The following formula was used in excel software for this purpose: “=IF(OR(A2>A1, A2<(A1-B1)),A1,A2)” where in column A the decreasing mass values of the y-axis in Figure E1 are displayed and B1 is the maximum expected combustion rate (≈ 0.1 kg/10sec). The result of the smoothing is illustrated in Figure E2.

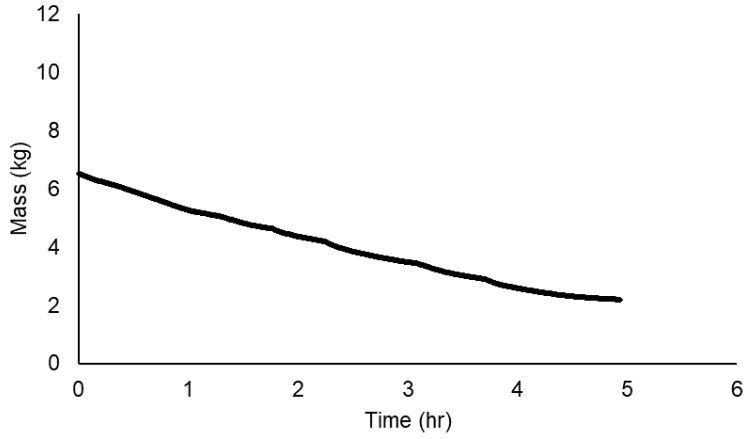

Figure E2: Processed fuel mass loss over time (P-5).

From this result set, the transient combustion rate (C_r) can be calculated using equation 4-2. This represents the local gradient of the data shown in Figure E2. Using the same software, the following equation was applied: "=(C1-C2)*(360)/(D2-D1)" where column C represents the processed mass loss data, and column D represents the time per ten second intervals, and a conversion factor of 360 is used to convert the transient combustion rate to kg/hr. The results of this are illustrated in Figure E3.

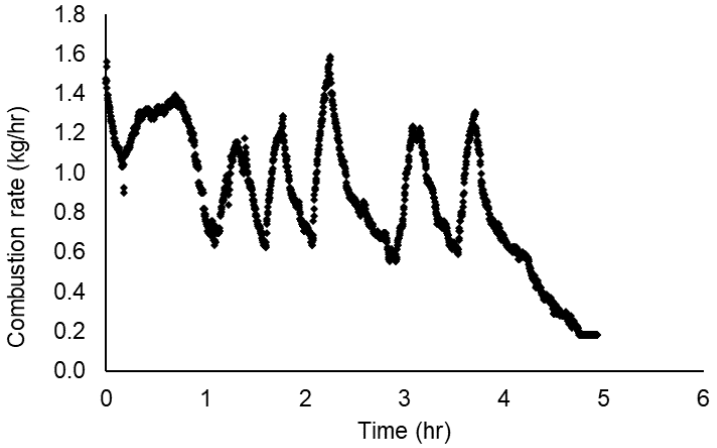

Figure E3: Transient combustion rate (P-5).

Using the transient combustion rate values presented in Figure E3, equation 4-3 is applied to determine the approximated molar flowrate of CO_2. This is calculated by applying the following formula: "=(E1)*(0.714)*(0.98)/(12.0107)*(1000)/(3600)" where column E is the transient combustion rate presented in Figure E3, the carbon fraction is 0.714, the α value for this run is 0.98, and the molar weight of carbon is 12.0107. The remaining constants is used to convert to a mol/s basis. The result of this equation is shown in Figure E4.

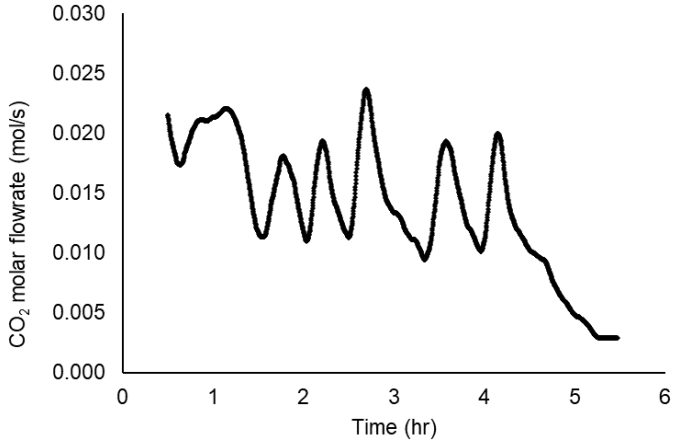

Figure E4: Calculated CO_2 molar flowrate (P-5).

The missing data at the start of the run is due to the time discrepancy between the emission data and the mass data. The total molar flowrate of the flue gas ($\dot{n}_{chim}$) can be approximated from the calculated CO_2 molar flowrate in Figure E4 using equation 4-5. This is calculated by applying the following formula: "=F1/[(G1/100)*(0.95)]" where column F is the molar flowrate of CO_2 as indicated in Figure E4, G1 refers to the CO_2 concentration (vol %) in the stack as measured by the Horiba PG 350 analyser (undiluted) and 0.95 is the dry to wet gas conversion factor to convert the value from a dry to a wet basis. The CO_2 concentration as measured during the experimental run is illustrated in Figure E5 while the calculated total molar flowrate of the flue gas for run P-5 is indicated in Figure E6.

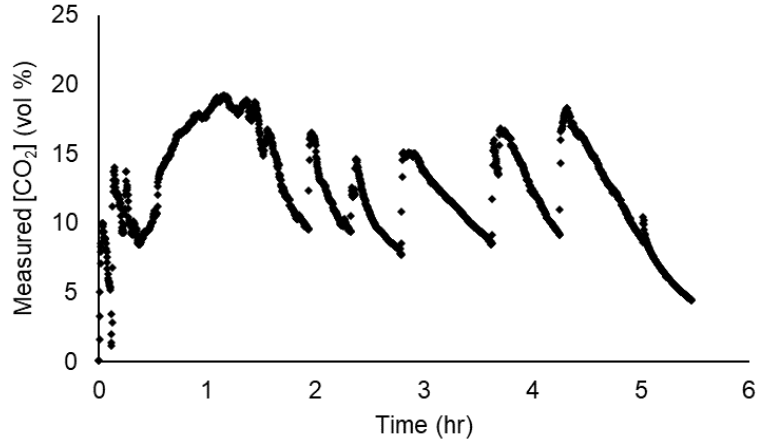

Figure E5: Undiluted CO_2 concentration measured by the Horiba PG 350 gas analyser (P-5).

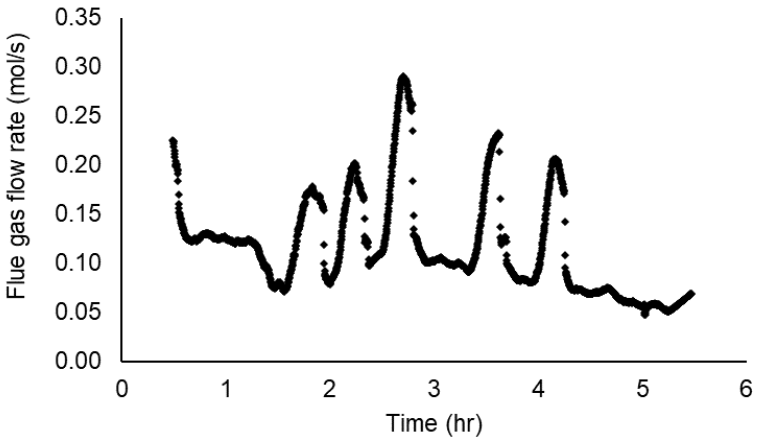

Figure E6: Approximated flue gas flowrate (P-5).

The mass flow of each pollutant (mg/s) is then calculated using the respective gas analyser results in combination with the total flue gas flowrate that was calculated above. This is done using equation 4-7. In Excel, the following formula is applied to each pollutant species: "=(G1/100)*(H1)*(44.01)*1000", where column G refers to the pollutant species of choice as measured by the gas analyser, column H is the calculated stack gas molar flowrate, 44.01 is the molar weight of CO_2 and the value is converted from g/s to mg/s by multiplying with 1000. This process is applied to all of the species (CO_2, CO, NO_X, SO_X) measured by the gas analyser in the chimney, but for illustration purposes the resulting mass flow rate of CO_2 is presented in Figure E7.

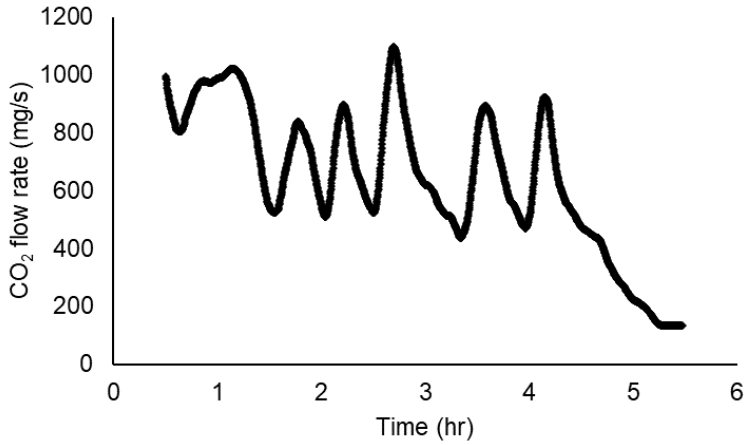

Figure E7: Calculated mass flowrate of CO2 (P-5).

The total mass of CO_2 emitted can be determined by calculating the area under the curve shown in Figure E7. This can be done for each measured pollutant. This is done via equation 4-9, however approximated integral calculation can also be applied using the formula: "=(Sum(I1:I2000)*10)/1000" where column I is the data set presented in Figure E7, I1 and I2000 is the first and last data point in this set respectively, and 10 is the measurement time interval between the data points (in seconds). The conversion is the made from mg to g and the result for total mass of CO_2 gas emitted in run P-5 was equal to 11502 g.

Before the emission factor can be calculated the calorific value must first be corrected to an ash free basis. This is done by using equation 4-10 and the CV value determined by the lab analyses. For the P-5 fuel, a CV of 20.3 MJ/kg and an ash yield of 25.7% was obtained. When substituting these values into equation 4-10, a corrected CV of 27.3 MJ/kg is calculated for the fuel. Finally, the emission factor of each species in g/MJ can be calculated using equation 4-11 together with the corrected CV, total mass of a species emitted and the total fuel mass loss during the run. For CO_2 the following formula was used: "=(11502)/(4.33*27.3)" which is equal to 97.13 g/MJ and falls within the confidence range of the value given in Table 5-8 (94 ± 5 g/MJ).

E.2 DETERMINING EMISSIONS MASS BALANCE

Using the method showcased in Section E.1, a carbon balance can be determined over the coal stove. Using the mass of CO_2 emitted (11502 g) and the mass of CO emitted (53 g) during the P-5 run, a carbon balance can be calculated over the combustion chamber using equations E-1 and E-2.

$$m_{C_{in}} = \Delta m_{fuel}\, x_c \qquad \text{E-1}$$

$$m_{C_{out}} = \frac{m_{CO_2} MW_C}{MW_{CO_2}} + \frac{m_{CO}\, MW_C}{MW_{CO}} \qquad \text{E-2}$$

$$m_{C_{in}} = (4.33\ kg)(0.71) = 3.09\ kg\ Carbon \qquad \text{E-3}$$

$$m_{C_{out}} = \frac{(11.502\ kg)\left(12.01 \frac{g}{mol}\right)}{\left(44.01 \frac{g}{mol}\right)} + \frac{(0.053\ kg)\left(12.01 \frac{g}{mol}\right)}{\left(28.01 \frac{g}{mol}\right)} = 3.19\ kg\ Carbon \qquad \text{E-4}$$

From the example calculations it can be seen that when comparing the carbon inlet and outlet of the combustion chamber (equations E-3 & E-4), a relative difference of 3% can be observed. This is mainly due to the assumptions used in this approximation (as stated in Section 4.2), in combination with the time discrepancy between the start of the mass data (started after the ignition phase) and emissions data (started before the ignition phase). For this reason, a confidence interval is always reported in Chapter 5 when referring to emission factors.

Using the approximation method discussed in Section 4.2 (equations 4-1 to 4-11) and the development of a species mass balance (using equations E-1 and E-2), an overall mass balance can be constructed including the main components (sulphur, nitrogen, oxygen, hydrogen). An overall mass balance for the P-5 run can be seen in Figure E-8.

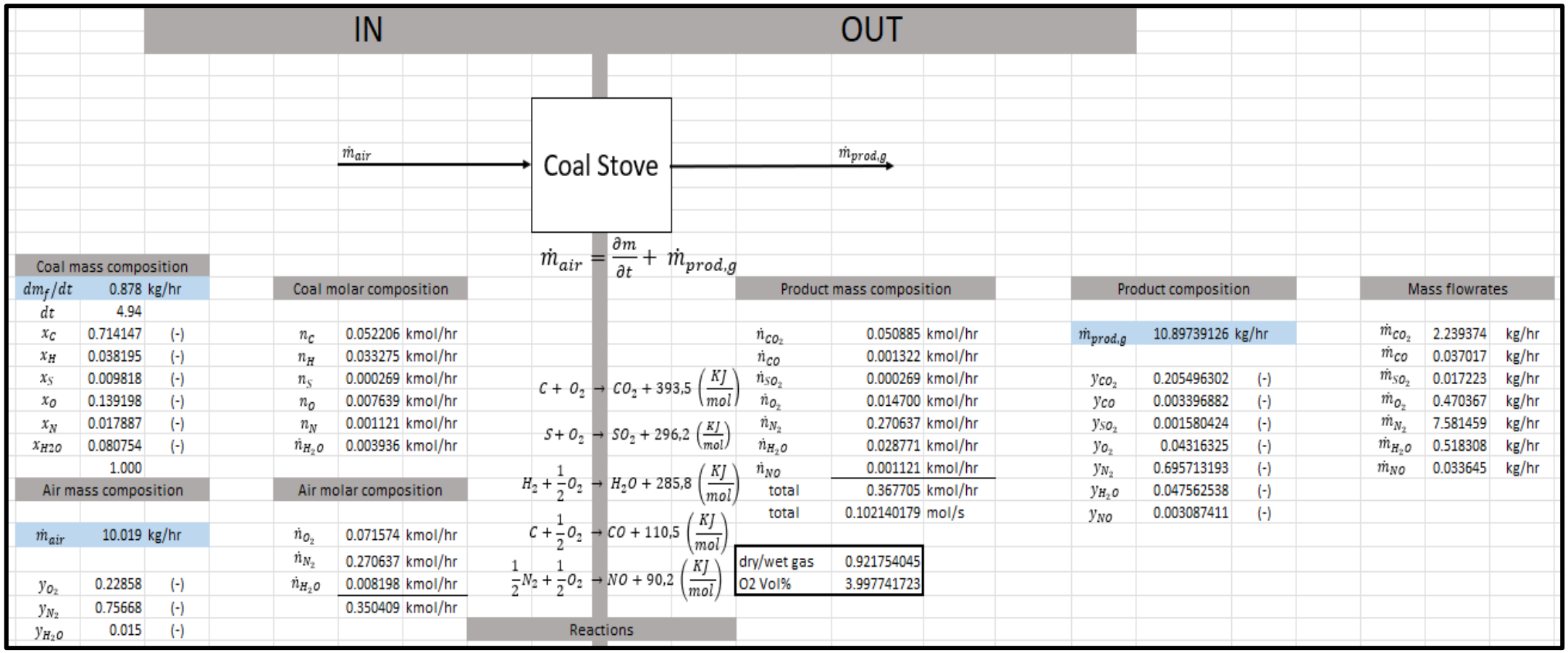

Figure E-8: Example of the overall mass balance for P-5 run.

E.3 DETERMINING OTHER EMISSION PARAMETERS

In Chapter 5, several emissions parameters, other than the emission factors, are displayed and discussed. The calculation of these parameters is possible by first applying the data processing methodology exhibited in Sections E.1 and E.2. Once the dynamic emissions data and the overall mass balance is determined, the following additional parameters can be calculated:

- The α value is calculated using Equation E-5. This value represents the fraction of carbon that oxidises to CO_2, whereas $(1-\alpha)$ represents the fraction of carbon that oxidises to CO.

$$\alpha = \frac{n_{CO_2}}{n_{CO_2} + n_{CO}} \qquad \text{E-5}$$

Where:

α is the fraction of carbon that oxidises to CO_2 *(-)*.
n_{CO_2} is the mole of CO_2 present in the flue gas *(mol/s)*.
n_{CO} is the mole of CO present in the flue gas *(mol/s)*.

- The CO:CO_2 ratio is calculated using equation E-6. This value represents the degree of complete combustion taking place, where a larger CO:CO_2 ratio indicates a greater degree of partial combustion.

$$CO{:}\,CO_2 = \frac{y_{CO}}{y_{CO_2}} \times 100 \qquad \text{E-6}$$

Where:

$CO{:}\,CO_2$ is the ratio of CO to CO_2 as a percentage *(%).*
y_{CO_2} is the vapor fraction of CO_2 in the flue gas *(vol.%).*
y_{CO} is the vapor fraction of CO in the flue gas *(vol.%).*

- The oxygen balance error is calculated using equation E-7. This error value indicates the relative difference between the inlet and outlet oxygen molecules.

$$\varepsilon_{O_2} = 1 - \frac{\left(\frac{1}{2}n_{CO} + \frac{1}{2}n_{NO} + n_{SO_2} + n_{CO_2} + n_{O_2\,out}\right)}{\left(\frac{m_{air}y_{O_2}}{MW_{O_2}}\right)} \qquad \text{E-7}$$

Where:

ε_{O_2} is the oxygen balance error *(%).*
n_{CO_2} is the mole of CO_2 present in the flue gas *(mol/s)*.
n_{CO} is the mole of CO present in the flue gas *(mol/s)*.
n_{NO} is the mole of NO present in the flue gas *(mol/s)*.
n_{SO_2} is the mole of SO_2 present in the flue gas *(mol/s)*.
$n_{O_2\,out}$ is the mole of O_2 present in the flue gas *(mol/s)*.
m_{air} is the mass of air entering the stove via the air inlet opening *(g/s).*

y_{O_2} is the vapor fraction of O_2 entering the stove *(vol.%).*
MW_{O_2} is the molecular weight of O_2 *(g/mol).*

- The average chimney velocity is calculated using equation E-8. This can either be determined from direct flue gas measurements or calculated using the ideal gas law approach.

$$\bar{v}_{chim} = \frac{\bar{n}_{chim} R\, T}{P\, A} \qquad \text{E-8}$$

Where:
$\bar{v}_{chim}$ is the average chimney velocity *(m/s).*
$\bar{n}_{chim}$ is the average total mole flowrate in the chimney *(mol/s).*
R is the molar gas constant *(8.314 J/K.mol).*
T is the temperature of the fluid *(K).*
P Is the pressure of the fluid *(Pa).*
A is the cross-sectional area of the chimney *(m^2).*

- The flue gas correction factor, lambda, is calculated using Equation E-9. This factor can be used to correct the gas analyser concentrations to quantitively compare results of two runs without the influence of oxygen dilution impacting the absolute values.

$$\lambda = \frac{n_{O_2\ in}}{n_{O_2\ in} - n_{O_2\ out}} = 1 + \frac{n_{O_2\ out}}{\left(\frac{1}{2} n_{CO} + \frac{1}{2} n_{NO} + n_{SO_2} + n_{CO_2}\right)} \qquad \text{E-9}$$

Where:
λ Is the flue gas concentration correction factor *(-).*
$n_{O_2\ in}$ Is the mole of O_2 entering the stove via the air inlet (mol).
$n_{O_2\ out}$ Is the mole of O_2 exiting the stove via the chimney (mol).
n_{CO_2} is the mole of CO_2 present in the flue gas *(mol/s)*.
n_{CO} is the mole of CO present in the flue gas *(mol/s)*.
n_{NO} is the mole of NO present in the flue gas *(mol/s)*.
n_{SO_2} is the mole of SO_2 present in the flue gas *(mol/s)*.

- The dry to wet gas correction factor is calculated using equation E-10. The flue gas sample moisture is removed using a combination of water traps, conditioning units, and filters. Therefore, concentrations reported by the gas analysers are on a dry basis. To convert these concentrations back to a wet basis, the correction factor is applied.

$$y_{d/w} = \frac{n_{chim} - n_{H_2O}}{n_{chim}} \qquad \text{E-10}$$

Where:
$y_{d/w}$ is dry to wet gas correction factor *(-).*
n_{chim} is the total mole of chimney gas on a wet basis *(mol).*
n_{H_2O} is the mole of H_2O in the stack gas *(mol).*

- The concentration of particulate matter in the stack gas is calculated Equation E-11. Using this equation, the total mass collected from the silica fibre thimble can be converted to a concentration.

$$[PM_T] = \frac{m_{f_T} - m_{i_T}}{V_{f_P} - V_{i_P}} \quad \text{E-11}$$

Where:

$[PM]_T$ is the PM concentration in the flue gas from the thimble mass *(mg/m^3).*
m_{f_T} is the final mass of the silica fibre thimble *(mg).*
m_{i_T} is the initial mass of the silica fibre thimble *(mg).*
V_{f_P} is the final volume reading on the aquaria pump *(m^3).*
V_{i_P} is the initial volume reading on the aquaria pump *(m^3).*

- The concentration of VOCs in the stack gas is calculated Equation E-12. Using this equation, the total mass collected from the activated carbon filter can be converted to a concentration.

$$[VOC] = \frac{m_{f_{CT}} - m_{i_{CT}}}{\dot{V}_P \Delta t} \quad \text{E-12}$$

Where:

$[VOC]$ is the VOC concentration in the flue gas *(mg/m^3).*
$m_{f_{CT}}$ is the final mass of the activated carbon filter *(mg).*
$m_{i_{CT}}$ is the initial mass of the activated carbon filter *(mg).*
$\dot{V}_P$ is the volume flow setting of the GilAir pump *(m^3/hr).*
Δt is the duration of the experiment *(hr).*

- The sulphur balance can be calculated using Equations E-13 – E-15. Here, the calculations for the total mass sulphur in the fuel, ash, and chimney pollutants are shown respectively. The error calculation for this mass balance is also shown in Equation E-17 to account for the undetected sulphur species. Additionally, the sulphur oxidation factors are calculated using Equation E-16. These factors indicate the fraction of sulphur in the fuel that oxidised to SO_X during combustion.

$$m_{S_{fuel}} = m_{i\,fuel}\, x_{S\,fuel} \quad \text{E-13}$$

$$m_{S_{ash}} = m_{ash}\, x_{S\,ash} \quad \text{E-14}$$

$$m_{S_{chim}} = \frac{MW_S}{MW_{SO_2}} \int_{t_f}^{t_i} (y_{SO_2})(\dot{n}_{chim})\left(MW_{SO_2}\right) dt \quad \text{E-15}$$

$$OF_S = \frac{m_{S_{chim}}}{m_{S_{fuel}}} \quad \text{E-16}$$

$$\varepsilon_S = \frac{m_{S_{fuel}} - m_{S_{ash}} - m_{S_{chim}}}{m_{S_{fuel}}} \times 100 \qquad \text{E-17}$$

Where:

$m_{S_{fuel}}$	is the mass of sulphur in the fuel *(g).*
$m_{i\ fuel}$	is the initial mass of fuel loaded at the start of the run *(g).*
$x_{S\ fuel}$	is the fraction of sulphur in the fuel *(-).*
$m_{S_{ash}}$	is the mass of sulphur in the ash *(g).*
m_{ash}	is the mass of ash collected at the end of the experiment *(g).*
$x_{S\ ash}$	is the fraction of sulphur in the ash *(-).*
$m_{S_{chim}}$	is the mass of sulphur in the flue gas *(g).*
MW_S	is the molecular weight of sulphur *(g/mol).*
MW_{SO_2}	is the molecular weight of SO_2 *(g/mol).*
y_{SO_2}	is the vapor fraction of SO_2 in the flue gas *(-).*
$\dot{n}_{chim}$	is the total mole flow of flue gas at time t *(mol/s).*
OF_S	is the sulphur oxidation factor *(-).*
ε_S	is the sulphur balance error caused by undetected species *(%).*

E.4 DETERMINING ENERGY TRANSFER RATES

In this section, an example calculation of the thermal data processing is given. The methodology given in Section 4.3 is applied to the P-5 run for illustration purposes. Equation 4-12 to 4-23 is used to calculate and populate the values in Table E-1. To calculate the energy delivered by convection, the first step is to identify the main areas of heat transfer and divide these areas into smaller segments that can be evaluated individually. This is shown in Figure 4-6. In Table E-1, the example calculation for one side of the stove is shown. This consists of six segments, namely the hopper top and bottom, combustion chamber top and bottom, and the heat exchanger top and bottom. The same methodology can be followed for the other stove segments, over the duration of the experiment.

Table E-1: Calculating energy delivered through convection.

Parameter	H Top	H Bot	CC Top	CC Bot	HX Top	HX Bot	Units	Determined
L_W	0.24	0.24	0.17	0.17	0.35	0.35	m	Measurement
L_H	0.26	0.26	0.26	0.26	0.26	0.26	m	Measurement
A	0.06	0.06	0.04	0.04	0.09	0.09	m^2	Equation 4-14
Gr_L	2.5×10^8	3.8×10^8	3.7×10^8	2.9×10^8	3.2×10^8	2.4×10^8	-	Equation 4-19
g	9.81	9.81	9.81	9.81	9.81	9.81	$m.s^{-2}$	Constant
β	0.0028	0.0025	0.0025	0.0027	0.0026	0.0028	K^{-1}	Equation 4-22
Lc	0.26	0.26	0.26	0.26	0.26	0.26	m	Equation 4-20
v	1.5×10^{-5}	1.5×10^{-5}	1.5×10^{-5}	1.5×10^{-5}	1.5×10^{-5}	1.5×10^{-5}	$m^2.s^{-1}$	Constant
T_s	426	510	507	449	467	416	K	Experimental
T_∞	298	298	298	298	298	298	K	Experimental
Pr	0.69	0.69	0.69	0.69	0.69	0.69	-	Equation 4-18
Ra_L	1.7×10^8	2.6×10^8	2.6×10^8	2.0×10^8	2.2×10^8	1.6×10^8	-	Equation 4-15
Nu_L	67.9	74.9	74.7	70.2	71.7	66.8	-	Equation 4-16
k	0.03	0.03	0.03	0.03	0.03	0.03	$W.m^{-1}.K^{-1}$	Constant
h	7.83	8.64	8.62	8.10	8.28	7.71	$W.m^{-2}.K^{-1}$	Equation 4-12 and 4-13
$\dot{Q}_{Con}$	63.47	116.08	80.46	54.72	127.43	83.31	W	Equation 4-12

To determine the energy delivered via radiation, the segmented area methodology is again applied. In Table E-2, the example calculation of radiation energy from one side of the stove is shown. Equation 4-24 is applied using the parameters shown in this table.

Table E-2: Calculating energy delivered through radiation.

Parameter	H Top	H Bot	CC Top	CC Bot	HX Top	HX Bot	Units	Determined
$\dot{Q}_{rad}$	85.56	204.48	140.48	79.23	194.88	109.28	W	Equation 4-24
A	0.06	0.06	0.04	0.04	0.09	0.09	m^2	Equation 4-14
ε	0.95	0.95	0.95	0.95	0.95	0.95	-	Constant
σ	$5.7x10^{-8}$	$5.7x10^{-8}$	$5.7x10^{-8}$	$5.7x10^{-8}$	$5.7x10^{-8}$	$5.7x10^{-8}$	$W.m^{-2}.K^{-4}$	Constant
T_s	426	510	507	449	467	416	K	Experimental
T_∞	298	298	298	298	298	298	K	Experimental

The stack losses can be calculated by evaluating the known emissions exiting the stack. The dry gases include CO_2, CO, NO, SO_2, O_2 and N_2. The wet gas stack loss evaluation includes the energy losses from both liquid and gas phase water. The liquid phase water accounts for only the inherent moisture in the fuel, whereas the vapour phase water accounts for inlet air moisture, vapourised fuel moisture, and water formed during the combustion reaction. The calculation of these stack losses is illustrated in Table E-3.

Table E-3: Calculating energy lost through stack emissions.

Parameter	CO_2	CO	NO	SO_2	O_2	N_2	H_2O (g)	H_2O (l)	Units	Determined
Q_{SL}	1390.6	36.28	0.99	3.64	480.40	5395.7	212.60	119.79	kJ	Equation 4-25 and 4-26
m_i	11.01	0.27	0.01	0.04	3.91	40.21	1.92	0.38	kg	Figure E-8
$C_{p\,i}$	0.98	1.05	1.00	0.64	0.95	1.04	1.97	4.18	$kJ.kg^{-1}.K^{-1}$	Literature
T	429	429	429	429	429	429	429	373	K	Experimental
T_{ref}	298	298	298	298	298	298	373	298	K	Experimental

From the results in this table, the energy of vaporisation of water should also be included in this calculation. This is determined by applying Equation 4-26. The energy of vaporisation (2441.7 kJ/kg) is multiplied with the mass of water, which produces a total of 4692 kJ of energy lost during the experiment. When all the stack losses are added from the respective species, both wet and dry, a total stack loss energy of 12.3 MJ was found for this example.

E.5 DETERMINING THE STOVE ENERGY BALANCE

In this section an example calculation of the energy balance for the P-5 runs is shown. The energy balance consists of five parts:

1. Energy generated through combustion (fired energy).
2. Energy delivered through free convection.
3. Energy delivered through radiation.
4. Energy losses through stack emissions.
5. Energy losses unaccounted for.

These five parameters are shown in Equation 4-29, where the total energy generated through combustion is equal to the total energy delivered through convection and radiation minus the sum of the losses. For the P-5 run, each of the five energy terms can be calculated as follows:

$$Q_F = \Delta m \times CV_{corr} = (4.23\ kg)\left(27.3\frac{MJ}{kg}\right) = 115.52\ MJ \quad \text{E-18}$$

$$Q_{SL} = \Sigma\, m_i C_{p\,i}\left(T - T_{ref}\right) + Q_{H_2O} = 1390.66\ kJ + 36.28\ kJ + 0.99\ kJ + 3.64\ kJ + 480.4\ kJ + 5395.71\ kJ + 212.6\ kJ + 119.79\ kJ + 4692.05\ kJ = 12.33\ MJ \quad \text{E-19}$$

$$Q_{rad} = \sum\left(\sum \sigma\varepsilon A_i\left(T_{s\,i}^4 - T_\infty^4\right)\right)\Delta t = 60.84\ MJ \quad \text{E-20}$$

$$Q_{con} = \sum\left(\sum h_i\, A_i\,(T_{s\,i} - T_\infty)\right)\Delta t = 35.76\ MJ \quad \text{E-21}$$

$$Q_{Error} = Q_F - Q_{SL} - Q_{rad} - Q_{con} = 115.52\ MJ - 12.33\ MJ - 60.84\ MJ - 35.76\ MJ = 6.59\ MJ \quad \text{E-22}$$

Where:

Q_F	is the energy generated through combustion *(MJ).*
Δm	is the difference between the initial and final mass of fuel *(kg).*
CV_{corr}	is the corrected calorific value for ash yield *(MJ/kg).*
Q_{SL}	is the total stack heat loss due to both dry gases and moisture *(MJ).*
m_i	is the total mass of pollutant species i emitted *(kg).*
$C_{p\,i}$	is the specific heat capacity of pollutant species i *(kJ/kg.K).*
T	is the stack outlet temperature *(K).*
T_{ref}	is the reference temperature (ambient) *(K).*
Q_{H_2O}	is the total heat loss due to moisture in stack emissions *(MJ).*
Q_{rad}	is the total heat transfer out of the body via radiation *(MJ).*
σ	is the Stefan-Boltzmann constant *(W/m^2K^4).*
ε	is the thermal emissivity *(-).*
A_i	is the area of stove segment i *(m^2).*

$T_{s\,i}$ is the stove surface temperature of segment i *(K).*
T_{∞} is the environment temperature *(K).*
Δt is the time between surface temperature measurements *(s).*
Q_{con} is the total heat transfer out of the body via convection *(MJ).*
h_i is the heat transfer coefficient calculated for stove segment i *(W/m^{2}K).*
Q_{Error} is the unaccounted energy losses and error *(MJ).*

From Equation E-22, an energy balance error of roughly 5.7% is calculated. As discussed in Chapter 4.3, this error is a sum of unaccounted energy losses. These losses include:

- Energy transfer through the bottom surfaces of the stove.
- Heating of the fuel.
- Heating of the stove material (metallic and refractory material).
- Energy losses through the dust and particulate matter in the stack.
- Energy losses through the water boiling test.
- Calculation approach and assumptions.

Even though there are multiple “energy pathways” that are not accounted for, the calculated energy balance error remains less than 10% which indicates that the calculation methodology followed in this study is sufficient to reach the aim and objectives set out in Chapter 1.

E.6 DETERMINING OTHER THERMAL PARAMETERS

In Chapter 5, focus is placed on thermal efficiencies and stove power ratings. In addition, the results of the water boiling test is also displayed and discussed. The calculation of these parameters is only possible by first applying the data processing methodology exhibited in Sections 4.3 and Annexures E.4 and E.5. Once the stove energy balance is determined, the following parameters can be calculated:

- The fired power of the stove-fuel combination is calculated using Equation E-23. This power rating indicates the average power that is produced through combustion. The combustion efficiency of the respective experiment is also reflected by this parameter.

$$P_F = \frac{\Delta m\ CV_{corr}}{\Delta t} = \frac{Q_F}{\Delta t} \qquad \text{E-23}$$

Where:

P_F	is the stove-fuel combination's fired power rating *(kW).*
Δm	is the difference between the initial and final mass of fuel *(kg).*
CV_{corr}	is the corrected calorific value for ash yield *(kJ/kg).*
Δt	is the duration of the experiment *(s).*
Q_F	is the energy generated through combustion *(kJ).*

- The delivered power of the stove-fuel combination is calculated using Equation E-24. This power rating conveys the average thermal power obtained from radiation and free convection.

$$P_D = \frac{Q_{rad}\ + Q_{con}}{\Delta t} \qquad \text{E-24}$$

Where:

P_D	is the stove-fuel combination's delivered power rating *(kW).*
Q_{rad}	is the total heat transfer out of the body via radiation *(kJ).*
Q_{con}	is the total heat transfer out of the body via convection *(kJ).*
Δt	is the duration of the experiment *(s).*

- The stove energy delivered efficiency is calculated using Equation E-25. The delivered efficiency indicates the fraction of energy that was transferred via conduction and radiation, as calculated by the methodology given in Section 4.3.

$$\eta_D = \frac{Q_{rad}\ + Q_{con}}{\mathrm{Q}_F} \times 100 \qquad \text{E-25}$$

Where:

η_D	is the stove-fuel combination's delivered energy efficiency *(%).*
Q_{rad}	is the total heat transfer out of the body via radiation *(MJ).*

Q_{con} is the total heat transfer out of the body via convection *(MJ).*
Q_F is the energy generated through combustion *(MJ).*

- The stove overall (total) thermal efficiency illustrates the amount of energy delivered via conduction and radiation compared to the potential energy from the loaded fuel. This efficiency reflects the accumulation of all the losses (combustion losses, stack emissions losses, and unaccounted energy transfer losses). This efficiency is calculated using Equation E-26.

$$\eta_{tot_1} = \frac{Q_{rad} + Q_{con}}{m_0\, CV} \times 100 \qquad \text{E-26}$$

Where:
η_{tot_1} is the stove-fuel combination's overall (total) energy efficiency *(%).*
Q_{rad} is the total heat transfer out of the body via radiation *(MJ).*
Q_{con} is the total heat transfer out of the body via convection *(MJ).*
m_0 is the mass of fuel loaded into the stove *(kg).*
CV is the calorific value if the fuel (a.d.b.) *(MJ/kg).*

In addition to the stove overall efficiency shown above, another overall efficiency parameter is displayed and discussed in this study. This overall efficiency is calculated using the British standard guideline for thermal performance assessment (BS 845-1:1987) [89]. Using this document as a guideline, the second overall thermal efficiency is defined as:

$$\eta_{tot_2} = 100\% - L_1 - L_2 - L_3 - L_4 \qquad \text{E-27}$$

Where:
η_{tot_2} is the stove-fuel combination's overall (total) energy efficiency *(%).*
L_1 is the loss due to sensible heat of the dry flue gases *(%).*
L_2 is the loss due to water vapour in the flue gases *(%).*
L_3 is the loss due to unburned gases in the stack gas *(%).*
L_4 Is the loss due to combustible matter in ash *(%).*

The η_{tot_1} is a calculation of the total efficiency with regards to the delivered energy for cooking and heating, while η_{tot_2} is a calculation of the total efficiency with regards to all the energy losses that might occur during operation. Theoretically η_{tot_1} and η_{tot_2} should be equivalent, however if an energy balance error exists as shown in Section E.5, these values will differ corresponding to the magnitude of the energy balance error.

- For the evaluation of the water boiling test, the cooking power and the cooking efficiency of the stove-fuel combination is also calculated. The cooking power is calculated using Equation E-28 and the cooking efficiency is calculated using Equation E-30.

$$P_C = \frac{Q_W}{\Delta t} \quad \text{E-28}$$

$$Q_W = m_{H_2O} \cdot Cp_{H_2O} (T_{boil} - T_0) \quad \text{E-29}$$

$$\eta_C = \frac{Q_W}{(m_0 - m_f)\, CV_{corr}} \times 100 \quad \text{E-30}$$

Where:

P_C	is the cooking power of the stove-fuel combination *(kW).*
Q_W	is the energy required to reach boiling point *(kJ).*
Δt	is the time that was required to reach boiling point *(s).*
m_{H_2O}	is the mass of water in the pot *(kg).*
Cp_{H_2O}	is the specific heat capacity of water in the liquid phase *(kJ/kg.K).*
T_{boil}	is the local boiling point temperature of water (368.9 *K).*
T_0	is the initial temperature of the water at the start of the test *(K).*
η_C	is the cooking efficiency *(%).*
m_0	is the fuel mass at the start of the test *(kg).*
m_f	is the fuel mass at the end of the run *(kg).*
CV_{corr}	is the calorific value corrected for ash yield *(kJ/kg).*

E.7 REAPEATABILITY CALCULATIONS

In this section, the calculations done for the experimental repeatability is shown. The repeatability analysis is conducted using three main statistic indicators:

- 95% confidence intervals.
- Standard deviation.
- 95% confidence interval error.

The calculation of these factors is done by applying Equation E-31 to E-34 on the results of the 5 identical runs. Similarly, the emission factors reported in Chapter 5 was also reported with a 95% confidence interval by applying the same methodology.

$$\bar{x} = \frac{1}{n}\sum_{i=1}^{n} x_i \quad \text{E-31}$$

$$\sigma = \sqrt{\frac{\sum(x_i - \bar{x})^2}{(n-1)}} \quad \text{E-32}$$

$$CI = \bar{x} \pm z\frac{\sigma}{\sqrt{n}} \quad \text{E-33}$$

$$For\ CI_{95\%}:\quad z = 1.96$$

$$\epsilon = \frac{CI_{95\%}}{\bar{x}} \times 100 \qquad \text{E-34}$$

Where:

$\bar{x}$	is the sample mean average *(-).*
n	Is the sample size (number of data points) *(-).*
x_i	is i^{th} sample in the set *(-).*
σ	Is the standard deviation of the data set *(-).*
CI	Is the confidence interval of the data set *(-).*
$CI_{95\%}$	Is the 95% confidence interval of the data set *(-).*
z	Is the confidence level value *(-).*
ϵ	Is the confidence level error *(%).*